Modeling Aqueous Organic Chemistry in Experimental and Natural Systems

by

Kirtland J Robinson

A Dissertation Presented in Partial Fulfillment
of the Requirements for the Degree
Doctor of Philosophy

Approved November 2017 by the
Graduate Supervisory Committee:

Everett Shock, Chair
Hilairy Hartnett
Ariel Anbar
Pierre Herckes

ARIZONA STATE UNIVERSITY

December 2017

ABSTRACT

In many natural systems aqueous geochemical conditions dictate the reaction pathways of organic compounds. Geologic settings that span wide ranges in temperature, pressure, and composition vastly alter relative reaction rates and resulting organic abundances. The dependence of organic reactions on these variables contributes to planetary-scale nutrient cycling, and suggests that relative abundances of organic compounds can reveal information about inaccessible geologic environments, whether from the terrestrial subsurface, remote planetary settings, or even the distant past (if organic abundances are well preserved). Despite their relevance to planetary modeling and exploration, organic reactions remain poorly characterized under geochemically relevant conditions, especially in terms of their reaction kinetics, mechanisms, and equilibria.

In order to better understand organic transformations in natural systems, the reactivities of oxygen- and nitrogen-bearing organic functional groups were investigated under experimental hydrothermal conditions, at 250°C and 40 bar. The model compounds benzylamine and α-methylbenzylamine were used as analogs to environmentally relevant amines, ultimately elucidating two dominant deamination mechanisms for benzylamine, S_N1 and S_N2, and a single S_N1 mechanism for deamination of α-methylbenzylamine. The presence of unimolecular and bimolecular mechanisms has implications for temperature dependent kinetics, indicating that Arrhenius rate extrapolation is currently unreliable for deamination.

Hydrothermal experiments with benzyl alcohol, benzylamine, dibenzylamine, or tribenzylamine as the starting material indicate that substitution reactions between these

compounds (and others) are reversible and approach metastable equilibrium after 72 hours. These findings suggest that relative ratios of organic compounds capable of substitution reactions could be targeted as tracers of inaccessible geochemical conditions.

Metastable equilibria for organic reactions were investigated in a natural low-temperature serpentinizing continental system. Serpentinization is a water-rock reaction which generates hyperalkaline, reducing conditions. Thermodynamic calculations were performed for reactions between dissolved inorganic carbon and hydrogen to produce methane, formate, and acetate. Quantifying conditions that satisfy equilibrium for these reactions allows subsurface conditions to be predicted. These calculations also lead to hypotheses regarding active microbial processes during serpentinization.

I dedicate this dissertation to my parents, Janet and Warren, and my brothers, Michael and Jeffrey. Mom and Dad, thank you for always being proud and encouraging. Bros, thank you for all the years of challenging me. Without any one of you, this work would not exist.

ACKNOWLEDGMENTS

This body of work required a great deal of effort beyond my own, including help from those who gave analytical support, expert advice, and hands-on mentorship, as well as those who provided professional and personal guidance. My first research experience was under Matt Golombek, a planetary geologist, who for some reason took on an undergraduate biologist and exposed him to thinking about the "bigger picture" in scientific exploration. Matt helped me find my next mentor, Mike Russell: an origins of life theorist. Mike paved the way for several new and exciting intellectual and analytical avenues, really allowing me to develop a nearly unhealthy addiction for science; he also helped me find my thesis advisor, Everett Shock.

Everett has had the largest role in shaping my approach to scientific exploration and thought. Everett has provided essential navigation, very literally at times as a field research guide through the bogs and "green blizzards" of Yellowstone National Park, more formally throughout my studies as one of the most meticulous skeptics that science has to offer, and at times more existentially as I consider my academic future. As anyone involved in a graduate program knows, the relationship between Ph.D. student and advisor can be a complicated one, but I am very fortunate to be able to consider Everett a true friend who has strived to keep my best interests in mind.

I thank my committee. Pierre Herckes has assisted me regarding theoretical atmospheric processes and in using his laboratory's gas chromatograph-mass spectrometer. Ariel Anbar has provided unique perspectives regarding isotope geochemistry, as well as mentorship for a teaching assistant role for the Habitable Worlds

course at Arizona State University. Hilairy Hartnett has provided valuable insights involving experimental, analytical, and statistical methods, which improved the quality of my data. Ian Gould has gone above and beyond in helping me understand and characterize the organic reactions that have been the focus of my experimental research.

There are also many early career scientists to thank. Chris Glein mentored me in lab first at ASU. Kris Fecteau provided mentorship for experiments, environmental analytical techniques, and performed inorganic ion chromatography analyses in this work. Christa Bockisch provided guidance for short time span experiments. Shaela Noble helped complete organic acid anion analysis. Natasha Zolotova provided instruction, assisted analytical efforts, and ensured instrumental accuracy and precision for dissolved inorganic and organic carbon analyses. Randall "Vince" Debes and Grayson Boyer also contributed to these analyses. Vince organized numerous field sampling expeditions relevant to this work. Alta Howells collected and analyzed dissolved gas samples for methane and hydrogen. James Leong contributed to field sampling efforts and performed silica concentration analysis. Alysia Cox contributed to field sampling efforts. Members of the Group Exploring Organic Processes in Geochemistry (GEOPIG), past and present, contributed to field sampling efforts or provided useful discussions over the years, including: Brian St Clair, Peter Canovas, Jeff Dick, Kristin Johnson, Jordan Okie, Apar Prasad, Tucker Eli, Jeff Havig, Panjai Prapaipong, and Ziming Yang. Others, many of whom are dear friends, also deserve my thanks for their useful insights, including: Robert Schmitz, Bennett Addison, Brian Woodrum, Adam Monroe, Iolanda Klein, Jessie Shipp, Jesse Coe, Aurelie Marcotte, Josh Nye, Meg Schmierer, Sarah Frey, Amisha Poret-Peterson, Trevor Bozeman, Stephen Romaniello, and Steve Davidowski.

TABLE OF CONTENTS

Page

LIST OF TABLES viii

LIST OF FIGURES ix

CHAPTER

1 INTRODUCTION 1

1.1 Deamination Reaction Mechanisms under Acidic Hydrothermal Conditions 2

1.2 Metastable Equilibrium Among Oxygen- and Nitrogen-Bearing Organic Compounds in Hydrothermal Experiments 4

1.3 A Thermodyanmic Assessment of Carbon Chemistry during Low-Temperature Continental Serpentinization 6

2 DEAMINATION REACTION MECHANISMS UNDER ACIDIC HYRDROTHERMAL CONDITIONS 10

2.1 Introduction 10

2.2 Experimental 20

2.3 Results and Discussion 28

2.4 Conclusions 57

2.5 Acknowledgements 58

3 METASTABLE EQUILIBRIUM AMONG OXYGEN- AND NITROGEN-BEARING ORGANIC COMPOUNDS IN HYDROTHERMAL EXPERIMENTS 59

3.1 Introduction 59

CHAPTER Page

3.2 Experimental 67

3.3 Results and Discussion.....73

3.4 Conclusions 95

3.5 Acknowledgements.....96

4 A THERMODYNAMIC ASSESSMENT OF CARBON CHEMISTRY DURING LOW TEMPERATURE CONTINENTAL SERPENTINIZATION 97

4.1 Introduction 97

4.2 Methods 106

4.3 Results and Discussion.....115

4.4 Concluding Remarks.....148

4.5 Acknowledgements.....150

5 FUTURE DIRECTIONS 152

REFERENCES..... 158

APPENDIX

A SUPPORTING DATA FOR CHAPTER 2 180

B SUPPORTING DATA FOR CHAPTER 3.....196

C ESTIMATING THERMODYNAMIC PROPERTIES OF PRIMARY, SECONDARY, AND TERTIARY AMINES AND AMINIUMS 203

D SUPPORTING DATA FOR CHAPTER 4 215

LIST OF TABLES

Table Page

1. Kinetics for Ring Substituted Compounds 48

LIST OF FIGURES

Figure Page

1. Structures and Abbreviations for the Amines Studied in this Work. 18
2. Experimental pH Relative to Empirically-Derived Literature pK_a Values 27
3. Reactant and Product Concentrations from Benzylamine Experiments..... 31
4. A Kinetic Model for the Hydrothermal Decomposition of Benzylamine 33
5. The Observed Rate Constant for Reaction of the Amine.....35
6. Proposed Mechanism for Formation of *p*-benzylbenzyl Alcohol..... 36
7. Kinetic Scheme for Reaction Conversion of Benzylamine 38
8. S_N1 (blue) and S_N2 (red) Reaction Mechanisms 41
9. Reactant and Product Concentrations from α-methylbenzylamine Experiments 43
10. A Kinetic Model for the Hydrothermal Decomposition of α-methylbenzylamine... 45
11. Hammett Plots for Deamination and other Substitution Reactions..... 51
12. Stoichiometric Ratios of Initial Reactants used in Experiments.....71
13. Experimentally Measured p*K*a Values vs. Temperature..... 72
14. Reactions used to Calculate Reaction Quotients..... 75
15. *Apparent Equilibrium* Reaction Quotients vs. Time..... 77
16. Cumulative Concentrations of Unidentified Multi-Ring Compounds vs. Time 81
17. Dehydrogenation of Dibenzylamine and Hydrogenolysis of Benzylamine..... 83
18. Ratio of the Total Concentrations of Dibenzylimine:Toluene vs. Time 85
19. Hydrothermal Reaction Network for C-, H-, O-, and N-Bearing Organics 88
20. Reaction Quotients vs. Time Compared to Calculated Reaction Constants 90
21. Cartoon Cross section of the Reaction Pathways of Carbon in Oman 105

Figure Page

22. Geologic map of the Samail Ophiolite with Sampling Locations 108

23. Aqueous Species Chemistry vs. pH in Samples from the Samail Ophiolite..... 117

24. Analysis of Carbonate Mineral Precipiation in Surface Fluids 120

25. Equilibrium Diagrams for Organic Compound Formation Reactions 128

26. Affinities for Potential Metabolic Reactions..... 139

27. Unconservative Mixing Trends for a Variety of Organic Analytes 142

28. Stable Carbon Isotopes of Dissolved Methane versus pH.....146

CHAPTER 1

INTRODUCTION

As evidence continues to emerge for the presence of organic material and liquid water in a variety of environments throughout the solar system, it seems that aqueous organic chemistry is common place in many planetary settings (e.g., Porco et al., 2006; Matson et al., 2007). According to accretionary heating models (e.g., Robuchon and Nimmo, 2011) and observations of carbonaceous meteorites (e.g., Pizzarello and Shock, 2010), aqueous organic chemistry should have been even more common following solar system formation. Water-rock reactions that are also expected to be common throughout the solar system, such as serpentinization (Holm et al., 2015), can produce conditions sufficient to generate a thermodynamic drive for organic synthesis from inorganic carbon (McCollom and Seewald, 2007; Etiope and Sherwood Lollar, 2013). While geologic settings can host a wide range of temperatures, pressures, and compositions, the effects of geochemically relevant conditions on relative rates of organic reactions and their resulting product distributions are not sufficiently characterized to model planetary environments.

In this study, we aim to characterize the kinetics, mechanisms, and equilibria for a variety of reactions involving oxygen- and nitrogen-bearing organic compounds. Hydrothermal experiments were performed involving model compound amines under acidic-buffered conditions in which two deamination mechanisms were elucidated and their kinetics quantified. These findings have implications for developing models for biomass degradation, and therefore for understanding nitrogen cycling. Similar unbuffered hydrothermal experiments demonstrate the reversibility of certain substitution

reactions between oxygen- and nitrogen-bearing organic compounds, as well as an approach toward metastable equilibrium. This suggests relative abundances of organic compounds involved in similar reactions might record the temperatures, pressures, or compositions of their source environments. Samples from a natural low temperature continental serpentinizing system were also analyzed, and metastable equilibria were evaluated for a variety of inorganic and organic carbon transformations, allowing predictions regarding conditions and active processes at the surface and in the subsurface.

1.1 Deamination Reaction Mechanisms under Acidic Hydrothermal Conditions

The nitrogen cycle on Earth is well characterized in terms of processes that take place at the surface of the Earth (e.g., Galloway et al., 2004; Knicker, 2004), but less so in deeper geologic settings (Berner, 2006; Boudou et al., 2008). However, as a result of biomass burial the amount of organic nitrogen in sediments and crustal rocks has been estimated to be greater than that of the biosphere (Boudou et al., 2008). While our understanding of organic nitrogen transformations at ambient conditions is aided by extensive studies of conventional gas phase and aqueous phase organic chemistry (Clayden et al., 2001) and biochemistry (Nelson et al., 2008), far less attention has been given to characterizing reactions at higher temperatures and pressures, and ranges of compositional conditions (such as pH) relevant to geologic settings.

Based on the structure of cellular material (Fernandez-Reiriz et al., 1989; Simon and Azam, 1989; Delgado et al., 2013), amino acids serve as the main reservoir for nitrogen in biomass, suggesting the reactivity of the amine functional group plays a central role in nitrogen cycling. Although many experimental studies have reported rates of amino acid decomposition under hydrothermal conditions, few have attempted to

describe the kinetics of competing reactions, and fewer still have characterized individual reaction mechanisms. As an example, comparing the well-characterized deamination reaction mechanism for aspartic acid at lower temperatures, ≤ 135°C (Bada and Miller, 1970), to the less-resolved multiple mechanisms for aspartic acid deamination at higher temperatures, 170 – 260°C (Cox and Seward, 2007; Faisal et al., 2007), suggests that deamination mechanisms change with temperature. Understanding mechanistic changes is crucial for extrapolating reaction rates across the temperature, pressure, and pH ranges common to natural, organic-rich, geologic environments.

As a step toward building useful models for amino acid reactivity, this study aims to provide a detailed description of the kinetics and mechanisms for deamination of primary and secondary amine functional groups under acidic hydrothermal conditions. Time series experiments were performed for hydrothermal deamination of model amine compounds based on benzylamine (**BA**) and α-methylbenzylamine (**α-CH_3-BA**), buffered at pH 3.3 at 250°C and 40 bar (P_{sat}). Deamination of the amines under these conditions forms alcohols as the major primary products. The deamination mechanisms were investigated by determining the kinetics of reaction of ring-substituted **BA** and **α-CH_3-BA** derivatives, which provided information on the nature of the charge buildup in the transition state. The results support nearly equal contribution from two substitution mechanisms, specifically S_N1 ($k_{SN1} \approx 2.4 \times 10^{-6}$ s^{-1}) and S_N2 ($k_{SN2} \approx 2.7 \times 10^{-6}$ s^{-1}), for the deamination of **BA** to form benzyl alcohol. In contrast, **α-CH_3-BA** deaminates almost exclusively via a much faster S_N1 mechanism ($k_{\alpha} \approx 7.6 \times 10^{-4}$ s^{-1}). Accordingly, under dilute, acidic hydrothermal conditions primary amines are expected to undergo essentially exclusive deamination followed by hydration to form alcohols. The

observation of two competing mechanisms for **BA** deamination/hydration implies that Arrhenius extrapolation of rate data to other temperatures is currently unreliable, since this is likely to be accompanied by a change in the dominant reaction mechanism. This observation of rapid substitution suggests that in the presence of nucleophiles that are stronger than water, amines can also react to generate other metastable organics, possibly producing larger compounds with heteroatoms.

1.2 Metastable Equilibrium Among Oxygen- and Nitrogen-Bearing Organic Compounds in Hydrothermal Experiments

Organic compounds are produced in geologic systems that are otherwise difficult to access (e.g., subterranean and extraterrestrial); if they are mobilized and released, they have the potential to bear signatures of their environments (Cruse and Seewald, 2006; Tassi et al., 2007). However, little is known about how relative abundances of many organic compounds are controlled by geochemical source conditions. One form of progress in this area is identifying organic reactions that are known to reach metastable equilibrium (Seewald, 1994; Seewald et al., 2006). This is because concentration ratios of compounds at equilibrium can be combined with thermodynamic calculations to assess temperature, pressure, and composition for unexplored environments. This type of analysis may even hold for ancient environments if ratios are preserved over time, as may be the case in carbonaceous meteorites (Pizzarello and Shock, 2010). Hydrothermal conditions promote rapid, reversible reactions between organic compounds, sometimes resulting in steady state ratios due to an approach toward metastable equilibrium (e.g., Shipp et al., 2014). Nitrogen-bearing organic compounds are typically abundant in natural systems, and their reactivity is particularly sensitive to pH conditions (e.g.,

Garrett and Tsau, 1972; Smith and Hansen, 1998), potentially allowing them to serve as tracers of acidity. However, there are few examples of reactions involving organic nitrogen compounds approaching metastable equilibrium under hydrothermal conditions.

The aim of this study is to characterize reversible and irreversible reactions between hydrothermally-treated alcohols, primary amines, secondary amines, tertiary amines, and their products. Four sets of aqueous experiments were performed with model organic compounds at 250°C and 40 bar (liquid/vapor saturation pressure of water, P_{sat}). The initial reactants for each set of experiments were benzyl alcohol, benzylamine, dibenzylamine, and tribenzylamine. In each case, the reactant solutions were prepared with the same bulk composition according to the amount of organic reactant added and the addition of varying amounts of ammonium hydroxide and ammonium chloride. After 2 hours of heating, all four of the initial reactants could be observed in each of the experiments, indicating rapid reversibility of amination/deamination substitution reactions. After 72 hours, reaction quotients for substitution reactions between the model compounds converged for each of the four sets of experiments, strongly suggesting an approach toward metastable equilibrium. The empirical reaction ratios are in good agreement with calculated equilibrium constants for the amination reactions. Similar, but even faster, convergences of compound ratios were observed for ether and imine formation reactions, providing evidence of metastable equilibrium for other ionic reaction mechanisms. Some compounds were identified whose ratios did not converge among the four experiments, including those from redox-sensitive reactions and electrophilic aromatic substitution reactions; thereforee, these products were distinguished as being linked to irreversible reactions.

These findings identify classes of organic compounds and reactions to target for environmental analysis that may reflect the conditions at which they last equilibrated. They also demonstrate experimental techniques that can be used to characterize reversible and irreversible reactions under hydrothermal conditions. The agreement between experimental results and independent thermodynamic calculations validates the methods and interpretations used for each.

1.3 A Thermodyanmic Assessment of Carbon Chemistry during Low Temperature Continental Serpentinization

Active serpentinizing environments have been investigated across a range of aqueous geochemical conditions, from near-critical submarine systems (e.g., Charlou et al., 2002) to near-ambient surface settings (e.g., Szponar et al., 2013), and various combinations of temperatures and pressures in between (e.g., Kelley et al., 2001). At this range of conditions, serpentinization generates high pH fluids bearing molecular hydrogen (Moody, 1976), which typically causes carbonate mineral precipitation and produces a thermodynamic drive for the chemical reduction of inorganic carbon to organic carbon, respectively (Kelemen et al., 2011). Observations of abundant methane and other small organic compounds support the notion that inorganic carbon reduction occurs (McCollom and Seewald, 2007; Etiope and Sherwood Lollar, 2013). Whether this occurs abiotically or biologically has implications for serpentinization's role in generating habitable conditions in both modern and prebiotic environments (Russell et al., 2010; Holm et al., 2015).

However, it still remains unclear what portion of these organic compounds are being actively added to solution from the abiotic reduction of inorganic carbon during

serpentinization, versus a variety of other processes (Etiope and Sherwood Lollar, 2013; McCollom, 2013b). These processes include the release of ancient organics from mineral inclusions that formed during crystallization and cooling of high-temperature ultramafic, as well as the thermogenic breakdown of dead biomass. Since these processes can also produce observable methane and other small organic compounds, disentangling the contribution from each process requires analytical strategies beyond simply quantifying compound concentrations. Sufficiently low temperature systems also have the potential to actively produce small organic compounds via microbial metabolisms, such as methanogenesis, which further challenges interpretations of abiotic methane formation mechanisms (Shrenk et al., 2013). Numerous strategies are in place for attempting to directly determine which source processes are producing which organic compounds, such as probing isotopic ratios that bear signatures of specific abiotic, thermogenic, or biological reactions (Etiope and Sherwood Lollar, 2013).

In this study, we borrow from these existing strategies and provide an additional technique for identifying source processes that employs thermodynamic calculations to infer where organic formation reactions take place in a low temperature serpentinizing system, at the Samail Ophiolite in the Sultanate of Oman. To perform this analysis, we collected water samples from shallow groundwater (Type I fluids), representative of input fluids to serpentinization, hyper-alkaline seeps (Type II fluids), representative of output fluids from serpentinization, and surface fluid mixing zones. We determined aqueous concentrations of molecular hydrogen, dissolved inorganic carbon (DIC), formate, acetate, methane and its stable carbon isotopic ratios, and a suite of other geochemical solutes.

These analyses indicate that the vast majority of DIC in Type I fluids that happens to undergo serpentinization precipitates in the subsurface as carbonate minerals; however, it seems that a significant amount of DIC is also converted into methane, formate, and acetate, and expelled at the surface in Type II fluids. Based on thermodynamic calculations, we generate a series of plausible hypotheses regarding the conditions under which each of these organic compounds last equilibrated, and in some cases how they have been perturbed away from equilibrium. Though we outline multiple possibilities, it seems most likely that acetate is actively forming in Type I and Type II fluids at the surface, as it has reached metastable equilibrium with measured abundances of H_2(aq) and DIC, the latter of which is buffered by carbonate minerals. Methane abundances in both fluid types are low relative to equilibrium with respect to DIC and H_2(aq), probably indicating that methane oxidation is actively occurring at the surface. Howeverm it may be the case that methane is formed in a carbon-limited zone in the deep subsurface. Formate is generally below detection in Type I fluids, but has high abundances relative to equilibrium in Type II fluids. This latter observation suggests that formate is either formed in the shallow subsurface, where DIC is still buffered by carbonate minerals but H_2(aq) is more abundant, or that formate is formed as a result of methane oxidation. Methane oxidation to carbon dioxide or formate is thermodynamically favorable, and evidence for this type of microbial metabolism is observed in the stable carbon isotopes of methane in fluid mixing zones, where the environment for redox chemistry is ideal. However, isotopic values in Type II fluids cannot rule out methane as biologically sourced from a carbon-limited zone in the deep subsurface.

In summary, the geochemical observations in this work support previous models of carbon flow through the Samail Ophiolite. Thermodynamic calculations present new evidence characterizing regions of the system within which organic formation reactions are occurring. Stable isotope trends in mixing fluids test and do not refute plausible hypotheses for microbial metabolisms, providing strong evidence for active microbial oxidation in surface fluids. Together, these techniques help to constrain conditions and identify potential active processes in surface and subsurface fluids that lead to carbon transformations during low temperature serpentinization.

CHAPTER 2

DEAMINATION REACTION MECHANISMS UNDER ACIDIC HYRDROTHERMAL CONDITIONS

2.1 Introduction

The large part of abiotic organic chemistry in nature takes place in the presence of water, with the most rapid and diverse reactions likely occurring in hydrothermal fluids. A wide range of organic compounds have been found in analyses of terrestrial hydrothermal systems (e.g., Leif and Simoneit, 1995; Proskurowski et al., 2008; Lang et al., 2010; Shock et al., 2013), as well as in carbonaceous meteorites and asteroids, which appear to have experienced heating in the presence of water (e.g., Cronin et al., 1988, Verdier-Paoletti et al., 2017). Experiments and thermodynamic models have demonstrated the potential for abiotic organic synthesis and increasing organic complexity under hydrothermal conditions (e.g., McCollom and Seewald, 2007; Shock et al., 2013). Models of heat generation during and after planetesimal formation suggest hydrothermal reaction conditions capable of driving organic reactions have existed throughout the solar system (e.g., Robuchon and Nimmo, 2011), and there is a growing body of evidence that there is *much more liquid water* in the rest of the solar system than there is on Earth alone (e.g., Encrenaz, 2008). There are, however, several challenges to the development of useful and predictive models of hydrothermal organic reactivity. Among these are that much of the work on hydrothermal organic chemistry to date has focused on determining reaction products; detailed mechanistic studies are rare. Another is that much of the traditional work on the mechanisms of organic reactions has tended to

focus on reactions in nonpolar solvents, at near-ambient conditions, often with rare metal catalysts or unstable synthetic reagents (Clayden et al., 2001).

Several of the more interesting features of hydrothermal organic chemistry arise from the behavior of liquid water at high temperatures. Specifically, the pK_a of H_2O at 250°C (at liquid/vapor saturation pressure, P_{sat}) is ~11; this results in a neutral pH of 5.5 and a pOH of 5.5 (Sweeton et al., 1974), and influences the equilibrium speciation of dissolved species and the kinetics of any reactions involving protons or hydroxide. Under these same hydrothermal conditions, the dielectric constant of H_2O lies between that of methanol and acetone under ambient conditions (25°C, 1 bar), mainly as a result of a decrease in hydrogen bonding at higher temperatures (Uematsu and Franck, 1980). Consequently, the solubility of organic compounds in water increases dramatically with increasing temperature, which means that hydrothermal fluids represent an excellent medium for organic chemical reactions. For example, the solubility constant (K_{sol}) for toluene in water is ~$10^{-2.2}$ at 25°C, but increases to ~$10^{-0.5}$ at 250°C; this translates roughly to a saturation change from ~0.006 to ~0.3 molal toluene (Anderson and Prausnitz, 1986; Brown et al., 2000). In addition to being a good solvent, hydrothermal water can act as a catalyst and a reagent in many reactions (e.g., Shipp et al., 2013; 2014).

With increasing temperature, the rates of organic reactions increase and the reactions are increasingly controlled by entropic rather than enthalpic effects. Consequently, reactions that are unlikely at ambient become possible at high temperatures. This results in hydrothermal organic product distributions that are often difficult to predict and explain based on corresponding reactions at ambient (Katritzsky et al., 2001; Rushdi and Simoneit, 2002; Yang et al., 2012), especially in the absence of

reliable mechanistic information. For example, hydration, hydrogenation, and carbon-carbon sigma bond breaking reactions have been found to occur via substitution, addition, and radical formation mechanisms (Glein, 2012; Yang et al., 2012; 2014; Shipp et al., 2013; 2014; Fecteau, 2016) for which there are no equivalent reactions at ambient. Reactions are often reversible under hydrothermal conditions, and metastable equilibrium may be achieved in certain cases (e.g., Seewald, 1994).

Understanding reaction mechanisms is necessary in order to build models for natural systems. For example, observed rates of compound degradation or formation may be determined by contributions from multiple mechanisms, that could even lead to the same products (see below) but have, for example, very different temperature dependencies. Also, the kinetics of different mechanisms may respond differently to other environmental parameters, such as pH or reactant concentration, the latter for example if the rate determining step for a mechanism is unimolecular or bimolecular. Quantitative descriptions of reactions in terms of rate order, rate constants, and how environment and temperature influence these quantitative descriptors should advance predictive models that may allow the relative rates of competing mechanisms to be extrapolated across a wide range of geochemical conditions and geochemically-relevant timescales. Our group has been building mechanistic and kinetic descriptions of organic hydrothermal reactions for organic structures containing C, H, and O (Glein, 2012; Yang et al., 2012; 2014; Shipp et al., 2013; 2014). Here we extend this work to a detailed mechanistic and kinetic description of nitrogen containing organic structures.

Characterizing the reactivity of organic nitrogen compounds under various geochemical conditions is crucial to develop models of the Earth's modern and ancient

global nitrogen cycles (Berner, 2006; Boudou et al., 2008), the habitability of planetary systems (Shock and Canovas, 2010; McCollum and Seewald, 2007), and perhaps even the emergence of life (Schoonen and Xu, 2001; Brandes et al., 2008; Martin and Russell, 2007). The major transformations of nitrogen compounds that can occur at ambient conditions have been extensively studied in conventional gas phase and aqueous phase organic chemistry studies (Clayden et al., 2001), and because of the importance of nitrogen containing structures in biochemistry, particular focus has been given to research aimed at characterizing the nitrogen cycle at the surface of the Earth (e.g., Galloway et al., 2004; Knicker, 2004). The broader topic of geological nitrogen cycling, which scales vast temperatures, pressures, and compositional changes, has received far less attention, particularly from a mechanistic organic perspective.

Proteins and nucleic acids serve as the main reservoirs of organic nitrogen common to all living organisms, with the former dwarfing the latter in terms of percent composition of N in cellular mass (Fernandez-Reiriz et al., 1989; Simon and Azam, 1989; Delgado et al., 2013). The quantity of organic nitrogen in sediments and crustal rocks is estimated to be significantly larger than that in the biosphere, mainly due to burial of biomass (Boudou et al., 2008). Buried material in ocean sediments eventually undergoes subduction, and exposure to increasing temperatures and pressures. A major initial reaction for proteins in water is hydrolysis to amino acids, especially at elevated temperatures (Kang and Chun, 2004; Rogalinski et al., 2005), suggesting that the reactions of amino acids, such as deamination, play a key role in governing geological nitrogen cycling. Indeed, high abundances of ammonium have been measured in both marine (e.g., Von Damm et al., 1985) and continental (e.g., Holloway et al., 2011)

sediment-hosted hydrothermal systems, implying significant nitrogen loss during hydrothermal processing of biomass. Similarly, amino acids and other primary amines may even be the dominant reservoirs for organic nitrogen in strictly abiotic systems, as suggested by analyses of soluble organic compounds in meteorites (e.g., Pizzarello and Shock, 2010). Meteoritic compounds potentially provide insight into the organic inventory of early planetary systems in the solar system. Thereforee, understanding the reactions of these compounds under conditions analogous to accretionary heating could provide insight into planetary habitability. Perhaps similar to sediment-hosted terrestrial systems, insoluble carbonaceous meteoritic materials have been shown to release ammonium when subjected to hydrothermal conditions at 300°C (Pizzarello et al., 2011). This suggests that the nitrogen-containing material had not previously been subjected to water under these conditions for a sufficient length of time to liberate nitrogen. Given that little is known about the variables governing these reactions, experimental investigations into the mechanisms of deamination of amines with respect to temperature and composition could help to put limits on ancient conditions and their evolution over geologic timescales.

Several studies of hydrothermal reactions of organic nitrogen compounds have been reported (e.g., Abraham and Klein, 1985; Katritzky et al., 1990; Benjamin and Savage, 2004), including those involving amino acids (e.g., Imai et al., 1999; Cleaves et al., 2009; Fuchida et al., 2014). Reactions of organic nitrogen can be sensitive to pH due to the basicity of amines and imines. Garrett and Tsau (1972) explored the pH-dependence (0.15 to 9.50) of solvolysis of cytosine and cytidine at lower temperatures (< 90°C), demonstrating both acid and base catalysis for this reaction. Smith and Hansen

(1998) also demonstrated both acid and base catalysis for peptide bond hydrolysis at low temperature (37°C) over a wide range of pH values (0 to 14). Bada and Miller (1970) studied the deamination of aspartic acid up to 135°C, also over a wide range of pH (1 to 13). This reaction was found to be subject to base catalysis only and inhibited at low pH , though there is some evidence that the reaction vessel material may have affected the reaction (Cox and Seward, 2007).

More recently, Faisal et al. (2007) found almost no effect of pH on the kinetics for aspartic acid deamination at higher temperatures (200 – 260°C); however, products due to reactions other than deamination complicated the mechanistic analysis. A detailed kinetic study by Cox and Seward (2007) under hydrothermal conditions (>170°C) found that aspartic acid decomposed by up to six different competing reactions, two of which were deaminations. Although these studies provide very useful information, the observations of multiple mechanisms and changes in mechanism with temperature suggest that Arrhenius rate extrapolations for organic reactions (e.g., Bada and McDonald, 1995; Radzicka and Wolfenden, 1996) be performed with caution, since reaction mechanisms may change with temperature.

While such studies have provided important information about possible reaction pathways involved in organic nitrogen degradation (e.g., Aubrey et al., 2009), preservation (e.g., Lee et al., 2014), and even synthesis (e.g., Marshall, 1994), few specific mechanisms for the hydrothermal reactions of amines have been reported. To some extent this is because mechanistic analysis is complicated when there are numerous competing reactions. In the case of amino acids, for example, potential reactions include deamination, decarboxylation, decarbonylation, and cyclization, among others (Imai et

al., 1999; Lemke, 2003; Lemke et al., 2009; Aubrey et al., 2009; Cleaves et al., 2009; Abdelmoez et al., 2010; Otake et al., 2011; McCollom, 2013a; Fuchida et al., 2014). It follows that making progress on mechanistic characterization will be facilitated by implementing strategies that can isolate specific reactions for analysis.

One way to simplify the problem of competing reactions is to minimize their number by using model compounds that are designed to probe specific reactions (e.g., Yang et al., 2012; Fecteau, 2016). Thus, reactions of individual functional groups in multi-functional group compounds can be targeted for study. Well-designed model compounds allow the effects of structural and electronic modifications near a functional group of interest to be studied and can provide valuable insight into reaction mechanisms. These techniques have been extensively exploited in conventional organic chemistry at ambient conditions, and were successfully used in an investigation of hydrothermal decarboxylation (Glein, 2012).

One important way to restrict the number of reactions available to amines is to isolate the unprotonated and protonated (aminium) forms, which are likely to undergo different reactions. Aqueous amines speciate according to Eq. (1),

$$\text{R-NH}_2 + \text{H}_2\text{O} \rightleftharpoons \text{R-NH}_3^+ + {}^-\text{OH} \qquad (1),$$

where R represents a generic organic functional group. Therefore, controlling experimental pH relative to the aminium pK_a under hydrothermal conditions is an important requirement for studying amine reaction mechanisms. Isolating individual

reaction mechanisms by controlling protonation state was successfully used in previous studies on the decarboxylation of carboxylic acids (Glein, 2012).

In the present study, high temperature phosphate buffers were used to control pH and isolate the reactions of protonated aminiums ($R\text{-}NH_3^+$). Few hydrothermal organic experimental studies attempt to control and characterize pH at high temperatures (≥ 150°C); those that do typically estimate the unbuffered solution pH (e.g., Lee et al., 2014) or buffer pH using mineral assemblages (e.g., Seewald, 2001). A feature of the present work is that aqueous buffers are used to control pH and maintain the amines in their protonated forms. Mineral buffers were specifically avoided to prevent any surface catalytic and/or reactive effects with organic compounds (McCollom, 2013b; Shipp et al., 2014) that would complicate mechanistic analysis. Although intermediate to low pH environments where amines are likely to be protonated are relevant to some basaltic and granitic hydrothermal systems (Henley et al., 1984), the main purpose of isolating reactions to the protonated forms is to simplify the experimental system in order to facilitate a step-wise mechanistic understanding of amine reactions. Specifically, at higher pH unprotonated amines hydrothermally decompose via multiple competing reactions that would require several experimental approaches in parallel to deconvolute the reaction mechanisms (Katritzky et al., 1990; 2001; Table A3).

Herein, the model organic compounds benzylamine (**BA**, Fig. 1) and α-methylbenzylamine (**α-CH_3-BA**, Fig. 1) were used in a complementary manner to investigate the hydrothermal deamination reaction mechanisms of primary (1°) and secondary (2°) α-carbon bonded aminiums. Subcritical hydrothermal experimental studies have previously been performed with benzylamine (Katritzky et al., 1990; 2001),

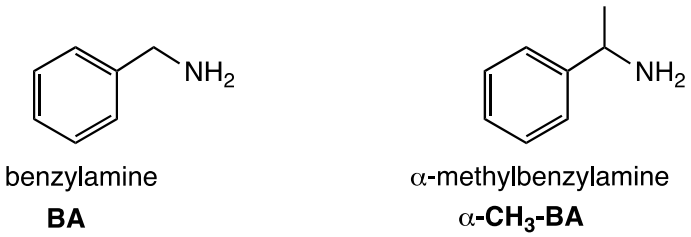

Fig. 1. Structures and abbreviations for the amines studied in this work. The α-methylbenzylamine **α-CH$_3$-BA** used was the single (S) enantiomer, see experimental.

similar benzyl carbon bonded amines (Abraham and Klein, 1985; Torry et al., 1992), and some other related amines (Katritzky, 1990; 2001). However, few mechanistic studies have been performed on amines while controlling pH at high temperatures. Unbuffered experimental studies have provided mechanistic insight at subcritical temperatures (≤ 340°C) for reactions with organic nitrogen, but not for deamination (Belsky and Brill, 1999; Li and Brill, 2003). Other researchers have characterized hydrolysis mechanisms in unbuffered, supercritical solution (Klein et al., 1990; Benjamin and Savage, 2004), the latter involving methylamine deamination. However, characterization of methylamine reactivity (Klein et al., 1990) is unlikely to be widely applicable to the behavior of other amines at subcritical temperatures, due to the unique behavior of supercritical water (Savage, 1999). Additionally, methylamine may not be a representative amine since it cannot deaminate via elimination to form an alkene, as does for example aspartic acid (Bada et al., 1970); nor is methylamine likely to form a formally charged intermediate due to the lack of neighboring functional groups that could provide charge stabilization (Schwarz, 2011).

Comparing the deamination rates of the primary amine **BA** and the secondary amine **α-CH$_3$-BA** not only provides insight into the mechanisms of their reactions, but also potentially provides useful insight into the chemistry of environmentally relevant amines. Many natural amines are bonded to differently substituted carbons, e.g., amino acids and various lipid structures (Sohlenkamp and Geiger, 2015). Aromatic model compounds were chosen for three reasons: 1) the aromatic ring is relatively inert and allows the reactivity of the aminium functional group to be studied in the absence of competing primary reactions, 2) classical, physical organic chemistry mechanistic probes

can be employed; specifically, ring-substituted derivatives can be used to probe charge generation in the rate determining steps (e.g., Brown and Okamoto, 1958), and 3) the majority of reaction products are readily extracted at the end of the experiments and their quantities can be accurately quantified using gas chromatography-flame ionization detection (GC-FID) methods (e.g., Yang et al., 2012). At 250°C, pH 3.3, and 40 bar (P_{sat}), deamination followed by hydration to form the corresponding alcohol was found to be the dominant primary reaction for the amines in the present study. The mechanisms were probed using ring-substituted benzylamines and α-methylbenzylamines with electron withdrawing and donating groups and concentration-dependent kinetic studies. These observations suggest the presence of two competing deamination mechanisms for benzylamine (i.e., S_N1 and S_N2), and a single deamination mechanism for α-methylbenzylamine (S_N1); these results have implications for extrapolating deamination rates across temperature.

2.2 Experimental

2.2.1 Materials

Reagents, buffers, standard compounds, and gases were purchased from Sigma-Aldrich (S-A), Alfa Aesar (AA), Oakwood Chemical (OC) Matrix Scientific (MS), Mallinckrodt (M), Synquest Laboratories (SL), Aldlab Chemicals (AC), Glycopep Chemicals (G.C.), and Praxair (PA) with the following specifications for purchased organic compounds: ≥ 99.5% benzylamine (S-A), > 98% 3-chlorobenzylamine (S-A), ≥ 98% 3-trifluromethylbenzylamine (S-A), ≥ 97% 3,5-Bis(trifluoromethyl)benzylamine (MS), ≥ 98% 3-methylbenzylamine(AA), ≥ 97% 3,5-dimethylbenzylamine, ≥ 97% 4-methylbenzylamine (S-A), 3-methoxybenzylamine (SL), ≥ 98% 4-methoxybenzylamine

(S-A), ≥ 98% 3-fluorobenzylamine (SL), ≥ 97% (S)-1-[3-(trifluoromethyl)phenyl]-ethylamine (SL), ≥ 97% (R)-1-[3,5-bis(trifluoromethyl)phenyl]-ethylamine (SL), ≥ 98% S-(-)-α-methylbenzylamine (S-A), ≥ 97% R-(+)-α-methylbenzyl alcohol (S-A), ≥ 97.0% dibenzylamine (S-A), ≥ 99.0% tribenzylamine (S-A), ≥ 99.8% benzyl alcohol (S-A), ≥ 99.0% *n*-benzylidenebenzylamine (S-A), ≥ 99.9% toluene (S-A), ≥ 95% 3-benzylbenzyl alcohol (AC), ≥ 95% 2-benzylbenzyl alcohol (AC), ≥ 98% (4-benzylphenyl)methanol (G.C.), ≥ 99% methanesulfonic acid (Acros Organics), ≥ 99.0% dodecane (S-A), ≥ 99.9%. Inorganic compounds included: ≥ 85.0% phosphoric acid (S-A Fluka Analytical), ≥ 99.9% monosodium (dihydrogen) phosphate (M), sodium bicarbonate (M), a mixed ion standard (Thermo Scientific, Waltham, MA, USA), and a mixed cation standard (Environmental Express, Charleston, SC, USA).

2.2.2 Analytical Procedures

Organic compounds were analyzed to confirm purity using a Varian CP-3800 Gas Chromatograph (GC) and a Bruker Scion 456 Gas Chromatograph (GC), both equipped with Varian CP-8400 auto-samplers, Supelco Equity^{TM}-5 columns (30m x 0.25mm x 0.5μm capillary fused silica), and flame ionization detectors (FIDs). For oven methods, peak assignment, and peak integration, Varian Star Chromatography: Integration Work Station software and Compass Chromatography Data System Version 3.0 Core Software were used by the GCs described above, respectively. Response factors for each compound relative to a fixed concentration (0.01 M) of the internal standard, dodecane, were calculated from three-point (for the ring substituted benzylamines) or five point (for all other compounds) linear calibration curves with $R^2 \geq 0.995$. Dichloromethane (DCM) was used as the solvent for all GC analyses. The GC method used an ultra-high purity (≥

99.999%) helium:sample split ratio of 15:1 for all calibration standards and experiments. The oven temperature profile method is summarized in Table A1; longer methods (≥ 60 min) were periodically conducted to look for products at longer retention times. A subset of experiments was also analyzed using a chiral column (Agilent J&W CP-Chirasil-Dex CB) with the same oven heating method.

Each compound of interest was verified by standard compound addition. A JEOL GCmate gas chromatograph/mass spectrometer (GC-MS, an Agilent 6890/5973 with the same Supelco Equity^{TM}-5 column as above) was also used to identify compounds based on their molecular ion fragments.

Yields of total ammonia (NH_3 + NH_4^+) were quantified via ion chromatography using suppressed conductivity detection. An aliquot (50 μL) of the aqueous phase of replicate experiments (quantitative GC and IC analyses could not be performed on the same sample) was diluted with deionized (DI) water (18.2 MΩ-cm from a Barnsted Nanopure DIamond purifier) to 5 mL, and injected in duplicate (2.5 mL) onto a Dionex DX-600 ion chromatography system via an AS-40 autosampler. The system was equipped with a 75 μL sample loop, CG-16 and CS-16 cation exchange columns, and a CERS500 electrolytically-regenerated suppressor and operated with Chromeleon software (version 6.8). The suppressor was regenerated via an external source of DI water to improve the signal-to-noise ratio of the analysis. Ammonium and other cations were eluted isocratically with 19 mM methanesulfonic acid at 0.5 mL/minute. Calibration was completed externally using a serial dilution of a commercially available mixed cation standard (Environmental Express, Charleston, SC, USA) that were fit with a second-order polynomial through the origin between 0.005 and 25 mg/L ammonium. Quantification

accuracy was verified by analysis of an independent mixed ion standard (Thermo Scientific, Waltham, MA, USA).

2.2.3 Experimental Procedures

Reaction solutions were prepared with DI water. Phosphoric acid and sodium phosphate buffers were used at double the concentration of the initial reactants to control solution pH under hydrothermal conditions. The correct proportions of the buffer species to achieve desired pH at high temperatures and pressures (3.3 at 250 °C and 40 bar) were calculated using the revised HKF equations of state from Tanger and Helgeson (1988), Shock et al. (1992), and the revised HKF parameters for $H_3PO_{4(aq)}$, $H_2PO_4^-$, HPO_4^{2-} PO_4^{3-}, and similar pyrophosphate species, that occur in significant abundance at high temperatures, from Shock et al. (1989; 1997) via the SUPCRT92 software package from Johnson et al. (1992) and the thermodynamic properties from Wagman et al. (1982) and Kelley (1960) and EQ36 (Wolery, 1992). These calculations revealed the required phosphate acid:salt ratios to reach the desired pH at high temperature, as well as the appropriate low-temperature pH (2.2 at 25 °C) at which reactant solutions should be prepared, which was verified with a Thermo Orion SB20 pH meter.

These solutions were bubbled in 7 mL Supelco clear glass vials with ultra-high purity, ≥ 99.999%, argon (PA) for ≥ 20 minutes before being loaded into silica tubes sealed at one end (eventual reaction vessels). Silica tubes were purchased from GM Associates and Technical Glass Products as 2 x 6 mm (inner diameter x outer diameter) “fused quartz” (silica) tubing. This material was used as the reaction container because previous studies showed that stainless steel and other container-materials can catalyze organic reactions (e.g., Kharaka et al., 1993; Bell et al., 1994). A welding torch (≥

99.95% H_2 (PA) and ≥ 99.5% O_2 (PA)) was used to seal the tube ends to produce closed reaction vessels. Upon loading the solution, the tubes were immediately immersed in liquid nitrogen to freeze the reactant solution, the tube headspace was briefly purged with argon, and the headspace was vacuum pumped to ≤ 100.0 millitorr to remove remaining atmospheric gases. Still submerged in liquid nitrogen above the height of the frozen reactants and under vacuum, the open ends of the tubes were sealed with the torch. Sealed reaction vessels were kept frozen and in the dark prior to conducting high-temperature experiments. Several frozen reaction vessels were thawed and analyzed without high-temperature exposure to confirm that no alteration to the initial reagent had occurred during storage.

For most experiments, a Varian GC oven (similar to the model mentioned above) was preheated with screw-capped iron pipes (to provide thermal inertia) to 250°C for ≥ 2 hours. As verified by two Fluke 52 II thermocouples, the air temperature within the preheated iron pipes varied spatially and temporally by no more than ± 2.5°C. Reaction vessels were placed inside the preheated iron pipes, and the temperature within the pipes was observed to stabilize after 30-60 minutes. Due to the temperature stabilization time of the vessels within the oven, rate constants for experimental reaction kinetics were calculated only from kinetic time series of experiments with ≥ 2 hours of heating time; the starting time, t = 0, for most reactions was considered to be 120 or 240 minutes of heating (t_{heat}, Table A2). For faster reactions, namely those involving S-(-)-α-methylbenzylamine, R-(+)-α-methylbenzyl alcohol, 4-methoxybenzylamine, and 3-methyl-α-methylbenzylamine, a brass block heating apparatus with cartridge heaters and an internal thermocouple was used to provide more contact and thus faster heating times

(as in Yang et al., 2014). The reaction vessels in the block heater had an observed temperature stabilization time of 5 minutes; therefore, rate constants derived from heating block experiments were calculated from kinetic time series of experiments with $t_{heat} \geq 5$ minutes of heating time.

At the end of each experiment, the reaction vessels were quickly removed from their heating source and submerged in room temperature water to rapidly quench the reactions and preserve the products. The time at which the reaction vessels were removed from the oven was considered the final experimental time (normalized for time of heating). After quenching the reactions in water, the reaction vessels were frozen and left in the dark until they were extracted and analyzed. Several duplicate experiments were immediately analyzed without the freezing step to verify that no significant changes in product distribution occurred during the freezing or storage processes.

Prior to extracting organic reaction products, the solutions were transferred to 7 mL Supelco clear glass vials with polytetrafluoroethylene/silicone septa lids. Then the solutions were brought to a pH of ~12 using 0.085 M potassium hydroxide (KOH in DI) saturated with dibasic sodium carbonate (Na_2CO_3; the solution bubbled if sample pH was insufficiently raised by the KOH, prompting further pH adjustment). This step was taken to deprotonate the amine functional groups and ensure they would partition into the DCM during liquid/liquid extraction. Dichloromethane, containing 0.01 M dodecane as an internal standard, was added to the solution in a 10:1 ratio for the liquid/liquid extraction procedure. This mixture was intermittently gently shaken for ≥ 15 minutes and the organic layer was separated and immediately taken for GC or GC-MS analysis.

In order to ensure reaction of only the protonated forms of benzylamine and α-methylbenzylamine, all experiments were buffered at pH 3.3. At this pH, the amines are more than 98% in the protonated forms if their pK_a values at 250°C are ~5 or greater. The pK_a values of several amines have been measured as a function of temperature; they decrease with increasing temperature, as shown in Fig. 2. The pK_a values of these amines are all 8.5 – 10.7 at 25°C, and all decrease to around 5 – 6 at 250°C, specifically, ammonium (pK_a = 5.2, Read, 1982), cyclohexaminium (pK_a = 6.0, Mesmer and Hitch, 1997), morpholinium (pK_a = 5.2, Ridley et al., 2000), dimethylaminium (pK_a = 6.1, Bénézeth et al., 2001), and ethanolaminium (pK_a = 5.5, Bénézeth et al., 2003). Benzylaminium, α-methylbenzylaminium, and ammonium have similar pK_a values at 25°C (9.4, 9.9, and 9.2, respectively; Richner, 2013; Gluck and Cleveland Jr., 1994; and Read, 1982, respectively). Although the pK_a values of benzylamine and α-methylbenzylamine have not been measured at high temperature, we expect they will follow the same general trend exhibited by the other amines, and their pK_a values should be in the range 5 – 6 at 250°C. Within this pK_a range, the amines should be almost completely protonated at pH 3.3 (Fig. 2). The ring substituted benzylamines included in the present study have pK_a values ranging from 8.6 to 9.6 (Blackwell et al., 1964) at 25°C (Fig. A1), and thus their unprotonated forms should exist only in very low abundance under experimental conditions.

Two separate time series experiments were performed with benzylamine at concentrations of 0.05 and 0.15 molal and phosphate buffer concentrations of 0.1 and 0.3 molal, respectively. The two concentrations allowed us to to determine the effect of reactant and buffer concentrations on reaction kinetics and provided a test for the

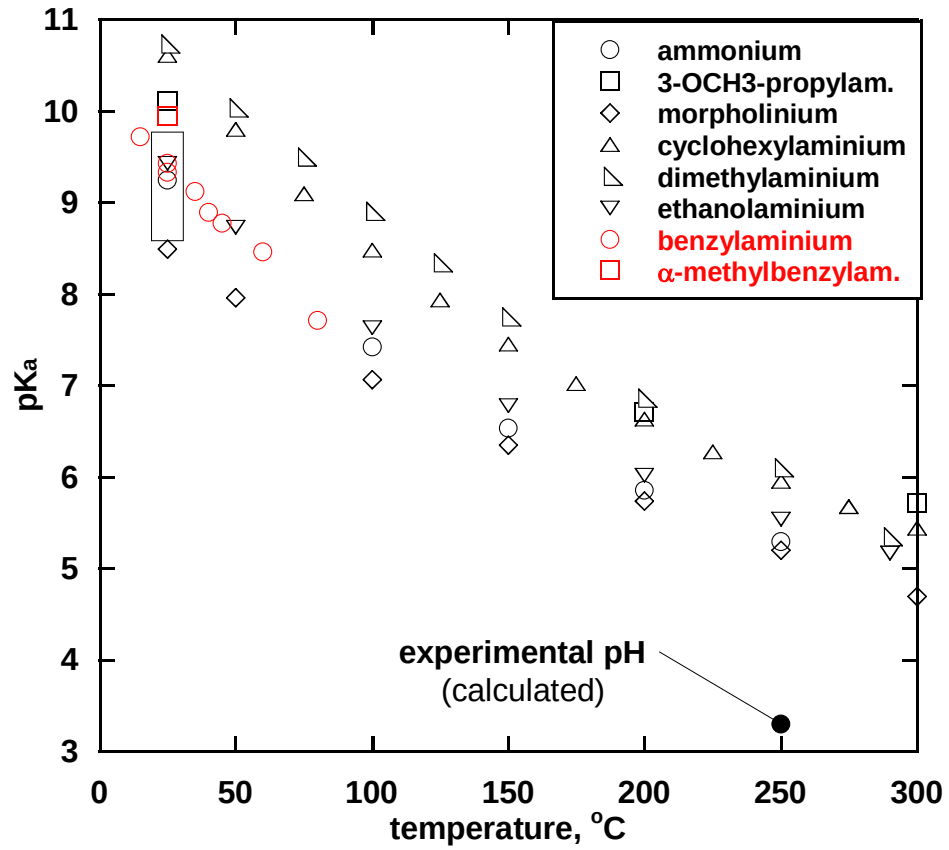

Fig. 2. Calculated experimental pH (single filled circle) and empirically-derived literature pK_a values (open symbols) vs. temperature for ammonium (Read, 1982) and a variety of protonated amines: 3-methoxypropylaminium (Rhee et al., 2010), morpholinium (Ridley et al., 2000), cyclohexylaminium (Mesmer and Hitch, 1977), dimethylaminium (Bénézeth et al., 2001; Bergström and Olofsson, 1977), ethanolaminium (Bénézeth et al., 2003), benzylaminium (Bunting and Stefanidis, 1990; Hanai et al., 1997; Richner, 2013), and α-methylbenzylaminum (Gluck and Cleveland, 1994). The calculations for experimental pH were performed using the program EQ36 (Wolery, 1992), SUPCRT92 (Johnson et al., 1992), and empirical data and estimated thermodynamic properties therein (Tanger and Helgeson, 1988; Shock et al., 1992; Wagman et al., 1982; Kelley, 1960; Shock et al., 1989; 1997). The box illustrates the range of empirically measured (Blackwell et al., 1964) and predicted pK_a values at 25°C for the ring-substituted benzylamine derivatives used in this study (Fig. A1). The experimental, phosphate-buffered pH was calculated using the thermodynamic properties of ammonia and ammonium as a proxy for benzylamine and its derivatives, since there are no published pK_a data for benzylamine above 80°C.

presence of 2nd order decomposition kinetics. Additionally, previous super- and near-critical hydrothermal experiments have demonstrated enhanced rates for the hydrolysis of benzyl-carbon-bonded amines with increasing ionic strength (Torry et al., 1992), so the two concentrations allowed an evalulation of this effect. Experiments with even higher concentrations of benzylamine and phosphate buffer were attempted, but abandoned due to problems with precipitation of solids upon reactant solution preparation, which complicated the experimental setup and cast doubt as to the reactant solubility at high temperature.

2.2.4 Kinetic Modeling

Kinetic models were developed to test whether a pseudo-first-order rate analysis would provide sufficiently accurate deamination reaction rates constants for the various benzylamines to yield insight into deamination reaction mechanisms. Kinetic modeling using simple 1st-order decay functions and consecutive 1st-order models was performed by fitting experimental data in KaleidaGraph software (version 4.1.0). More complex kinetic models utilized the COPASI program (version 4.20); all COPASI rate constants in this study were solved using the "Levenberg-Marquardt" method. Identical products formed by multiple different irreversible reactions were tracked in some models according to which reaction formed them by running a "time course" method. Additional details regarding the kinetic models employed are provided in Sections 2.3.2 and 2.3.3 below.

2.3 Results and Discussion

2.3.1 Benzylaminium (BA) reaction paths

Reaction of benzylamine (**BA**) at 250°C, 40 bar, and pH 3.3 for 20 hours results in 33% conversion to benzyl alcohol and ammonium (NH_4^+), which are each formed in near stoichiometric equivalence to **BA** loss during this reaction time (Table A2 and A3). This suggests that substitution of the amine by water is the primary reaction path for the benzylamine, *via* the protonated form, **BAH**$^+$. Unless otherwise specified in this manuscript, all reactions of the various benzylamines under the experimental conditions are assumed to proceed via their protonated forms, and so reaction of **BA** is understood to imply reaction *via* **BAH**$^+$.

Although the reaction yields benzyl alcohol and NH_4^+ as essentially the only products at early times, other minor products were detected, including: dibenzylamine, toluene, dibenzylimine, and tribenzylamine. Of these minor products, toluene was formed as < 0.2 mole% of total product yield at early reaction times. Toluene is typically the major product in unbuffered supercritical and subcritical hydrothermal experiments involving **BA** (Houser et al., 1989; Katritzky et al., 1990; 2001), which suggests toluene is a product of reactions involving unprotonated **BA** rather than **BAH**$^+$.

At later reaction times, numerous other small peaks were observed in the GC chromatograms (Fig. A2) with retention times that correspond to structures containing two, three, and four phenyl rings. These products may be similar to those observed in previous hydrothermal **BA** experiments by Katritzky et al. (1990; 2001) that were performed with higher **BA** concentrations and unbuffered conditions. Multi-ring products can form via electrophilic aromatic substitution of the primary product benzyl alcohol (mechanisms are discussed below).

At later reaction times, multi-ring products constitute a larger portion of the total product mixture, and specific electrophilic aromatic substitution products (**EAS** products**)** could be clearly identified. In particular, the *ortho*-, *meta*-, and *para*-isomers of benzyl-benzyl alcohol were identified by comparison with authentic standards (see further below). After 140 hours (longest reaction time) these three products contributed ~10 mole% of total products, normalized to number of phenyl rings (e.g., 1 eq. benzyl-benzyl alcohol ≡ 2 eq. phenyl rings). Support for electrophilic aromatic substitution reactions of benzyl alcohol also comes from separate experiments performed starting with α-methylbenzylamine as well as the chiral compound R-(+)-α-methylbenzyl alcohol (see Section 2.3.3 and Appendix A). **EAS** products have also been detected in other hydrothermal experiments starting with benzyl alcohol (Fecteau, 2016). Any kinetic reaction scheme must, therefore, take these secondary electrophilic aromatic substitution reactions into account.

2.3.2 Kinetics of the BA Reaction

The decrease in concentration of **BA** with time, and concomitant rise in the concentrations of benzyl alcohol (**BAL**) and NH_4^+ as the products is shown in Fig. 3. Under the experimental conditions, **BA** is almost exclusively in the reactive protonated form, $\mathbf{BAH^+}$. The benzyl alcohol concentration increases at early times and later decreases due to secondary electrophilic aromatic substitution reactions mentioned above. The benzyl alcohol concentration is lower than that of NH_4^+ at all reaction times due to these follow-up reactions, which limit the maximum attainable concentration of benzyl alcohol. A kinetic model that includes conversion of **BA** to **BAL**, and the follow-up reactions is shown in Fig. 4.

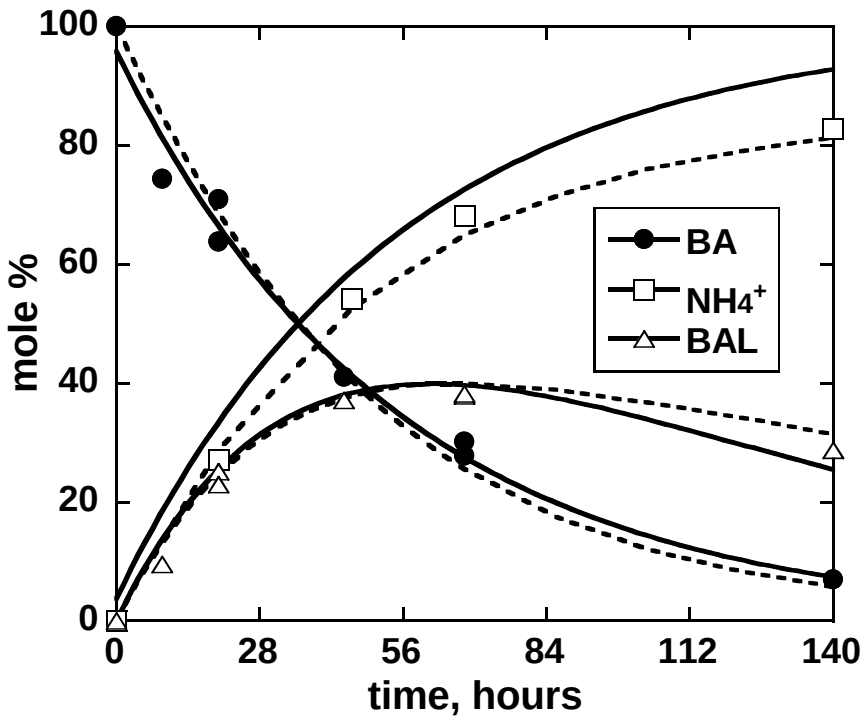

Fig. 3. Reactant and product concentrations vs. time in hydrothermal experiments (250°C, P_{sat}) with 0.05 molal benzylamine, **BA**, buffered at pH 3.3 using phosphate salts. The solid curve through the **BA** data (filled circles) represents the best fit to a first-order kinetic model, Eq. (2). The solid curve through the benzyl alcohol, **BAL**, data (open triangles) represents the best fit to a consecutive first-order kinetic model, Eq. (4). The NH_4^+ data (open squares) are not fit with an equation, but are compared to predicted NH_4^+ concentrations (solid curve) assuming **BA** deamination follows 1:1 stoichiometry with deamination, Eq. (3). The dotted lines represent best fits to a kinetic model that includes second-order reactions for the decomposition of benzyl alcohol (see Fig. 7). For visual clarity, the data are presented as mole% of BA at t = 0, with products normalized to zero mole% for t = 0. Duplicate experiments can be seen for some reaction times. Analytical uncertainties (±1 standard deviation for triplicate GC injections for organics and duplicate injections for NH_4^+) are smaller than the data points.

In principle, conversion of **BA** to **BAL** is reversible. Under the experimental conditions, however, the reverse reaction is negligible since the experiments are performed at very low reactant concentration that drive the reaction toward the alcohol and ammonia. The experiments are also performed at low pH, and under these conditions the nitrogen leaves as NH_3 and will be rapidly protonated to NH_4^+. This also precludes the reverse reaction since the protonated NH_4^+ is neither basic nor nucleophilic enough to react with the alcohol product. The rate constant for reaction of the **BA** is thus assumed to be pseudo-first-order and irreversible (k_{obs}^1, Fig. 4). The electrophilic aromatic substitution and other follow-up reactions of the benzyl alcohol were also modeled using collective, irreversible 1st-order kinetics (k_{obs}^2).

This consecutive first-order decay model was used to fit the time-dependent data shown in Fig. 3 according to Eq. (2 – 4):

$$[\mathbf{BA}] = [\mathbf{BA}]_0 \, e^{-k_{obs}^1 t} \qquad (2),$$

$$[NH_4^+]_p = 100 - [\mathbf{BA}] \qquad (3),$$

$$[\mathbf{BAL}] = (k_{obs}^1 \, [\mathbf{BA}]_0)/(k_{obs}^2 - k_{obs}^1) \, (e^{-k_{obs}^1} - e^{-k_{obs}^2}) \qquad (4),$$

where [**BA**] is the concentration of **BA** at a given time, $[\mathbf{BA}]_0$ is the concentration of **BA** at time zero, [**BAL**] is the concentration of benzyl alcohol, and $[NH_4^+]_p$ is the predicted concentration of NH_4^+ assuming it is produced in a 1:1 stoichiometric ratio to **BA** loss. The values of the rate constants that gave the best fit to the data, shown as the solid lines in Fig. 3, are 5.1×10^{-6} s^{-1} and 4.0×10^{-6} s^{-1} for k_{obs}^1 and k_{obs}^2, respectively. These observed rate constants can be deconstructed into more elementary rate constants. As

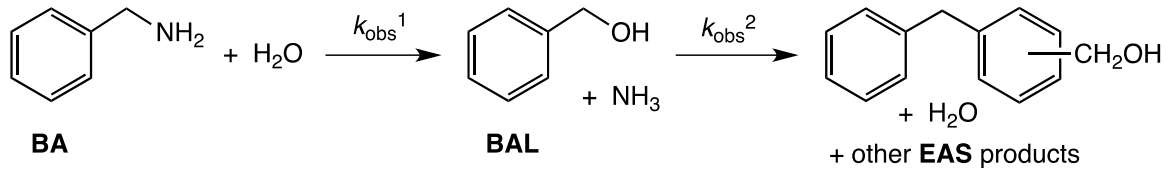

Fig. 4. A kinetic model for the hydrothermal decomposition of benzylamine, **BA**. The observed rate constants for the decomposition of **BA** (k_{obs}^{1}) and the decomposition of benzyl alcohol, **BAL**, (k_{obs}^{2}) were modeled using irreversible, first-order kinetics (see text). Reactions of both the amine and the alcohol are assumed to proceed via their protonated forms, which are not shown (see text).

discussed above, under the experimental conditions **BA** will be protonated, and it is the protonated form, **BAH**$^+$, that reacts (Fig. 5). The rate constants for protonation, $k_{+H^+}^{BA}$, and deprotonation, $k_{-H^+}^{BA}$, can be assumed to be much larger than the rate constant for the deamination of **BAH**$^+$, $k_r^{BAH^+}$, thereforee reversible protonation can be represented as an equilibrium process. The ratio of $k_{+H^+}^{BA}$ to $k_{-H^+}^{BA}$ is equal to the equilibrium constant for reversible protonation, K^{BA}. The equilibrium constant can be used with the experimental pH to calculate the fraction of **BAH**$^+$ present in experiments, f(BAH^+) (Fig. 5). With an experimental pH of 3.3 and an estimated minimum value for K^{BA} of 10^5 (pK_a = 5) (see Section 2.2.3 and Fig. 2), more than 98% of **BA** will be in the protonated **BAH**$^+$ form, i.e., f(BAH^+) > 0.98. The rate constant for the deamination of BAH+, $k_r^{BAH^+}$, is equal to the observed rate constant, k_{obs}^1, multiplied by f(BAH^+). Because f(BAH^+) is nearly unity, $k_{obs}^1 \approx k_r^{BAH^+}$. Accordingly, although we refer to **BA** reactions, since total benzylamine concentrations are determined after extraction and GC analysis, it is the protonated **BAH**$^+$ form that reacts, and for which the reaction mechanisms are relevant.

The situation for k_{obs}^2 for **BAL** is similar. It is also determined by the rate constant for reaction of the protonated alcohol multiplied by the fraction of the alcohol that is in the protonated form (Fig. 6). Unlike the amine, the fraction of the alcohol in the protonated form was not estimated since the follow-up electrophilic aromatic substitution reaction mechanisms were not the focus of this work. Reaction of the benzyl alcohol to form **EAS** and other products was considered to be pseudo-first-order based on the assumption that the concentration of phenyl rings in solution is roughly constant. The formation mechanism for one of the benzyl alcohol derived **EAS** products that was positively identified in the product mixture, *para*-benzylbenzyl alcohol, is shown

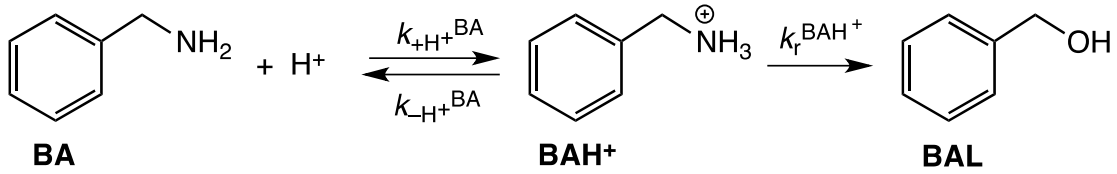

$$f(BAH^+) = \frac{[BAH^+]}{[BAH^+] + [BA]} = \frac{[H^+]\,K^{BA}}{1 + [H^+]\,K^{BA}} \qquad K^{BA} = \frac{k_{+H^+}^{BA}}{k_{-H^+}^{BA}}$$

$$k_{obs}^{1} = f(BAH^+)\,k_r^{BAH^+}$$

Fig. 5. The observed rate constant for reaction of the amine, k_{obs}^{1}, is given by the fraction of the amine that is in the protonated form f(BAH^+), multiplied by the rate constant for reaction of the protonated form, k_r^{BAH+}.

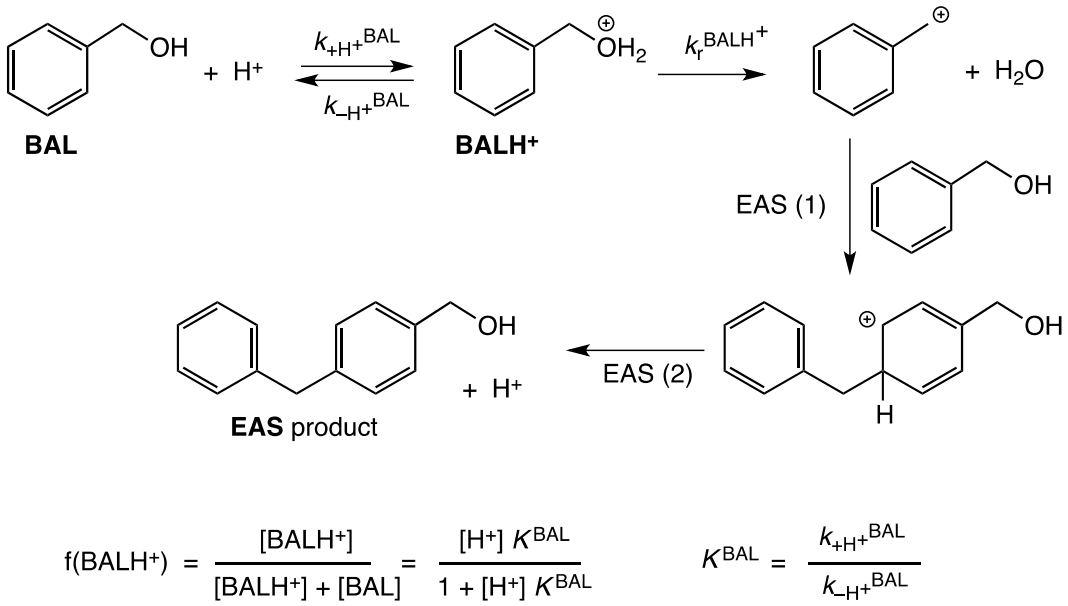

$$f(BALH^+) = \frac{[BALH^+]}{[BALH^+] + [BAL]} = \frac{[H^+]\,K^{BAL}}{1 + [H^+]\,K^{BAL}} \qquad K^{BAL} = \frac{k_{+H^+}^{BAL}}{k_{-H^+}^{BAL}}$$

Fig. 6. Proposed mechanism for formation of *p*-benzylbenzyl alcohol from benzyl alcohol (**BAL**), as an example electrophilic aromatic substitution product (**EAS** product), which builds up at later reaction times. The electrophilic aromatic substitution mechanism consists of two steps: first, addition of the cation to an aromatic ring, EAS (1), and second, loss of a proton to regenerate a new substituted aromatic ring, EAS (2). The observed rate constant for reaction of the alcohol, k_{obs}[2], is given by the fraction of the alcohol in the protonated form f($BALH^+$), multiplied by the rate constant for reaction of the protonated form, $k_r^{BALH^+}$.

in Fig. 6. Protonation of the benzyl alcohol, similar to protonation of the starting amine, generates a very good leaving group for the alcohol, i.e., water. Loss of water from the protonated alcohol forms a benzyl cation, which can in principle react with any aromatic ring in solution via the conventional two-step electrophilic aromatic substitution mechanism, i.e., addition of the cation to the benzene ring of an aromatic compound, EAS (1), followed by deprotonation to form a new substituted aromatic structure, EAS (2) (Fig. 6). Corresponding electrophilic aromatic substitution reactions can, in principle, occur with any aromatic molecule in solution, including an aromatic product of a prior electrophilic aromatic substitution reaction. On this basis, we assume a roughly constant concentration of aromatic ring structures that can react with benzyl alcohol; this allows the additional assumption of pseudo-first-order kinetics for the follow-up reactions of the benzyl alcohol.

To test the assumptions of pseudo-first-order-kinetics, a more complex kinetic model that describes the benzyl alcohol reaction as a *second-order* process involving the reaction of two benzyl alcohol molecules was considered (Fig. 7). The rate of reaction of the benzyl alcohol is now described by a second-order rate constant, $k_{obs}^{(2)}$. In addition to the first-order reaction to form the alcohol, the starting amine is allowed to react with the alcohol product in another second-order reaction, fit with the same rate constant, $k_{obs}^{(2)}$ (Fig. 7). In this model, the time-dependent concentrations of **BA** and benzyl alcohol were fitted using a non-linear least-squares method to give the best values for the two rate constants, k_{obs}^{1} and $k_{obs}^{(2)}$. These best fit values were 4.8×10^{-6} s^{-1} and 4.8×10^{-5} M^{-1} s^{-1}, respectively.

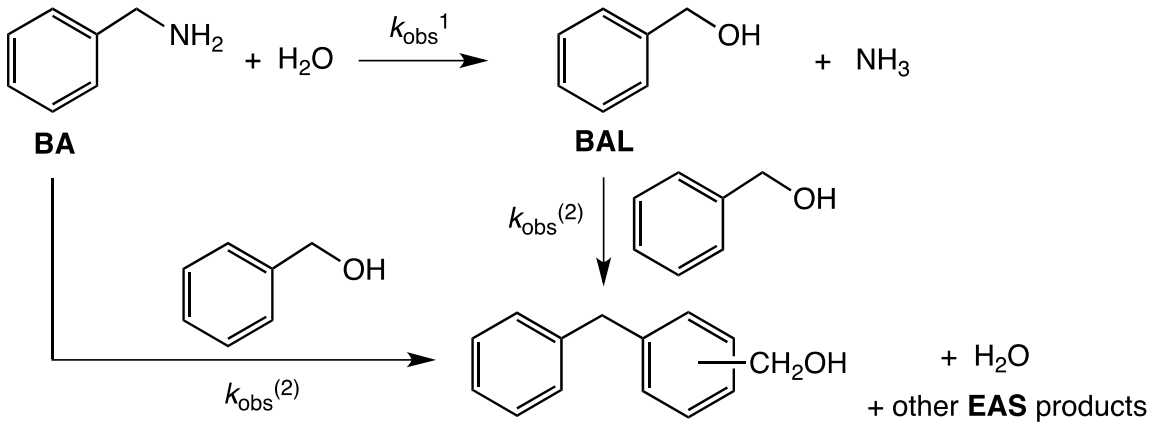

Fig. 7. Kinetic scheme for reaction conversion of benzylamine, **BA**, into benzyl alcohol, **BAL**, k_{obs}^{1}, and reaction of the alcohol to give electrophilic aromatic substitution products *via* second-order reaction with another alcohol, $k_{obs}^{(2)}$, and also via a second-order reaction with the starting amine, with the same rate constant, $k_{obs}^{(2)}$. This kinetic model is compared to the simpler, consecutive first-order model of Fig. 4.

The values of the first-order rate constants for reaction of the amine to give the alcohol, k_{obs}^1, are 5.1×10^{-6} s^{-1} for the simple, first-order model (Fig. 4) and 4.8×10^{-6} s^{-1} for the model that includes the second-order reactions (Fig. 7). The difference in these two values is small, because the majority of the amine decomposes via the first-order process. As mentioned above, after ~30% conversion of the amine, no **EAS** products are detectable; they only become significant for amine conversions approaching 70%. The results from the kinetic model that includes the second-order pathways suggest, via a "time course" method (Section 2.2.4), that only 10% of the amine reacts via second-order reaction with the alcohol product after 140 hours.

The significance of competing second-order reactions was further investigated by determining the dependence of **BA** reaction kinetics on the concentration of the amine. Two time-series experiments were performed to compare reaction kinetics for 0.05 molal amine with those of 0.15 molal amine (Table A4); the corresponding phosphate buffer concentrations were 0.1 molal and 0.3 molal, respectively. Loss of the amine at 0.15 molal could be described by first-order kinetics ($R^2 = 0.992$) with a k_{obs}^1 of $(6.9 \pm 0.5) \times 10^{-6}$ s^{-1}. This value is larger than the corresponding rate constant for 0.05 molal amine by a factor of only 1.4. Pure second-order kinetics would be expected to increase the observed first-order rate constant, k_{obs}^1, by a factor of 9 at the start of the reaction when tripling the concentration of reactant. This observation, together with the small difference in the k_{obs}^1 for the two kinetic models (i.e., Fig. 4 vs. Fig. 7), and the fact that the amine decay kinetics fit well to a first-order model (Fig. 3), suggest the simpler first-order kinetic model gives reaction rate constants that are sufficiently accurate for the present

study. This is especially evident when considering that the rate constants for ring substituted compounds range over almost four orders of magnitude (see below).

Two possible mechanisms for the substitution reaction to form benzyl alcohol can be considered (Clayden et al., 2001), Fig. 8. In the first (S_N1), unimolecular C–N bond cleavage in the protonated benzylaminium forms a benzyl cation, with NH_3 as a leaving group. Subsequent C–O bond formation occurs by water addition to the cation, followed by deprotonation to form the alcohol. The first step is rate determining in this mechanism, since energy is required to break the C–N bond. In the second mechanism (S_N2), water attacks the protonated amine, the C–O bond forms and the C–N bond breaks at the same time (a concerted reaction). Subsequent deprotonation forms the alcohol, and the rate determining step is the concerted bond breaking/bond making step. Under the experimental conditions, the NH_3 that leaves in both the S_N1 and the S_N2 reactions will be quickly protonated to form NH_4^+. Mechanisms involving radical intermediates are not considered since no significant quantities of expected radical products, such as toluene or bibenzyl (combined < 0.6 mole%), were observed even at the longest time experiments (140 hrs).

Although the rate determining step in the S_N2 mechanism is a bimolecular reaction between the protonated amine and water, the reaction will obey pseudo-first-order kinetics because water is the solvent, and its concentration is much larger than that of the amine and changes negligibly over the timescale of the reaction progress. Since both are formally first-order for the protonated amine, the S_N1 and S_N2 mechanisms would be indistinguishable in the absence of additional mechanistic information. It is

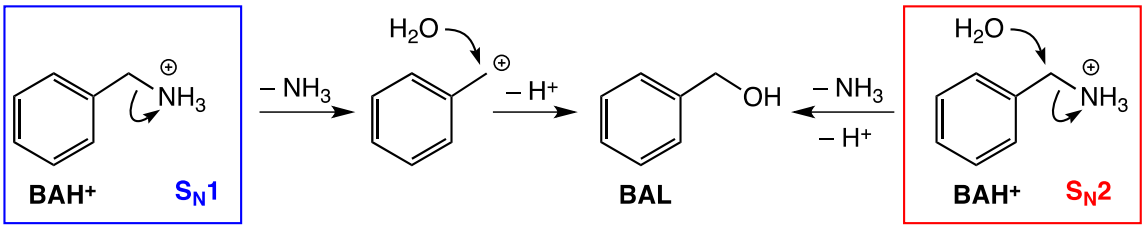

Fig. 8. S_N1 (blue) and S_N2 (red) reaction mechanisms for the substitution reaction of **BAH**$^+$ to form **BAL**.

important to distinguish between these two mechanisms so that useful kinetic models of reactivity can be developed. For example, the two mechanisms would be expected to have different temperature-dependent changes in rate, since one is unimolecular and the other is bimolecular, the former being more entropically favored. Thus, a series of experiments were performed on structural derivatives of **BA** in order to determine whether the S_N1 or the S_N2 mechanism was the most important in the formation of benzyl alcohol (see Section 2.3.4).

2.3.3 α-methylbenzylaminium (α-CH_3-BA) kinetics

Similar experiments as a function of time were performed with 0.05 molal α-methylbenzylamine, **α-CH_3-BA**, under the same conditions as those for **BA**. A methyl group on the α-carbon of **α-CH_3-BA** compared to **BA** should influence the relative rates of the S_N1 and the S_N2 reaction mechanisms quite differently. This methyl group should increase the rate of amine decomposition via the S_N1 reaction compared to **BA** because the methyl group will stabilize the intermediate benzyl cation via hyperconjugation. In addition, the presence of this methyl group should decrease the rate of **α-CH_3-BA** decomposition via the S_N2 mechanism compared to **BA**, because steric hindrance decreases the rate of nucleophilic attack by H_2O or other nucleophiles (Clayden et al., 2001). The time-dependence of the loss of **α-CH_3-BA** is shown in Fig. 9, along with the formation of α-methylbenzyl alcohol (**α-CH_3-BAL**) and styrene. Unlike with **BA**, alkene formation (styrene in this case) is possible for **α-CH_3-BA** via an elimination mechanism. The data in Fig. 9 indicate that after ~20 mins the alcohol and styrene reach a near-constant ratio, suggesting that formation of styrene from the alcohol by dehydration is rapid and reversible. Similar to **BA**, the sum of the **α-CH_3-BAL** and the styrene (~50

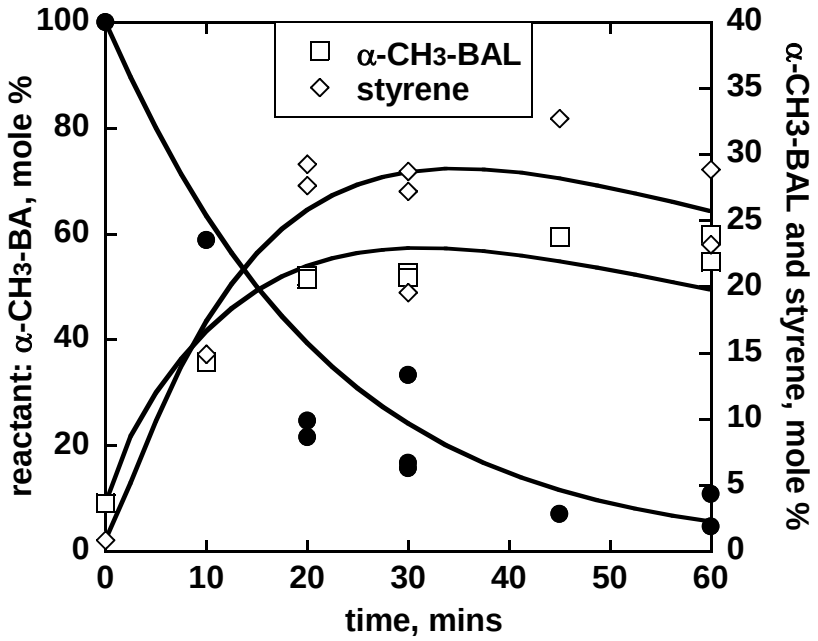

Fig. 9. Reactant and product concentrations vs. time for experiments with 0.05 molal α-methylbenzylamine, **α-CH3-BA**, solutions phosphate-buffered at pH 3.3 at 250°C. The curves through the data points for **α-CH3-BA** (closed circles), α-methyl benzyl alcohol (**α-CH3-BAL**, open squares), and styrene (open diamonds), represent the best fits to the data using the kinetic model summarized in Fig. 10, that includes first-order reaction of **α-CH3-BA** to give **α-CH3-BAL**, and second-order reaction of **α-CH3-BAL** with **α-CH3-BA** and **α-CH3-BAL** to give electrophilic aromatic substitution products. For clarity, the data are plotted as mole% of **α-CH3-BA** at t = 0 (see Table A2 for molal concentrations). The concentration scale on the left is for **α-CH3-BAL** and the concentration scale on the right is for right is **α-CH3-BAL** and styrene. Duplicate experiments can be seen for certain time points. Analytical uncertainties (±1 standard deviation for triplicate GC injections) are smaller than the data points.

mole% at t = 60 min) is less than the quantity of **α-CH$_3$-BA** lost (~90 mole% at t = 60 min), presumably due to reactions that give **EAS** products analogous with those from benzyl alcohol. The kinetic scheme for the **α-CH$_3$-BA** reaction is shown in Fig. 10. The values of the rate constants k_{obs}^{1}, $k_{obs}^{(2)}$, k_{obs}^{3f} and k_{obs}^{3r} that give the best fit to the data (the solid lines in Fig. 9) are 7.0×10^{-4} s^{-1}, 2.3×10^{-2} M^{-1} s^{-1}, 6.9×10^{-3} s^{-1} and 5.3×10^{-3} s^{-1}, respectively. Fitting the **α-CH$_3$-BA** concentration alone to first-order kinetics gives a value for k_{obs}^{1} of 7.6×10^{-4} s^{-1}. Since this value is within 10% of k_{obs}^{1} for the more complex model (i.e., 7.0×10^{-4} s^{-1}) we assumed that first-order decay fits are sufficiently accurate for all substituted benzylamine compounds in the present study.

The absolute values of k_{obs}^{3f} and k_{obs}^{3r} are not accurate, because the rates of these two processes are significantly faster than the rate at which the alcohol is formed from the amine and thus their values cannot be obtained from the data. The ratio $k_{obs}^{3f}/k_{obs}^{3r}$, however, determines the ratio of styrene to alcohol, and this ratio is determined with much higher accuracy. The ratio represents an empirical equilibrium constant for alcohol/alkene interconversion of 1.3. Both benzyl alcohol, **BAL**, and the α-methylbenzyl alcohol, **α-CH$_3$-BAL**, form electrophilic aromatic substitution products (**EAS** products), presumably via benzyl cations that are formed by elimination of water after protonation. The value of the second-order rate constant for reaction to give **EAS** products, $k_{obs}^{(2)}$, is 480 times larger for **α-CH$_3$-BAL** than for **BAL**. This difference can be explained in terms of the relative stabilities of the intermediate benzyl cations. The α-methyl substituent in **α-CH$_3$-BAL** stabilizes the benzyl cation via hyperconjugation. This makes it easier to form and results in a faster reaction. The pseudo-first-order rate constant for

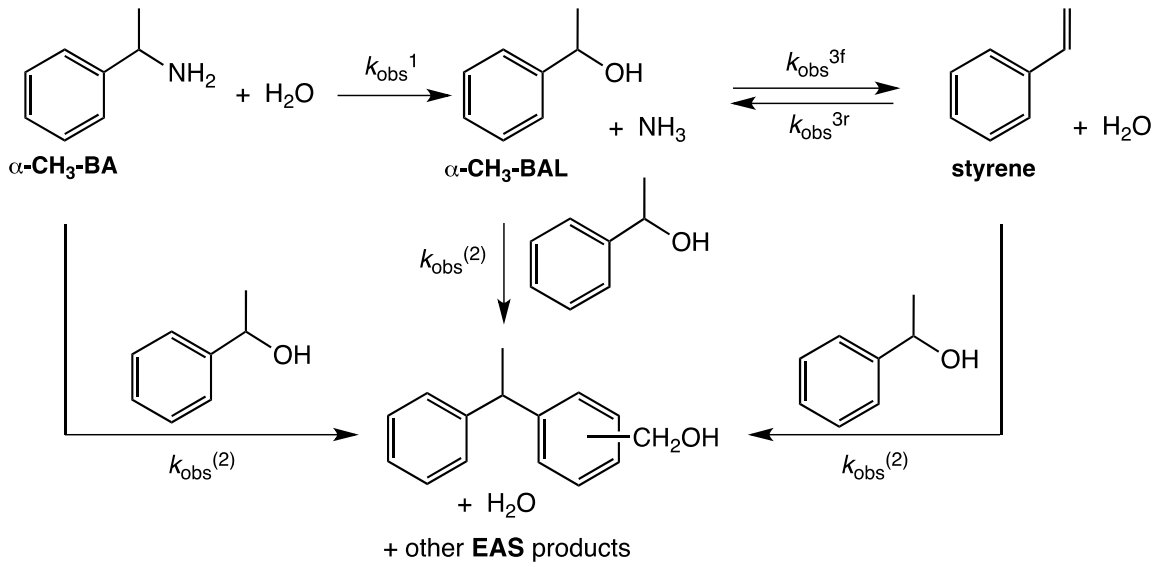

Fig. 10. A kinetic model for the hydrothermal decomposition of **α-CH$_3$-BA**. The rate constant for the deamination/dehydration of **α-CH$_3$-BAH+** (k_{obs}^{1}) was modeled using irreversible first-order kinetics. The resulting α-methylbenzyl alcohol (**α-CH$_3$-BAL**) can dehydrate reversibly to form **styrene** (k_{obs}^{3f} and k_{obs}^{3r}). Secondary benzyl cations (not shown) are assumed to be present in equilibrium with **α-CH$_3$-BAL**, and can undergo electrophilic aromatic substitution with phenyl rings in solution, including **α-CH$_3$-BAL** itself and **α-CH$_3$-BA** to form multi-ring electrophilic aromatic substitution products (**EAS** products), with a second-order rate constant $k_{obs}^{(2)}$.

formation of the alcohol **α-CH$_3$-BAL** from the amine **α-CH$_3$-BA**, k_{obs}^1, is larger than the corresponding rate constant for conversion of **BA** to **BAL** by a factor of 150. This observation can be explained in the same way if this reaction proceeds *via* an S_N1 mechanism (Fig. 8), since this reaction for **α-CH$_3$-BA** would generate the same, more stable, benzyl cation intermediate as in the corresponding alcohol reactions.

In Fig. 10, styrene is shown as a product of elimination of H_2O from the primary alcohol product, even though in principle styrene could also be formed in an elimination reaction of the starting amine. However, two lines of evidence suggest that elimination from the amine does not occur to a significant degree. First, at early reaction times the ratio of **α-CH$_3$-BAL** to styrene is much larger than unity and approaches 0.8 at later times (Fig. 10, Table A5). This suggests the alcohol is the primary product of reaction of the amine, not styrene, and that styrene is indeed formed as a secondary reaction of the alcohol. Second, hydrothermal reaction of the (R)-enantiomer of **α-CH$_3$-BAL**, R-(+)-α-methylbenzyl alcohol, forms the corresponding (S)-enantiomer much faster than it produces styrene; i.e., substitution is much faster than elimination. See Appendix A for more details on these experiments and discussion regarding these lines of evidence.

Overall, these findings suggest that **α-CH$_3$-BA** primarily undergoes reaction to form the corresponding alcohol via an S_N1 mechanism. The rate of reaction of **α-CH$_3$-BA** increases relative to **BA**, consistent with an S_N1 mechanism for both of these amines. However, it is also theoretically possible that **BA** actually reacts via an S_N2 mechanism, and that the addition of the α-methyl substituent to **BA** simply decreases the rate of the S_N2 mechanism and increases the rate of the S_N1 mechanism, i.e., effectively switching the mechanism from S_N2 for **BA** to S_N1 for **α-CH$_3$-BA**. This is possible because the α-

methyl substituent will sterically hinder nucleophilic attack in an S_N2 attack, reducing its rate. The α-methyl substituent will also stabilize the carbocation intermediate formed in an S_N1 reaction via hyperconjugation and increase the reaction rate. Further experiments were performed using ring-substituted benzylamines to probe the deamination/hydration substitution reaction mechanisms for both compounds.

2.3.4 Ring substituent effects

Experiments were performed with ring substituted **BA** and **α-CH_3-BA** derivatives, at 0.05 molal and the same experimental conditions. Ring substituents were chosen that would either donate electron density to the benzene ring (electron donating groups) or withdraw electron density from the benzene ring (electron withdrawing groups). Electron donating groups are expected to greatly increase the rate of reaction if a positive charge is generated in the benzene ring in the rate determining step, as would be the case for the S_N1 mechanism that forms a benzyl cation intermediate (Fig. 8, blue). Electron withdrawing groups are correspondingly expected to strongly decrease the rate of an S_N1 reaction because they destabilize the benzyl cation intermediate. The S_N2 mechanism does not result in build-up of charge in the benzene ring in an intermediate or transition state (Fig. 8, red), so ring substituents are expected to have a relatively weak influence on the rate of an S_N2 reaction. In this way, substituent effects can provide information on reaction mechanisms.

Rate constants for the decay of the variously ring-substituted **BA** and **α-CH_3-BA** derivatives are summarized in Table 1. The rate constants were obtained assuming pseudo-first-order kinetic fits. The R^2 values for each kinetic fit are included in Table 1 (see Table A2 for a more extensive summary of the experimental data). From Table 1 it is

Table 1
Hammett parameters (σ^+) and rate constants (log *k*) for ring-substituted BA and α-CH_3-BA compounds.

Substituent(s)	σ^+ [a]	log *k*, s^{-1} [c]
BA compounds		
4-OCH_3	-0.648	-2.23
4-CH_3	-0.256	-4.62
3,5-diCH_3	-0.13 [b]	-4.81
3-CH_3	-0.065	-5.05
H (BAH+)	0	-5.29
3-OCH_3	0.047	-5.13
3-F	0.352	-5.68
3-Cl	0.399	-5.59
3-CF_3	0.52	-5.49
3,5-diCF_3	1.04	-5.70
α-CH_3-BA compounds		
3-CH_3	-0.065	-2.73
H (α-CH_3-BAH+)	0	-3.10
3-CF_3	0.52	-4.37
3,5-diCF_3	1.04 [b]	-5.67

[a] σ^+ values were obtained from Gordon and Ford, 1972.
[b] This was calculated by multiplying meta-σ^+ value by 2.
[c] These values were calculated from 1st order kinetics fits to the data.

clear that electron donating substituents, such as $–OCH_3$, increase the reaction rate constant by orders of magnitude for both **BA** and **α-CH_3-BA**. This strongly suggests a positively charged intermediate and transition state, consistent with an S_N1 mechanism. In addition, electron withdrawing substituents, such as $–CF_3$, decrease the reaction rate constants by orders of magnitude for **α-CH_3-BA**, again consistent with an S_N1 mechanism. Electron withdrawing substituents have a much weaker effect on the rate constant for reaction of **BA**, suggesting only a weak build-up of charge in the transition state for the rate determining step, consistent with an S_N2 mechanism.

This discussion of substituent effects can be put in a quantitative framework by using a Hammett analysis. Here, the electron donating and withdrawing abilities of substituents are quantified by assigning them a σ value; the σ parameter is a quantitative measure of their influence on a related reaction. In the original work by Hammett (1935), substituent effects were quantified in terms of their influence on the ionization constant for benzoic acid. More appropriate for the present reaction are substituent σ values derived from rate constants for the closely related S_N1 solvolysis reaction of α,α-dimethylbenzyl chloride (*tert*-cumyl chloride) reported by Brown and Okamoto (1958). The substituent effects for this reaction were given the specific label σ^+, since they quantify the influence of the substituent on a reaction that generates a positive charge on a benzene ring in the rate-determining step.

The Hammett equation, Eq. (5):

$$\log k_x = \rho\sigma^+ + b, \qquad (5),$$

represents a linear free energy relationship if the substituent effects on the rate-determining step for *tert*-cumyl chloride solvolysis is directly proportional to the substituent effects on the rate-determining step for the reaction of interest (Brown and Okamoto, 1958). In this version of the equation, k_x is the rate constant for the reaction of the ring-substituted benzylamines (where the subscript x represents the substituent; e.g., "H" for the parent), ρ is a constant for the reaction that characterizes its sensitivity to the substituent effects, and b is the y-intercept that, assuming a perfect fit, is equal to log k_H.

For reactions that generate a positive charge on a benzene ring, electron donating substituents have negative σ^+ values and electron withdrawing substituents have positive σ^+ values (Brown and Okamoto, 1958). Thus, a Hammett plot with σ^+ values has a negative slope for a reaction that builds-up positive charge in the ring in the rate-determining step. Table 1 includes the σ^+ values for each of the ring substituents (Gordon and Ford, 1972), together with the first-order rate constants for the decomposition of each of the substituted and parent compounds (log k_x, s^{-1}).

The Hammett plot for this data is shown in Fig. 11. According to the Hammett relationship, a constant reaction mechanism for all of the substituted structures should result in a linear relationship; This is observed for **α-CH$_3$-BA** hydrolysis (straight dashed line). A linear least squares regression fit this data with an R^2 of 0.997 and a slope of -2.50 (ρ1α, Fig. 11, left). The negative slope and linear correlation strongly support a constant mechanism for all of the substituted α-methylbenzylamines, which generates a positively charged transition state, i.e., reaction via the S_N1 mechanism. In turn, this is in agreement with the observation of faster reaction for the unsubstituted **α-CH$_3$-BA** compared to unsubstituted **BA** discussed above. Thereforee, the first-order rate constant

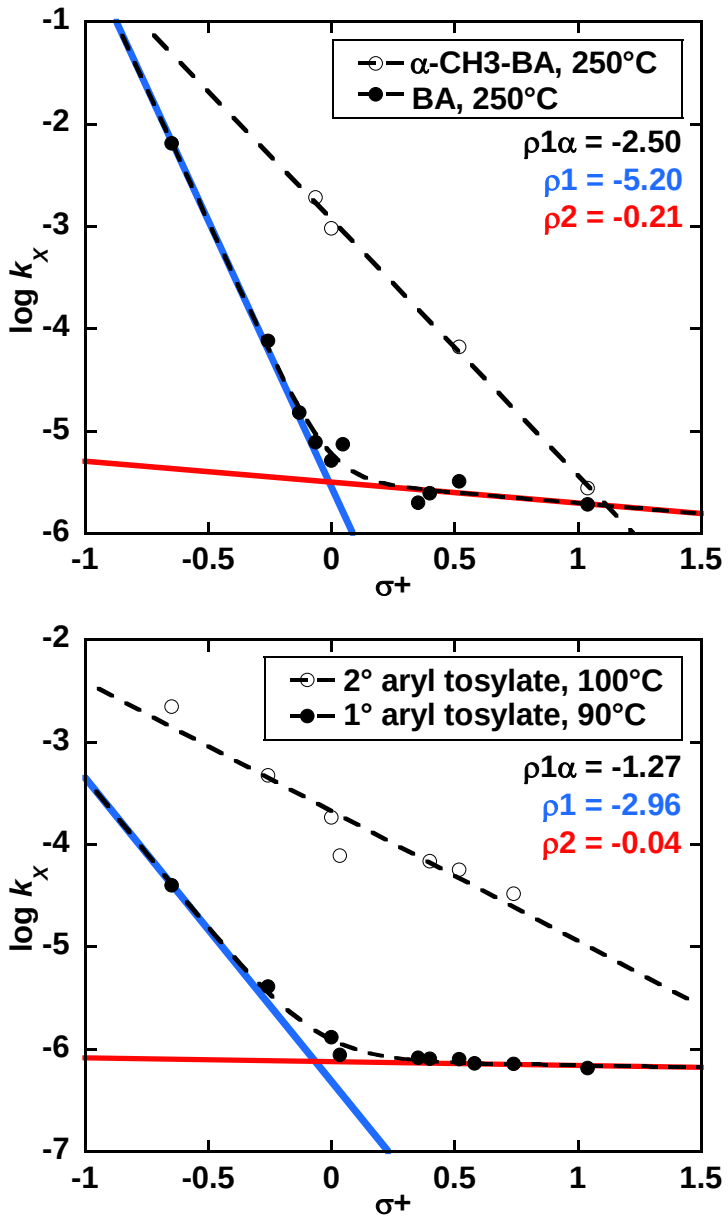

Fig. 11. Top, a Hammett plot based on 250°C deamination/hydration kinetics for ring-substituted **BA** (filled circles) and **α-CH$_3$-BA** (open circles) from data compiled in Table 1. Two additive linear functions were used to fit the **BA** data (curved dashed line), and the best fit parameters were used to solve for the linear functions associated with a positively charged transition state (blue line) and a more neutrally charged transition state (red line). The data for **α-CH$_3$-BA** were fit with a single linear function (straight dashed line). The reaction constants (ρ), equal to the slope of each linear function, are displayed on the plot. Bottom, another Hammett plot following the same formatting, based on the 90-100°C acetolysis of two aryl tosylates is shown for comparison. This plot was constructed using data compiled from the following studies: Winstein et al., 1952; Winstein et al., 1953; Lancelot et al., 1969; S. Harris et al., 1969; Coke et al., 1969.

for the decomposition of **α-CH$_3$-BA** is attributed to an S_N1 reaction mechanism ($k_\alpha \approx 7.6 \times 10^{-4}$ s^{-1}).

The relationship for **BA** (curved dashed line), however, is clearly non-linear. Curved Hammett plots are usually taken as strong evidence for a change in mechanism with changes in the substituents ability to stabilize or destabilize charge (see below). In this case, the two competing mechanisms are likely to be S_N1 and S_N2. To properly describe the Hammett relationship for all of the substituted **BA**, the contributions of each of these mechanisms needs to be considered. The rate constant for the **BA** structures was modeled as a linear sum of rate constants for the two mechanisms. Each mechanism is

described by its own linear Hammett relationship, according to Eq. (6):

$$\log k_x = \log [10^{(\rho 1 * \sigma^+ - b1)} + 10^{(\rho 2 * \sigma^+ - b2)}] \qquad (6).$$

This equation was fit to the data using nonlinear least squares regression analysis to solve for the parameters ρ1, b1, ρ2, and b2. For this equation, ρ1 and b1 are the reaction constant and y-intercept for the S_N1 mechanism, while ρ2 and b2 are the reaction constant and y-intercept for the S_N2 mechanism. The best fit values for each parameter are as follows: ρ1 = -5.20, b1 = -5.55 (S_N1 reaction), ρ2 = -0.21, and b2 = -5.50 (S_N2 reaction).

The b1 and b2 intercept values obtained from the best fit of Eq. (6) were used to calculate the contribution of each mechanism to the reaction of the parent, unsubstituted

BA. This analysis gave an S_N1 contribution of ~47% and an S_N2 contribution of ~53%. From these percentage contributions, rate constants for the individual mechanisms were obtained, i.e., $k_{SN1} \approx 2.4 \times 10^{-6}$ s^{-1} and $k_{SN2} \approx 2.7 \times 10^{-6}$ s^{-1}. For comparison with ring substituted benzylamines, reaction of 4-methoxybenzylamine (most electron donating) had more than 99.9% contribution from S_N1, while reaction of 3,5-bis(trifluoromethyl)benzylamine (most electron withdrawing) had more than 99.9% contribution from S_N2.

The reaction constant ($\rho 1$) for the S_N1 mechanism for the benzylamines is much more negative than the reaction constant ($\rho 1\alpha$) for the S_N1 mechanism for **α-CH_3-BA** (-5.20 vs. -2.50, respectively). This is expected, because the α-methyl group should stabilize the charged transition state and delocalize charge away from the ring due to hyperconjugation, thus making reaction kinetics less sensitive to ring substituent effects compared to the benzylamines.

The dependence of the rate constants on substituents shown in Fig. 11 is consistent with other mechanistic studies of substitution reactions reported in the literature. Specifically, studies of lower temperature (90-100°C) acetolysis of substituted 1-phenyl-2-ethyl tosylates (Lancelot et al., 1969; Winstein et al., 1952; Harris et al., 1969; Winstein et al., 1953; Coke et al., 1969) give a Hammett plot with curvature very similar to that for **BA** (Fig. 11). Again, a switch from an S_N1-like mechanism (in the area of strong dependence on substituent) to an S_N2 mechanism (in the area of weak dependence on substituent) was proposed to account for this behavior. For these structures a simple S_N1 mechanism is not possible because the leaving group is on a primary carbon atom. Instead, a mechanism in which the tosylate leaves by anchimeric

assistance from the benzene ring was proposed. This still generates a positive charge on the benzene ring, but the structure of the cation is somewhat different. The reaction parameters for this data are $\rho 2 = -0.04$ in the S_N2 region (even smaller than for **BA**), and $\rho 1 = -2.96$ in the S_N1-like region. This is also smaller than the reaction constant for **BA** in the S_N1 region, which may be because the structure of the cation intermediate is simply not the same for both reactions.

The Hammett plot for substituted secondary tosylates exhibits similar behavior to the secondary **α-CH$_3$-BA** (Fig. 11). The plot for the secondary tosylates exhibits a linear trend ($R^2 = 0.954$), and has a negative slope with reaction constant $\rho 1\alpha = -1.27$ (Fig. 11). Just as for **α-CH$_3$-BA**, this indicates a single mechanism for all structures that generate a positive charge on the benzene ring. Like the **BA** and **α-CH$_3$-BA** again, the reaction constant for the secondary structures ($\rho 1\alpha = -1.27$) represents a less negative slope than that for the primary structures discussed above ($\rho 1 = -2.96$), presumably due to charge delocalization into the α-methyl group, which reduces the charge on the ring, and thus the sensitivity to ring substituents.

Comparison of the Hammett plots for the amine hydrothermal substitutions with those for more conventional S_N1 reactions also supports our mechanistic interpretation. Solvolysis of α,α-dimethylbenzyl chloride and ionization reactions of diphenyl methanol and triphenyl methanol all generate benzyl cations. The reaction constants for these processes are $\rho = -4.54$, $\rho = -4.74$ and $\rho = -3.44$, respectively (Brown and Okamoto, 1958). Here again, the reaction constant is less negative for the carbons that have more extensive delocalization of the positive charge away from the benzyl carbon. Thus, the mechanistic conclusions related to the hydrothermal substitution reactions of **BA** and **α-**

CH_3-BA derived from the Hammett analysis are in accord with the literature on closely related reactions.

2.3.5 Implications for modeling

Primarily, the results of this study serve as a warning that Arrhenius style rate extrapolation under hydrothermal conditions should be treated with caution, especially in the case of kinetic modeling of organic compound reactions whose mechanisms remain unknown.

Evidence for two competing mechanisms, S_N1 and S_N2, during the hydrothermal reactions of **BA** at low pH has implications for kinetic modeling of experimental and natural systems. Each mechanism contributes roughly equally to **BA** deamination under the experimental conditions, and yet these two mechanisms give identical products for **BA** and thereforee would be indistinguishable in the absence of the substituent studies described here. Since the unimolecular S_N1 mechanism is more entropically favorable than the bimolecular S_N2 mechanism, the S_N1 would be expected to become increasingly favored with increasing temperature. Correspondingly, the S_N2 would be expected to be favored over S_N1 at lower temperatures. Thereforee, a linear extrapolation of observable reaction rate constants across hydrothermal temperature regimes using Arrhenius methods would not be reliable or valid for this particular reaction. Proper characterization of the reaction mechanism with temperature would require developing Hammett relationships at different temperatures (e.g., 200 and 300°C) so that S_N1 and S_N2 mechanisms and their Arrhenius parameters could be quantified at different temperatures.

For the **α-CH_3-BA** reactions, the rate constants for the S_N1 mechanism could be more reliably extrapolated to higher, subcritical temperatures without further mechanistic

investigation since we expect the S_N1 mechanism will dominate at higher temperatures and that competing S_N2 reaction could be ignored. Extrapolation to lower temperatures, however, would be unreliable since it is not known at what temperature the S_N2 mechanism may become significant, or even dominate the decomposition kinetics. Other mechanisms for amine decomposition may also be possible at lower temperatures. Bada and Miller (1970) described an elimination deamination mechanism for aspartic acid, which also has an amine bonded to a secondary carbon just like **α-CH_3-BA**.

The structures studied here are model amines, chosen so that substituent effects could be properly explored to obtain mechanistic insight. However, the rates of their reactions may be related to those of more common naturally occurring amines if the reactions proceed via intermediates of similar stability. Based on kinetic studies of carbocation formation for various chlorides and tosylate compounds (Beste and Hammett, 1940; Brown and Rei, 1964; Schadt et al., 1976; Fujio et al., 1990; Fujio et al., 1994), it can be approximated that 2° benzyl cations have similar stabilities to 3° alkyl cations, and that 1° benzyl cations have similar stabilities to 2° alkyl cations. On this basis, the reaction rate of **α-CH_3-BA** might be similar to those of alkyl amines that form tertiary cation intermediates, and the reaction rate of **BA** might be similar to alkyl amines that form a secondary cation intermediates under acidic hydrothermal conditions. Our work also suggests that under these conditions, substitution mechanisms uncovered here may even outcompete previously proposed lower temperature deamination (elimination) mechanisms for amino acids (Bada and Miller, 1970).

The present results suggest that acidic, dilute hydrothermal conditions should result in almost exclusive deamination of amines to form alcohols as primary products by

hydration. Rapid deamination would be consistent with observations of abundant NH_4^+ in (intermediate pH) sediment-hosted hydrothermal systems (Von Damm et al., 1995; Holloway et al., 2011) and hydrothermally-treated carbonaceous meteoritic material (Pizzarello et al., 2011). Thus, one should expect that amines make up a disproportionately small component of aqueous organic nitrogen in acidic hydrothermal ($\geq$ 250°C) systems. The observation of rapid substitution for the compounds studied here suggests that related substitution reactions should occur in the presence of nucleophiles other that water, which could be even more reactive. Examples include unprotonated amines (Brotzel et al., 2006), carbanions, and sulfides. Such reactions could generate larger, more stable organic compounds, perhaps containing heteroatoms via either an S_N1 or S_N2 mechanism.

2.4 Conclusions

This study uses model compounds and traditional techniques from physical organic chemistry to determine the mechanisms for deamination/hydration reaction of primary amines under acidic, hydrothermal conditions. The influence of substrate concentration, the effect of an α-methyl substituent, and aromatic ring substituent effects on reaction kinetics were quantified and interpreted mechanistically. The mechanistic analysis demonstrated two competing substitution mechanisms (S_N1 and S_N2) and allowed determination of the individual rate constants for each of the two mechanisms for deamination of **BA** and its substituted analogues at 250°C and 40 bar (P_{sat}). The mechanistic analysis suggests an S_N1 deamination mechanism for **α-CH_3-BA** and its substituted analogues. Based on these findings, **BA** kinetics cannot be reliably extrapolated across temperature using Arrhenius methods without further experiments

characterizing the temperature dependence of each mechanism. On the other hand, **α-CH_3-BA** kinetics can be more confidently extrapolated using Arrhenius methods at least to higher temperatures where unimolecular mechanisms such as S_N1 are expected to dominate. This study provides an experimental framework for targeting individual reactions using model compounds that can be used to understand organic chemistry under geochemically relevant conditions.

2.5 Acknowledgements

I thank Kris Fecteau for ion chromatroraphy analyses of ammonium, Pierre Herckes at ASU for guidance with and use of his research group's GC-MS, and Christa Bockisch for guidance using the brass block heating apparatus. I also thank all other official and honorary members of the Hydrothermal Organic Geochemistry (HOG) group at Arizona State University for vital discussion at weekly group meetings, including Chris Glein, Jessie Shipp, Ziming Yang, Kristin Johnson, Josh Nye, and Ted Lorance. My thesis advisor, Everett Shock, and other mentors, including Ian Gould, Hilairy Hartnett, and Lynda Williams all played crucial roles in this work. This work was supported by National Science Foundation grants OCE-0826588 and OCE-1357243, and NASA Habitable Worlds grant NNX16AO82G.

CHAPTER 3

METASTABLE EQUILIBRIUM AMONG OXYGEN- AND NITROGEN-BEARING ORGANIC COMPOUNDS IN HYDROTHERMAL EXPERIMENTS

3.1 Introduction

Recent advances in organic compound analysis have enabled the detection of organic compounds in environments once thought to be devoid of organic carbon, such as crack surfaces (e.g., Tingle et al., 1990) and interiors of igneous rocks (e.g., Potter and Konnerup-Madsen, 2003), as well as volcanic gases (e.g., Graeber et al, 1979; Giggenbach et al., 1994; Tassi et al., 2007). With decreasing detection limits, the diversity and complexity of identified organics also continue to increase, generally accompanied by more accurate and precise quantification. Organic molecules containing the elements most abundant in living systems (C, H, O, and N) have been observed in comets (Mumma and Charnley, 2011) and meteorites (Pizzarello and Shock, 2010), primordial representatives of our local system, as well as in distant nebulae (Ehrenfreund and Charnley, 2000) and (more preliminarily) in exoplanetary atmospheres (Swain et al., 2008; Tsiaras et al, 2016). In some of these systems, organic inventories represent one of the most compositionally diverse data sets that can be feasibly attained. The potential for organic richness is often introduced in organic chemistry classrooms with the following type of example: there are 3 structural isomers for the chemical formula C_5H_{12}, 14 isomers for $C_5H_{12}O$, and 182 for $C_5H_{12}NO$. In nature, organic richness is exemplified outside of the biosphere by the current cumulative identification of more than 1000 different abiotically formed organic compounds in meteorites (Pizzarello and Shock, 2010).

In addition to their abundance and compositional diversity, organic compounds make for good analytical targets because they are often volatile and can escape from the natural systems in which they are produced, which are sometimes difficult to directly access. This makes them attractive targets for probing hidden processes, such as those taking place in Earth's subsurface or in extraterrestrial environments. One of the best examples for this potential is the discovery of a suite of small organic compounds in the water ice plumes rising from Saturn's moon, Enceladus (e.g., Porco et al, 2006; Matson et al., 2007). There is some evidence that Jupiter's moon, Europa, also has plumes, which NASA's Europa Clipper mission is designed to investigate for organic compounds via a spacecraft mass spectrometer (Brockwell et al., 2016). Therefore, characterizing conditions under which certain organic compounds are generated, and which classes of compounds bear signatures of their source environments, could aid in natural system exploration. Indeed, organic compounds may even provide information regarding processes and conditions from the distant past if they are preserved over long timescales, as with certain deep-circulating terrestrial fluids (e.g., Lippmann-Pipke et al., 2011; Young et al., 2017) and meteorites (e.g., Cronin et al., 1988).

One key factor affecting the preservation of organic compounds is the diversity of organic functional groups that allow the potential for numerous reactions with a vast range of temperature-dependent reaction rates. A general rule for chemistry is that as temperatures are lowered reaction rates become slower (Arrhenius, 1889); however, while this suggests colder temperatures are ideal for eventual organic preservation, higher initial temperatures may be required for abiotic organic transformations to generate compositions that reflect the local conditions that control them (Tassi et al., 2007,

McCollom, 2013b). High temperatures also mobilize organic compounds, via vaporization or dissolution in water (Shock et al., 2013, and references therein), releasing them from geologic systems. Ideal organic analytes from inaccessible systems of interest will have been subjected to high temperatures to equilibrate, traveled with some mobile phase to become accessible, and experienced temperature quenching to preserve organic abundances. One type of environment that generally satisfies these criteria is a hydrothermal system with fluids that migrate outward from planetary interiors. Thus, characterizing hydrothermal organic reactions may aid in developing the use of organic compounds as predictive tools regarding inaccessible environments.

Many organic reactions that are irreversible at ambient conditions (25°C, 1 bar) become rapidly reversible under hydrothermal conditions, as demonstrated in many experimental studies (e.g., Yang et al., 2012; Shipp et al., 2013; 2014). In some experiments, reversibility has resulted in an approach toward metastable equilibrium, as evidenced by steady state ratios of organic compounds that in some cases are in near-agreement with equilibrium values from thermodynamic calculations (Seewald, 1994; Seewald et al., 2006). Because reaction ratios approaching metastable equilibrium are dependent on temperature and pressure, these latter variables can be determined if concentration data are combined with thermodynamic data for a given reaction. Similarly, compositional variables (e.g., reactant or product concentrations) can be determined if temperatures and pressures are well-constrained.

Such calculations have been performed for several environmental systems to determine if certain organic reactions approach metastable equilibrium, and at what conditions they last equilibrated. In certain oil field brines with moderate temperatures

(~90 to 150°C) and long fluid duration (millions of years), metastable equilibrium was identified for redox reactions between a variety of carboxylic acids, alkanes, and inorganic carbon sources (Helgeson et al, 1993). Importantly, light hydrocarbon abundances do not seem to approach metastable equilibrium values in these systems, suggesting higher temperatures may be required for certain reactions to proceed. In higher temperature submarine hydrothermal systems (>185°C) at Juan de Fuca Ridge, reactions involving light hydrocarbons plus those involving unsaturated hydrocarbons were investigated to constrain subsurface fluid temperatures (Cruse and Seewald, 2006); the results demonstrate a significant temperature difference between the source fluids for two sites, which is corroborated by other geochemical observations. Notably, the organic reactions investigated by Cruse and Seewald (2006) seem to have last equilibrated at different temperatures, suggesting some reactions may be better for investigating higher temperature systems and others better for lower temperature systems. Temperature and reduction/oxidation (redox) source conditions have been predicted for volcanic gases from many different systems according to various combinations of ratios for CO_2, light hydrocarbons, and associated alkenes (Giggenbach et al., 1994; Tassi et al., 2005; Taran and Giggenbach, 2003). Some of these volcanic gas studies indicate that minimum temperatures are required to reach metastable equilibrium between alkanes, but importantly, not all organic reaction ratios reflect equilibrium at higher temperatures (e.g., Tassi et al., 2007); this implies some reactions must remain kinetically inhibited.

Collectively, these studies demonstrate that different organic compounds may serve as better tools in certain environments than others. They also highlight the need for experimental characterization of organic reactions as irreversible vs. reversible under a

diversity of conditions. In addition, thermodynamic analyses of organic compounds have been applied successfully to only a few natural systems (e.g. Cruse and Seewald, Tassi et al., 2007; Helgeson et al., 1993); these types of calculations have also only been performed for a tiny fraction of the potential organic reactions, mainly the C-, H-, and sometimes O-bearing organic compounds mentioned above. This is in part because thermodynamic data and estimation strategies are relatively scarce for aqueous organic compounds (as compared to gas and liquid phase organics); this is especially true for N-bearing organics when compared to C-, H-, and O-bearing organics (Cabani et al., 1981; Domalski and Hearing, 1993; Belousov and Panov, 1994; Plyasunov and Shock, 2001: numerous references in each). Measurements of thermodynamic property data (e.g., calorimetric and volumetric measurements) are often motivated by the exploration of fundamental physical chemistry (e.g., Archer, 1987; Fenclová et al., 2004), or by industrial and engineering applications (e.g., Shvedov and Tremaine, 1997; Xie and Tremaine, 1999; Collins et al., 2000); these types of studies do not always produce thermodynamic data relevant to environmentally-abundant compounds. However, on occasion the collection of thermodynamic data has been motivated by natural system exploration (e.g., Nichols and Wadso, 1975; Nichols et al., 1976; Touhara et al., 1982; Jolicoeur et al., 1986). Experiments that identify which hydrothermal organic reactions approach metastable equilibrium, and thus would be useful analytical targets in natural systems, could provide guidance and motivation for expanding thermodynamic data sets for individual compounds or reactions relevant to natural system exploration.

Expanding experiments to include organic nitrogen reactions is particularly attractive because N-bearing organics make up a large portion of the organic material in

the biosphere (Fernandez-Reiriz et al., 1989; Simon and Azam, 1989; Delgado et al., 2013), and because the total amount of organic nitrogen that is buried in the terrestrial geosphere may be even greater (Berner, 2006; Boudou et al., 2008). A diversity of organic nitrogen compounds has also been identified in hydrothermally-altered meteorites (e.g., Pizzarello and Shock, 2010), suggesting that the presence of such compounds could be expected in similar abiotic extraterrestrial environments. Many organic nitrogen reactions are very sensitive to pH (e.g., Garrett and Tsau, 1972; Smith and Hansen, 1998) and have the potential to reflect of acidity levels in subsurface fluids. For example, aqueous amines exist in protonated ($R–NH_3^+$) and unprotonated ($R–NH_2$) forms, according to Eq. (7):

$$R–NH_2 + H_2O \rightleftharpoons R–NH_3^+ + OH^- \qquad (7).$$

There is some evidence these forms undergo different hydrothermal reactions that result in different products, some that form reversibly and others irreversibly (e.g., comparing Katritzky et al., 1990; 2001 to Chapter 2 herein). Much is already known about the volatilities of aqueous amines due to their long-time use as anti-corrosives in boiler systems (e.g., Maguire, 1954), more recent interests in amine transport during atmospheric processes (e.g., Leng et al., 2015), and their geo-engineering applications for CO_2 capture (e.g., Du et al., 2017). This makes them even better targets as organics that might be expelled from geologic systems in plumes of gas.

Reversibility has been observed for individual reactions involving amines in some hydrothermal studies, but an approach to metastable equilibrium has only been rarely

demonstrated, especially for multiple, simultaneous reactions. In a detailed kinetics study, Radzicka and Wolfenden (1996) reported empirical equilibrium constants for a variety of hydrothermal (≤ 160°C) amide bond formation reactions by calculating the ratio of forward and reverse reaction rate constants. In terms of whether these reactions actually reach metastable equilibrium, however, no explicit evidence was presented demonstrating these reactions would reach consistent reaction ratios, or whether competing reactions might cause departures from steady state.

Bada and Miller (1968; 1970) comprehensively characterized the primary deamination mechanism for aspartic acid under moderate hydrothermal conditions (≤ 135°C) via a detailed experimental kinetics analysis, demonstrating reversibility as well as rate dependencies on temperature and pH. In these experiments, product concentrations from aspartic acid deamination level off over time, hinting at an approach to steady state. The authors (Bada and Miller, 1968) calculated equilibrium constants for this reaction by letting the forward deamination reaction run to long times; we note they did not obtain reaction ratios from the reverse reaction at long time scales. The authors also point out that ionizable species (such as amines) in reactions of interest can produce *apparent equilibrium* reaction quotients that vary with pH (true equilibrium ratios do not vary with composition, including pH). *Apparent equilibrium* reaction quotients are calculated using the total (protonated and unprotonated) concentrations of products and reactants. This is a useful concept because analytical techniques often yield total concentrations.

Recently, amino acid degradation experiments by Lee et al. (2014) demonstrated an approach toward metastable equilibrium over time for the reversible reaction of

glutamic acid to pyroglutamic acid (i.e., amide bond formation). Their evidence included reaction ratios calculated for the forward reaction that appear to reach consistent values over time. The authors went on to identify an irreversible reaction step in their degradation reaction network that was primarily responsible for the cumulative mass lost from glutamic acid and its reversibly formed products. Characterizing processes that deplete certain organic reservoirs is useful because it could provide comparable timescales of preservation for organic compounds involved in reactions that reach metastable equilibrium.

To build upon this useful body of experimental work, the present study was designed to test whether multiple simultaneous organic reactions would reach metastable equilibrium in a hydrothermal system involving C-, H-, O-, and N-bearing organics. Four sets of experiments were performed, each with a different initial organic compound. Each compound was expected to be part of the same reaction network in a series of potentially reversible amination reactions, from an alcohol to a primary (1°) amine, then a secondary (2°) amine, and then a tertiary (3°) amine. Model compounds with aromatic rings were used to ensure that most organic products could be accurately and precisely quantified using a single analytical technique, gas chromatography. These compounds were: benzyl alcohol, benzylamine, dibenzylamine, and tribenzylamine. The four experimental reactant solutions were prepared with the same bulk composition according to the amount of each initial organic reactant and the addition of ammonium hydroxide (NH_4OH) and ammonium chloride (NH_4Cl); thus, the starting compounds could all theoretically interconvert with one another via the substitution of organic functional groups, water, and ammonia.

Amination reaction quotients calculated over time from these experiments compared to calculated equilibrium constants for amination reactions, provide strong evidence that reactions between the four organic reactants approach metastable equilibrium. Trends in *apparent equilibrium* reaction quotients (i.e., Bada and Miller, 1968) over time provided similar evidence of an approach to metastable equilibrium for two other substitution reactions; these reactions involved new products (not used as reactants), an ether and an imine. There is strong evidence for the irreversible formation of toluene; this reaction has redox implications for the experimental system. Additionally, there is some indication that a diverse suite of multi-ring products forms irreversibly via electrophilic aromatic substitution reactions. This study demonstrates an approach toward metastable equilibrium by multiple, simultaneous organic reactions between C-, H-, O-, and N-bearing organics. It also provides analytical and experimental techniques for robustly testing reversibility vs. irreversibility for hydrothermal reaction networks.

3.2 Experimental

This section describes the materials and techniques used to setup and analyze hydrothermal experiments performed with aqueous organic compounds as well as NH_4OH and NH_4Cl in anoxic, silica glass reaction vessels. It also outlines some calculations performed to establish whether a similar pH could be assumed for experiments containing different initial reactant solutions. Many of the experimental and analytical techniques herein follow those in Chapter 2, as indicated below when relevant.

3.2.1 Materials

Reagents, buffers, standard compounds, and gases were purchased through Sigma-Aldrich (S-A), Mallinckrodt (M), Aldlab Chemicals (AC), Glycopep Chemicals

(G.C.), and Praxair (PA) with the following specifications: ≥ 99.5% benzylamine (S-A), benzylamine hydrochloride (S-A), ≥ 97.0% dibenzylamine (S-A), ≥ 99.0% tribenzylamine (S-A), ≥ 99.8% benzyl alcohol (S-A), ≥ 99.0% *n*-benzylidenebenzylamine (S-A), ≥ 99.9% toluene (S-A), ≥ 99.0% dodecane (S-A), ≥ 99.9% sodium bicarbonate (M), ≥ 99.99% ammonium chloride (S-A), 14.8 M ammonium hydroxide (EMD Chemicals Inc.), ≥ 99.0% bibenzyl (S-A), ≥ 96.0% stilbene (S-A), ≥ 99.0% benzyl ether (S-A), ≥ 99.5% benzaldehyde (S-A), ≥ 95% 3-benzylbenzyl alcohol (AC), ≥ 95% 2-benzylbenzyl alcohol (AC), ≥ 98.0% (4-benzylphenyl)methanol (G.C.), ≥ 99.999% ultra high purity (UHP) helium (PA), ≥ 99.999% UHP argon (PA), ≥ 99.95% H_2 (PA), and ≥ 99.5% O_2 (PA), ≥ 99% methanesulfonic acid (Acros Organics), mixed ion standard (Thermo Scientific, Waltham, MA, USA), and mixed cation standard (Environmental Express, Charleston, SC, USA). Reaction vessel materials were purchased from GM Associates and Technical Glass Products as 2 x 6 mm (inner diameter x outer diameter) "fused quartz" (silica) tubing.

3.2.2 Analytical techniques

Gas chromatography flame ionization detection (GC-FID) and mass spectrometry (GC-MS) were employed to ensure organic compound purity and to develop calibration curves used to quantify product abundances in experiments, as previously described in Chapter 2. Unlike the previous methods, however, response factors derived from dibenzylamine and tribenzylamine calibration curves were used to estimate total concentrations of numerous low abundance unidentified compounds that populated the two phenyl and three phenyl ring-bearing product regions of the GC chromatograms, respectively. Benzyl ether calibration curves were used to obtain the approximate

concentrations for the identified benzyl-benzyl ethers, which were included in cumulative two ring product estimates. Liquid/liquid organic extraction and sample storage methods for experimental analysis exactly followed those of Chapter 2. Concentrations of total ammonia ($NH_3 + NH_4^+$, referred to as ΣNH_3 for the remainder of this study) were quantified via ion chromatography with suppressed conductivity detection for a subset of experiments. The aqueous phases of replicate 72-hour experiments (quantitative GC and IC analysis could not be performed on the same sample) for each of the four sets of experiments (described below in Section 3.2.3) were analyzed using methods described in Chapter 2. The abundances of nitrogen-bearing organic compounds were used to estimate the ΣNH_3 for all other experimental time points, as described in Appendix B and shown in Table B1.

3.2.3 Experimental setup

Reactant solutions were prepared using anoxic methods; 300 μL was loaded into each silica glass reaction vessel and sealed, as described in Chapter 2. The reaction vessels were placed in preheated screw-capped iron pipes in a 250°C oven; this was considered the experimental starting time (t = 0 hours). Note that this is different from the methods in Chapter 2, where the designated starting time began after a heating period, because the study focused on kinetics. At the end of the desired reaction time, the pipes were removed from the oven and submerged in room temperature water to quench the experiments. The reaction vessels were then subsequently frozen until analysis. Details concerning the equipment and techniques used regarding the anoxic, heating, quenching, and storage methods can be found in Chapter 2.

Four aqueous reactant solutions with different starting materials were prepared for each set of experiments according to the initial reactant ratios in Fig. 12. Alcohol experiments were prepared with 0.5 molal benzyl alcohol, 0.25 molal NH_4Cl, and 0.25 molal ammonium hydroxide (NH_4OH). Primary amine experiments were prepared with 0.25 molal benzylamine and 0.25 molal benzylamine hydrochloride. Secondary amine experiments were prepared with 0.25 molal dibenzylamine and 0.25 molal NH_4Cl. Tertiary amine experiments were prepared with 0.167 molal tribenzylamine, 0.25 molal NH_4Cl, and 0.083 molal NH_4OH. Each reactant solution was prepared with the same bulk composition, based on the stoichiometry shown in Fig. 12; thus, they all could hypothetically be transformed into one another via substitution reactions.

Aqueous amines, like NH_3, rapidly speciate into protonated and unprotonated forms (see Eq. 7). The speciation of amines in water therefore affects solution pH. Additionally, the protonated and unprotonated forms of the various amines are expected to have unique reaction paths (compare Chapter 2 with Katritzky et al., 1990; 2001). Equal molar concentrations of protonated and unprotonated amines (including NH_3) were added to all experiments in an attempt to establish pH-buffered conditions via the reactants themselves (Fig. 12). The four sets of experiments were expected to have similar initial pH and fairly consistent pH over reaction time due to the similar 25°C pK_a values for ammonium (9.2; Read, 1982), benzylaminium (9.4; Carothers et al., 1927; Richner, 2013), and dibenzylaminium (8.52; Graton et al., 2001) (tribenzylaminium has an abnormal pK_a, discussed below). Additionally, changes in experimentally determined pK_a values across temperature for a variety of other aminium compounds are fairly consistent, as seen in Fig. 13. For experiments starting with benzyl alcohol (not shown in

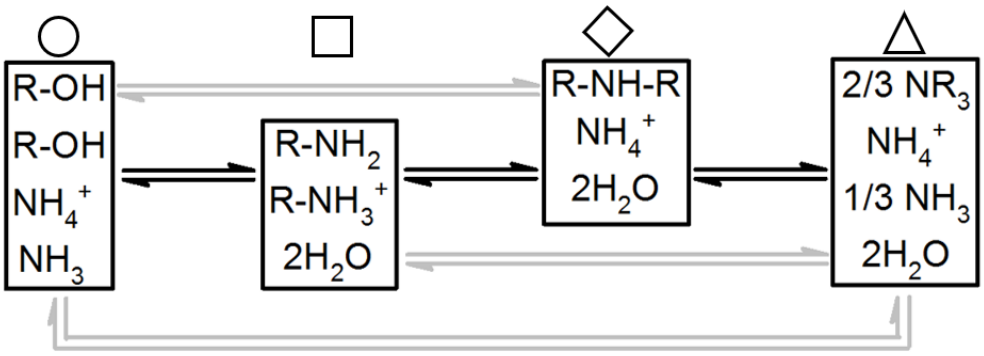

Fig. 12. Stoichiometric ratios of initial reactants used in each of the four sets of hydrothermal (250°C, 40 bar) experiments. Black reversible arrows indicate bulk transformations that produce and then increase the degree of amines via amination reactions from left to right, beginning with alcohols and ending with tertiary amines. Grey reversible arrows indicate chemical mass balance between all initial reactants. Preparation of experiments included the following reactants: (with corresponding short hand): benzyl alcohol (R-OH), ammonium chloride (NH_4^+ in this figure only), ammonium hydroxide (NH_3 in this figure only), benzylamine ($R\text{-}NH_2$), benzylamine hydrochloride ($R\text{-}NH_3^+$), dibenzylamine (R-NH-R), and tribenzylamine (NR_3). Since water is the solvent and its concentration changes negligibly during reactions, its stoichiometry can be ignored. The geometric symbols are used to illustrate experimental results from different starting reactant solutions in Fig. 15 and 20.

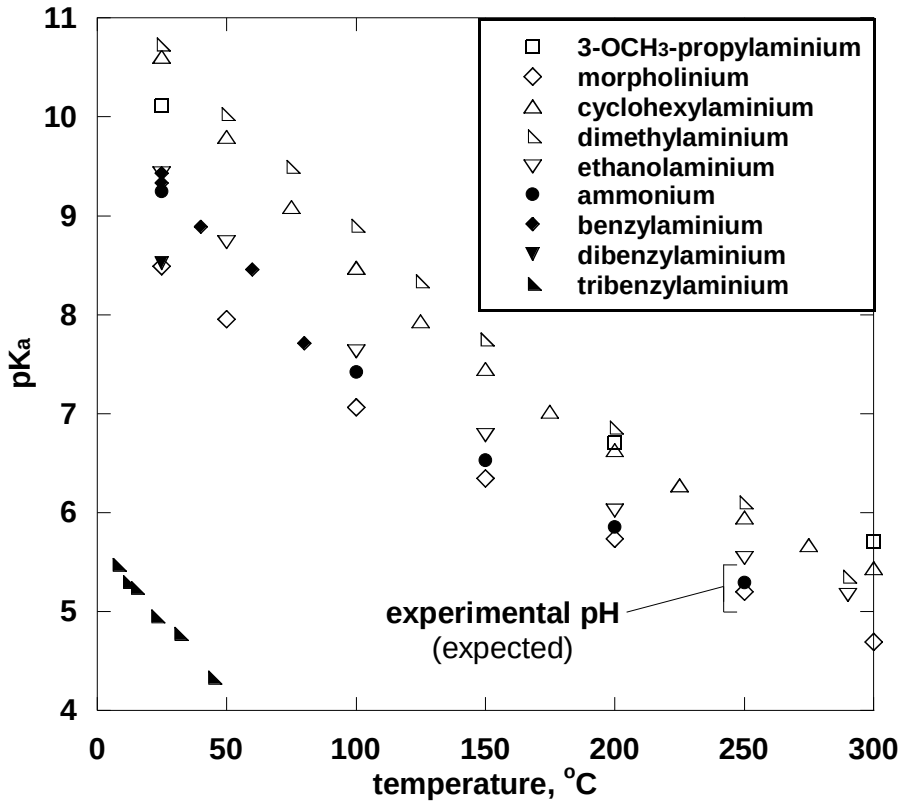

Fig. 13. Experimentally measured pK_a values vs. temperature for ammonium (Read, 1982) and a variety of protonated amines, including: 3-methoxypropylaminium (Rhee et al., 2010), morpholinium (Ridley et al., 2000), cyclohexylaminium (Mesmer and Hitch, 1977), dimethylaminium (Bénézeth et al., 2001; Bergström and Olofsson, 1977), ethanolaminium (Bénézeth et al., 2003), benzylaminium (Bunting and Stefanidis, 1990; Hanai et al., 1997; Richner, 2013), dibenzylaminium (Graton et al., 2001), and tribenzylaminium (Canle L. et al., 2004). Since ΣNH_3, Σbenzylamine (analogous to ΣNH_3), and/or Σdibenzylamine, are the most abundant buffer species for all experiments at any given time (even for tribenzylamine experiments), the pH is expected to fall within the pK_a values of the aminium compounds at 250°C (P_{sat}). Modified after Fig. 2 in Chapter 2.

the figure), which presumably has very little effect on solution pH, equilibrium between NH_3 and NH_4^+ was expected to provide sufficient pH-buffering capacity. Tribenzylaminium is an anomalously acidic aminium (pK_a = 4.9 at 25°C; Canle L. et al., 2004). Because of this, thermodynamic calculations were performed to test the buffer capacity of NH_3/NH_4^+ in the tribenzylamine experimental time series using the chemical speciation software EQ36 (Wolery, 1992) and thermodynamic data and property estimations therein (Kelley, 1960; Wagman et al., 1982; Tanger and Helgeson, 1988; Shock et al., 1989; 1990; 1992; 1997). The results of the calculations indicate that a 0.25 molal NH_4Cl and 0.25 molal NH_4OH solution at room temperature (measured $pH_{25°C}$ = 9.3) would have a pH of 5.4 at 250°C. Tribenzylamine was conservatively assumed to have no basic (proton accepting) properties. This is shown to be a good assumption according to thermodynamic estimations explained in more detail in Appendix C. Accordingly, a solution of 0.083 molal NH_4OH and 0.25 molal NH_4Cl was mixed at room temperature (measured $pH_{25°C}$ = 8.9), leaving out the 0.167 molal tribenzylamine. The calculated pH for this solution at 250°C was 5.0. This conservative assumption sets a maximum pH deviation (-0.4) at the outset of tribenzylamine experiments; this difference should decrease in magnitude as tribenzylamine reacts to form other amines (see below).

3.3 Results and Discussion

The hydrothermal experiments (250°C, P_{sat}) with different initial organic reactants (i.e., benzyl alcohol, benzylamine, dibenzylamine, and tribenzylamine (Fig. 12)), each produce detectable abundances of the three other compounds even at the shortest reaction time (2 hours; Table B2). At the longest reaction time (72 hours), each set of experiments produces similar compositions of buffering species (amines and ΣNH_3) supporting our

expectations that the pH for all sets of experiments should be very similar. Additionally, by 72 hours ammonia and ammonium are the dominant buffering species in all four sets of experiments. Toluene and dibenzylimine were also detectable throughout all experiments, resulting from reduction and oxidation (redox) reactions, respectively. Two minor products were also monitored throughout experiments, benzyl ether and benzaldehyde; the latter is also an oxidation product relative to the starting materials. A gas chromatogram of the major products is shown in Fig. B1. Determining whether reactions involving these eight compounds approach metastable equilibrium was the focus of this study.

3.3.1 Reversible substitution reactions

Substitution reactions involve the loss of one organic functional group and replacement by another. The formation of all four initial reactants in each experiment starting with only one compound suggests that substitution reactions occur, and are probably reversible under experimental conditions. Whether substitution reactions between organic compounds in this study were approaching metastable equilibrium was assessed by calculating *apparent equilibrium* reaction quotients for a variety of reactions in each experiment. Balanced reaction equations for a series of substitution reactions are shown in Fig. 14. These reactions are (1) dehydration of benzyl alcohol and amination by NH_3 to form benzylamine and H_2O, (2) deamination of benzylamine and amination by benzylamine to form dibenzylamine and NH_3, and (3) deamination of benzylamine and amination by dibenzylamine to form tribenzylamine and NH_3. Reactions (4) and (5) show substitution reactions involving the initial reactants as well as novel products. These reactions are: (4) dehydration of benzyl alcohol and reaction with another benzyl alcohol

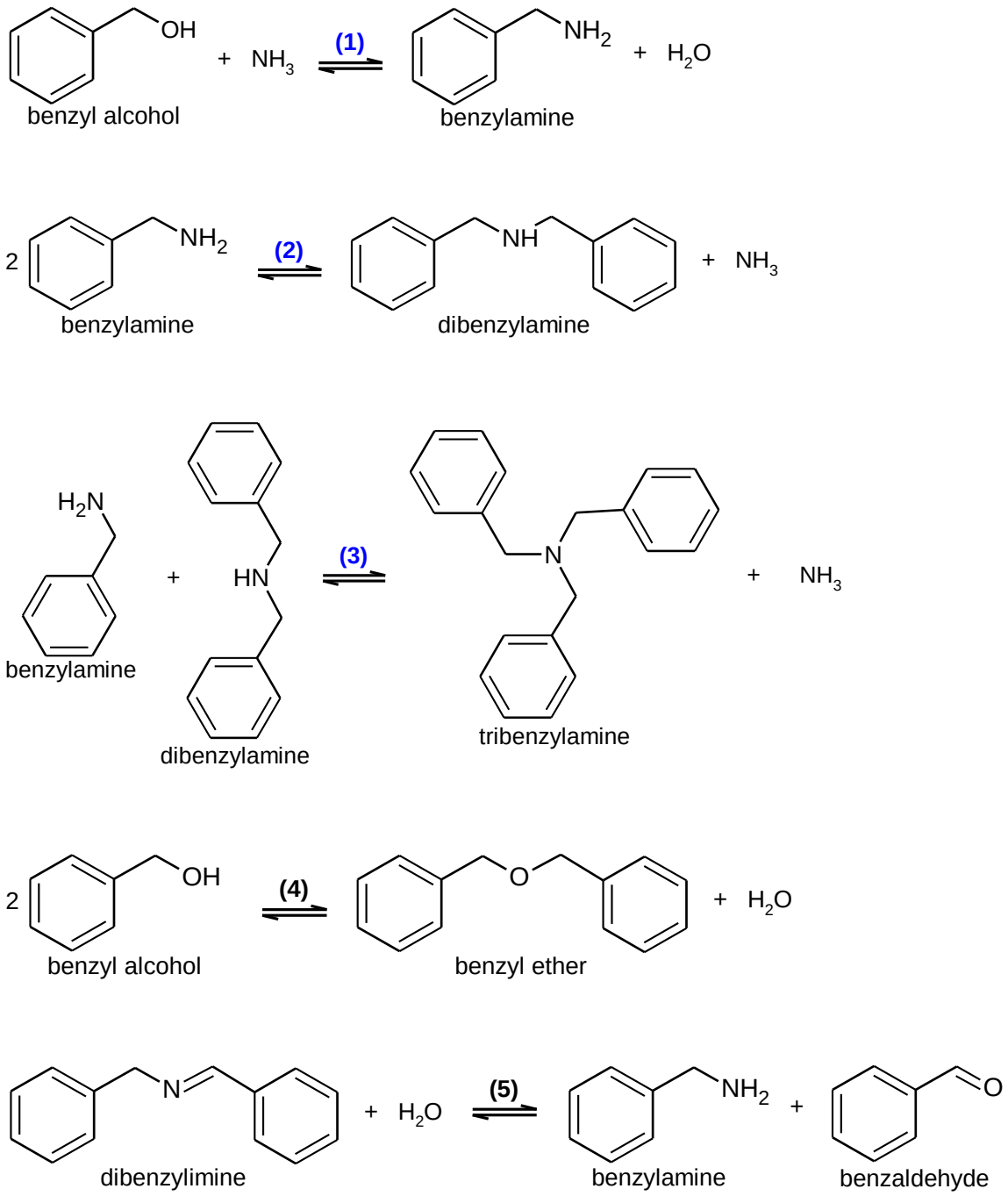

Fig. 14. Balanced reactions used to calculate reaction quotients for experiments, shown in Fig. 15 and 20. Reactions (1), (2), and (3) are amination reactions that that produce primary, secondary, and tertiary amines, respectively. Reactions (4) and (5) each involve at least one novel compound that was not used as an initial reactant in the experiments. All are substitution reactions except (5), which is technically an addition reaction followed by an elimination reaction; overall reaction (5) substitutes one organic functional group for another.

to form benzyl ether and H_2O, and (5) hydration of dibenzylimine followed by deamination to form benzaldehyde and benzylamine. The last reaction (5) is technically an addition reaction followed by an elimination reaction, but the combined effect of these two processes results in the substitution of one functional group for another. All of these reactions are expected to take place via ionic mechanisms (Clayden et al., 2001).

Reactions (1 – 3) in Fig. 14, numbered blue, share similarities to the reaction equations used to demonstrate stoichimetric balance for the reactant solutions shown in Fig. 12. Each number represents an amination reaction that increases the degree of the product amine. Unlike the stoichiometry shown in Fig. 12, the reaction equations in Fig. 14 are written with neutral species only. Alternative amination reactions to those shown in Fig. 14 can be written, but only three can be considered without redundancy. This stems from the fact that there are six different compounds involved in these amination reactions and four different compounds involved in each reaction (two reactants and two products). Reactions (1), (2), and (3) were chosen over alternatives based on organic chemistry principles of nucleophilicity, steric hindrance, and leaving group stability (Clayden et al., 2001). *Apparent equilibrium* reaction quotients (Bada et al., 1970) were calculated for Reactions (1 – 5) (Fig. 14) using total compound concentrations, as approximations for activities, for each set of experiments over time, as shown in Fig. 15. When calculating reaction quotients, H_2O was was assumed to be in its pure standard state since it was the experimental solvent; thus, H_2O is not shown in the calculation. Each plot in this Fig. 15 represents a different reaction, and each geometric symbol indicates which starting compound reacted to produce the given *apparent equilibrium* reaction quotient. The general trend for plots (1), (2), and (3) in Fig. 15 is a convergence

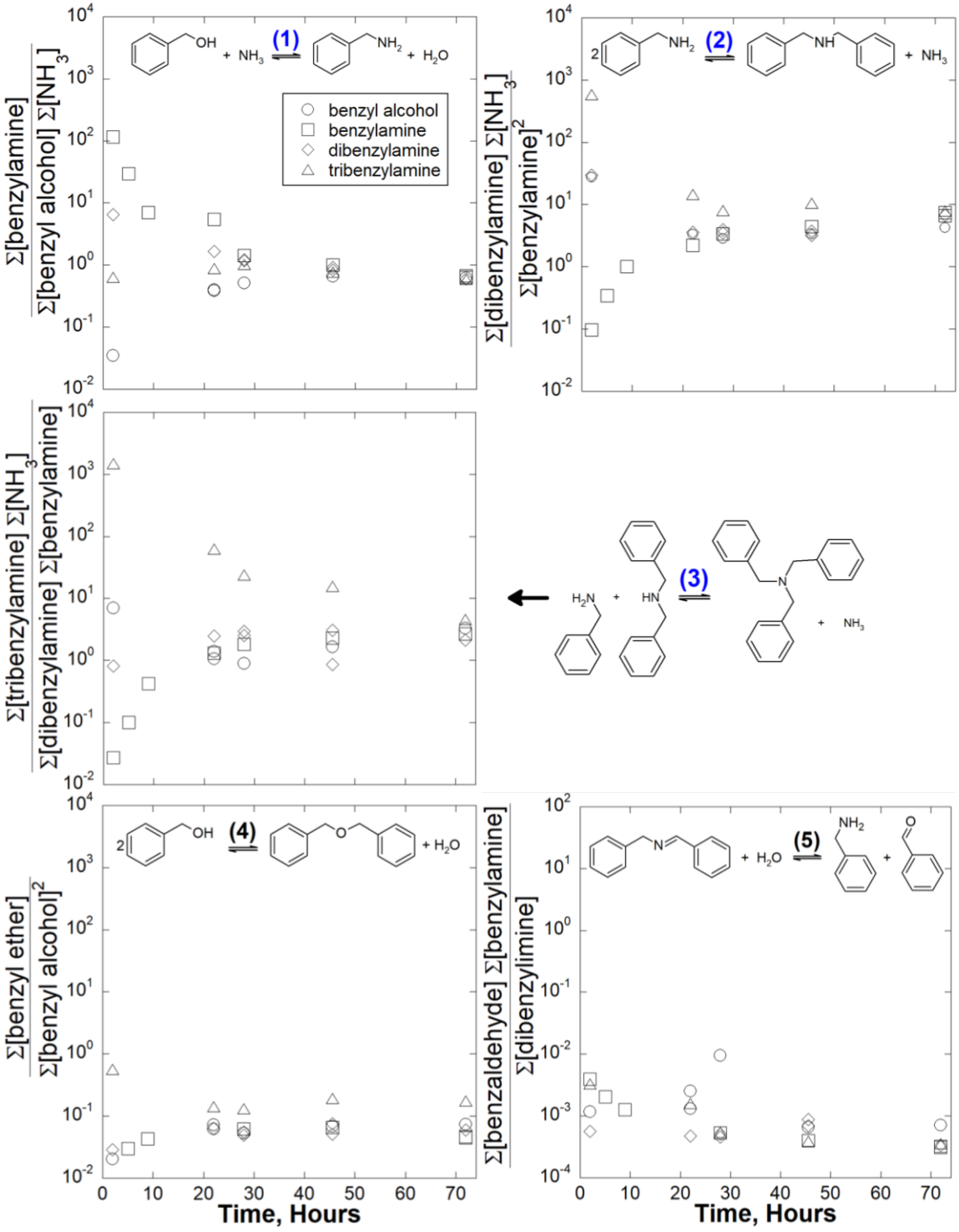

Fig. 15. *Apparent equilibrium* reaction quotients vs. time, calculated using total compound concentrations (Σ) as measured by GC or IC, for experiments conducted at 250°C and P_{sat}. Values are shown for four sets of experiments with different initial organic reactants, as indicated by geometric symbols. The reactions represented are shown and numbered, corresponding to Fig. 14. The convergence of *apparent equilibrium* reaction quotients over time provides evidence for reversibility and an approach toward metastable equilibrium from the different starting conditions.

of *apparent equilibrium* reaction quotients (geometric symbols) over time, regardless of starting composition. This provides strong evidence for the reversibility of these amination reactions, as well as an approach toward metastable equilibrium. For each reaction (one per plot), compound ratios from different experiments converge at different rates. For example, the *apparent equilibrium* reaction quotients for benzylamine formation from benzyl alcohol (1) seem to converge by 45.5 hours, while those for tribenzylamine formation from benzylamine and dibenzylamine (3) seem to converge by 72 hours, suggesting more rapid reversibility for benzylamine formation. The *apparent equilibrium* reaction quotients calculated for reaction (4) are very near in value after only 2 hours, and also remain fairly consistent over time, suggesting this reaction approaches metastable equilibrium very quickly. The same can be seen for reaction (5).

Deviations from these general trends of convergence for the calculated *apparent equilibrium* reaction quotients seem to be mainly attributable to the set of experiments with tribenzylamine as the initial reactant (triangles). These experiments are typically the slowest to achieve stable reaction ratios. We hypothesize that this is due to the anomalously low pK_a of tribenzylamine, which likely favors its neutral form relative to the other amines (Fig. 13). Protonated amines are much better "leaving groups" than unprotonated amines (Clayden et al., 2001), based on the pK_b (a proxy for stability) of NH_3 versus NH_2^-, and thus participate more readily in substitution reactions shown in Fig. 14. Indeed, experiments starting with benzylamine and dibenzylamine both show ~64% conversion by 22 hours; in contrast, tribenzylamine experiments at similar times have less conversion (~53%). Note, the conversion calculations were performed after normalizing the initial reactants to 100% at 2 hours to avoid irregularities in

decomposition rates that may have been caused by reaction vessel heating times upon placement into the oven (Section 3.2.3).

3.3.2 Irreversible substitution reactions

Although there is strong evidence for an approach toward metastable equilibria for the reactions mentioned above, there is an overall loss of mass from compounds in the apparent metastable system of C-, H-, O-, and N-bearing organics over reaction time. By 72 hours, the seven organic compounds shown in Fig. 14. only account for ~50 mole% of the starting materials (Table B2); mole% was calculated in terms of phenyl rings (e.g., 1 equivalent of dibenzylamine ≡ 2 equivalents of phenyl rings). Therefore, one or more of these compounds must undergo reactions not represented in Fig. 14 and 15.

As with tribenzylamine, benzyl alcohol also decomposes more slowly than the other amines (~36% conversion at 22 hours). This can be attributed to the fact that benzyl alcohol should be the least protonated of the initial reactants, and hydroxide (OH^-) is a worse leaving group than NH_3 (based on pK_b). There is evidence that the small fraction of benzyl alcohol that becomes protonated is highly reactive (Chapter 2), but it mostly dehydrates and (re)hydrates via the water solvent to reform benzyl alcohol. Previous hydrothermal experiments suggest that benzyl alcohol undergoes dehydration followed by electrophilic aromatic substitution reactions with phenyl groups in solution (Fecteau, 2016), especially under acidic conditions (Chapter 2). This latter finding follows the same logic concerning leaving groups: since H_2O is a better leaving group than OH^- according to pK_b. In previous studies, the *ortho*, *para*, and *meta* isomers of benzyl-benzyl alcohol were identified as electrophilic aromatic substitution products (Fecteau, 2016; Chapter 2). In the present study, the same three isomers were detected in all 72-hour experiments.

The summed concentration of benzyl-benzyl alcohol isomers is greatest in experiments with benzyl alcohol as the initial reactant (~1.5 mole%, in terms of phenyl rings) relative to experiments with amines as the initial reactants (~0.5 mole%). This finding corroborates evidence from the studies mentioned above, that benzyl alcohol serves as a precursor to electrophilic aromatic substitution reactions under hydrothermal conditions.

In addition to the benzyl-bendzyl alcohol isomers, numerous other small peaks (> 100 peaks at 72 hours) were observed in the GC-FID chromatograms (Fig. B1). These compounds were not identified, but the apparent high diversity and low abundance of these products supports the occurrence of electrophilic aromatic substitution reactions, since electrophilic aromatic subsitution reactions are expected to be nonselective due to the high reactivity of benzyl cations with variety of different aromatic structures in solution. The retention times of these unidentified peaks correspond to distinct two, three, and four phenyl ring-bearing product regions of the chromatograms. The groups of peaks look similar to those observed in Chapter 2, which provided evidence for electrophilic aromatic substitution reactions involving benzyl alcohol. The four ring product region was composed of mostly small, poorly resolved peaks. Because no four ring products were identified, any proxy compound would lilkely be unreliable for estimating product abundances. Therefore, cumulative concentrations were only estimated for two and three ring product regions (see Section 3.2.2 and Table B2).

Estimates of two and three ring product concentrations are shown in Fig. 16. The highest concentrations of the multi-ring compounds are found in benzyl alcohol experiments (circles). Additionally, tribenzylamine expriments accumulate the least of

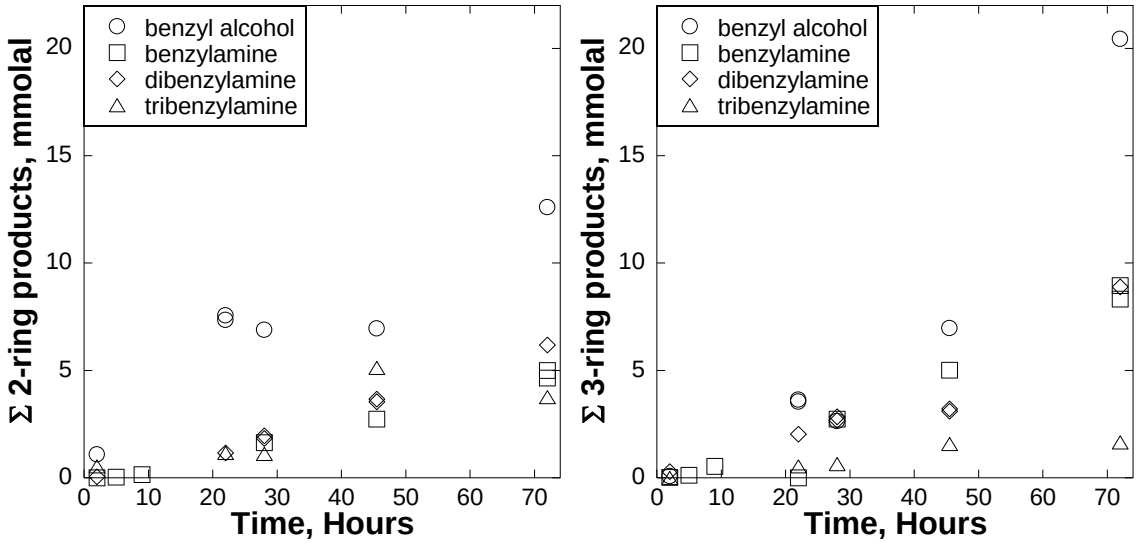

Fig. 16. Cumulative concentrations of unidentified multi-ring compounds vs. time for the four sets of experiments, that began with benzyl alcohol (circles), benzylamine (squares), dibenzylamine (diamonds), and tribenzylamine (triangles). Unidentified two ring products (left) were quantified using the GC-FID response factor of dibenzylamine, and unidentified 3-ring products (right) were quantified using the response factor of tribenzylamine (Section 3.2.2).

these two and three ring products over time. This is presumably because these same experiments accumulate benzyl alcohol more slowly than the other amine experiments (Table B2). Since these findings corroborate evidence for electrophilic aromatic substitution reactions of benzyl alcohol from previous studies (Fecteau, 2016; Chapter 2), we hypothesize that these unidentified multi-ring compounds are mainly products of electrophilic aromatic substitution reactions.

Since electrophilic aromatic substitution reactions produce C–C bonds, which are recalcitrant with respect to further substitution chemistry, it is possible they represent an irreversible loss of mass from the metastable reservoir of C-, H-, O-, and N-bearing organics (Fig. 14 and 15). If the proposed electrophilic aromatic substitution products are forming reversibly, their concentrations over time should level off and approach steady state concentrations. However, for each set of experiments the sums of these unidentified products do not reach consistent values, and in some cases, increase more over time (Fig. 16). In experiments starting with benzyl alcohol, cumulative concentrations of the seven reversibly formed organic compounds (Fig. 14) decrease faster than in the other sets of experiments and show no sign of approaching steady state (Table B2). This suggests that the formation of electrophilic aromatic substitution products from benzyl alcohol could be a dominant irreversible reaction pathway from the metastable system.

3.3.3 Redox Reactions

The production of dibenzylimine and toluene during each of the four sets of experiments indicates that organic carbon oxidation and reduction reactions are occuring. The formation of these two compounds involve production and consumption of hydrogen atoms (H), respectively, as shown in Fig. 17.

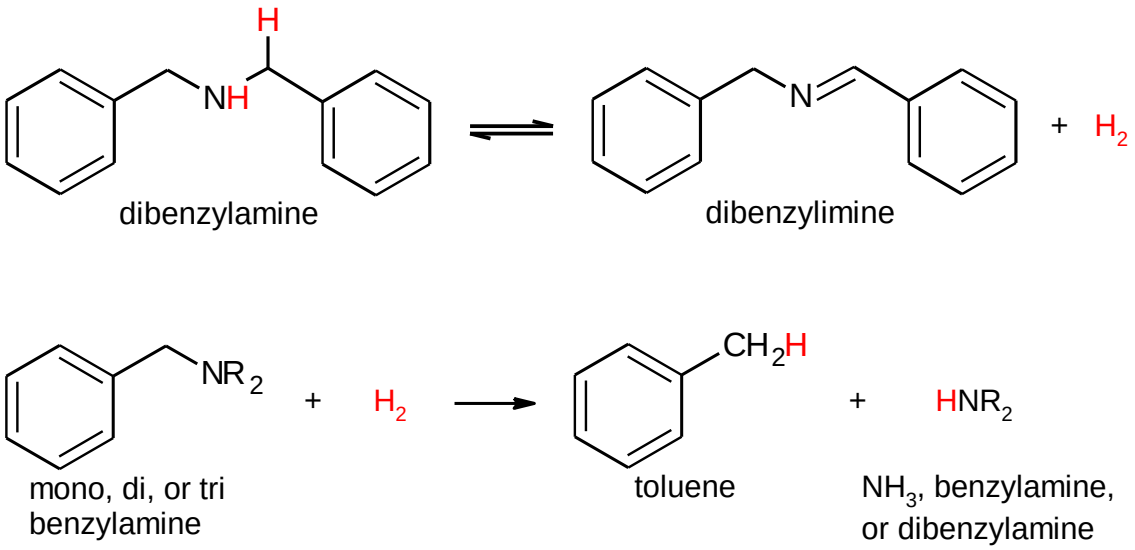

Fig. 17. Redox reactions showing the dehydrogenation of dibenzylamine to form dibenzylimine (top), and the reductive hydrogenolysis of mono, di, or tribenzylamine to form toluene and an amine of a lower degree. The transfer of hydrogen atoms (H) is tracked with red labels, illustrating that the reactions might be linked by H_2 production and consumption. If the two reactions are combined, H_2 cancels from the products and reactants. The single arrow indicates that toluene formation is proposed to be irreversible (see below).

In order to test whether these redox reactions are linked by the transfer of hydrogen, the dibenzylimine:toluene ratio was calculated for all experiments, as seen in Fig. 18. Except for a single experiment, these ratios are always ≥ 1. At early reaction times the ratios range from ~1 to 17; at longer times the ratios converge and approach values slightly greater than unity (1.14 to 1.18 at 72 hours). Based on these trends, we hypothesize that dibenzylimine and H_2 are produced first via dibenzylamine oxidation (i.e, dehydrogenation, top reaction in Fig. 17). Next, the resulting H_2 is proposed to participate in hydrogenolysis of amines in solution to form toluene and NH_3 (bottom reaction in Fig. 17). Note, this interpretation requires H_2 to be available first for C–N bonds to be reduced in this way.

Further evidence for this series of reactions comes from the differences in the dibenzylimine:toluene ratios for the four sets of experiments at 2 and 22 hours, prior to their convergence (Fig. 18). First, the generally high dibenzylimine:toluene ratios for benzyl alcohol experiments (shown as circles) indicate that toluene formation is sluggish relative to dibenzylimine formation in those experiments. This could be because the homolytic dissociation energy of C–O bonds is greater than that of C–N bonds (~83 vs ~72 kcal $mole^{-1}$, respectively; Blanksby and Ellison, 2003); therefore, toluene is formed more slowly from benzyl alcohol than from the amines. At longer reaction times, after sufficient concentrations amines are produced via the amination of benzyl alcohol, toluene concentrations approach those of dibenzylimine. Additionally, the descending dibenzylimine:toluene ratios correlates to their descending pK_a values for each of the starting amines used in experiments. This suggests that their neutral, unprotonated

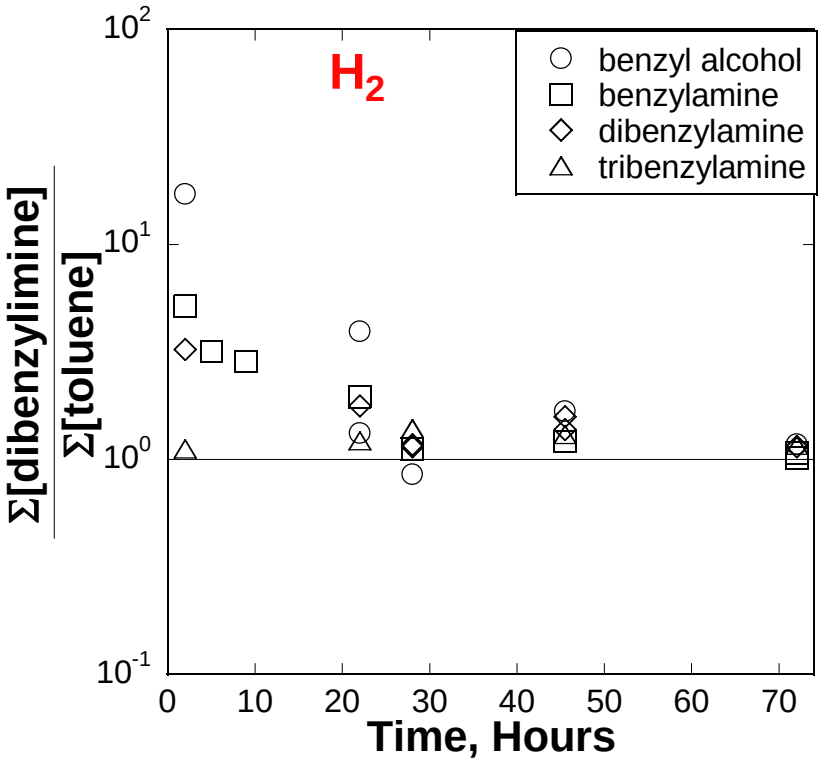

Fig. 18. The ratio of Σdibenzylimine:Σtoluene vs. time in each of the four sets of experiments, that began with benzyl alcohol (circles), benzylamine (squares), dibenzylamine (diamonds), and tribenzylamine (triangles).

forms undergo hydrogenolysis, while their protonated forms do not (or do so much more slowly). Previous experiments under similar low pH (3.3) buffered hydrothermal conditions (250°C), demonstrated that benzylamine produces very little toluene (< 0.2 mole% at 140 hours; see Chapter 2). In constrast, in unbuffered experiments that should heavily favor unprotonated benzylamine, toluene is the dominant product (~73 mole% at 120 hours; Katritzky et al., 1990). Accordingly, the solution pH (5.4) in the present study relative to the two aforementioned (Katritzky et al., 1990; Chapter 2) is intermediate, and intermediate amounts of toluene were observed (~1 to 5 mole % toluene at 72 hours). This suggests an intermediate amount of toluene would be expected at time scales comparable to the two aforementioned studies. Therefore, higher pH seems to promote the hydrogenolysis of amines to form alkyl groups and ammonia. Bibenzyl, a common product of benzyl radical coupling, was also observed in 72-hour experiments at concentrations up to ~1 mole %, suggesting that the mechanism for hydrogenolysis may involve radical intermediates.

The potential for the reversibility of both redox reactions (Fig. 17) was investigated with additional experiments. A 142-hour experiment with 0.5 molal toluene and 0.5 molal NH_4OH was performed (in duplicate) under the same hydrothermal conditions as the other experiments. No benzylamine or other products were observed, indicating toluene formation was not reversible. A similar experiment, with 0.25 molal dibenzylimine and 0.1 molal phosphate buffer (calculated pH of ~4 at 250°C), generated ~0.01 molal (4 mole%) dibenzylamine after 8 hours. This suggests that dibenzylimine reduction is fairly rapid, and further that dibenzylamine dehydrogenation is potentially

reversible. It was not obvious which organic product was oxidized to provide H or H_2 needed for the reduction to dibenzylamine.

3.3.4 Hydrothermal reaction pathways for C-, H-, O-, and N-bearing organics

This study into potential reversibility and metastable equilibria for substitution and redox reactions between C-, H-, O-, and N-bearing organic compounds under hydrothermal conditions has provided sufficient information to generate a reaction pathway scheme (Fig. 19). The initial reactants used in experiments are shown in boxes and their interconversion reactions are numbered in blue (as in Fig. 14). The proposed reversible reactions (parallel opposing arrows) are informed in most cases by the convergence of *apparent equilibrium* reaction quotients, as with reactions (1 – 5) from Fig. 14 and 15. In certain cases, reversible vs. irreversible reactions (single arrows) were determined by additional experiments, as with dibenzylimine and toluene formation (Section 3.3.3). There is also evidence for irreversible electrophilic aromatic substitution reactions that form multi-ring products, based on the steadily increasing concentrations of unidentified 2 and 3 phenyl ring products over time (Fig. 16), in addition to the expectation that typical C–C bonds are less reactive in terms of substitution chemistry than C–O or C–N bonds (Clayden et al., 2001).

3.3.5 Independent equilibrium constant calculations

In experiments with different starting compositions, the observation of *apparent equilibrium* reaction quotients converging to similar values over time provides strong evidence for an approach to metastable equilibrium (as in Fig. 15). For the amination reactions (1 – 3) of Fig. 14, we further tested the approach to metastable equilibrium by comparing independently calculated equilibrium constants for these

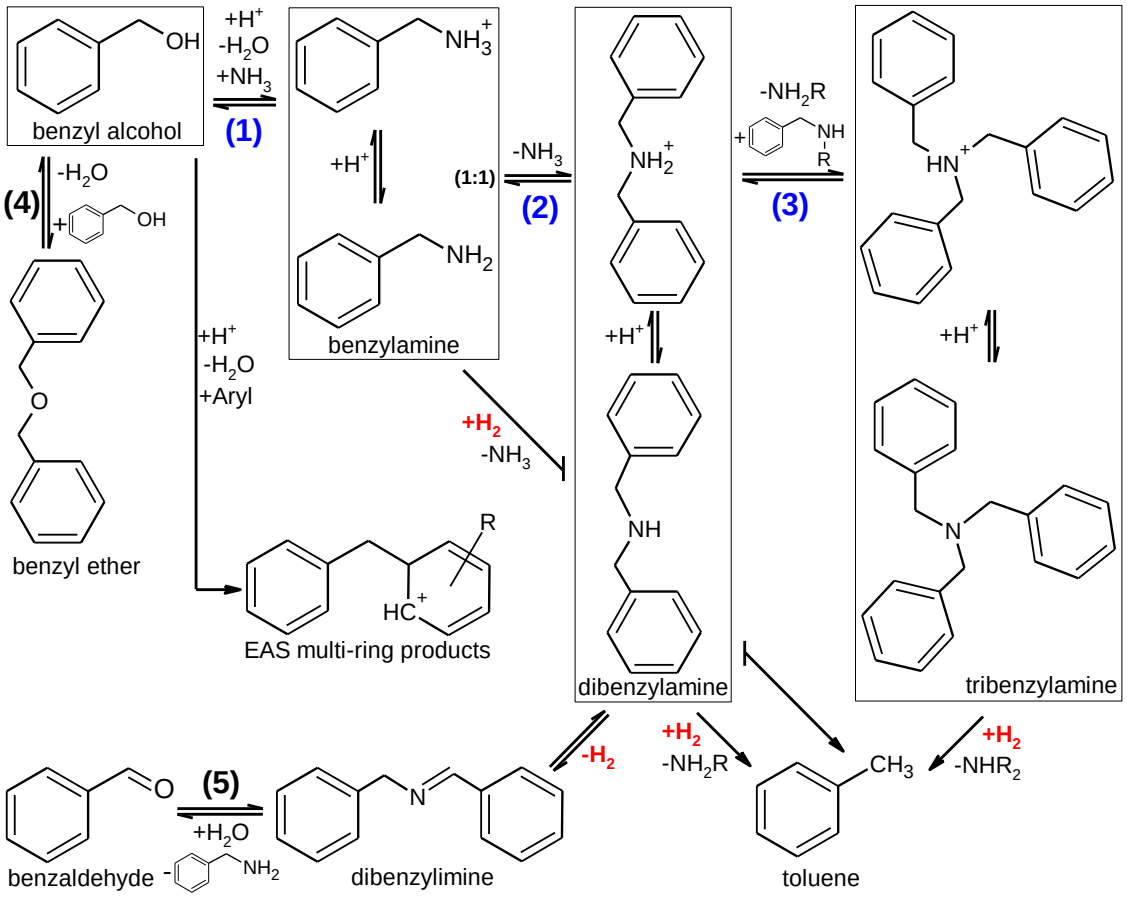

Fig. 19. A proposed hydrothermal reaction network for C-, H-, O-, and N-bearing organic compounds observed in experiments (250°C, P_{sat}). Parallel opposing arrows indicate reversible reactions, while single arrows indicate irreversible reactions. Numbered reactions (blue for amination/deamination) follow those in Fig. 14. Redox reactions are identified by addition or loss of H_2, labeled red as in Fig. 18. Products of electrophilic aromatic substitution reactions are labeled "EAS multi-ring products."

reactions with the experimentally-determined (empirical) reaction quotients. To make this comparison, it was necessary to calculate the concentrations of the neutral forms of the amines and NH_3, since *apparent equilibrium* reaction quotients (Bada et al., 1970) that use total concentrations, as in Fig. 15, do not relate to individual reactions, and thus cannot becompared to reaction equilibrium constants. Quantifying the neutral species required calculating dissociation constants for the aminium species. The estimates of the amination reaction constants and aminium dissociation constants were achieved at experimental conditions (250°C, P_{sat}) by using existing standard state thermodynamic data (at 25°C), new group contribution correlation strategies for primary, secondary, and tertiary amines and aminiums, and the revised Helgeson-Kirkham-Flowers (HKF) equations of state via the Microsoft Excel-based Deep Earth Water (DEW) model (Kelley, 1960; Wagman et al., 1982; Tanger and Helgeson, 1988; Shock et al., 1989; 1990 Sverjensky et al., 2014). A complete description of these methods, including previous literature sources, is found in Appendix C.

The results of these thermodynamic calculations are shown in Fig. 20. The reaction quotients for the amination reactions (1 – 3) from Fig. 14 were calculated with only neutral compound concentrations for each of the four sets of experiments over time, along with equilibrium constants calculated for each amination reaction using the HKF equations of state. The calculations assume concentrations are equal to activities, while H_2O is treated as being in its standard state, and does not appear in the reaction quotient for reaction (1). The empirical reaction quotients are mostly in good agreement with the independently calculated equilibrium constants. The independently calculated equilibrium constants for reactions (1), (2), and (3) are 2.30, 1.02, and 1.02, respectively.

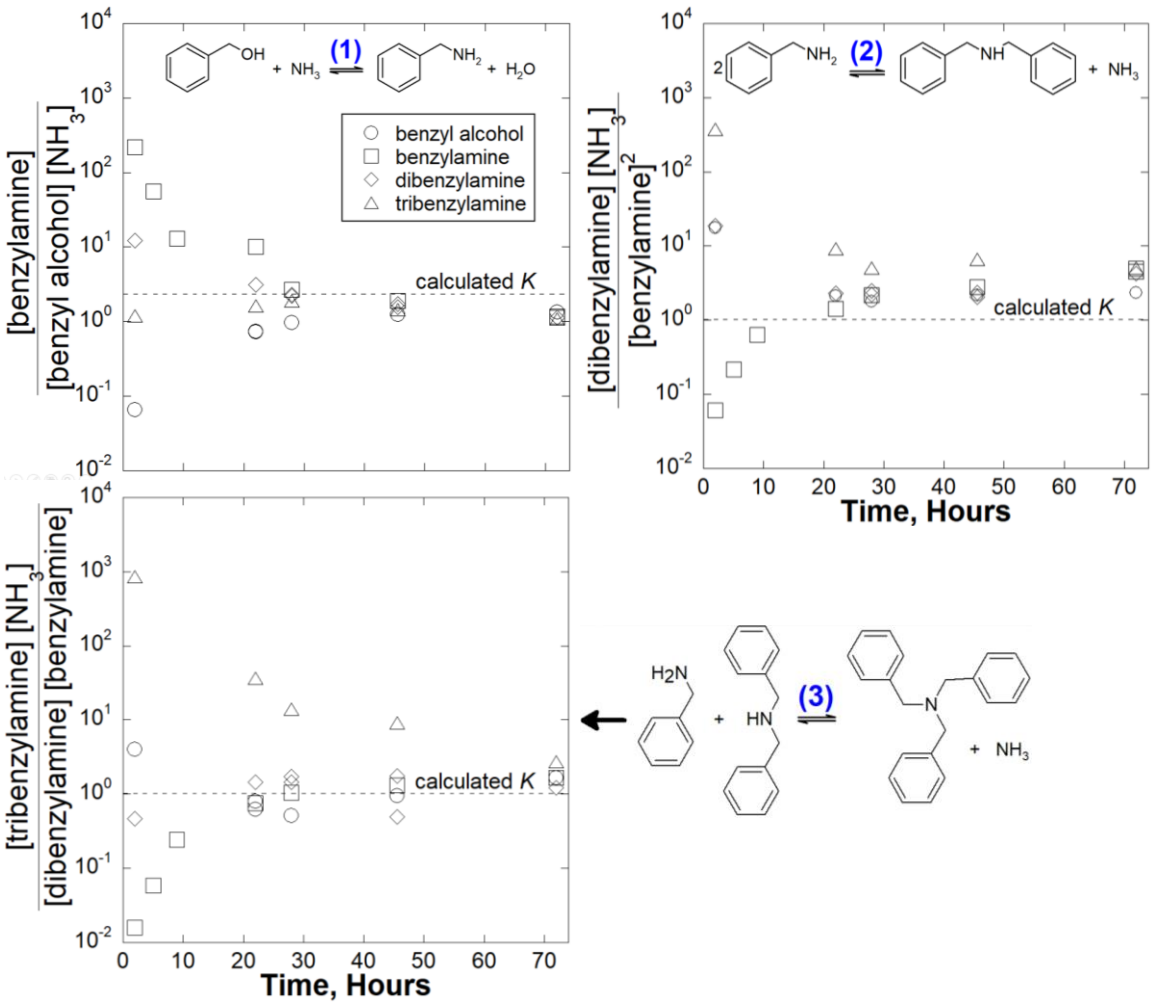

Fig. 20. Reaction quotients calculated using neutral compound concentrations vs. time, compared to calculated equilibrium constants (dashed lines) for each reaction (250°C and P_{sat}). Data symbols and depicted reactions follow those in Fig. 14 and 15. Amine dissociation constants, used to calculate neutral compound concentrations, and reaction equilibrium constants were both calculated using a variety of thermodynamic data and estimation strategies (Appenidx C).

Comparatively, the empirical 72-hour reaction quotients averaged from the four sets of experiments at 72 hours are 1.17 ± 0.10, 4.24 ± 1.11, and 1.78 ± 0.55, respectively (uncertainties are ±1 standard deviation).

The deviation from agreement between the empirical reaction quotients and the calculated equilibrium constants (Fig. 20) may be systematic, according to whether benzylamine is a reactant or a product in the reaction. For example: when benzylamine is a product, as for reaction (1), the reaction quotient is slightly lower than the equilibrium constant; when benzylamine is a reactant, as for reaction (3), the reaction quotient is slightly higher than the equilibrium constant; lastly, when there are two benzylamines in the reactant, as for reaction (2), the reaction quotient is much higher than the equilibrium contant. This trend suggests that benzylamine is somewhat depleted relative to metastable equilibrium for these reactions. A possible cause is the participation of benzylamine in other reactions that have competitive rates relative to reactions (1 – 3). It seems plausible that benzylamine would be more reactive than the other amines due to the fact that its single phenyl ring causes steric hindrance (Clayden et al., 2001), specifically for S_N2 reaction mechanisms, which are shown to be relevant in Chapter 2.

The calculated equilibrium constants for amination reactions (2) and (3) are the same because the thermodynamic property estimation scheme involves group contribution correlations that are additive and follow strong linear trends (Fig. C1 and C2). For example, the differences in thermodynamic properties between NH_3 and methylamine, methylamine and dimethylamine, and dimethylamine and trimethylamine, are approximately the same (Fig. C1). If this estimation scheme holds for a wider diversity of amines, then equilibrium constants for substitution reactions between amines

that have similar functional groups will be near unity, with little preference in favorability for products or reactants. This suggests that reactions (2) and (3) may not be ideal targets for exploring environmental systems because their equilibrium constants, and thus their reaction ratios, would not change significantly with changes in temperature and pressure. On the other hand, reaction (1) has an equilibrium constant that is highly dependent on temperature and pressure because the alcohol and the amine have different temperature and pressure dependent thermodynamic properties.

Comparison of the equilibrium constants provides strong evidence that the trends in organic concentrations in these experiments represent an approach to metastable equilibrium, rather than an approach to arbitrary steady state ratios. Furthermore, the empirical results provide support for the methods used to combine existing thermodynamic data, the new group contribution scheme, and the HKF equations of state in order to predict equilibrium constants for amines and aminiums under hydrothermal conditions.

3.3.6 Implications for natural systems

Based on the findings in this study, hydrothermal conditions (250°C, P_{sat}) are expected to induce rapid substitution reactions that approach metastable equilibrium on short timescales (days) for several organic compounds, including: alcohols, primary, secondary, and tertiary amines, ethers, imines, and aldehydes. Accordingly, on geologic timescales (millennia) and/or with environmental catalysts (e.g., minerals; McCollom, 2013b) present, approach toward metastable equilibrium for these classes of substitution reactions might be expected at much lower temperatures. Environmental compounds involved in similar reactions and their thermodynamic properties could therefore reflect

temperature and pressure conditions of the systems that produced them. Similarly, if temperature and pressure conditions are well-constrained then unknown compositional variables could be calculated for individual reactions. The equilibrium constants estimated for the amination reactions above indicate that substitution reactions involving different heteroatoms in organic functional groups (such as alcohols reacting to form amines; Fig. 14), will possess greater temperature and pressure dependencies than reactions involving similar function groups (such as amines reacting to form amines). This concept not only provides a framework that guides the choice of analytical targets in the environment, but also motivates thermodynamic measurements needed to expand the property estimates herein to wider classes of environmentally-relevant amines.

Most of the organic functional groups produced in these experiments are abundant in the natural world, composing amino acids (amines, alcohols), carbohydrates (alcohols, ethers), nucleobases (imines, amines), and certain lipid headgroups and linkages (amines, alcohols, ethers). Therefore, these natural compounds may be similarly (highly) reactive under hydrothermal conditions, and could serve as targets within organic reservoirs whose functional group compositions potentially reflect metastable equilibrium conditions. The rapid reversibility of substitution reactions involving heteroatom leaving groups (e.g. H_2O, NH_3, amines, and alcohols) allows speculation that similar or better leaving groups also undergo substitution chemistry under hydrothermal conditions. Some groups that likely fit this criterion (based on pK_b) include esters, thioesters, thiols, and carbon-bonded phosphates, all of which are relevant to biological systems.

The results in this study also indicate that C-, H-, O-, and N-bearing organic reservoirs under hydrothermal conditions are expected to lose mass irreversibly to

electrophilic aromatic substitution reactions involving alcohols. Since relatively high activation energies are required to break phenyl group aromaticity, the occurrence of this bond-breaking process during electrophilic aromatic substitution suggests that almost any C–C pi bond will readily react via this process to irreversibly form a new C–C bond and an adjacent or resonance-allowed hydroxyl (C–OH) group (Clayden et al., 2001). Over sufficiently long timescales, iterations of this process will theoretically produce ever larger organic compounds, for which intramolecular electrophilic aromatic substitution reactions may occur. Eventually having grown large enough to become insoluble in water and populated with conjugated double bonds, such products may begin to resemble coal (Vandenbroucke and Largeau, 2007).

Another irreversible reaction for which there is evidence in this study is the hydrogenolysis of neutral mono, di, or tribenzylamines to form toluene and NH_3 or a lower-degree amine (Fig. 17). Although the C–O bond takes more energy to break than the C–N bond (Blanksby and Ellison, 2003), it is possible that on geologic time scales the hydrogenolysis of alcohols could be a significant source of alkyl group formation. The irreversible loss of heteroatoms in this way represents a path toward enrichment of alkanes within organic reservoirs under reducing (H_2-abundant) conditions. This hydrogenolysis path may be an alternative or parallel model for petroleum formation, that differs from the typical model involving the decarboxylation of fatty acids to form alkanes (Vandenbroucke and Largeau, 2007).

The results of this study show strong evidence that an approach to metastable equilibrium occurs for hydrothermal substitution reactions involving organic compounds. Ideal natural system test cases for metastability between similar C-, H-, O-, and N-

bearing organic include those rich in organic carbon and NH_3, such as the sediment-hosted hydrothermal systems of Guaymas Basin in the Gulf of California (Von Damm et al., 1985), and the Washburn Hot Springs in Yellowstone National Park (Holloway et al., 2011), among others. These active hydrothermal systems also possess mid-pH fluids, which allow unprotonated nucleophiles (e.g., $R–NH_2$) and protonated leaving groups (e.g., NH_3 for $R–NH_3^+$) to exist simultaneously; this should increase the rate of substitution reactions. If more cases of organic metastability can be verified and corroborated with thermodynamic calculations in these well-studied natural systems, then these tools may be applied to plumes of fluids issuing from less accessible systems, such as subducting slabs or the icy ocean worlds of our outer solar system. Additionally, for organic nitrogen rich meteorites with reasonable constraints on duration of hydrothermal exposure, these tools could be applied to make inferences about ancient solar system conditions.

3.4 Conclusions

Hydrothermal experiments, with constant temperature, pressure, and bulk composition, deomstrated that rapid and reversible transformations take place between: benzyl alcohol, benzylamine, dibenzylamine, and tribenzylamine. Convergence of the organic reaction quotients between experiments over time implies that metastable equilibrium is achieved for the following substitution reactions: (1) dehydration of benzyl alcohol and amination by NH_3 to form benzylamine and water, (2) deamination of benzylamine and amination by benzylamine to form dibenzylamine and NH_3, and (3) deamination of benzylamine and amination by dibenzylamine to form tribenzylamine and NH_3. Similarly, reaction quotients converged for (4) alcohol condensation to form ethers

and (5) hydration and deamination of dibenzylimine to form benzaldehyde and benzylamine. Mass loss to the resulting metastable C-, H-, O-, and N-bearing organic system is attributed to irreversible electrophilic aromatic substitution reactions of benzyl alcohol with phenyl rings and to irreversible reductive hydrogenolysis of amines to form toluene. The oxidation of dibenzylamine to form dibenzylimine and H_2 appears to be reversible, but the amine reduction to toluene seems to irreversibly consume available H_2; therefore, the reverse formation of dibenzylamine is inhibited. The approach toward metastable reaction quotients indicates that measurements of alcohols, amines, and NH_3 escaping from otherwise inaccessible natural systems could be supplemented with thermodynamic calculations to assess geochemical variables such as temperature, pressure, and composition.

3.5 Acknowledgements

I thank Kris Fecteau for ion chromatroraphy analyses of ammonium, Pierre Herckes at ASU for guidance with and use of his research group's GC-MS. I thank all other official and honorary members of the Hydrothermal Organic Geochemistry (HOG) group at Arizona State University for vital discussion at weekly group meetings, including: Chris Glein, Jessie Shipp, Ziming Yang, Kristin Johnson, Christa Bockisch, Josh Nye, and Ted Lorance. My thesis advisor, Everett Shock, and other mentors, including: Ian Gould, Hilairy Hartnett, and Lynda Williams all played crucial roles in this work. This work was supported by National Science Foundation grants OCE-0826588 and OCE-1357243, and NASA Habitable Worlds grant NNX16AO82G.

CHAPTER 4

A THERMODYNAMIC ASSESSMENT OF CARBON CHEMISTRY DURING LOW-TEMPERATURE CONTINENTAL SERPENTINIZATION

4.1 Introduction

Serpentinization of ultramafic rocks is a common water-rock reaction in the solar system, likely for much of its history. This idea is supported by terrestrial observations, characterization of meteorites, remote sensing of solar system objects, and by theoretical models (Holm et al., 2015). This widespread geochemical process has become a focus of the astrobiological community because it generates aqueous conditions that have implications for planetary habitability and for prebiotic chemistry (Russell et al., 2010, Holm et al., 2015). Serpentinization is also being examined in an anthropocentric context, due to the potential ability for natural serpentinizing systems to sequester atmospheric carbon dioxide (Kelemen and Matter, 2008).

During serpentinization, ferromagnesian minerals are hydrated and partially oxidized by H_2O to produce hydrous silicates, ferric minerals, and molecular hydrogen (Moody, 1976). Calcium hydroxide is also generated during mineral transformation, which increases the pH of solution and causes the precipitation of dissolved inorganic carbon as carbonate minerals (McCollom and Bach, 2009; Kelemen et al., 2011). When reduced fluids encounter inorganic carbon and other oxidants, there is an energetic drive to produce organic carbon and initiate other reduction/oxidation (redox) reactions, respectively (Shock et al., 2010; Canovas et al., 2017). Many redox reactions are sluggish (kinetically inhibited) at low temperatures and thus, can be catalyzed by life and harnessed for metabolic energy (Shock and Boyd, 2015). The presence of abundant

metals like iron and nickel, potentially capable of catalyzing hydrogenation reactions in serpentinizing systems, may promote a variety of abiotic organic synthesis reactions (McCollom, 2013b).

Current NASA mission plans for a fly-by of Jupiter's icy ocean moon, Europa, will feature a spacecraft equipped to analyze organic compounds in rising plumes (via mass spectrometry; Brockwell et al., 2016) that may be linked to serpentinization occurring beneath a subsurface ocean (Vance et al., 2016). Evidence already exists for molecular hydrogen and a suite of small organics within plumes rising from an alkaline subsurface ocean on Saturn's icy moon, Enceladus (Porco et al., 2006; Matson et al., 2007; Waite et al., 2017). As more organic observations are obtained, interpreting the sources of these compound distributions will rely on studies that characterize abiotic versus biological contributions to organic transformations during serpentinization as a function of temperature, pressure, and geochemical composition. Quantifying fluxes of volatile organic compounds for a range of serpentinizing environments on Earth may ultimately help to determine whether anthropogenic carbon sequestration in these systems is a feasible idea or not. Relevance to these wide-ranging endeavors, which have significant scientific and public interest, suggest that investigations into carbon chemistry during serpentinization have a high potential to produce results with broad applications.

4.1.1 Organic compound production in natural serpentinizing systems

As mentioned above, an energetic drive to transform inorganic carbon into organic carbon exists in serpentinizing environments, primarily resulting from the production of H_2. Molecular hydrogen has been detected and quantified in many systems suspected to have active serpentinization, and often serves as a primary diagnostic tool

for identifying such systems. In marine serpentinizing environments, abundant H_2 has been measured in the warm (< 100°C) carbonate-precipitating fluids of the Lost City hydrothermal vents (Kelley et al., 2001; Proskurowski et al., 2006), and in the more magmatically influenced (> 350°C) fluids of the Rainbow vent field (Charlou et al., 2002). A handful of other hot (295 - 355°C) Mid-Atlantic Ridge hydrothermal fields like Logatchev 1, Ashadze 1, Ashadze 2 (Charlou et al., 2002; Proskurowski et al., 2006; Charlou et al., 2010), and the hot (> 370°C) Nibelungen hydrothermal field (Melchert et al., 2008) of the southern Mid-Atlantic Ridge have also been shown to have abundant H_2.

Continental systems suspected of undergoing present or past serpentinization also exist. Hydrogen measurements have been made for many low temperature (< 50°C) sites, including the Samail Ophiolite of Oman (Neal and Stanger, 1983; Paukert, 2014; Miller et al., 2016; Rempfert et al., 2017; Canovas et al., 2017), the focus of this study, as well as the Tablelands Ophiolite of Newfoundland, Canada (Szponar al., 2013), the Cedars Peridotite of California, USA (Morrill et al., 2013), the Zambales Ophiolite of the Philippines (Abrajano et al., 1988), Socorro Island of Mexico (Taran et al., 2010), and the Tekirova Ophiolite of Turkey (Hosgormez et al., 2008; Etiope et al., 2011). Hydrogen in continental serpentinizing systems is typically measured as percent volume from sampled gases, though some studies report dissolved hydrogen, $H_2(aq)$, concentrations (Szponar et al., 2013; Canovas et al., 2017). These concentrtions are typically lower than in submarine systems, but in certain cases reach millimolar levels in subsurface samples taken from boreholes (Paukert, 2014; Miller et al., 2016; Rempfert et al., 2017).

Abundant methane (CH_4) and other organic compounds often accompany H_2 in serpentinizing systems. From the same corresponding studies listed above, high

abundances of CH_4 have also been measured in Lost City, Rainbow, Logatchev 1, Ashadze 1 and 2, Nibelungen, the Samail Ophiolite, Tablelands, Zambales, The Cedars, and Socorro, as well as at Conical Seamount and South Chamorro Seamount in the Mariana Forearc (Mottl et al., 2003), Logatchev 2 (Charlou et al., 2010), and at Gruppo di Voltri of Italy (Cipolli et al., 2004). Consistent observations of abundant CH_4 in serpentinizing systems suggests that CH_4 formation might be inherent to this geochemical process, even in the lower-temperature continental systems. A variety of non-biological processes that could generate CH_4 in these systems are summarized in reviews by McCollom and Seewald (2007), Etiope and Sherwood Lollar (2013), and McCollom (2013b). These processes include: thermogenic degradation of biomass, the release of microfluidic inclusions during water rock reactions, and abiotic CH_4 generation from an inorganic carbon source. Evidence for these non-biological processes in active systems comes from examining the relative concentrations of light hydrocarbons and their stable carbon and hydrogen isotope ratios (e.g., Proskurowski et al., 2008; Taran et al., 2010; Etiope et al., 2011; Szponar et al., 2013; Morrill et al., 2013). Typically, these hydrocarbons are enriched in heavier isotopes. The investigations and reviews above also contain isotopic and other techniques used for disentangling non-biological sources from each other and distinguishing biological sources. Several argue that active abiotic inorganic carbon reduction is the dominant source of CH_4 in low temperature systems.

In contrast, abiotic experimental studies sometimes display inconsistent trends in isotopic fractionation, likely as a result of minor differences in experimental conditions (see McCollom, 2013b and references therein). As an example, variations in the percent of inorganic carbon converted to CH_4 can greatly affect resulting isotopic ratios of

reactants in closed systems due to Rayleigh fractionation. Experiments have also yet to demonstrate inorganic carbon reduction to CH_4 under geochemically relevant conditions below temperatures at which life is known to persist, e.g., 122°C (Cowan, 2004; Takai, 2008). Recent taxonomic investigations have reported evidence for methanogenic and methanotrophic microbial communities in certain serpentinite-hosted ecosystems (Bradley and Summons, 2010; Shrenk et al., 2013; Miller et al., 2016; Rempfert et al., 2017). Aside from the obvious caveat that methanogens produce CH_4, the potential presence of both communities in these systems complicates interpretations of isotopic analyses with respect to abiotic and biological processes since the former is expected to deplete heavier isotopes in CH_4 reservoirs (e.g., Valentine et al., 2004), and the latter is expected to enrich heavier isotopes (e.g., Templeton et al., 2006; Rasigraf et al., 2012). Thermodynamic calculations have shown that methanogenesis is energetically viable in fluids undergoing active serpentinization (Canovas et al., 2017), and thus ancient processes and higher temperature conditions need not be invoked to explain the presence of CH_4. Thereforee, it seems likely that generation of CH_4 during low-temperature serpentinization is partially the result of biological processes, maybe even to a greater extent than from abiotic processes. The results presented herein provide evidence for microbial metabolisms involving CH_4 in a serpentinizing system.

In addition to methane, small organic acids have been observed in fluids associated with serpentinites, sometimes as a substantial percentage of the dissolved organic carbon (DOC; Haggerty and Fisher, 1992; Lang et al., 2010). Haggerty and Fisher (1992) observed significant formate and acetate abundances (and more rarely, low propionate and malonate abundances) in serpentine-associated interstitial fluids from the

Mariana forearc. When detected, formate was generally the dominant organic acid observed, with concentrations on the order of 100 μM (but ranging up to 2.272 mM); acetate concentrations were typically in the 10s of μM. The authors suggest that the presence of these organic acids is most likely due to the degradation of more complex organic material, possibly via alkaline hydrolysis of ester functional groups; however, they could not speculate whether such a degradation process was predominantly microbially or thermally mediated. In either case, the complex organic material being degraded seems to be biologically sourced in these sediments; this falls into a similar category as thermogenic-degradation of biomass to produce CH_4.

In hyper-alkaline vent fluids discharging from the actively-serpentinizing Lost City hydrothermal field, Lang et al. (2010) observed similarly high formate and acetate abundances (36-158 μmol kg^{-1} and 1-35 μmol kg^{-1}, respectively). In order to examine the sources of these compounds, the authors present: stable carbon isotopic ratios ($\delta^{13}C$) for formate and acetate approximated from isotopic DOC measurements, relative abundances of formate and acetate in mixing fluids, thermodynamic calculations for DIC-H_2-formate equilibrium, and results from previous theoretical and laboratory studies (e.g., Shock, 1992; Shock and Schulte, 1998; McCollom and Seewald, 2003). With these data, they conclude that formate is likely formed via abiotic reduction of inorganic carbon, and that acetate is likely formed via microbial metabolism. However, with regard to the potential abiotic production of formate, even though the reaction is thermodynamically favorable, this is instrinsically true for the reaction whether it proceeds abiotically or via a biological process, and the fluids sampled are well within the temperature limit of life (Lang et al, 2010; Takai, 2008; Cowan, 2004). They also suggest that formate bears an abiotic

signature in its enriched $\delta^{13}C$ values. However, in addition to uncertainties associated with these values being approximated, the carbonate minerals of the Lost City vent chimneys can have anomalously enriched $\delta^{13}C$ values as well, weakening this particular line of evidence. Therefore, it seems that a biological source for formate cannot be ruled out in this system.

Lang et al. (2010) also calculated apparent temperatures of equilibration among DIC, H_2, and formate, based on fluid geochemistry, but did not generate reasonable temperature predictions; their calculations yield colder values than were measured in sampled fluids. We took a similar thermodynamic approach in the current study at the Samail Ophiolite, and generated useful predictions regarding formate formation under different subsurface conditions that might have existed prior to discharge and sampling of serpentinized fluids. Though different in temperature, these predictions may apply to Lost City as well (see below).

More convincing evidence exists for abiotic formate production from inorganic carbon in higher temperature, lower pH systems, such as the Mid-Cayman, Von Damm deep sea hydrothermal vents (McDermott et al., 2015). These hydrothermal systems have temperatures up to 226°C and high H_2 concentrations (~18 mM). They are hosted in gabbro, basalt, and ultramafic rock, though based on an average observed pH of ~6, these fluids are clearly not dominated by serpentinization geochemistry to the extent of Lost City fluids, which have pH up to 11. Nevertheless, the study provides useful insights regarding formate formation in higher temperature natural systems that may capture the hotter side of the transition from biological to abiotic inorganic carbon reduction. While McDermott et al. (2015) use a similar thermodynamic drive argument to that of Lang et

al. (2010), the temperatures of their samples are generally high enough to exclude biological production; although, the possibility of thermogenic breakdown of biomass cannot be excluded. The Von Damm fluid calculations show metastable equilibrium among DIC, H_2, and formate in near-endmember fluids (226°C) and most hydrothermal-seawater mixing fluids (114-151°C), most of which are above the current demonstrated temperature limit of life (Takai, 2008; Cowan, 2004). This apparently rapid equilibration makes thermogenic breakdown seem much like likely. While this last study provides fairly strong evidence that formate can form abiotically in high temperature serpentinizing environments, it seems less likely that this is the case at the near-ambient conditions (~20 – 60°C), addressed in the current study.

4.1.2 Active serpentinization in the Samail Ophiolite

We made field measurements and collected samples at the actively-serpentinizing system of the Samail Ophiolite, in the Sultanate of Oman, during January 2014. An overview of serpentinization in this continental system is described in Kelemen et al. (2011). Focusing specifically on the reaction pathways of carbon, this overview is illustrated in Fig. 21 and can be summarized in three simplified steps: (1) Meteoric water in equilibrium with atmospheric CO_2 reacts with previously altered peridotite at or near the surface to produce circumneutral magnesium bicarbonate (Mg-HCO_3) fluids. (2) Some of these Mg-HCO_3 fluids permeate deeper into the subsurface and react with fresh, unaltered peridotite, through serpentinization, to produce calcium hydroxide (Ca-OH) fluids and molecular hydrogen (H_2). The increase in pH results in the precipitation of magnesium and calcium carbonate minerals, such as magnesite ($MgCO_3$) and dolomite

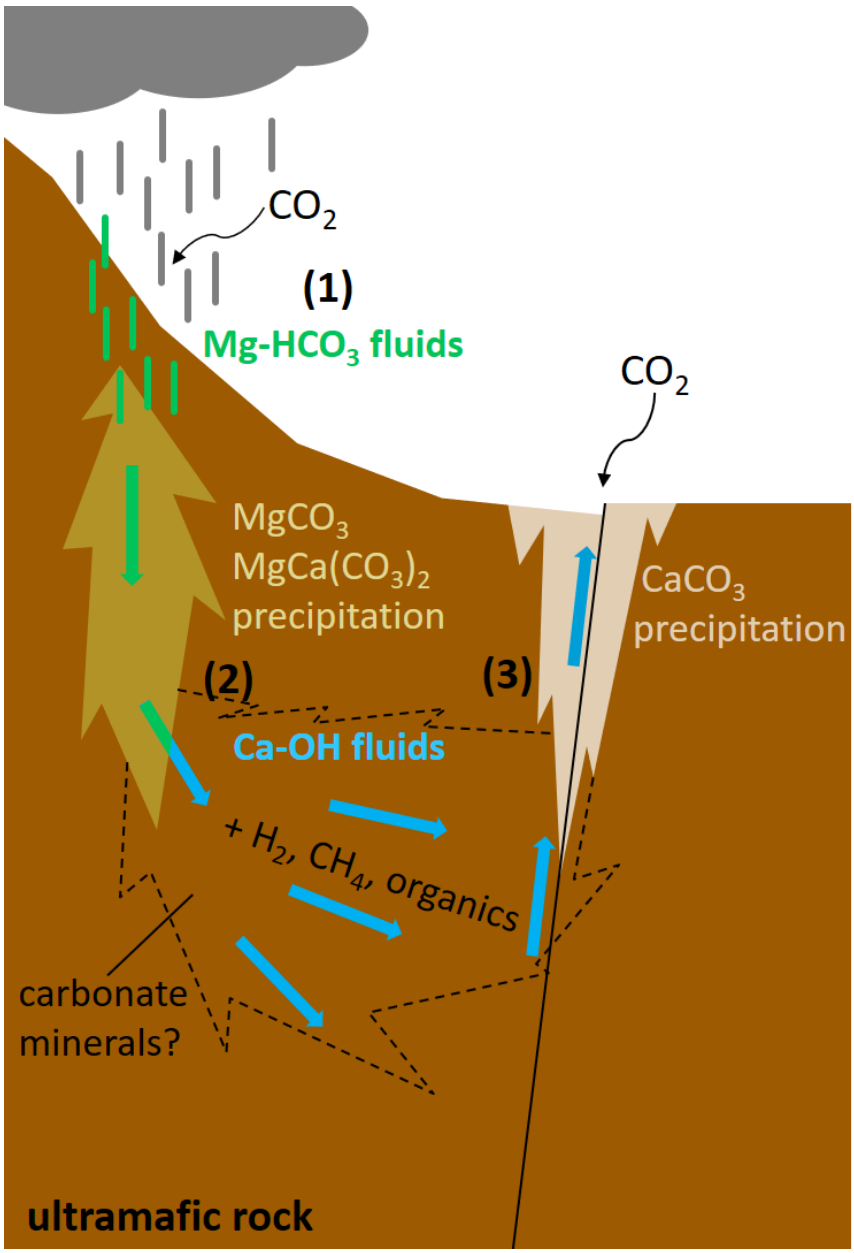

Fig. 21. Cartoon cross section showing the reaction pathways of carbon during low temperature serpentinization in the Samail Ophiolite, as described in Kelemen et al. (2011) and summarized in the text with corresponding steps (1 – 3). The flow of water through the system is indicated with arrows. Regions of magnesium-rich and calcium-rich carbonate mineral precipitation are shown as yellow and beige polygons, respectively. A region potentially depleted of carbonate minerals is invoked with a dashed outline based on observations by Paukert (2014) and results below.

($MgCa[CO_3]_2$). The production of H_2 generates a thermodynamic drive to reduce inorganic carbon to organic carbon, potentially reflected in observations of CH_4 and organic acids (Miller et al., 2016). (3) The serpentinizing Ca-OH fluids eventually return to the surface, and upon encountering atmospheric CO_2, calcium carbonate minerals precipitate, dominantly in the form of calcite ($CaCO_3$).

Kelemen et al. (2011), and other authors, refer to Mg-HCO_3 fluids at the surface as shallow groundwater Type I fluids and to Ca-OH fluids that have resurfaced as Type II fluids. Based on tritium-helium dating techniques, Type I fluids develop in shallow aquifers over 20-40 years; Type II fluids reside in the subsurface for > 60 years (Paukert, 2014) and cannot be better constrained by these dating techniques. However, reaction path models by Paukert et al. (2012) suggest that Type II fluids may take as long as 500-6,500 years to reach their composition between pH 11-12. Noble gas and stable water isotopic measurements suggest Type II fluids may have recharged as far back as the glacial period of the late Pleistocene (15 to 25 ka). The reaction path models also indicate that during the development of Type II fluids, magnesite, dolomite, and calcite should precipitate in the subsurface in a molar ratio of ~500:10:1, respectively. Stable isotope studies performed on carbonate mineral samples from this system provide formation temperature estimates of 23-60°C (Kelemen et al., 2011; Streit et al., 2012). In short, it appears that hyper-alkaline Type II fluids have undergone gradual serpentinization at near-ambient temperatures in the subsurface for at least thousands of years before discharging from the Samail Ophiolite.

4.2. Methods

Geochemical sampling and in-field measurements for this study took place at the following locations in the Sultanate of Oman: Falej, Qafifah, Al-Banah, and the Dima Wa Al Tayeen Municipality, as indicated in Fig. 22. These efforts took place during January 2014. Laboratory geochemical analyses took place at the W. M. Keck Foundation Laboratory for Environmental Biogeochemistry, the Goldwater Environmental Lab, and the GEOPIG (Group Exploring Organic Processes in Geochemistry) Lab; all are at Arizona State University.

4.2.1 Field Measurements

The pH of Type I groundwater fluids, Type II hyperalkaline fluids, and mixtures of these two fluids was analyzed in the field using a WTW 3110 meter with WTW SenTix 41-3 probe. Conductivity and temperature were measured using a YSI Model 30 probe and meter. The following dissolved species concentrations were analyzed using a Hach 2800 or 2400 Spectrophotometer: ferrous iron (Method 8146), high range oxygen (Method 8166), low range oxygen (Method 8316), and total sulfide (Method 8131), according to methods described in Hach (2007).

4.2.2 Sample collection and Laboratory Analyses

Water samples from hyper-alkaline springs and shallow groundwater pools were collected for laboratory geochemical analyses using a polytetrafluoroethylene (PTFE) scoop. Subsurface water samples were collected using a steel bailer lowered into boreholes. For both surface and subsurface sampling, the collected water was transferred to a one liter Nalgene high density polyethylene (HDPE) bottle. The bottle had a polypropylene tube inserted through a hole cut into the lid leading to a 140 mL plastic syringe (Covidien, Inc.). All plastic components were rinsed three times with each

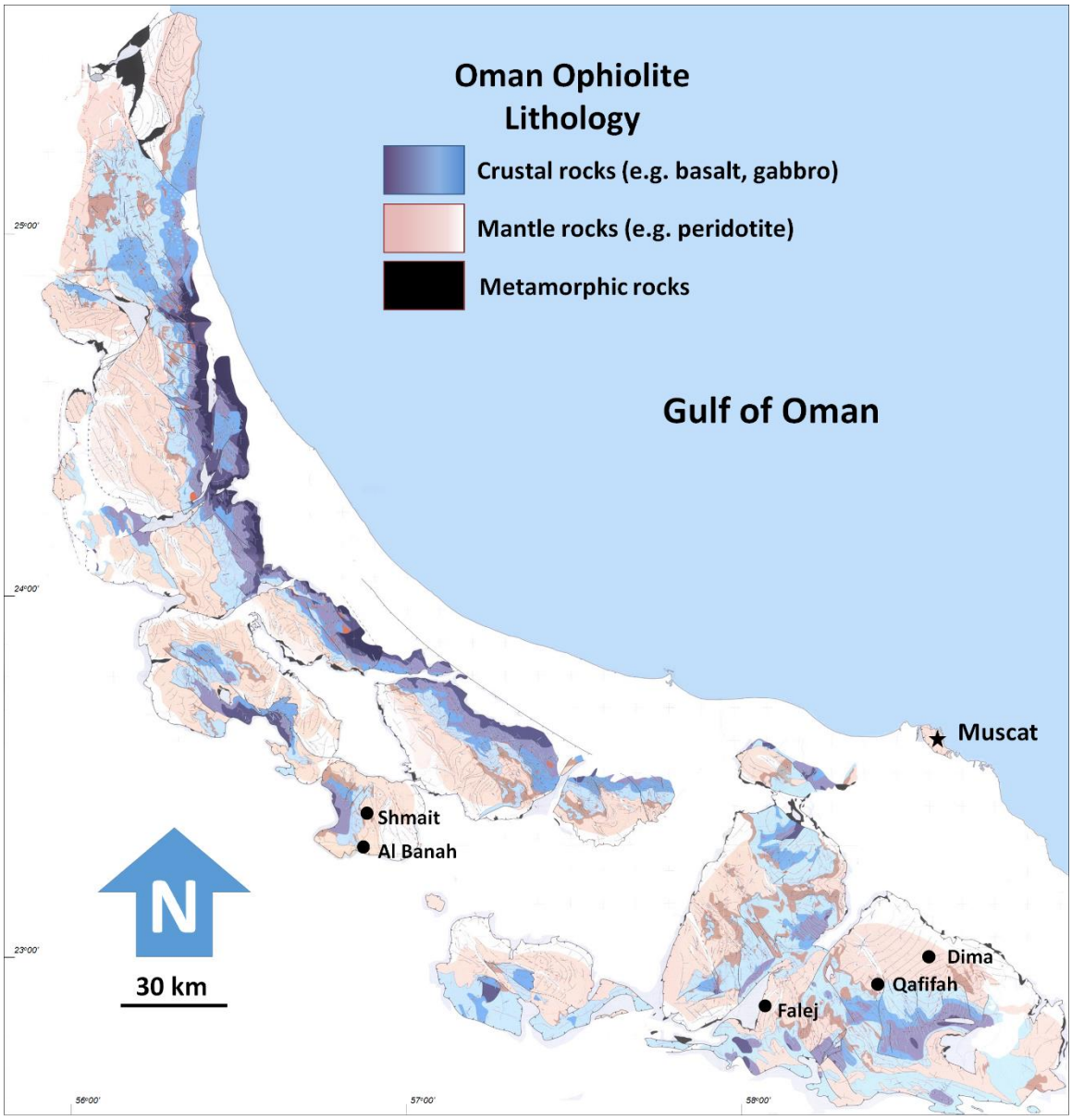

Fig. 22. Geologic map of the Samail Ophiolite, modified after Nicolas and Boudier (2001) by James Leong, with labeled sampling sites marked with filled circles. The capitcal city of Oman, Muscat, is also indicated with a filled star.

sample prior to filtration. This (mostly) closed-system setup was designed to minimize contamination and exchange of volatiles between the sample and the atmosphere as it was being apportioned into different types of sample containers.

Each sample was filtered through an Acrodisc® Supor® 0.8/0.2 μm filter membrane to remove particulates and cells; filters were rinsed with >130 mL of sample prior to sample collection for the analyses herein. Filtered water was collected in various sample containers (see below) for different types of analyses in the following order (with specified volume): dissolved inorganic carbon (DIC; ~40 mL), major dissolved cation (~30 mL), major dissolved anion (~30 mL), dissolved trace element analysis (~60 mL, not reported herein), dissolved organic carbon (DOC) (~40 mL), and organic acid anions (~30 mL). The sequence of sample bottle filling was chosen to preserve samples on the front end that might suffer from atmospheric exchange, and to reduce organic contaminants inherent to the filter via rinsing for samples later in the sequence.

Water samples for DIC were collected in 40 mL VWR CS24 amber glass vials with butyl rubber septa (which have low permeability to gases), both of which were soaked in 10-20% hydrochloric acid for > 12 hours, then rinsed with deionized water (DI) and dried prior to field work. Samples for DOC were collected in 40 mL VWR trace clean amber glass vials with polytetrafluoroethylene (PTFE) septa (which do not leech significant organics). Prior to field work, DOC vials were muffled at 500°C for > 12 hours, the PTFE septa were soaked in DI for > 12 hours then dried, and each bottle was spiked with 100 μL of 85% Sigma-Aldrich phosphoric acid to drive off inorganic carbono as CO2, with the added benefit of sterilizing sample fluids upon collection, and thus preserve the DOC.

Major dissolved ion samples were collected in 30 mL HDPE Nalgene bottles. Both major ion bottles were frozen until analysis upon return to the GEOPIG Lab. Cation bottles were spiked with 95 µL of methane sulfonic acid prior to field work in 2014 in order to prevent precipitation of calcium carbonate or other minerals that might sequester cations.

Samples for organic acid analysis were collected in 20 mL Qorpak amber glass bottles with PTFE cap inserts. The amber glass bottles and their PTFE cap inserts were rinsed three times with DI, and then the cap inserts were soaked for 24 hours. The glass bottles then baked in a muffle furnace at 500°C for 24 hours in order to remove any potential residual organic carbon. Then the cap inserts were dried and these bottles were closed for transport to the field. Upon return from the field, the amber glass bottles were refrigerated until analysis. All samples were analyzed within five weeks of their collection.

Dissolved gas samples were collected using a peristaltic pump to transfer water samples into a plastic syringe, where they were gently shaken in order to allow dissolved gases to equilibrate with a headspace. The headspace was injected into evacuated Mylar bags for storage. Details regarding dissolved gas sample collection are found in Canovas et al. (2017).

4.2.3 Laboratory Analyses

Dissolved inorganic carbon (DIC) and dissolved organic carbon (DOC) measurements were performed using an OI-Analytical total organic carbon (TOC) analyzer coupled to a continuous flow Thermo Electron DeltaPlus Advantage isotope ratio mass spectrometry (IRMS). The setup and methods for the coupled TOC-IRMS

were derived from Gilles St-Jean (2003). Briefly, the method consists of heating, followed by acidification of the sample with phosphoric acid to drive off the DIC as carbon dioxide (CO_2), which is sent to the IRMS. This is followed by continued heating and the addition of sodium persulfate to oxidize and then drive off the DOC as CO_2, which is sent to the IRMS as a separate aliquot. Though both measurements were made for each DIC and DOC vial, because of the different sample bottle preparation techniques, only DIC values from DIC-prepped vials and only DOC values from DOC-prepped vials are reported herein.

Concentrations of major anions (Cl^-, SO_4^{2-}, NO_3^-) and major cations (Na^+, Ca^{2+}, Mg^{2+}, NH_4^+) were determined on separate Dionex DX-600 ion chromatography systems in the GEOPIG lab using suppressed conductivity detection and operated by Chromeleon software (version 6.8), following methods in Fecteau (2016). The anion system employs a potassium hydroxide eluent generator, a carbonate removal device, and AS11-HC/AG11-HC columns. The hydroxide concentration of the eluent is held isocratically at 5 mM for 5 minutes, followed by a non-linear (i.e., Chromeleon curve 8) hydroxide concentration gradient applied over 31 minutes, after which the column is re-equilibrated at 5 mM hydroxide for 10 minutes before the next sample injection. The eluent flow rate is held constant at 1.0 mL/minute. The cation system is equipped with CS-16 and CG-16 columns and cations are eluted isocratically with 19 mM methanesulfonic acid (MSA) at 0.5 mL/minute. Both systems are plumbed with an external source of deionized water for suppressor regeneration to improve the signal-to-noise ratio of the analyses. Injection volumes are 100 µL and 75 µL for anions and cations, respectively. Quantification is achieved externally via calibration curves constructed from a series of dilutions of mixed-

ion standards (Environmental Express, Charleston, SC, USA). Quantification accuracy is verified daily by analysis of an independent mixed ion standard (Thermo Scientific, Waltham, MA, USA). Uncertainties in reported inorganic ion concentrations are estimated to be ± 5%.

Dissolved gas measurements of methane (CH_4) concentrations were analyzed using a gas chromatograph with a flame ionization detector (GC-FID, Peak Laboratories, LLC). Hydrogen (H_2) concentrations were analyzed via a GC with a reductively coupled photometric detector (GC-RCP), following the methods described in greater detail in Canovas et al. (2017). Both instruments used are in the GEOPIG laboratory at Arizona State University. Gas bags were analyzed ~1 year later for $\delta^{13}CH_4$. In order to test for leaks, since they could cause unintended fractionation, the bags were first reanalyzed for CH_4 concentrations and those with significant (> 1 standard deviation) decreases in their concentrations were discarded. Those that hadn't leaked were injected in triplicate into a Picarro cavity ring-down spectrometer G2201-I equipped with a small-sample isotope module. Ultra Zero Air from Praxair was used as the carrier and for diluting samples and standards; standards were purchased from Air Liquide and used to make three-point calibration curves with R^2 values > 0.999, with the following $\delta^{13}CH_4$ values: -69 ± 1, -36 ± 1, and 5 ± 1 ‰, all at 500 ppmV concentrations. Each sample was diluted to approximately 500 ppmV (when possible) and 20 mL of the resulting diluted sample was injected into the instrument.

Organic acid analysis was performed using a Dionex ICS-1500 ion chromatograph equipped with a Dionex IonPac® ICE-AS6 ion exclusion column (9 x 250 mm), a Dionex AMMS-ICE 300 suppressor, a Dionex DS6 heated conductivity cell

detector, and a Dionex AS40 autosampler. Samples were spiked with 25 μL of 3.75 M hydrochloric acid prior to analysis so that sample pH was < 7, in order for organic acids to speciate into the proper proportions of protonated versus unprotonated for interaction with the column. Each sample was run twice, and each run consisted of duplicate injections. The first run used 0.60 mM heptafluorobutyric acid (HFBA) as an eluent, and was designed to isolate the formate peak from coeluting interferences. The second run used 0.15 mM HFBA to isolate the acetate peak. In both cases the eluent flow rate was set to 1.00 mL/min. The suppressor regenerant used was 5.00 mM tetrabutylammonium hydroxide (TBAOH), set to a nitrogen pressure-driven flow of ~3mL/min. Five-point calibration curves with $R^2 > 0.993$ were generated for formate and acetate using standards purchased from High-Purity Standards. Natural sample peaks were verified in all cases by overlaying sample and standard chromatograms, and in some cases verified by standard addition. Instrument detection limits for organic acid anions were ~0.2 μM.

4.2.4 Thermodynamic Methodology

In order to investigate carbon transformations involving inorganic and organic carbon species in Type I and Type II fluids, calculations were performed using the measured concentrations of the dissolved species described above. For near-endmember Type I and Type II fluids, activities of H_2(aq) and CO_3^{2-} that satisfied equilibrium conditions were calculated for organic formation reactions as well as carbonate mineral precipitation reactions. These equilibrium activities were compared to actual H_2(aq) and CO_3^{2-} from sample measurements (the latter calculated using DIC and pH) in order to assess what processes may have caused fluid chemistry to deviate from equilibrium with respect to certain reactions.

For all of these calculations, it was necessary to speciate solutions using the analytical aqueous geochemistry data, meaning that electrolyte complexes were accounted for and activities were calculated for chemical species in their free forms. This process utilized the software package EQ3 (Wolery, 1992), its associated estimation strategies (Shock et al., 1989; Shock et al., 1992; Shock et al., 1997), and existing thermodynamic data (Wagman et al., 1982; Shock and Helgeson, 1990;). The resulting activities were used to calculate activity products (*Q*, also known as reaction quotients) for separate reactions between methane, formate, acetate, and the corresponding reaction species for each individual sample site. In some cases, only partial activity products were calculated, appointing the activities, aCO_3^{2-} and aH_2, as variables. As mentioned above, comparing these partial activity products to equilibrium constants (*K*) derived from SUPCRT92 (Johnson et al., 1992) for mineral and organic formation reactions allowed the quantification of theoretical equilibrium activities for those geochemical variables that satisfy equilibrium, and thus generated hypotheses regarding active processes in the surface and subsurface, whether abiotic or biological (see below).

Affinities were calculated for carbonate mineral precipitation reactions and for a non-exhaustive set of redox reactions potentially relevant to microbial metabolisms involving formate, acetate, and methane, according to Eq. (8):

$$A = RT \ln(K/Q) \qquad (8),$$

where R is the universal gas constant, T is the temperature in Kelvin, and A is the affinity, or the free energy available for a reaction. A positive affinity calculated for a

given reaction means that it is thermodynamically favorable proceeding as written from left to right. The inspiration and methods for these calculations come from Shock et al. (2010), who calculated and ranked affinities for an extensive set of redox reactions in the hot springs of Yellowstone National Park. Affinity calculations for this work were performed for samples taken from shallow groundwater (Type I) fluids, serpentinized (Type II) fluids, and mixtures of these fluids.

4.3. Results and Discussion

Carbon chemistry is central to many processes during low temperature serpentinization. It is involved in the precipitation of carbonate minerals as fluids become more alkaline. It is inherent to any biological structures that exist in the system, and potentially powers biological metabolisms via carbon redox reactions (Canovas et al., 2017). The following results of geochemical and thermodynamic analyses explore existing models of carbon flow within the fluids of the Samail Ophiolite (Kelemen et al., 2011) and expand upon what is known about transformations between inorganic and organic carbon reservoirs during low temperature serpentinization.

4.3.1 General visual observations

Shallow groundwater (Type I) fluids and serpentinized (Type II) fluids are often observed in similar geographic locations, as described in Kelemen et al. (2011). Type I fluids often have visible signs of photosynthesis (green pigments), and Type II fluids do not. Instead, Type II fluids often have visible signs of carbonate precipitation as brittle, white films forming on the surface of stagnant pools, or white flocculant material at the bottom of pools and outflow channels. This makes Type II fluids visually easy to distinguish. Both fluids typically have distinct sources; we attempted to sample both

types as endmembers, and in some cases across regions where their outflow channels mixed together. The geochemistry of these fluids suggests that some mixing may also occur in the subsurface; silica concentrations were used as proxies for the extent of this mixing (see below). The compilation of geochemical data used in this study can be found in Tables D1 – D4.

4.3.2 Aqueous inorganic chemistry

Many of the geochemical measurements in the present study corroborate descriptions of carbon flow through low temperature actively serpentinizing systems from previous studies (Barnes and O'Neil 1969; Barnes et al. 1967, 1978), and other more quantitative investigations (Bruni et al. 2002, Cipolli et al. 2004, Kelemen at al., 2011). Measurements of pH from Type I shallow groundwater fluids at the Samail Ophiolite yield circumneutral values, ranging from ~7 to 9; the pH of Type II hyperalkaline fluids is generally ~11.5; fluids mixing at the surface span an intermediate pH range. At intermediate pH, the geochemical analytes typically span an intermediate concentration range with respect to the analyte concentrations at pH extremes (Fig. 23).

According to the model presented in Kelemen et al. (2011, and references therein) the carbon in the actively-serpentinizing Samail Ophiolite is primarily derived from the atmosphere. In surface fluids, dissolved inorganic carbon (DIC) concentrations have an inverse linear correlation with pH, as shown in Fig. 23a. Due to differences in pH, DIC should be predominantly in the form of bicarbonate (HCO_3^-) in Type I fluids and carbonate (CO_3^{2-}) in Type II fluids. The fact that DIC in Type II fluids is relatively low is consistent with dolomite and magnesite precipitation as alkalinity increases during serpentinization (Kelemen et al., 2011; Paukert et al. 2012), as summarized in

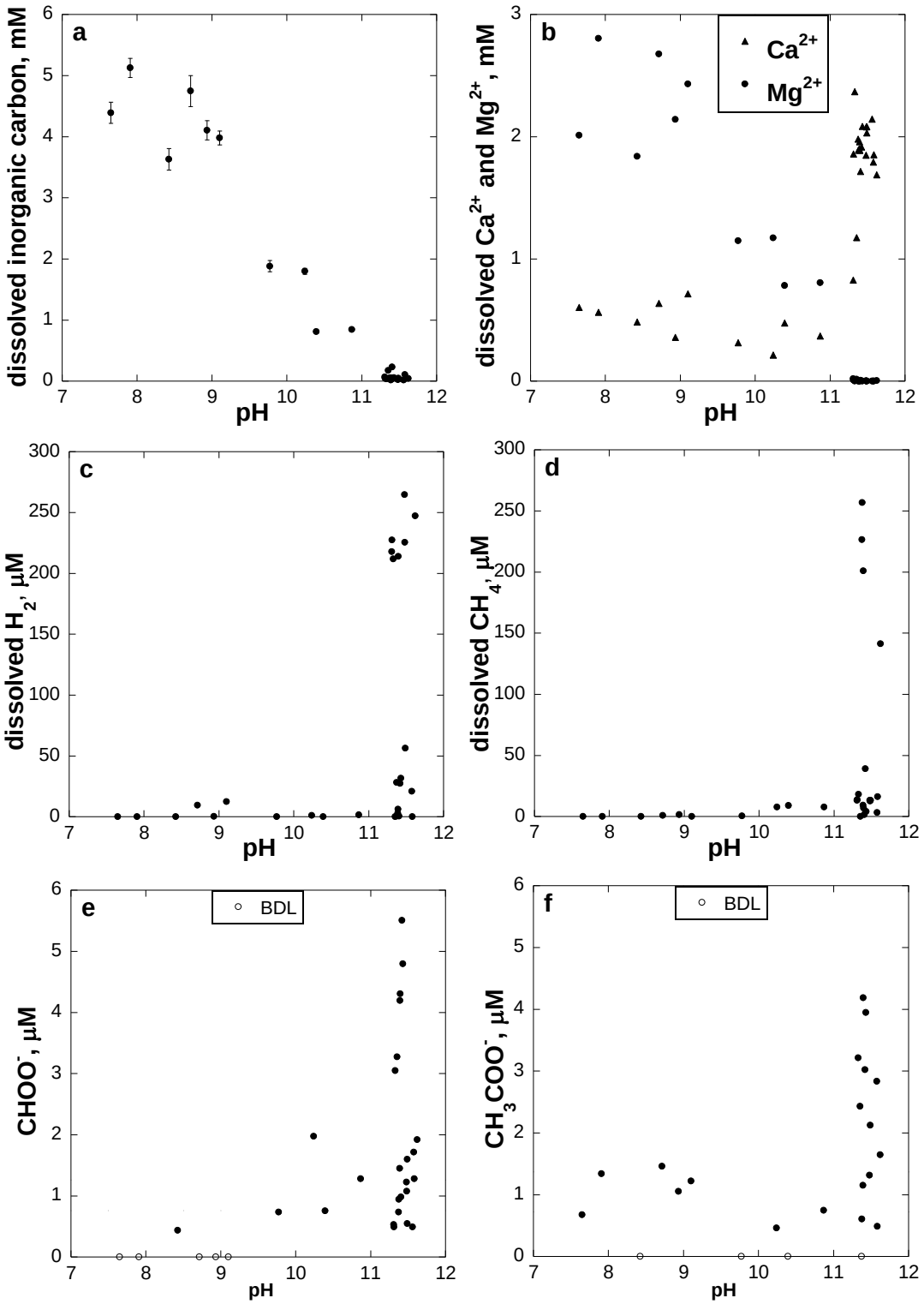

Fig. 23. Aqueous species concentrations vs. pH from shallow groundwater and hyperalkaline seeps, Type I and Type II fluids, respectively. Samples at intermediate pH values are from mixtures of these fluids that occur naturally at the surface. The data used to make these plots are found in Table D1, D2, and D4.

Section 4.1.2. Dissolved magnesium (Mg^{2+}) follows a similar trend to the DIC; it is abundant in Type I fluids (> 1.8 mmolal) from the weathering of altered peridotite at the surface and depleted in Type II fluids (< 0.01 mmolal), owing to the precipitation of magnesium-rich carbonate minerals in the subsurface as Type I fluids transform into Type II fluids (see Fig. 23). In contrast, dissolved calcium (Ca^{2+}) is roughly a factor of 4 more concentrated in Type II fluids (~2.0 mmolal) than in Type I (~0.5 mmolal), owing to the exclusion of Ca^{2+} from transforming minerals during serpentinization in the subsurface. Calcium is roughly the same concentration across low and intermediate pH (~7-11) and is depleted relative to hyper-alkaline fluids (pH > 11). The difference in behavior of these divalent cations across intermediate pH suggests differences in Mg^{2+} versus Ca^{2+} carbonate mineral precipitation rates may be occurring in these mixing zones.

We investigated this notion of preferential precipitation of certain carbonate minerals was investigated by performing thermodynamic affinity calculations to assess carbonate mineral saturation states (in fluid samples) with respect to calcite, magnesite, and dolomite, according to Eq. (9 – 11):

$$Ca^{2+} + CO_3^{2-} \rightleftharpoons CaCO_3 \text{ (calcite)} \quad (9),$$

$$Mg^{2+} + CO_3^{2-} \rightleftharpoons MgCO_3 \text{ (magnesite)} \quad (10), \text{ and}$$

$$Mg^{2+} + Ca^{2+} + 2CO_3^{2-} \rightleftharpoons MgCa(CO_3)_2 \text{ (dolomite)} \quad (11).$$

The results of these calculations (Fig. 24a) indicate that Type I fluids are generally at saturation with respect to all three minerals, while Type II fluids are saturated with respect to calcite only, and undersaturated with respect to magnesite and dolomite. This suggests that Type I fluids are in contact with all three minerals and their DIC is buffered according to their pH and divalent cation concentrations. On the other hand, Type II fluids have not been in contact with magnesite or dolomite recently and seem to be actively precipitating calcite. Samples of these two fluids mixing at the surface, which occupy intermediate pH, are saturated with respect to calcite and magnesite and oversaturated with respect to dolomite, suggesting formation of the latter may be inhibited in real time.

Inhibition of rapid precipitation of Mg^{2+} minerals is supported by the mixing trends shown in (Fig. 24b), the result of sampling across a single mixing zone, which includes data from a Type I fluid sample, a Type II fluid sample, and two samples from where these two fluids mix (Fig. 1D – 3D). Sodium (Na^{+}) is higher in Type II fluids than in Type I fluids, potentially due to a longer duration of water-rock interaction, and is expected to mix conservatively at the surface mixing zone that was sampled. Analysis of aqueous cations shows a conservative mixing trend of Mg^{2+} versus Na^{+} between both types of fluid, compared with the unconservative mixing trend of Ca^{2+} versus Na^{+}, and DIC versus Na^{+}. The low Ca^{2+} and DIC in the two mixing sites suggests that calcite is actively precipitating, corroborating the visual observations of white mineral precipitation mentioned above, as well as previous mineralogical studies which have identified calcite as the dominant carbonate mineral at hyperalkaline springs. (Kelemen et al., 2011, Streit et al., 2012).

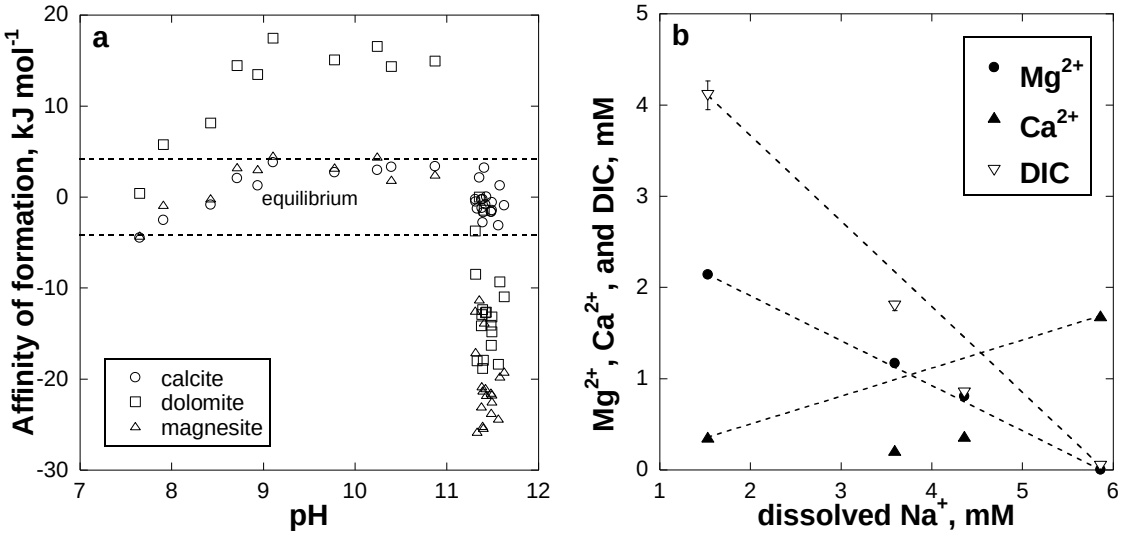

Fig. 24. On the left, affinity calculations for the reaction of aqueous species to form carbonate minerals, Eq. (9 – 11), versus pH for Type I and Type II fluids, as well as fluid mixing zones. Calculations were performed using spring geochemistry to obtain activity products using the software program EQ36 (Wolery, 1992), while the program SUPCRT92 (Johnson et al., 1992) was used to obtain equilibrium constants. Positive affinities indicate that minerals are oversaturated while negative affinities indicate minerals are undersaturated with respect to fluid chemistry. Calculations for mineral formation reactions that yield affinities between -4.184 and 4.184 kJ mol^{-1} (± 1 kcal mol^{-1}) are considered to be at equilibrium saturation. On the right are DIC and cation measurements from samples at a single mixing site where a Type I fluid mixes with a Type II fluid. Given that sodium is presumed to mix conservatively, the plot indicates that Mg^{2+} mixes conservatively as well, while Ca^{2+} and DIC do not. This suggests that calcium-rich carbonate minerals, such as calcite, are actively precipitating upon mixing of these two fluids.

Evidence for various states of mineral saturation, as well as active precipitation in these different fluids, allows for predictions to be made regarding DIC abundances for fluids of different composition within the subsurface. For example, since calcium hydroxide rich Type II fluids are actively precipitating calcite and have not achieved equilibrium with atmospheric carbon dioxide, these fluids should be actively deviating from subsurface compositions that are more depleted of inorganic carbon. The abundance and speciation of DIC in surface versus subsurface fluids has implications for the production of organic carbon compounds, whether by biological and abiotic processes (see below).

Volatile species measured in fluids of the Samail Ophiolite span wide concentration ranges. Dissolved hydrogen concentrations in Type II fluids exceed those in Type I fluids typically by ~1 to 3 orders of magnitude, the large variation resulting from wide concentration ranges in both fluids, but more so in Type II fluids (Fig. 23c, Table D2). Visual observations in the field suggest that in most cases low H_2(aq) concentrations in Type II fluids ($\geq$ 0.476 μmolal) come from sampling larger stagnant pools of fluid that presumably have been subject to degassing and atmospheric mixing. However, in some cases fluids sampled after very short residence times at the surface also have low H_2(aq) concentrations. Therefore, in addition to degassing there are likely other surface or subsurface processes causing H_2(aq) concentrations to range widely. One possible alternative process is microbial hydrogen oxidation. Evidence for this exists based on sequencing of 16S rRNA genes closely related to aerobic hydrogen oxidizers, performed on filtrides of water sampled from peridotite hosted boreholes (Miller et al., 2016; Rempfert et al., 2017). The range of H_2(aq) concentrations in Type I fluids (0.01 to

0.24 μmolal), all anomalously high for typical freshwater at the surface of the Earth, can be attributed to gases from serpentinization separating from subsurface Type II fluids and diffusing upward through Type I fluids, providing a unique habitat for microorganisms. These observations suggest that Type II fluids may be subject to H_2 loss before reaching the surface, and thereforee could contain higher H_2(aq) concentrations in the subsurface. This notion is supported by measurements from boreholes in the Samail Ophiolite that find millimolar concentrations of H_2(aq) (Paukert et al, 2014; Miller et al., 2016; Rempfert et al., 2017). Greater H_2(aq) concentrations in the subsurface are invoked in hypotheses regarding the formation of formate in Type II fluids (see below).

4.3.3 Aqueous organic chemistry

Dissolved methane, CH_4(aq), concentrations generally follow a similar trend to H_2(aq) concentrations across pH, with a higher and larger range of CH_4(aq) concentrations for Type II fluids (3.98 μmolal to 242.42 μmolal) and a lower and smaller range for Type I fluids ($\leq$ 0.63 μmolal) (Fig. 23d). However, sites with the highest CH_4(aq) do not typically have the highest H_2(aq), and vice versa, as seen by comparing Table D2 and D4. Instead, the observation that the highest abundance CH_4(aq) sites have lower H_2(aq) may be indicative of H_2(aq) consumption during the reduction of DIC to produce CH_4(aq).

Formate and acetate concentrations measured in fluid samples follow similar general trends to H_2(aq) and CH_4(aq) across pH (Fig. 23e and 21f, respectively). Most formate concentrations in Type I fluids are below the detection limit of the instrument, while acetate concentrations in these fluids are on average lower than those measured in Type II fluids. In Type II fluids formate is never below detection limits, ranging from

0.43 to 5.93 μmolal. Only a single acetate measurement from Type II fluids was below detection limits, otherwise ranging from 0.40 to 4.19 μmolal. Formate and acetate concentrations have a weak direct correlation with one another, which can be surmised from Table D4. This suggests that formate and acetate may have minor commonalities in terms of processes affecting their production and consumption within the system. It is possible that dissolution of atmospheric formic and acetic acid contributes to high abundances observed in Type II fluids, since this is extremely thermodynamically favorable at high pH (Ervens et al., 2003). However, there is not enough available data to constrain contributions process at this time, so this possibility is not addressed in the current study (addressed in Chapter 5).

There is not an obvious trend with DOC versus pH, and thus this particular relationship is not shown in any figures, but the data can be compared in Table D1 and D4. This is probably because DOC potentially represents a large diversity of individual compounds that are affected by many different processes. However, DOC concentrations relative to other organic compounds from multiple samples across a single mixing zone may reflect biological processes, as discussed below. Notably, formate and acetate typically compose < 5% of the DOC in Type I fluids, and > 10% in Type II fluids.

4.3.4 Classifying near-endmember (N-E) Type I and Type II fluids

Based on the data presented in Fig. 23, it can be seen that pH separates variations between Type I and Type II fluid geochemistry quite distinctly for most species. However, as described above, Type II fluids with pH above 11 often have a wide range of concentrations of species relevant to serpentinization and carbon chemistry, making it difficult to identify a representative endmember for this fluid. A likely cause for these

large variations is mixing with atmospheric fluids, including air and Type I fluids, at or below the surface. Mixing with Type I fluids is expected to cause more rapid changes than atmospheric exchange. Small amounts of exposure to these fluids could cause large changes in Type II fluid geochemistry due to the introduction of atmospherically derived inorganic carbon to relatively depleted fluids, the exsolution of gases derived from the subsurface, and the reaction of reduced compounds, including organics, with atmospheric oxygen. However, small amounts of mixing may not significantly affect the pH of hydroxide-rich Type II fluids, and furthermore, proton (H^+) concentrations are not expected to behave conservatively upon mixing for a variety of reasons.

Outside of the conservative mixing of solutions, H^+ concentrations can be affected by certain mineral precipitation and dissolution reactions. Type II fluids are oversaturated with respect to brucite, $MgOH_2$ (Paukert et al., 2012), the precipitation of which would decrease pH. Conversely, Type II fluids are undersaturated with respect to magnesite and dolomite (Fig. 24a), which if contacted should dissolved and increase the pH. Additionally, numerous redox reactions become available when reduced fluids mix with oxidized fluids, many of which produce or consume H^+ (Shock et al., 2010, Canovas et al., 2017), see below. Perhaps related to redox chemistry is the observation that pH increases down Type II fluid outflow channels that are in contact with the atmosphere; we observed this for two outflow channels, as indicated in Table D1. Together, these theoretical expectations and empirical observations suggest that increasing pH may not be the best indicator of pristine fluids, especially for Type II water.

Instead, work by Leong et al. (in prep) suggests that aqueous silica concentrations, presented in Table D3, may best serve to characterize the extent of

mixing between Type I and Type II fluids both at the surface and into the subsurface, and thus also serve to identify near-endmember fluids for each water type. Silica is expected to mix conservatively between fluids in this system due to its lack of involvement in redox chemistry, as well as its relatively sluggish kinetics associated with silicate mineral precipitation and dissolution at ambient conditions, based on field observations (Paukert et al., 2012; Chavanac et al., 2013) and kinetic studies (Schott et al., 2009). The use of silica(aq) as a conservative mixing species also possesses a unique advantage over non-redox species which are highly soluble, e.g., Na^+, because equilibrium silica(aq) concentrations can be independently derived from thermodynamic reaction path modeling for an endmember Type II fluid that has undergone serpentinization, reaching equilibrium between chrysotile and brucite (Leong et al., in prep). No equivalent reaction exists for determining a Na^+ concentration for a Type II fluid. This reaction path modeling allows Leong et al., (in prep) to compare empirical and theoretical silica(aq) values for Type II fluids, which find good agreement.

As a result, silica(aq) concentrations were used to classify near-endmember Type I and Type II fluids in this study according to the highest and lowest measuremeants from fluid samples, respectively; see Appendix D (text and Table D3). For the remainder of this study, these near-endmember fluids will be referred to as N-E Type I and N-E Type II fluids. Using this characterization, we assess the differences in energetics between N-E fluids for a variety of carbon transformation reactions via thermodynamic calculations. These calculations are designed to generate and test hypotheses regarding the sources and sinks of inorganic carbon and organic carbon during low temperature serpentinization.

4.3.5 Thermodynamic modeling of organic carbon formation reactions

As described above, the production of H_2 in the presence of inorganic carbon during serpentinization theoretically generates an energetic drive for the formation of organic compounds. Given that methane, formate, and acetate are generally observed in greater abundance in Type II fluids relative to Type I fluids (Fig. 23d – f), we hypothesize that these compounds are formed from redox reactions along the flow path of water in this system. Also mentioned above, Type II fluids issuing at the surface are estimated to have residence times in the subsurface of up to 6,500 years (Paukert et al., 2012) and may travel to kilometer depths (Kelemen et al., 2011), potentially allowing for a large gradient of fluid compositions and habitats in which organic compounds could be produced. Identifying the conditions under which individual organic compounds form could help to predict the location of active processes, which may include microbial communities metabolizing different carbon species.

We performed thermodynamic calculations to assess whether organic compound abundances from water samples were in equilibrium with their associated N-E Type I and N-E Type II fluid chemistries. If an organic compound was out of equilibrium, we hypothesized active processes at the surface that could account for the perturbation from equilibrium observed, or we determined plausible differences in subsurface conditions that would satisfy equilibrium for the concentrations of organic compounds observed. Organic compound formation was considered from DIC and H_2, with equilibrium abundances calculated from combining activity products with equilibrium constants, according to the redox reactions shown in Eq. (12 – 14):

$$CO_3^{2-} + 4H_2(aq) + 2H^+ \rightleftharpoons CH_4(aq) + 3H_2O \qquad (12)$$

$$CO_3^{2-} + H_2(aq) + H^+ \rightleftharpoons CHOO^- + H_2O \quad (13)$$

$$2CO_3^{2-} + 4H_2(aq) + 3H^+ \rightleftharpoons CH_3COO^- + 4H_2O \quad (14)$$

Results from these calculations, which determine the equilibrium activities of H_2 and CO_3^{2-} for the above reactions, are shown as lines or bands in Fig. 25 for near-endmember (N-E) Type I fluids, plot a, and N-E Type II fluids, plot b. Near-endmember fluids were designated by silica(aq) abundances in water samples, as described briefly in Section 4.3.4 and in more detail in Appendix D (Leong et al., in prep). Equilibrium activity calculations were performed at the temperatures measured for each sample (solid lines), plotted as bands to show the ranges of results from the samples, and then again at 60°C (dashed lines) for only the maximum values, since carbonate mineral formation has been estimated to have occurred up to that temperature in the active system (Kelemen et al., 2011; Streit et al., 2012). More details on how these calculations were performed can be found summarized in Section 4.2.4.

Equilibrium activities can be compared to actual H_2(aq) and CO_3^{2-} activities of individual fluid samples, which are shown as square symbols on the plots. Some data points are colored in the case that an organic analyte necessary for performing calculations for a given reaction is below the detection limit of the instrument (BDL); in those samples equilibrium activities (bands) were calculated using instrumental detection limit values for organic compounds. By comparing the activities of H_2(aq) and CO_3^{2-} in fluid samples to their equilibrium activities, these plots allow one to quantify changes in

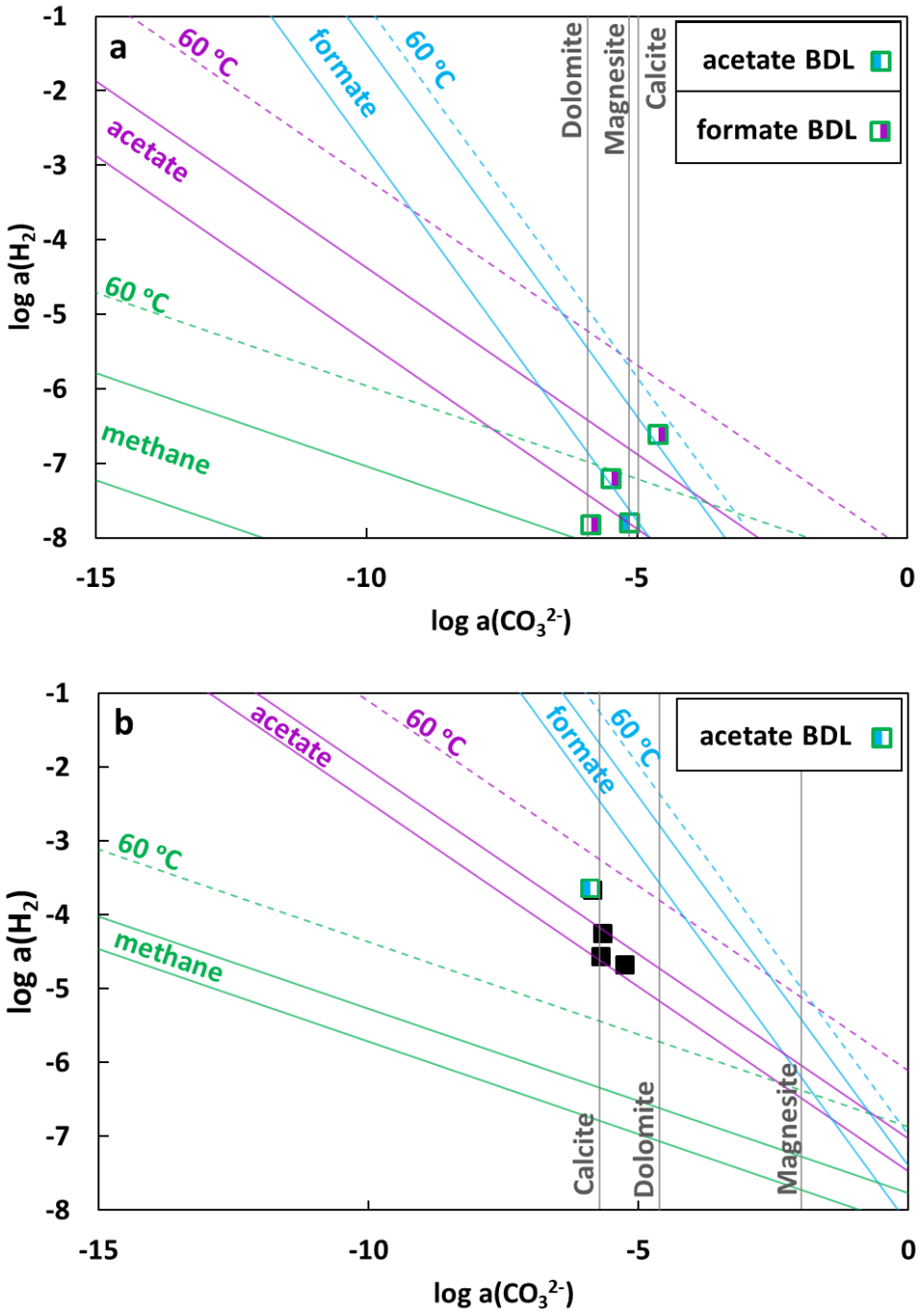

Fig. 25. Equilibrium activity diagrams for carbonate mineral and organic compound formation reactions. Equilibrium values of $aH_2(aq)$ and aCO_3^{2-} for each reaction (lines) can be compared to actual activities of these species in near-endmember (N-E) Type I fluids (a) and N-E Type II fluids (b). Colored symbols indicate organic measurements for particular samples that were below the detection limits of the instrument (BDL). Black symbols contain all measurements. Equilibrium values of aCO_3^{2-} (grey lines) for carbonate minerals were calculated as averages for the fluid samples in each plot.

the geochemistry of the samples, in terms of aH_2 and aCO_3^{2-}, that would satisfy equilibrium for the different organic compound formation reactions.

Simply put, if a symbol in the plot falls on a given line, the corresponding organic compound formation reaction is at equilibrium in that sample. If a symbol plots above a line, then that organic formation reaction is out of equilibrium in that sample and would need to proceed from left to right to approach equilibrium, i.e., reactant to product ratios are too high relative to equilibrium. Conversely, if a symbole plots below a line, then that organic formation reaction is also out of equilibrium in that sample, but would need to proceed from right to left to approach equilibrium.

Based on these calculations, Fig. 25a shows that N-E Type I fluids are generally in equilibrium with the carbonate minerals calcite, magnesite, and dolomite, as well as the organic compounds formate, and acetate, according to Eq. (9 – 11, 13, 14), respectively. Notably, however, most formate measurements are BDL, so for its formation reaction this is less certain. Additionally, N-E Type I fluids are slightly out of equilibrium with respect to the methane formation reaction, Eq. (12), having too little an abundance of products relative to reactants, e.g., too little methane relative to the geochemistry of the fluids. However, when calculations are performed at the maximum estimated carbonate formation temperatures for the system, 60°C (Kelemen et al., 2011; Streit et al., 2012), N-E Type I fluids appear to be essentially in equilibrium with respect to Eq. (12) according to the general agreement between the data points and the range of values covered between the solid and dashed green lines. The reliability of using this upper temperature for N-E Type I fluid calculations is discussed below.

The relationships between N-E Type I fluid geochemistry and calculated equilibrium activities serve to generate hypotheses concerning the origins of methane, formate, and acetate in shallow groundwater fluids. As mentioned above, the formation reaction for acetate appears to be at equilibrium in N-E Type I fluids, which implies that forward and reverse reactions for Eq. (14) proceed sufficiently faster than competing reactions that would perturb equilibrium. Abiotic redox reactions that form organic compounds from DIC and H_2(aq) have typically been shown to be inhibited under a variety of experimental conditions up to 200°C (see McCollom, 2013b and references therein). Because of the low temperatures (Kelemen et al., 2011; Streit et al., 2012) and short residence times (Paukert et al., 2012) estimated for shallow groundwater fluids of the modern Samail Ophiolite, we hypothesize that an approach toward metastable equilibrium for acetate formation, Eq. (14), is facilitated and catalyzed by microorganisms in N-E Type I fluids or host sediments at the surface where fluid samples were collected.

The source of CH_4(aq) in N-E Type I fluids is less certain due to its low abundance relative to equilibrium with DIC and H_2(aq), as well as its volatility. While calculations performed at 60°C satisfy equilibrium for the methane formation reaction, Eq. (12), there is no evidence that suggests Type I shallow groundwater fluids reach these temperatures, since the annual average air temperature is 30°C and the geothermal gradient is 24°C per kilometer depth in the region (Paukert, 2014). Therefore, it seems that Eq. (12) does not reach equilibrium in N-E Type I fluids.

It is possible that CH_4(aq) formation is kinetically inhibited from reaching equilibrium, but given that acetate is in equilibrium with N-E Type I fluid geochemistry,

and should require more reaction steps to form than CH_4(aq) from DIC and H_2(aq), this kinetic explanation is unsatisfactory without further investigation into microbial processes. Diffusion of H_2 from deeper Type II fluids upward into Type I fluids could explain why CH_4(aq) activities are relatively low, since H_2(aq) is on the reactant side of Eq. (12), but again requires that acetate equilibrates with H_2 via Eq. (14) faster than CH_4 does via Eq. (12). Exsolution is not considered as an explanation for relatively low CH_4(aq) abundances, since CH_4(aq) should degas more slowly than H_2(aq).

A more likely contributing factor for relatively low CH_4 abundances in N-E Type I fluids is microbial oxidation of CH_4(aq), shown to be thermodynamically favorable in Type I fluids for aerobic as well as anaerobic metabolisms, with O_2 as an oxidant as well as NO_3^-, NO_2^-, or SO_4^{2-}, respectively (Canovas et al., 2017, and below). For this hypothesis to be sensible, oxidation of CH_4(aq) would also need to be significantly faster than oxidation of H_2(aq), since H_2(aq) is a reactant in Eq. (12), and has a larger stoichiometric coefficient in the reaction than CH_4(aq). This means that changes in H_2(aq) abundance cause larger perturbations to the reaction quotient than changes in CH_4(aq). A potential caveat to this hypothesis is that acetate does not seem to undergo oxidation in a way that perturbs it from equilibrium with Eq. (14), despite acetate oxidation also being quite energetically favorable (see below).

Narrowing down this list of plausible hypotheses could be achieved by identifying potential microbial metabolisms involving involving these organic compounds occurring in N-E Type I fluids or host sediments at the surface. Through sequencing, Rempfert et al. (2017) identified 16S rRNA genes closely related to methylotrophs, methanogens, and aerobic hydrogen oxidizers, as well as identifications suggestive of acetogenesis in

peridotite hosted fluids with pH ≤ 8.5 from boreholes in the Samail Ophiolite, which provides some validation for the above hypotheses. However, though somewhat compositionally similar, as indicated by similar aqueous silica concentrations, it is uncertain how relevant the communities of these subsurface fluids might be to the N-E Type I fluids from the present study, which were sampled at the surface. Additionally, the pumping methods used in Rempfert et al. (2017) to obtain borehole fluids could conceivably cause mixing of both fluid types (I and II), mixing their microbial communities during sampling. As investigations continue into comparisons between subsurface and surface taxonomy (A. Howells, personal communication, October 20, 2017), further clarity for the above hypotheses could be gained from microbial incubation experiments by comparing rates of organic acid, H_2, and methane redox metabolisms.

Unlike N-E Type I fluids, 23b shows that N-E Type II fluids only approach equilibrium with respect to calcite saturation and acetate formation from DIC and H_2(aq), Eq. (9) and (14), respectively. This observation finds commonalities with similar observations of metastable equilibrium achieved between acetate and calcite in sedimentary basins (Helgeson et al., 1993), suspected to be biologically mediated. Although notably, the Samail Ophiolite is a much lower temperature system in which metastable equilibrium is achieved between these carbon species.

Also in N-E Type II fluids, CH_4(aq) is extremely low in abundance relative to equilibrium for Eq. (12), while formate is actually high in abundance relative to equilibrium for Eq. (13), the latter a similar observation to Lang et al. (2010), who suggest that formate at Lost City is abiotically produced. At ambient conditions in the Samail Ophiolite, it is more likely that biology exploits carbon redox reactions (Shock

and Boyd, 2015), and as mentioned above, this can be hypothesized for acetate in Type I fluids, suggesting contact with microbial communities operating metabolisms for both the forward and reverse reactions for Eq. (14). Since some portion of Type I fluid is presumed to permeate into the subsurface and undergo serpentinization, it may have potential to "seed" the rest of the system, including Type II fluids, with organisms capable of similar metabolic reactions. While microbially-mediated pathways seem to achieve acetate formation equilibrium in both N-E Type I and N-E Type II fluids, the same cannot be said for organic formation reactions of formate and methane, Eq. (12) and (13), respectively, which are both extremely out of equilibrium in N-E Type II fluids.

Similar to N-E Type I fluids, low CH_4(aq) abundances relative to equilibrium in N-E Type II fluids could also be explained by kinetic inhibition of Eq. (12), as well as methane oxidation metabolisms which are also thermodynamically favorable in Type II fluids (Canovas et al., 2017). These hypotheses bear the same caveats as their analogs for Type I fluids (see above). In addition to assuming that these disequilibria describe geochemical or biochemical processes largely responsible for the composition of N-E Type II fluids, we also consider the possibility that these organic abundances are representative of previous equilibrium states under different geochemical conditions. This different approach seems sensible given that N-E Type II surface fluids have only just been exposed to surface conditions prior to sampling and, as mentioned previously, rapid calcite precipitation at Type II surface seeps indicates that these fluids are rapidly exchanging with the atmosphere and thereforee far from equilibrium. Prior to surfacing, these fluids potentially have thousands of years (Paukert et al., 2012) to reach equilibrium with respect to the organic formation reactions of interest.

Here we quantify potential compositional differences in Type II fluids prior to reaching the surface that satisfy equilibrium for formate and methane reactions, Eq. (12) and (13), and could be possible in the subsurface. As seen in Fig. 25b, N-E Type II surface fluids have extremely low abundances of CH_4(aq) relative to H_2(aq) and CO_3^{2-}, requiring activities of CO_3^{2-} and/or H_2(aq) several orders of magnitude lower to satisfy equilibrium. Therefore, these calculations allow for the possibility that CH_4(aq) last equilibrated in a carbon and/or hydrogen limited zone in the subsurface. However, it is difficult to conceptualize how H_2(aq) could be lower in abundance in subsurface Type II fluids, given that the formation of Type II fluids and H_2(aq) are entangled in the subsurface via serpentinization, and H_2(aq) abundances should be generally increasing with depth due to decreasing atmospheric exchange. Therefore, we rule this possibility out and instead hypothesize that CH_4(aq) in N-E Type II fluids is produced and last equilibrates in an extremely carbon-limited zone in the subsurface ($aCO_3^{2-} \leq 10^{-14}$), with similar or greater levels of H_2(aq) as measured in Type II surface fluids, prior to atmospheric infiltration or exchange. A similar general hypothesis is proposed in Miller et al. (2016) on the basis of borehole fluid CH_4 stable carbon isotopes, which we discuss below with additional isotopic analyses. Such an environment would be undersaturated with respect to carbonate minerals, and thereforee devoid of them. The hypothesis for a carbon limited zone also finds support from preliminary work on samples from deep wells by Paukert (2014), which suggests that calcite is less common below 150 meters depth. A similar carbon limitation hypothesis was not considered to explain low CH_4 abundances for Type I fluids, due to the short residence times and signatures of atmospheric influence in the geochemistry of these fluids (Paukert et al., 2012).

In contrast to CH_4(aq), equilibrium is satisfied for the formate formation reaction, Eq. (13), under conditions where H_2(aq) and/or CO_3^{2-} activities are greater than what is measured in N-E Type II surface fluids. However, it is difficult to conceptualize how CO_3^{2-} could be higher in abundance in subsurface Type II fluids, given that the atmosphere should have less influence with increasing depth, and Mg^{2+} concentrations are far too low in N-E Type II fluids to suggest recent contact with Mg^{2+}-rich carbonate minerals, which would buffer CO_3^{2-} at greater abundacnes. Thereforee we hypothesize that formate is produced and last equilibrates in the subsurface under similar geochemical conditions, except with more abundant H_2, prior to transport to the surface where H_2 is lost via atmospheric exchange.

Although perhaps counterintuitive, this hypothesis is not mutually exclusive with the formation of CH_4(aq) in a carbon limited zone of the subsurface. Instead, since this hypothesis requires greater activity of H_2(aq) at depth, it simply requires even lower activities of CO_3^{2-} in a carbon-limited zone where CH_4(aq) is formed, presumably deeper in the system. Accordingly, these two hypotheses suggest formate forms shallower, in the upper 150 meters of the subsurface, where atmosphere has infiltrated to precipitate calcite (Paukert, 2014), which buffers CO_3^{2-} activities, but H_2(aq) has not yet sufficiently diffused out of N-E Type II fluids. Measurements of H_2(aq) down boreholes by Paukert (2014) and Miller et al., (2016) yield millimolar abundances, which is up to a factor of 4 greater than the highest H_2(aq) concentrations measured in Type II surface fluids herein (Fig. 23c). These observations provide some support for a suitable subsurface environment in which formate is produced and equilibrates in Type II fluids, but these particular H_2(aq) concentrations are still insufficient for satisfying equilibrium. If formate

is formed in the subsurface, we expect that a subsurface microbial community is responsible for forward and reverse formate formation reactions that allow Eq. (13) to approach equilibrium.

Another hypothetical process that could simultaneously explain the relatively high abundances of formate and the relatively low abundances of CH_4(aq) in N-E Type II fluids is microbial oxidation of CH_4(aq) to formate, which does not proceed with the final oxidation step for some portion of carbon. Thermodynamic calculations show that aerobic methane oxidation to formate as the product is quite energetically favorable in Type II fluids ($\Delta_r G \approx$ -100 kJ/mol e^-), see below. Based on culture sequencing of methanotrophs and methylotrophs, formate is produced during oxidation of C1 compounds as a discrete molecule (Ward et al., 2004), and methylotrophs do not necessarily have to proceed with the final oxidation step (Chistoserdova et al., 2004), though this latter study reports that after formate is excreted into culture medium, it is later consumed via some other metabolic process during growth. In part this hypothesis could also help to explain low CH_4(aq) abundances relative to equilibrium for Eq. (12), if cumulative forms of CH_4(aq) oxididation are significantly faster than H_2(aq) oxidation.

This set of hypotheses for formate formation could also potentially apply to observations of formate at the Lost City hydrothermal vents (Lang et al., 2010), since formate abundances are also high relative to equilibrium with DIC and H_2(aq) in that system. Additionally, findings by Haggerty and Fisher (1992), described in Section 4.1.1, also suggest that high levels of formate in serpentinite-hosted ecosystems may be the product of biomass degradation in organic rich sediments. While it seems that there is not comparably abundant organic material in the hyperalkaline fluids of either the Samail

Ophiolite or Lost City, the possibility that an overabundance in these fluids relative to equilibrium may be the product of biomass degradation cannot be ruled out, since microbial communities are present.

Sequencing work has also been performed on subsurface Type II fluids from boreholes, with studies by both Rempfert et al. (2017) and Miller et al. (2016) identifying 16S rRNA genes closely related to those of methylotrophs, methanogens, aerobic hydrogen oxidizers, as well as identifications suggestive of other relevant metabolic pathways, including acetogenesis, fermentation, and small organic acid oxidation (Rempfert et al. (2017). As mentioned above, fluids in these previous studies are not perfect analogs to the surface fluids sampled in this study. This is even more so the case when comparing Type II fluids between studies, as subsurface fluids from the studies with sequencing have silica(aq) concentrations that are greater by at least a factor of 5 in high pH peridotite hosted samples, likely an indication of subsurface mixing with Type I fluids (Leong et al., in prep). Still, the fluids in these sequencing studies have otherwise very similar geochemistry to the samples in the current study, and provide some credibility to the hypotheses for N-E fluids herein.

As with Type I fluids, the hypotheses above concerning organic formation reactions in Type II fluids can be tested by expanding taxonomic investigations to surface fluids, and moving into the realm of investigating relative metabolic rates for redox reactions involving CH_4(aq), H_2(aq), formate, and acetate. The sequencing results of Rempfert (2017) and Miller et al., (2016) certainly provide sufficient confidence that such work would yield some amount of activity from metabolic processes. The organic formation reactions that have been calculated to be in equilibrium with respect to surface

fluid chemistry also allow us to more confidently make predictions regarding microbial metabolisms in these environments. Specifically, we predict that the metabolic potential exists and is active for reversible acetate formation, Eq. (13), in surface environments with N-E Type II fluids and N-E Type I fluids. In contrast, multiple hypotheses remain plausible for organic formation reactions that calculations have revealed to be out of equilibrium with respect to fluid geochemistry in samples. Because these hypotheses involve different biological processes, we used additional geochemical observations below to test for the presence of active metabolic processes.

4.3.6 Evidence for active metabolic processes involving carbon

To gain energy from serpentinizing environments, microorganisms catalyze a diversity of redox reactions (Canovas et al., 2017). It follows that mixtures of oxidant-rich Type I shallow groundwater fluids and reductant-rich Type II serpentinized fluids make for ideal environments for redox metabolisms to operate. To test this, affinity calculations were performed, as described in Section 4.2.4, which quantify the energy available for a non-exhaustive set of potential metabolic reactions involving methane, formate, and acetate.

These affinity calculations are presented as energy ranges in Fig. 26 in near-endmember (N-E) Type I fluids, N-E Type II fluids, and all other samples, termed "Mixing fluids." This figure shows the energetics for a variety of different reactions in which all three organic compounds are oxidized, coupled to the reduction of dissolved oxygen (O_2), nitrate (NO_3^-), sulfate (SO_4^{2-}), and carbonate (CO_3^{2-}). Affinity values are also shown for reactions involving the reduction of formate and acetate, coupled to the oxidation of H_2(aq), as well as a fermentative reaction, acetate decarboxylation (reaction

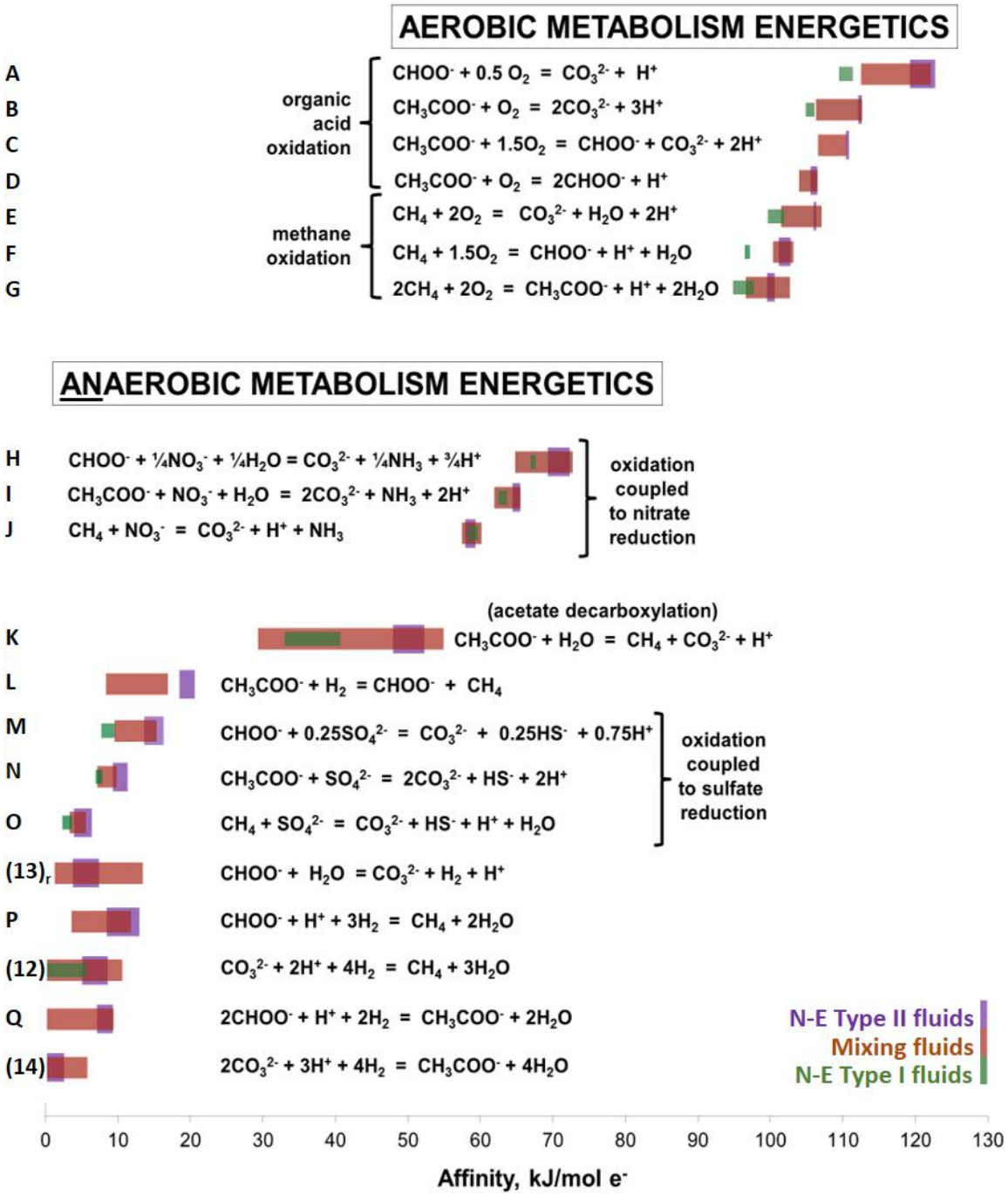

Fig. 26. Affinities for potential metabolic reactions involving formate ($CHOO^-$), acetate (CH_3CHOO^-), and methane (CH_4). Reaction affinities are shown in kJ per mole of electrons transferred, and as energy ranges calculated for N-E Type II fluids (purple), N-E Type I fluids (green), and all other samples, termed "Mixing fluids" (orange). All species in these reactions are in their aqueous forms. This diagram was calculated using the same style of affinity calculations as the central focus of Shock et al., 2010 and Canovas et al., 2017.

K). Each equation in the figure is thermodynamically favorable if the net reaction proceeds, as written, from left to right; accordingly, none are energetically favorable to proceed from right to left. Notably, Eq. (12 – 14) used in Fig. 25 can be found among these reactions, with Eq. (13) being written in reverse, labeled $(13)_r$, since N-E Type II fluids have a high abundance of formate relative to equilibrium with respect to Eq. (13).

Specific reactions will be referred to below when considering hypotheses regarding potential metabolic pathways that could explain organic abundances relative to thermodynamic equilibrium from Section 4.3.5. More broadly, to be gleaned from this figure is the fact that N-E Type I fluids have the lowest average energy yields for essentially all reactions. This seems to follow common logic, as N-E Type I fluid samples are derived from shallow groundwater, so they have been in greater contact with the atmosphere and are already quite oxidized. On the other hand, Type II fluids have the highest average energy yields for essentially all reactions. Again, this follows common logic, given that these fluids have been in contact and equilibrating with reduced minerals in the subsurface for up to thousands of years (Paukert et al., 2012), and just prior to sampling they are exchanging with the atmosphere for the first time, which creates redox disequilibria and thus enormous amounts of chemical potential energy. All reactions shown are more energetically favorable in N-E Type II fluids than in N-E type I fluids, with the exception of CH_4 oxidation via NO_3^- reduction (reaction J). Interestingly however, the maximum energies available for a variety of reactions in "Mixing fluids" sometimes exceed the energies available in Type II fluids. Thereforee the general hypothesis that mixtures of Type I and Type II fluids should provide ideal environments for redox metabolisms finds some support in these thermodynamic calculations.

To further test the general hypothesis that carbon redox metabolisms should be enhanced during the mixing of Type I and Type II fluids, an examination of geochemical data was performed across a single mixing zone, which was first mentioned above in the context of calcite precipitation, Fig. 24. As above, Na^+ concentrations from this fluid mixing zone are used to test conservative mixing trends, in this case for a variety of organic analytes, as shown in Fig. 27. As a reminder, the Type I fluid sample in these plots has the lowest Na^+ concentration, the Type II fluid sample has the highest Na+ concentration, and thereforee the two mixing zone samples have intermediate Na^+ concentrations according to their degree of mixing.

In Fig. 27a, CH_4(aq) is shown to have the highest abundance in the Type II fluid sample and the lowest abundance in the Type I fluid sample, with an unconservative mixing trend for the mixing samples, which are low abundance in CH_4(aq) by ~50 – 75 μM relative to conservative mixing (dashed line). Since CH_4 is volatile, it is possible that degassing partially contributes to this trend. However, if degassing were the only process affecting this trend, it would be expected that the two mixing zones would have different amounts of CH_4(aq), since time is required for fluid mixing to occur across the landscape (Fig. 1D – 3D). Instead, the two mixing sites have CH_4(aq) values that are not significantly different, suggesting degassing may not be a rapid process relative to the timescales of mixing. Both mixing fluids are also orders of magnitude above CH_4(aq) saturation from the atmosphere, suggesting even though there is a drive for degassing of CH_4, it may actually be quite slow relative to mixing. Therefore we conclude that a significant amount of CH_4(aq) is being oxidized during the mixing of Type I fluids and Type II fluids in this location.

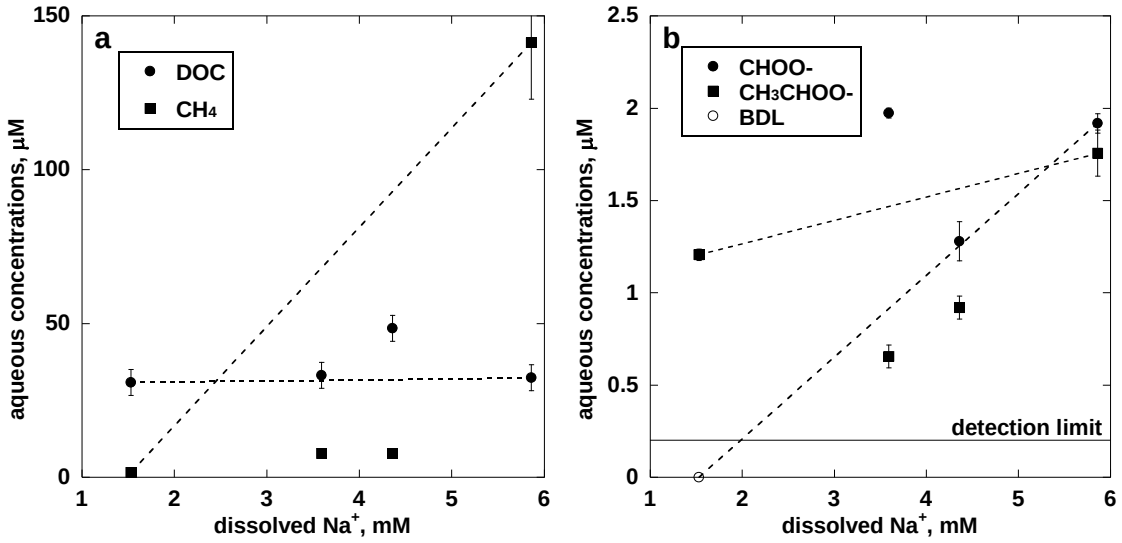

Fig. 27. Unconservative mixing trends for a variety of organic analytes. Plot "a" shows dissolved organic carbon (DOC) and CH_4(aq) concentrations versus Na^+ concentrations, while plot "b" shows formate ($CHOO^-$) and acetate (CH_3COO^-) concentrations versus Na^+ concentrations. Note that conservative mixing line was drawn to a value of 0.0 µM formate, but this value could be up to that of the detection limit of the instrument, depicted on the plot.

Conversely, total dissolved organic carbon (DOC) concentrations, which do not include CH_4(aq) concentrations by nature of analysis (Section 4.2.3), can be seen spiking in one mixing zone sample by ~20 μM. This is potentially a signature of CH_4(aq) being partially oxidized into organic carbon of intermediate oxidation states and released into the extracellular environment. The other source of this DOC production could be from the chemical reduction of DIC. However, although DIC decreases in this mixing zone sample relative to conservative mixing, it is matched by a decrease in Ca^{2+} (Fig. 24), which suggests that the DIC decrease is due to precipitation of calcite, as described in Section 4.3.2. It is possible that dissolution of atmospheric CO_2 could provide additional inorganic carbon that gets reduced to DOC. Still, these unconservative mixing trends together provide some support that active biological CH_4(aq) oxidation is occurring in this mixing zone. Additional isotopic evidence supporting this notion is discussed below. In some sense this mixing zone represents an extreme analog with regard to the mixing of oxidants into Type II fluids as they surface. It follows that when Type II fluids encounter atmospheric fluids, microbial CH_4 oxidation could be contributing to the low CH_4(aq) abundances observed relative to equilibrium for the CH_4 formation reaction, Eq. (12), illustrated in Fig. 25b.

Like CH_4(aq), acetate concentrations are also low relative to conservative mixing in mixing samples, as shown in Fig. 27b. Acetate is actually unique relative to other organic analytes in that concentrations are lower in both mixing zones than concentrations in either the Type I or Type II fluid, also indicating that mixing zone conditions are causing it to be consumed by some process. One possible abiotic explanation for this, supported by calcite precipitation experiments performed by Haile

(2011), is that acetate anions may be depleted from solution in mixing zones by adsorbing to the surface of actively precipitating calcite, which is occurring rapidly according to our interpretations in Section 4.3.2. Alternatively, but not mutually exclusive, some portion of acetate may be consumed via potential oxidation (Rempfert et al., 2017), reduction, or decarboxylation metabolisms by microorganisms in mixing zones, a subset of which are shown to be favorable in Fig. 26 (reactions B, C, D, I, K, L, and N).

Some of these reactions indicate that it is thermodynamically favorable to produce formate from redox reactions involving acetate (reactions C, D, and L). This could also explain why formate has a high abundance relative to conservative mixing while acetate has a low abundance relative to conservative mixing in the same sample Fig. 27b. Notably, the sample with high relative formate concentrations is not the same sample that has a high relative DOC concentration, so these observations are seemingly governed by different processes. In addition to production from acetate, it is also thermodynamically favorable to produce formate from oxidation of CH_4 (reaction F). This reaction was discussed in Section 4.3.5 as a possible explanation for why N-E Type II fluids have low CH_4(aq) abundances and high formate abundances relative to equilibrium for Eq. (12) and (13), respectively. The increase in formate in the mixing sample seems to strengthen this hypothesis, making this potential metabolic pathway a good target for taxonomic investigations as well as microbial incubation experiments that analyze for in situ methane consumption and formate production, along the lines of analyses performed on cultures (Chistoserdova et al., 2004).

More generally, active CH_4(aq) oxidation of any kind was investigated from a via

the analysis of stable carbon isotopic ratios for CH_4 in dissolved gas samples, abbreviated as $\delta^{13}CH_4(aq)$. As described above in Section 4.1.1, numerous investigations into natural serpentinizing systems have attempted to use $\delta^{13}C$ measurements to characterize the source of CH_4. Here we present $\delta^{13}CH_4(aq)$ across pH for our entire sample set where measurements were possible (Fig. 28, geochemistry compiled in Tables D2 and D4). Values of $\delta^{13}CH_4(aq)$ for the single mixing zone discussed above could not be compared to one another with completeness because the Type II dissolved gas sample from the single mixing zone leaked prior to isotopic analysis, and could not be analyzed, but the remaining three values can be identified in Table D4. However, Fig. 28 still seems to possess strong general trends across our entire sample set, probably due to pH still reflecting mixing, if only at a course grained level compared to silica(aq), for O_2-rich Type I fluids and CH_4-rich Type II fluids, which we expect to enhance microbial $CH_4(aq)$ oxidation.

A characteristic of these data is consistency in $\delta^{13}CH_4(aq)$ values between each set of near-endmember (N-E) fluid samples. Two N-E Type I fluid samples (only two out of four samples were able to be analyzed due to leakage), which are between pH of 7 and 8, possess the most depleted $\delta^{13}CH_4(aq)$ values, below -30 ‰. Similarly, four N-E Type II fluid samples (four out of five were able to be analyzed), which all have pH values of ~11.5, possess $\delta^{13}CH_4(aq)$ values between -12 and -7 ‰. All but one of the remaining Type II dominated fluids between pH 11.3 and 11.7 range in $\delta^{13}CH_4(aq)$ between -12 and -4 ‰. The depleted $\delta^{13}CH_4(aq)$ values in N-E Type I fluids appear to be nearly in equilibrium with CH_4 from air sampled in Oman, likely due to atmospheric exchange. On the other hand, N-E Type II fluids appear to have their own unique signature, perhaps

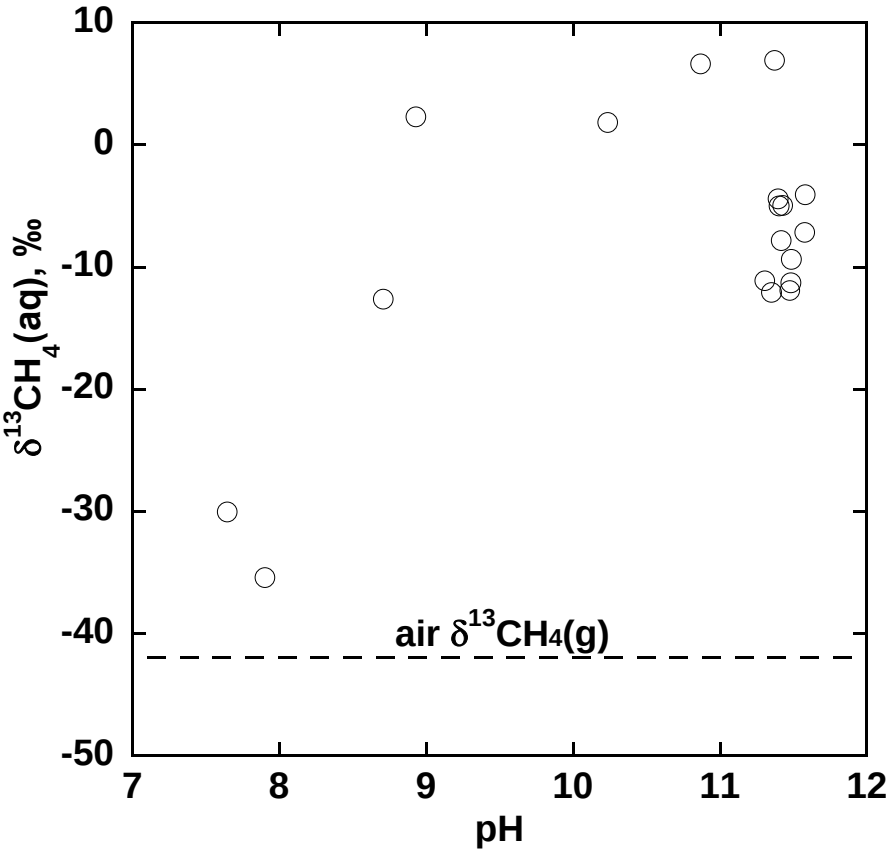

Fig. 28. Stable carbon isotopes of dissolved methane, $\delta^{13}CH_4(aq)$, versus pH, for fluid samples from the Samail Ophiolite. Average analytical uncertainties of one standard deviation from three injections are typically 2 – 3 ‰ for dissolved gas samples, and the analytical uncertainty of four replicate samples is ~10 ‰ for the value reported for "air" collected in Oman, due to atmospheric concentrations being low for the analytical technique used; exact uncertainties for each dissolved gas sample can be found in Table D4.

preserved from the deep or shallow subsurface. The $\delta^{13}CH_4(aq)$ values for N-E Type II fluids are relatively enriched compared to other serpentinizing systems, which are already often enriched relative to most other natural systems (e.g., Etiope and Sherwood Lollar, 2013). As Miller et al. (2016) note, this could either be due to an enriching process like preferential microbial oxidation of $^{12}CH_4(aq)$ over $^{13}CH_4(aq)$, or reduction of inorganic carbon in a carbon-limited zone of the subsurface, where nearly complete conversion takes place. This notion is also echoed by the thermodynamic calculations presented in Section 4.3.5, in which extremely low aCO_3^{2-} activities satisfy equilibrium for the methane formation reaction, Eq. (12). Additionally, we note that Mg^{2+}-rich carbonate minerals, expected to precipitate in the subsurface (Kelemen et al., 2011; Paukert et al., 2012), contain very similar $\delta^{13}C$ ranges (Mervine et al., 2014) to the $\delta^{13}CH_4(aq)$ we report from Type II fluids, which would be expected from complete reduction of a mineral reservoir to $CH_4(aq)$.

The most revealing trend in Fig. 28 is that the most positive $\delta^{13}CH_4(aq)$ values are in mid-pH samples, which are representative of mixing zones. It does not seem likely that these relatively positive values are simply a result of preferential degassing of $^{12}CH_4$, since some Type II dominated fluids with pH $\geq$ 11 are stagnant pools that should also be actively degassing. Degassing is a form of atmospheric exchange, and should also be accompanied by dissolution of atmospheric CH_4, which is relatively depleted in $^{13}CH_4$. Additionally, experiments regarding the kinetic isotope fractionation of CH_4 during gas exchange yield enrichment factors that are inadequate to explain the high $\delta^{13}CH_4(aq)$ values seen in mixing zones (Knox et al., 1992).

Consequently, high $\delta^{13}CH_4(aq)$ values in mid-pH mixing zones, ranging up to 6.6

± 2.5 ‰, are likely the result of microbial CH_4(aq) oxidation. This conclusion fits with the observation that CH_4(aq) concentrations are depleted relative to conservative mixing across the single mixing zone examined in this study, as demonstrated in Fig. 27. Therefore, this isotopic signature provides additional support for the hypothesis that microbial oxidation may be causing CH_4(aq) activities to be low relative to equilibrium, Eq. (12), in N-E Type I and N-E Type II fluids. A single high pH, Type II dominated fluid, with silica levels indicative of some subsurface mixing with Type I fluids, also possesses a high $\delta^{13}CH_4$(aq) value of 6.9 ± 1.9 ‰ (Table D1, D3, D4), providing some additional validation for this hypothesis.

4.4 Concluding remarks

A suite of geochemical analyses, including measurements of organic compounds, was performed on samples from shallow groundwater (Type I) and serpentinized (Type II) fluids sampled at surface springs from the Samail Ophiolite, in the Sultanate of Oman. Trends in the concentrations of aqueous carbon compounds and dissolved species were examined in near-endmember (N-E) fluids of both types, as well as mixtures of these fluids, to gain insights regarding carbon transformations during low temperature serpentinization. Thermodynamic calculations revealed which carbon species are in equilibrium in each type of fluid, and for those that are in disequilibrium, hypotheses were generated invoking active abiotic or biological processes as the cause. These hypotheses were tested by investigating changes in individual organic abundances and methane stable carbon isotopes across mixing Type I and Type II fluids, since these were expected to be ideal environments for active microbial redox metabolisms.

Based on the analyses of dissolved species, Organic compounds formate, acetate, and methane are all more abundant in Type II fluids than in Type I fluids, by varying degrees. Aqueous H_2 and other reduced species are also more abundant in Type II fluids, while DIC is depleted from Type II fluids. Given the likelihood that Type I fluids adequately represent the source fluid that is transformed into Type II fluids, it seems that the reducing conditions generated by serpentinization drive the reduction of inorganic carbon to form organic carbon.

According to the thermodynamic calculations, acetate is in equilibrium with DIC and H_2(aq) in both N-E Type I and N-E Type II fluids. Given that redox reactions are sluggish at low temperatures, we view this as strong evidence that microbial metabolisms control the forward and reverse formation reaction of acetate from these inorganic components. This may be the case for formate in N-E Type I fluids as well, but the majority of formate measurements were below instrumental detection limits in these fluids. Formate is in overabundance relative to equilibrium with DIC and H_2(aq) in N-E Type II fluids that we sampled. We hypothesize that this is because it formed and last equilibrated in the subsurface, where there is more H_2, and/or because microbial CH_4(aq) oxidation near the surface is generating formate. These are not mutually exclusive hypotheses. Additionally, CH_4(aq) is in low abundance relative to equilibrium with DIC and H_2(aq) in both fluid types, especially in Type II fluids. This is in agreement with the latter hypothesis of formate generation via CH_4(aq) oxidation. However, it could also be the case that CH_4(aq) formed in a deeper carbon-limited zone in the subsurface. Each metabolism invoked for a hypothesis was shown to be thermodynamically favorable under environmental conditions.

Trends in organic compounds across mixing zones of oxidized Type I fluids and reduced Type II fluids suggest CH_4(aq) oxidation to dissolved organic carbon and formate may be occurring. Enriched $\delta^{13}CH_4$(aq) values in mixing zones relative to Type I and Type II fluids reinforces this hypothesis. Similarly, Type II fluids have enriched $\delta^{13}CH_4$(aq) values relative to other natural systems, including serpentinizing ones, which supports the hypothesis that CH_4(aq) oxidation may be the cause of low CH_4(aq) abundance relative to equilibrium with DIC and H_2. Alternatively, enriched $\delta^{13}CH_4$(aq) values may be indicative of a very carbon-limited zone in the deep subsurface where virtually all inorganic carbon is converted into CH_4(aq). This alternative hypothesis could also explain why CH_4(aq) appears to be in low abundance at the surface, since equilibrium calculations are performed for fluids that are not carbon limited, since they are in contact with the atmosphere and are actively precipitating calcite.

It is important to note that none of these hypotheses are mutually exclusive. Ongoing taxonomic investigations of the microbial communities should help to test these hypotheses. A greater degree of clarity could be added by microbial incubation experiments that measure relative rates of organic production and consumption under environmentally relevant conditions. In addition to generating and testing a set of hypotheses regarding carbon cycling during low temperature serpentinization, this study provides a thermodynamic framework for predicting subsurface conditions and active processes in low temperature serpentinizing fluids.

4.5 Acknowledgements

I especially thank Jeurg Matter and Peter Kelemen for geographical, administrative, and cultural guidance in navigating the country of Oman. I also thank the

government administrators and locals of Oman, who made this scientific exploration possible, and who always made us feel welcome in an unfamiliar place. Shaela Noble was instrumental for organic acid anion analysis. Inorganic ion analyses were performed by Kris Fecteau. Dissolved gas measurements were performed by Alta Howells. James Leong is responsible for silica measurements and modified Fig 22. Grayson Boyer and Randall “Vince” Debes both contributed to dissolved inorganic and organic carbon analyses, under the guidance of Natasha Zolotova, in the Keck Lab. Tom Colella provided guidance and assistance for methane stable isotopes analyses conducted in the Goldwater Environmental Lab. Alysia Cox and Everett Shock both performed a variety of field sampling efforts that contributed to this work, and I also thank those official and honorary members of the Group Exploring Organic Processes in Geochemistry (GEOPIG) who contributed useful weekly discussions at Arizona State University, including Peter Canovas, Tucker Eli, and Josh Nye. This work was supported by NASA exobiology (NNX12AB38G), the NSF Integrated Earth Systems grant (EAR-1515513), and the NASA NAI Rock-Powered Life group (NNA15BB02A)

CHAPTER 5

FUTURE DIRECTIONS

In this work the kinetics, mechanisms, and equilibria of oxygen- and nitrogen-bearing organic compounds were investigated in the context of natural system modeling and exploration. Hydrothermal experiments with model amines elucidated reaction mechanisms for deamination under acidic conditions; similar, unbuffered experiments identified a variety of reversible substitution reactions that approached metastable equilibrium; and finally, analyses of inorganic and organic carbon species in a natural low-temperature serpentinizing system allowed predictions to be made regarding conditions and active processes in surface and subsurface environments. Each of these findings has prompted new inquiries, and here I recommend follow-up investigations that could improve the applications of this research, which potentially extend from Earth systems to other planetary environments.

The determination that two competing mechanisms (yielding an identical product, benzyl alcohol) are responsible for the deamination of protonated benzylamine, reveals the importance of characterizing mechanisms. Since one of these mechanisms is unimolecular and the other is bimolecular, the former should dominate at higher temperatures, because it is entropically favored, and the latter should dominate at lower temperatures. However, both the temperature at which this transition occurs and how sharp the temperature transition is remain unknown. Whether a similar transition exists for α-methylbenzylamine, which has a single unimolecular deamination mechanism, also remains unknown. Mechanistic characterization of aspartic acid deamination at low temperatures (≤ 135°C; Bada et al., 1970) suggests that there may be mechanistic

transitions for deamination at low temperatures in addition to substitution reactions. Experiments exploring these mechanistic transitions across narrower temperature ranges, with both these compounds and with different amines, could be used to develop predictors for these transitions regarding a wide range of environmentally relevant amines. Deamination reaction mechanisms for the unprotonated amines, at higher pH, also need to be investigated to make predictions regarding amine reactivty in natural systems.

Additional amines should be selected for hydrothermal experiments to bridge the gap between the more easily investigated mechanisms of model compounds and those of environmentally-relevant compounds, since reactivities will differ depending on compound structure. The mechanistic influences of the phenyl ring on the reactions of model compounds studied in this work need to be evaluated. This could be achieved via ring substituent experiments with 2-phenylethan-1-amine derivatives; compared to benzylamine this compound has an additional CH_2 between the amine and the ring, which would provide insights regarding aliphatic amine reaction mechanisms. It would also be wise to compare mechanistic influences from a variety of other structures found in natural compounds, such as amino acids. The challenge in doing this is that amino acids have multiple reactive functional groups and undergo several competing hydrothermal reactions (e.g. Imai et al., 1999; Lemke, 2003; Aubrey et al., 2009; Cleaves et al., 2009), which obscure mechanistic kinetic studies (Cox and Seward, 2006). However, mechanistic investigations of hydrothermal decarboxylation have already been performed for the model compound, phenylacetic acid (Glein, 2012). A logical next step is to investigate multi-functional group model compounds with both amines and carboxylic

acids, and eventually "phasing out" the aromatic structure. Some ideal amino acids to compare would be phenylglycine and phenylalanine, the latter of which has an extra CH_2 group, following the same logic as above. Studies of this kind may ultimately aid development of models that consider relative rates of abiotic degradation of biomass at different conditions on the Earth, as well as the persistence of organic nitrogen in abiotic planetary environments.

The approach toward metastable equilibrium in hydrothermal experiments for oxygen- and nitrogen-bearing organic compounds demonstrates that certain hydrothermal substitution reactions have the potential to produce ratios of organic compounds that reflect environmental conditions. In order to find quantitative application in natural systems, this experimental observation of model compound behavior will need to be tested using environmentally relevant compounds, for reasons concerning reactivity mentioned above. For systems with biological influence (essentially all terrestrial systems), biogenic amines, such as amino acids, are the most logical compounds to test experimentally due to their high abundance. The meteorite record also shows that amino acids are abundant in abiotic environments as well (Pizzarello and Shock, 2010). By targeting amino acids, direct comparisons can be made between experimental and environmental observations regarding metastability; conveniently, these metastability investigations would run parallel to those recommended above for mechanistic investigation. In addition to lab experiments, the terrestrial hydrothermal environments that have received considerable attention to date could be further investigated to probe metastable equilibrium, by first quantifying abundances of relevant compounds, like those mentioned above. Ideal candidate systems include the Von Damm submarine

hydrothermal vents and the Washburn hot springs of Yellowstone National Parks, both of which are rich in organic material and ammonium (Von Damm et al., 1985; Holloway et al., 2011). In a decade or so, NASA's Europa Clipper mission is expected to return analyses for a wide diversity of organic compounds in plumes rising into space from the icy moon, which might be linked to a subsurface ocean (Brockwell et al., 2016). With our current knowledge, the relative abundances of most organic compounds measured in this way would find little quantitative use. The experimental and environmental investigations into metastability recommended above, however, may allow us to use such data to infer subsurface temperatures, pressures, and compositional variables.

The equilibrium calculations for carbon transformation reactions at the Samail Ophiolite suggest that a variety of biological processes govern formate, acetate, and methane production and consumption during low-temperature serpentinization. However, in some instances multiple, plausible hypotheses still exist that require further microbiological investigations which are beyond the scope of this study. Sequencing, performed by other researchers (Miller et al., 2016; Rempfert et al., 2017) on samples from Oman, has identified close relatives of known microorganisms potentially capable of metabolizing hydrogen, methane, formate, and acetate; however, it is unclear if these genomic data sets, acquired from subsurface samples, are relevant for surface communities. Still, until taxonomic data sets are reported for surface fluids, these sequencing studies provide motivation to investigate rates of various metabolisms. Ideally, in situ studies will measure fluxes of relevant compounds in incubation experiments, or better yet, use isotopic labels to track carbon atoms as they undergo redox transformations into different metabolites, as in Urschel et al. (2015). The

calculations performed herein allowed hypotheses to be made about where various organics formed in the subsurface of the Samail Ophiolite. These hypotheses may soon be tested during the ongoing Oman Drilling Project (Matter et al., 2015), by analyzing similar species and determining whether their activities in the subsurface match the calculated activities in this study. The final important point to address in order to move this work forward, is the potential for atmospherically-derived organic acids to contribute to the high abundances of organic acid anions in Type II hyperalkaline fluids; the high pH of these fluids potentially promotes extensive dissolution (Ervens et al., 2003). These tests would be best done in the field, by collecting Type II water samples and performing dissolution rate experiments via exposure of samples to the atmosphere for different periods of time. These experiments would potentially find relevance with respect to all continental serpentinizing systems.

Characterizing carbon transformations during low temperature serpentinization will ultimately lead to expectations regarding abiotic versus biological production and consumption of organic compounds. These expectations will allow for assessing the habitability of modern and ancient planetary environments suspected to host serpentinization. If abiotic and biological carbon transformations can be quantitatively disentangled, relative organic compound abundances in extraterrestrial serpentinizing environments may also indicate whether such systems are currently inhabited.

The recommendations above each represent large undertakings that include experimental and field investigations. The potential future experiments outlined here are valuable because they attempt to bridge the gap between model compounds and environmentally relevant species. The field work suggested would test a variety of

hypotheses, and ultimately test the application of thermodynamic models to low-temperature systems as a means to explore active processes at the surface and in the subsurface. Together, the work herein and the potential future directions outlined represent an effort to better model aqueous organic chemistry in natural systems.

REFERENCES

Abdelmoez, W., Yoshida, H., and Nakahasi, T. (2010). Pathways of amino acid transformation and decomposition in saturated subcritical water conditions. *International Journal of Chemical Reactor Engineering*, *8*(1).

Abraham, M. H. (1984). Thermodynamics of solution of homologous series of solutes in water. *Journal of the Chemical Society, Faraday Transactions 1: Physical Chemistry in Condensed Phases*, *80*(1), 153-181.

Abraham, M. A., and Klein, M. T. (1985). Pyrolysis of benzylphenylamine neat and with tetralin, methanol, and water solvents. *Industrial and Engineering Chemistry Product Research and Development*, *24*(2), 300-306.

Abrajano, T. A., Sturchio, N. C., Bohlke, J. K., Lyon, G. L., Poreda, R. J., and Stevens, C. M. (1988). Methane-hydrogen gas seeps, Zambales Ophiolite, Philippines: Deep or shallow origin? *Chemical Geology*, *71*(1-3), 211-222.

Allred, G. C., and Woolley, E. M. (1981). Heat capacities of aqueous acetic acid, sodium acetate, ammonia, and ammonium chloride at 283.15, 298.15, and 313.15 K: ΔC°p for ionization of acetic acid and for dissociation of ammonium ion. *The Journal of Chemical Thermodynamics*, *13*(2), 155-164.

Anderson, F. E., and Prausnitz, J. M. (1986). Mutual solubilities and vapor pressures for binary and ternary aqueous systems containing benzene, toluene, m-xylene, thiophene and pyridine in the region 100–200° C. *Fluid Phase Equilibria*, *32*(1), 63-76.

Archer, D. G. (1987). Heat capacities of aqueous decyland dodecyl-trimethylammonium bromides from 324.6 to 374.6 K. *The Journal of Chemical Thermodynamics*, *19*(4), 407-415.

Arrhenius, S. (1889). Quantitative relationship between the rate a reaction proceeds and its temperature. *Journal of Physical Chemistry*, *4*, 226-248.

Aston, J. G., Sagenkahn, M. L., Szasz, G. J., Moessen, G. W., and Zuhr, H. F. (1944). The heat capacity and entropy, heats of fusion and vaporization and the vapor pressure of trimethylamine. The entropy from spectroscopic and molecular data. *Journal of the American Chemical Society*, *66*(7), 1171-1177.

Aubrey, A. D., Cleaves, H. J., and Bada, J. L. (2009). The role of submarine hydrothermal systems in the synthesis of amino acids. *Origins of Life and Evolution of Biospheres*, *39*(2), 91-108.

Bada, J. L., and Miller, S. L. (1968). Equilibrium constant for the reversible deamination of aspartic acid. *Biochemistry*, *7*(10), 3403-3408.

Bada, J. L., and Miller, S. L. (1970). Kinetics and mechanism of the reversible nonenzymic deamination of aspartic acid. *Journal of the American Chemical Society*, *92*(9), 2774-2782.

Bada, J. L., and McDonald, G. D. (1995). Amino acid racemization on Mars: Implications for the preservation of biomolecules from an extinct Martian biota. *Icarus*, *114*(1), 139-143.

Barnes, I., LaMarche, V. C., and Himmelberg, G. (1967). Geochemical evidence of present-day serpentinization. *Science*, *156*(3776), 830-832.

Barnes, I., and O'neil, J. R. (1969). The relationship between fluids in some fresh alpine-type ultramafics and possible modern serpentinization, western United States. *Geological Society of America Bulletin*, *80*(10), 1947-1960.

Barnes, I., O'neil, J. R., and Trescases, J. J. (1978). Present day serpentinization in New Caledonia, Oman and Yugoslavia. *Geochimica et Cosmochimica Acta*, *42*(1), 144-145.

Bell, J. L., Palmer, D. A., Barnes, H. L., and Drummond, S. E. (1994). Thermal decomposition of acetate: III. Catalysis by mineral surfaces. *Geochimica et Cosmochimica Acta*, *58*(19), 4155-4177.

Belousov, V. P., and Panov, M. I. (1994). *Thermodynamic Properties of Aqueous Solutions of Organic Substances*. CRC.

Belsky, A. J., and Brill, T. B. (1999). Spectroscopy of hydrothermal reactions. 14. kinetics of the pH-sensitive mminoguanidine− semicarbazide− cyanate reaction network. *The Journal of Physical Chemistry A*, *103*(39), 7826-7833.

Bénézeth, P., Palmer, D. A., and Wesolowski, D. J. (2001). Potentiometric study of the dissociation quotients of aqueous dimethylammonium ion as a function of temperature and ionic strength. *Journal of Chemical and Engineering Data*, *46*(2), 202-207.

Bénézeth, P., Wesolowski, D. J., and Palmer, D. A. (2003). Potentiometric study of the dissociation quotient of the aqueous ethanolammonium ion as a function of temperature and ionic strength. *Journal of Chemical and Engineering Data*, *48*(1), 171-175.

Benjamin, K. M., and Savage, P. E. (2004). Hydrothermal reactions of methylamine. *The Journal of Supercritical Fluids*, *31*(3), 301-311.

Bergström, S., and Olofsson, G. (1977). Thermodynamic quantities for the dissociation of the methylammonium ions between 273 and 398 K. *The Journal of Chemical Thermodynamics*, *9*(2), 143-152.

Berner, R. A. (2006). Geological nitrogen cycle and atmospheric N2 over Phanerozoic time. *Geology*, *34*(5), 413-415.

Beste, G. W., and Hammett, L. P. (1940). Rate and mechanism in the reactions of benzyl chloride with water, hydroxyl ion and ccetate ion 1. *Journal of the American Chemical Society*, *62*(9), 2481-2487.

Blackwell, L. F., Fischer, A., Miller, I. J., Topsom, R. D., and Vaughn, J. (1964) Dissociation of benzylammonium ions. *Journal of the Chemical Society (Resumed)*, *694*, 3588-3591.

Blanksby, S. J., and Ellison, G. B. (2003). Bond dissociation energies of organic molecules. *Accounts of Chemical Research*, *36*(4), 255-263.

Boudou, J. P., Schimmelmann, A., Ader, M., Mastalerz, M., Sebilo, M., and Gengembre, L. (2008). Organic nitrogen chemistry during low-grade metamorphism. *Geochimica et Cosmochimica Acta*, *72*(4), 1199-1221.

Bradley, A. S., and Summons, R. E. (2010). Multiple origins of methane at the Lost City Hydrothermal Field. *Earth and Planetary Science Letters*, *297*(1), 34-41.

Brandes, J. A., Hazen, R. M., and Yoder Jr, H. S. (2008). Inorganic nitrogen reduction and stability under simulated hydrothermal conditions. *Astrobiology*, *8*(6), 1113-1126.

Brockwell, T. G., Meech, K. J., Pickens, K., Waite, J. H., Miller, G., Roberts, J., Lunine, J., and Wilson, P. (2016, March). The mass spectrometer for planetary exploration (MASPEX). In *Aerospace Conference, 2016 IEEE*, 1-17.

Brotzel, F., Chu, Y. C., and Mayr, H. (2007). Nucleophilicities of primary and secondary amines in water. *The Journal of Organic Chemistry*, *72*(10), 3679-3688.

Brown, H. C., and Okamoto, Y. (1958). Electrophilic substituent constants. *Journal of the American Chemical* Society, *80*(18), 4979-4987.

Brown, H. C., and Rei, M. H. (1964). Comparison of the effect of substitutents at the 2-position of the norbornyl system with their effect in representative secondary aliphatic and alicyclic derivatives. evidence for the absence of nonclassical stabilization of the norbornyl cation. *Journal of the American Chemical Society*, *86*(22), 5008-5010.

Brown, J. S., Hallett, J. P., Bush, D., and Eckert, C. A. (2000). Liquid-liquid equilibria for binary mixtures of water + acetophenone, + 1-octanol, + anisole, and + toluene from 370 K to 550 K. *Journal of Chemical and Engineering Data*, *45*(5), 846-850.

Bruni, J., Canepa, M., Chiodini, G., Cioni, R., Cipolli, F., Longinelli, A., Marini, L., Ottonello, G., and Zuccolini, M. V. (2002). Irreversible water–rock mass transfer

accompanying the generation of the neutral, Mg–HCO 3 and high-pH, Ca–OH spring waters of the Genova province, Italy. *Applied Geochemistry*, *17*(4), 455-474.

Bunting, J. W., and Stefanidis, D. (1990). A systematic entropy relationship for the general-base catalysis of the deprotonation of a carbon acid. A quantitative probe of transition-state solvation. *Journal of the American Chemical Society*, *112*(2), 779-786.

Cabani, S., Conti, G., and Lepori, L. (1974). Volumetric properties of aqueous solutions of organic compounds. III. Aliphatic secondary alcohols, cyclic alcohols, primary, secondary, and tertiary amines. *The Journal of Physical Chemistry*, *78*(10), 1030-1034.

Cabani, S., Mollica, V., Lepori, L., and Lobo, S. T. (1977). Volume changes in the proton ionization of amines in water. 2. Amino alcohols, amino ethers, and diamines. *The Journal of Physical Chemistry*, *81*(10), 987-993.

Cabani, S., Gianni, P., Mollica, V., and Lepori, L. (1981). Group contributions to the thermodynamic properties of non-ionic organic solutes in dilute aqueous solution. *Journal of Solution Chemistry*, *10*(8), 563-595.

Canle, L., Demirtas, I., Freire, A., Maskill, H., and Mishima, M. (2004). Base strengths of substituted tritylamines, N-alkylanilines, and tribenzylamine in aqueous solution and the gas phase: steric effects upon solvation and resonance interactions. *European Journal of Organic Chemistry*, *2004*(24), 5031-5039.

Canovas, P. A., Hoehler, T., and Shock, E. L. (2017). Geochemical bioenergetics during low-temperature serpentinization: An example from the Samail Ophiolite, Sultanate of Oman. *Journal of Geophysical Research: Biogeosciences*, *122*(7), 1821-1847

Carothers, W. H., Bickford, C. F., and Hurwitz, G. J. (1927). The preparation and base strengths of some amines. *Journal of the American Chemical Society*, *49*(11), 2908-2914.

Carson, A. S., Laye, P. G., and Yürekli, M. (1977). The enthalpy of formation of benzylamine. *The Journal of Chemical Thermodynamics*, *9*(9), 827-829.

Charlou, J. L., Donval, J. P., Fouquet, Y., Jean-Baptiste, P., and Holm, N. (2002). Geochemistry of high H 2 and CH 4 vent fluids issuing from ultramafic rocks at the Rainbow hydrothermal field (36 14′ N, MAR). *Chemical Geology*, *191*(4), 345-359.

Charlou, J. L., Donval, J. P., Konn, C., Ondréas, H., Fouquet, Y., Jean-Baptiste, P., and Fourré, E. (2010). High production and fluxes of H2 and CH4 and evidence of abiotic hydrocarbon synthesis by serpentinization in ultramafic-hosted hydrothermal systems on the Mid-Atlantic Ridge. *Diversity of Hydrothermal Systems on Slow Spreading Ocean Ridges, American Geophysical Union, Washington, D. C,* 265-296.

Chavagnac, V., Ceuleneer, G., Monnin, C., Lansac, B., Hoareau, G., and Boulart, C. (2013). Mineralogical assemblages forming at hyperalkaline warm springs hosted on ultramafic rocks: a case study of Oman and Ligurian ophiolites. *Geochemistry, Geophysics, Geosystems*, *14*(7), 2474-2495.

Chistoserdova, L., Laukel, M., Portais, J. C., Vorholt, J. A., and Lidstrom, M. E. (2004). Multiple formate dehydrogenase enzymes in the facultative methylotroph Methylobacterium extorquens AM1 are dispensable for growth on methanol. *Journal of Bacteriology*, *186*(1), 22-28.

Cipolli, F., Gambardella, B., Marini, L., Ottonello, G., and Zuccolini, M. V. (2004). Geochemistry of high-pH waters from serpentinites of the Gruppo di Voltri (Genova, Italy) and reaction path modeling of CO_2 sequestration in serpentinite aquifers. *Applied Geochemistry*, *19*(5), 787-802.

Clayden, J., Warren, W., Greeves, N., and Wothers, P. (2001). Organic Chemistry. *Oxford University Press*.

Cleaves, H. J., Aubrey, A. D., and Bada, J. L. (2009). An evaluation of the critical parameters for abiotic peptide synthesis in submarine hydrothermal systems. *Origins of Life and Evolution of Biospheres*, *39*(2), 109-126.

CODATA. (1978). Recommended key values for thermodynamics, 1977. Report of the CODATA Task Group on key values for thermodynamics, 1977. *Jour. Chem. Thermodynamics*, *10*, 903-906.

Coke, J. L., McFarlane, F. E., Mourning, M. C., and Jones, M. G. (1969). Carbonium ions. II. Mechanism of acetolysis of 2-phenylethyltosylate. *Journal of the American Chemical Society*, *91*(5), 1154-1161.

Collins, C., Tobin, J., Shvedov, D., Palepu, R., and Tremaine, P. R. (2000). Thermodynamic properties of aqueous diethanolamine (DEA), N, N-dimethylethanolamine (DMEA), and their chloride salts: Apparent molar heat capacities and volumes at temperatures from 283.15 to 328.15 K. *Canadian Journal of Chemistry*, *78*(1), 151-165.

Cowan, D. A. (2004). The upper temperature for life–where do we draw the line?. *Trends in Microbiology*, *12*(2), 58-60.

Cox, J. D., and Pilcher, G. (1970). Thermochemistry of Organic and Organometallic Compounds. *Academic: London.*

Cox, J. S., and Seward, T. M. (2007). The hydrothermal reaction kinetics of aspartic acid. *Geochimica et Cosmochimica Acta*, *71*(4), 797-820.

Cronin, J. R., Pizzarello, S., and Cruikshank, D. P. (1988). Organic matter in carbonaceous chondrites, planetary satellites, asteroids and comets. *Meteorites and the Early Solar System, 1*, 819-857.

Cruse, A. M., and Seewald, J. S. (2006). Geochemistry of low-molecular weight hydrocarbons in hydrothermal fluids from Middle Valley, northern Juan de Fuca Ridge. *Geochimica et Cosmochimica Acta*, *70*(8), 2073-2092.

Delgado, F. F., Cermak, N., Hecht, V. C., Son, S., Li, Y., Knudsen, S. M., Olcum, S., Higgins, J. M., Chen, J., Grover, W. H., and Manalis, S. R. (2013). Intracellular water exchange for measuring the dry mass, water mass and changes in chemical composition of living cells. *PloS one*, *8*(7), e67590.

Domalski, E. S., and Hearing, E. D. (1993). Estimation of the thermodynamic properties of C-H-N-O-S-halogen compounds at 298.15 K. *Journal of Physical and Chemical Reference Data*, *22*(4), 805-1159.

Du, Y., Yuan, Y., and Rochelle, G. T. (2017). Volatility of amines for CO 2 capture. *International Journal of Greenhouse Gas Control*, *58*, 1-9.

Ehrenfreund, P., and Charnley, S. B. (2000). Organic molecules in the interstellar medium, comets, and meteorites: A voyage from dark clouds to the early Earth. *Annual Review of Astronomy and Astrophysics*, *38*(1), 427-483.

Encrenaz, T. (2008). Water in the solar system. *Annual Review of Astronomy and Astrophysics 46*(1), 57-87.

Ervens, B., Herckes, P., Feingold, G., Lee, T., Collett, J. L., and Kreidenweis, S. M. (2003). On the drop-size dependence of organic acid and formaldehyde concentrations in fog. *Journal of Atmospheric Chemistry*, *46*(3), 239-269.

Etiope, G., Schoell, M., and Hosgörmez, H. (2011). Abiotic methane flux from the Chimaera seep and Tekirova ophiolites (Turkey): Understanding gas exhalation from low temperature serpentinization and implications for Mars. *Earth and Planetary Science Letters*, *310*(1), 96-104.

Etiope, G., and Sherwood Lollar, B. (2013). Abiotic methane on Earth. *Reviews of Geophysics*, *51*(2), 276-299.

Faisal, M., Sato, N., Quitain, A. T., Daimon, H., and Fujie, K. (2007). Reaction kinetics and pathway of hydrothermal decomposition of aspartic acid. *International Journal of Chemical Kinetics*, *39*(3), 175-180.

Fecteau, K. M. (2016). *Organic Carbon in Hydrothermal Systems: From Phototrophy to Aldehyde Transformations* (Doctoral dissertation, Arizona State University).

Fenclová, D., Perez-Casas, S., Costas, M., and Dohnal, V. (2004). Partial molar heat capacities and partial molar volumes of all of the isomeric (C3 to C5) alkanols at infinite dilution in water at 298.15 K. *Journal of Chemical and Engineering Data*, *49*(6), 1833-1838.

Fernández-Reiriz, M. J., Perez-Camacho, A., Ferreiro, M. J., Blanco, J., Planas, M., Campos, M. J., and Labarta, U. (1989). Biomass production and variation in the biochemical profile (total protein, carbohydrates, RNA, lipids and fatty acids) of seven species of marine microalgae. *Aquaculture*, *83*(1-2), 17-37.

Florián, J., and Warshel, A. (1999). Calculations of hydration entropies of hydrophobic, polar, and ionic solutes in the framework of the Langevin dipoles solvation model. *The Journal of Physical Chemistry B*, *103*(46), 10282-10288.

Fuchida, S., Masuda, H., and Shinoda, K. (2014). Peptide formation mechanism on montmorillonite under thermal conditions. *Origins of Life and Evolution of Biospheres*, *44*(1), 13-28.

Fujio, M., Goto, M., Susuki, T., Akasaka, I., Mishima, M., and Tsuno, Y. (1990). Substituent Effects. XXI. Solvolysis of Benzyl Tosylates. *Bulletin of the Chemical Society of Japan*, *63*(4), 1146-1153.

Fujio, M., Susuki, T., Goto, M., Tsuji, Y., Yatsugi, K. I., Saeki, Y., Hong, K. S., and Tsuno, Y. (1994). Solvent effects on the solvolysis of benzyl p-toluenesulfonates. *Bulletin of the Chemical Society of Japan*, *67*(8), 2233-2243.

Galloway, J. N., Dentener, F. J., Capone, D. G., Boyer, E. W., Howarth, R. W., Seitzinger, S. P., Asner, G.P., Cleveland, C.C., Green, P.A., Holland, E.A., and Karl, D. M. (2004). Nitrogen cycles: past, present, and future. *Biogeochemistry*, *70*(2), 153-226.

Garrett, E. R., and Tsau, J. (1972). Solvolyses of cytosine and cytidine. *Journal of Pharmaceutical Sciences*, *61*(7), 1052-1061.

Giggenbach, W. F., Sheppard, D. S., Robinson, B. W., Stewart, M. K., and Lyon, G. L. (1994). Geochemical structure and position of the Waiotapu geothermal field, New Zealand. *Geothermics*, *23*(5-6), 599-644.

Gill, S. J., Nichols, N. F., and Wadsö, I. (1976). Calorimetric determination of enthalpies of solution of slightly soluble liquids II. Enthalpy of solution of some hydrocarbons in water and their use in establishing the temperature dependence of their solubilities. *The Journal of Chemical Thermodynamics*, *8*(5), 445-452.

St-Jean, G. (2003). Automated quantitative and isotopic (13C) analysis of dissolved inorganic carbon and dissolved organic carbon in continuous-flow using a total organic carbon analyser. *Rapid communications in mass spectrometry*, *17*(5), 419-428.

Glein, C. R. (2012). *Theoretical and Experimental Studies of Cryogenic and Hydrothermal Organic Geochemistry*. (Doctoral dissertation, Arizona State University).

Gluck, S. J., and Cleveland Jr., J. A. (1994) Capillary zone electrophoresis for the determination of dissociation constants. *Journal of Chromatography A*, *680*(1), 43-48

Gordon, A. J., and Ford, R. A. (1972). Chemist's Companion: A Handbook of Practical Data, Techniques, and References. *New York: Wiley*.

Graeber, E. J., Modreski, P. J., and Gerlach, T. M. (1979). Compositions of gases collected during the 1977 east rift eruption, Kilauea, Hawaii. *Journal of Volcanology and Geothermal Research*, *5*(3-4), 337-344.

Graton, J., Berthelot, M., and Laurence, C. (2001). Hydrogen-bond basicity pK_{HB} scale of secondary amines. *Journal of the Chemical Society, Perkin Transactions 2*, (11), 2130-2135.

Hach, D. (2007). *2800 Spectrophotometer: Procedures Manual*. Hach Company, Germany.

Haggerty, J. A., and Fisher, J. B. (1992). Short-chain organic acids in interstitial waters from Mariana and Bonin forearc serpentines: Leg 125. In *Fryer, P., Pearce, JA, Stokking, LB, et al., Proc. ODP, Sci. Results*, *125*, 387-395.

Hammett, L. P. (1935). Some Relations between Reaction Rates and Equilibrium Constants. *Chemical Reviews*, *17*(1), 125-136.

Hanai, T., Koizumi, K., Kinoshita, T., Arora, R., and Ahmed, F. (1997). Prediction of p*K*a values of phenolic and nitrogen-containing compounds by computational chemical analysis compared to those measured by liquid chromatography. *Journal of Chromatography A*, *762*(1), 55-61.

Harris, J. M., Schadt, F. L., Schleyer, P. V. R., and Lancelot, C. J. (1969). Participation by neighboring aryl groups. V. Determination of assisted and nonassisted rates in primary systems. Rate-product correlations. *Journal of the American Chemical Society*, *91*(26), 7508-7510.

Helgeson, H. C., Knox, A. M., Owens, C. E., and Shock, E. L. (1993). Petroleum, oil field waters, and authigenic mineral assemblages Are they in metastable equilibrium in hydrocarbon reservoirs. *Geochimica et Cosmochimica Acta*, *57*(14), 3295-3339.

Henley, R. W., Barton, P. B., Truesdell, A. H., & Whitney, J. A. (1984). *Fluid-Mineral Equilibria in Hydrothermal Systems* (Vol. 1). El Paso, TX: Society of Economic Geologists.

Høiland, H. (1986). Partial molar volumes of biochemical model compounds in aqueous solutions. *Thermodynamic Data for Biochemistry and Biotechnology*, 17-44.

Holloway, J. M., Nordstrom, D. K., Böhlke, J. K., McCleskey, R. B., and Ball, J. W. (2011). Ammonium in thermal waters of Yellowstone National Park: processes affecting speciation and isotope fractionation. *Geochimica et Cosmochimica Acta*, *75*(16), 4611-4636.

Holm, N. G., Oze, C., Mousis, O., Waite, J. H., and Guilbert-Lepoutre, A. (2015). Serpentinization and the formation of H2 and CH4 on celestial bodies (planets, moons, comets). *Astrobiology*, *15*(7), 587-600.

Hosgormez, H., Etiope, G., and Yalçin, M. N. (2008). New evidence for a mixed inorganic and organic origin of the Olympic Chimaera fire (Turkey): a large onshore seepage of abiogenic gas. *Geofluids*, *8*(4), 263-273.

Houser, T. J., Tsao, C. C., Dyla, J. E., Van Atten, M. K., and McCarville, M. E. (1989). The reactivity of tetrahydroquinoline, benzylamine and bibenzyl with supercritical water. *Fuel*, *68*(3), 323-327.

Imai, E. I., Honda, H., Hatori, K., Brack, A., and Matsuno, K. (1999). Elongation of oligopeptides in a simulated submarine hydrothermal system. *Science*, *283*(5403), 831-833.

Jenny, E. F., and Winstein, S. (1958). 14C-Umlagerung, Salzeffekte und Ionenpaar-Rückkehr in der Solvolyse von [2-(p-Anisyl)-äthyl]-p-toluolsulfonat. *Helvetica Chimica Acta*, *41*(3), 807-823.

Johnson, J. W., Oelkers, E. H., and Helgeson, H. C. (1992). SUPCRT92: A software package for calculating the standard molal thermodynamic properties of minerals, gases, aqueous species, and reactions from 1 to 5000 bar and 0 to 1000 C. *Computers and Geosciences*, *18*(7), 899-947.

Jolicoeur, C., and Lacroix, G. (1976). Thermodynamic properties of aqueous organic solutes in relation to their structure. Part III. Apparent molal volumes and heat capacities of low molecular weight alcohols and polyols at 25 C. *Canadian Journal of Chemistry*, *54*(4), 624-631.

Jolicoeur, C., Riedl, B., Desrochers, D., Lemelin, L. L., Zamojska, R., and Enea, O. (1986). Solvation of amino acid residues in water and urea-water mixtures: volumes and

heat capacities of 20 amino acids in water and in 8 molar urea at 25 C. *Journal of Solution Chemistry*, *15*(2), 109-128.

Jones, F. M., & Arnett, E. M. (2007). Thermodynamics of ionization and solution of aliphatic amines in water. *Progress in Physical Organic Chemistry, 11*, 263-322.

Kang, K. Y., and Chun, B. S. (2004). Behavior of hydrothermal decomposition of silk fibroin to amino acids in near-critical water. *Korean Journal of Chemical Engineering*, *21*(3), 654-659.

Katritzky, A. R., Lapucha, A. R., and Siskin, M. (1990). Aqueous high-temperature chemistry of carbo-and heterocycles. 12. Benzonitriles and pyridinecarbonitriles, benzamides and pyridinecarboxamides, and benzylamines and pyridylamines. *Energy and Fuels*, *4*(5), 555-561.

Katritzky, A. R., Nichols, D. A., Siskin, M., Murugan, R., and Balasubramanian, M. (2001). Reactions in high-temperature aqueous media. *Chemical Reviews*, *101*(4), 837-892.

Kelemen, P. B., and Matter, J. (2008). In situ carbonation of peridotite for CO2 storage. *Proceedings of the National Academy of Sciences of the U.S.A.*, *105*(45), 17295-17300.

Kelemen, P. B., Matter, J., Streit, E. E., Rudge, J. F., Curry, W. B., and Blusztajn, J. (2011). Rates and mechanisms of mineral carbonation in peridotite: natural processes and recipes for enhanced, in situ CO2 capture and storage. *Annual Review of Earth and Planetary Sciences*, *39*, 545-576.

Kelley, K. K. (1960). High Temperature Heat Content. *Heat Capacity, and Entropy Data for Inorganic Compounds, US Bureau Mines Bull, 584*.

Kelley, D. S., Karson, J. A., Blackman, D. K., and Fruh-Green, G. L. (2001). An off-axis hydrothermal vent field near the Mid-Atlantic Ridge at 30 degrees N. *Nature*, *412*(6843), 145.

Kharaka, Y. K., Carothers, W. W., and Rosenbauer, R. J. (1983). Thermal decarboxylation of acetic acid: implications for origin of natural gas. *Geochimica et Cosmochimica Acta*, *47*(3), 397-402.

Klein, M. T., Torry, L. A., Wu, B. C., Townsend, S. H., and Paspek, S. C. (1990). Hydrolysis in supercritical water: Solvent effects as a probe of the reaction mechanism. *The Journal of Supercritical Fluids*, *3*(4), 222-227.

Knicker, H. (2004). Stabilization of N-compounds in soil and organic-matter-rich sediments—what is the difference? *Marine Chemistry*, *92*(1), 167-195.

Knox, M., Quay, P. D., and Wilbur, D. (1992). Kinetic isotopic fractionation during air-water gas transfer of O2, N2, CH4, and H2. *Journal of Geophysical Research: Oceans*, *97*(C12), 20335-20343.

Lancelot, C. J., and Schleyer, P. V. R. (1969). Participation by neighboring aryl groups. I. Determination of assisted and nonassisted solvolysis rates by Hammett correlation. *Journal of the American Chemical Society*,*91*(15), 4291-4294.

Lang, S. Q., Butterfield, D. A., Schulte, M., Kelley, D. S., and Lilley, M. D. (2010). Elevated concentrations of formate, acetate and dissolved organic carbon found at the Lost City hydrothermal field. *Geochimica et Cosmochimica Acta*, *74*(3), 941-952.

Lebedeva, N. D. (1966). Heats of Combustion and Formation of Aliphatic Tertiary Amine Homologues. *Russian Journal of Physical Chemistry*, *40*(11), 1465.

Lee, N., Foustoukos, D. I., Sverjensky, D. A., Hazen, R. M., and Cody, G. D. (2014). Hydrogen enhances the stability of glutamic acid in hydrothermal environments. *Chemical Geology*, *386*, 184-189.

Leif, R. N., and Simoneit, B. R. T. (1995). Ketones in hydrothermal petroleums and sediment extracts from Guaymas Basin, Gulf of California. *Organic Geochemistry*, *23*(10), 889-904.

Leng, C., Kish, J. D., Roberts, J. E., Dwebi, I., Chon, N., and Liu, Y. (2015). Temperature-dependent Henry's law constants of atmospheric amines. *The Journal of Physical Chemistry A*, *119*(33), 8884-8891.

Lemke, K. H. (2003). *Peptide Synthesis under Simulated Deep-Sea Hydrothermal Conditions*. Stanford University. (Doctoral dissertation, Stanford University).

Lemke, K. H., Rosenbauer, R. J., and Bird, D. K. (2009). Peptide synthesis in early Earth hydrothermal systems. *Astrobiology*, *9*(2), 141-146.

Li, J., and Brill, T. B. (2003). Spectroscopy of hydrothermal reactions 25: Kinetics of the decarboxylation of protein amino acids and the effect of side chains on hydrothermal stability. *The Journal of Physical Chemistry A*, *107*(31), 5987-5992.

Lippmann-Pipke, J., Lollar, B. S., Niedermann, S., Stroncik, N. A., Naumann, R., van Heerden, E., and Onstott, T. C. (2011). Neon identifies two billion year old fluid component in Kaapvaal Craton. *Chemical Geology*, *283*(3), 287-296.

Maguire, J. J. (1954). After boiler corrosion. *Industrial and Engineering Chemistry*, *46*(5), 994-997.

Marshall, W. L. (1994). Hydrothermal synthesis of amino acids. *Geochimica et Cosmochimica Acta*, *58*(9), 2099-2106.

Matter, J. M., Kelemen, P. B., and Teagle, D. A. H. (2015, December). Scientific Drilling in the Samail Ophiolite, Sultanate of Oman. In *AGU Fall Meeting Abstracts*. V11A-3055.

McCollom, T. M., and Seewald, J. S. (2003). Experimental constraints on the hydrothermal reactivity of organic acids and acid anions: I. Formic acid and formate. *Geochimica et Cosmochimica Acta*, *67*(19), 3625-3644.

Martin, W., and Russell, M. J. (2007). On the origin of biochemistry at an alkaline hydrothermal vent. *Philosophical Transactions of the Royal Society of London B: Biological Sciences*, *362*(1486), 1887-1926.

Matson, D. L., Castillo, J. C., Lunine, J., and Johnson, T. V. (2007). Enceladus' plume: Compositional evidence for a hot interior. *Icarus*, *187*(2), 569-573.

McCollom, T. M., and Seewald, J. S. (2007). Abiotic synthesis of organic compounds in deep-sea hydrothermal environments. *Chemical Reviews*, *107*(2), 382-401.

McCollom, T. M., and Bach, W. (2009). Thermodynamic constraints on hydrogen generation during serpentinization of ultramafic rocks. *Geochimica et Cosmochimica Acta*, *73*(3), 856-875.

McCollom, T. M. (2013a). The influence of minerals on decomposition of the n-alkyl-α-amino acid norvaline under hydrothermal conditions. *Geochimica et Cosmochimica Acta*, *104*, 330-357.

McCollom, T. M. (2013b). Laboratory simulations of abiotic hydrocarbon formation in Earth's deep subsurface. *Reviews in Mineralogy and Geochemistry*, *75*(1), 467-494.

McDermott, J. M., Seewald, J. S., German, C. R., and Sylva, S. P. (2015). Pathways for abiotic organic synthesis at submarine hydrothermal fields. *Proceedings of the National Academy of Sciences of the U.S.A.*, *112*(25), 7668-7672.

Melchert, B., Devey, C. W., German, C. R., Lackschewitz, K. S., Seifert, R., Walter, M., Mertens, C., Yoerger, D. R., Baker, E. T., Paulick, H., and Nakamura, K. (2008). First evidence for high-temperature off-axis venting of deep crustal/mantle heat: The Nibelungen hydrothermal field, southern Mid-Atlantic Ridge. *Earth and Planetary Science Letters*, *275*(1), 61-69.

Mervine, E. M., Humphris, S. E., Sims, K. W., Kelemen, P. B., and Jenkins, W. J. (2014). Carbonation rates of peridotite in the Samail Ophiolite, Sultanate of Oman, constrained through 14 C dating and stable isotopes. *Geochimica et Cosmochimica Acta*, *126*, 371-397.

Mesmer, R. E., and Hitch, B. F. (1977). Base strength of amines at high temperatures. Ionization of cyclohexylamine and morpholine. *Journal of Solution Chemistry*, *6*(4), 251-261.

Miller, H. M., Matter, J. M., Kelemen, P., Ellison, E. T., Conrad, M. E., Fierer, N., Ruchala, T., Tominaga, M., and Templeton, A. S. (2016). Modern water/rock reactions in Oman hyperalkaline peridotite aquifers and implications for microbial habitability. *Geochimica et Cosmochimica Acta*, *179*, 217-241.

Moody, J. B. (1976). Serpentinization: a review. *Lithos*, *9*(2), 125-138.

Morrill, P. L., Kuenen, J. G., Johnson, O. J., Suzuki, S., Rietze, A., Sessions, A. L., Fogel, M.L., and Nealson, K. H. (2013). Geochemistry and geobiology of a present-day serpentinization site in California: The Cedars. *Geochimica et Cosmochimica Acta*, *109*, 222-240.

Mottl, M. J., Komor, S. C., Fryer, P., and Moyer, C. L. (2003). Deep-slab fluids fuel extremophilic Archaea on a Mariana forearc serpentinite mud volcano: Ocean Drilling Program Leg 195. *Geochemistry, Geophysics, Geosystems*, *4*(11).

Mumma, M. J., and Charnley, S. B. (2011). The chemical composition of comets—Emerging taxonomies and natal heritage. *Astronomy and Astrophysics*, *49*(1), 471.

Neal, C., and Stanger, G. (1983). Hydrogen generation from mantle source rocks in Oman. *Earth and Planetary Science Letters*, *66*, 315-320.

Nelson, D. L., Lehninger, A. L., and Cox, M. M. (2008). P*rinciples of Biochemistry*. Macmillan.

Nichols, N., and Wadsö, I. (1975). Thermochemistry of solutions of biochemical model compounds 3. Some benzene derivatives in aqueous solution. *The Journal of Chemical Thermodynamics*, *7*(4), 329-336.

Nichols, N., Sköld, R., Spink, C., and Wadsö, I. (1976). Thermochemistry of solutions of biochemical model compounds 6. α, ω-dicarboxylic acids, -diamines, and -diols in aqueous solution. *The Journal of Chemical Thermodynamics*, *8*(10), 993-999.

Olofsson, G., Oshodj, A. A., Qvarnström, E., and Wadsö, I. (1984). Calorimetric measurements on slightly soluble gases in water enthalpies of solution of helium, neon, argon, krypton, xenon, methane, ethane, propane, n-butane, and oxygen at 288.15, 298.15, and 308.15 K. *The Journal of Chemical Thermodynamics*, *16*(11), 1041-1052.

Otake, T., Taniguchi, T., Furukawa, Y., Kawamura, F., Nakazawa, H., and Kakegawa, T. (2011). Stability of amino acids and their oligomerization under high-pressure conditions: implications for prebiotic chemistry. *Astrobiology*, *11*(8), 799-813.

Pagé, M., Huot, J. Y., and Jolicoeur, C. (1993). A comprehensive thermodynamic investigation of water–ethanolamine mixtures at 10, 25, and 40° C. *Canadian Journal of Chemistry*, *71*(7), 1064-1072.

Parks, G. S., Todd, S. S., and Moore, W. A. (1936). Thermal data on organic compounds. XVI. Some heat capacity, entropy and free energy data for typical benzene derivatives and heterocyclic compounds. *Journal of the American Chemical Society*, *58*(3), 398-401.

Paukert, A. N., Matter, J. M., Kelemen, P. B., Shock, E. L., and Havig, J. R. (2012). Reaction path modeling of enhanced in situ CO2 mineralization for carbon sequestration in the peridotite of the Samail Ophiolite, Sultanate of Oman. *Chemical Geology*, *330*, 86-100.

Paukert, A. (2014). *Mineral carbonation in mantle peridotite of the Samail Ophiolite, Oman: Implications for permanent geological carbon dioxide capture and storage*. (Doctoral dissertation, Columbia University).

Pizzarello, S., and Shock, E. (2010). The organic composition of carbonaceous meteorites: The evolutionary story ahead of biochemistry. *Cold Spring Harbor Perspectives in Biology*, *2*(3), a002105.

Pizzarello, S., Williams, L. B., Lehman, J., Holland, G. P., and Yarger, J. L. (2011). Abundant ammonia in primitive asteroids and the case for a possible exobiology. *Proceedings of the National Academy of Sciences of the U.S.A.*, *108*(11), 4303-4306.

Plyasunov, A. V., and Shock, E. L. (2001). Correlation strategy for determining the parameters of the revised Helgeson-Kirkham-Flowers model for aqueous nonelectrolytes. *Geochimica et Cosmochimica Acta*, *65*(21), 3879-3900.

Porco, C. C., Helfenstein, P., Thomas, P. C., Ingersoll, A. P., Wisdom, J., West, R., Neukum, G., Denk, T., Wagner, R., Roatsch, T., Kieffer, S., Turtle, E., McEwen, A., Johnson, T. V., Rathbun, J., Vererka, J., Wilson, D., Perry, J., Spitale, J., Brahic, A., Burns, J. A., DelGenio, A. D., Done, L., Murray, C. D., and Squyres, S. (2006). Cassini observes the active south pole of Enceladus. S*cience*, *311*(5766), 1393-1401.

Potter, J., and Konnerup-Madsen, J. (2003). A review of the occurrence and origin of abiogenic hydrocarbons in igneous rocks. *Geological Society, London, Special Publications*, *214*(1), 151-173.

Proskurowski, G., Lilley, M. D., Kelley, D. S., and Olson, E. J. (2006). Low temperature volatile production at the Lost City Hydrothermal Field, evidence from a hydrogen stable isotope geothermometer. *Chemical Geology*, *229*(4), 331-343.

Proskurowski, G., Lilley, M. D., Seewald, J. S., Früh-Green, G. L., Olson, E. J., Lupton, J. E., Sylva, S. P., and Kelley, D. S. (2008). Abiogenic hydrocarbon production at Lost City hydrothermal field. *Science*, *319*(5863), 604-607.

Radzicka, A., and Wolfenden, R. (1996). Rates of uncatalyzed peptide bond hydrolysis in neutral solution and the transition state affinities of proteases. *Journal of the American Chemical Society*, *118*(26), 6105-6109.

Rasigraf, O., Vogt, C., Richnow, H. H., Jetten, M. S., and Ettwig, K. F. (2012). Carbon and hydrogen isotope fractionation during nitrite-dependent anaerobic methane oxidation by Methylomirabilis oxyfera. *Geochimica et Cosmochimica Acta*, *89*, 256-264.

Read, A. J. (1982). Ionization constants of aqueous ammonia from 25 to 250° C and to 2000 bar. *Journal of Solution Chemistry*, *11*(9), 649-664.

Rempfert, K. R., Miller, H. M., Bompard, N., Nothaft, D., Matter, J. M., Kelemen, P., Fierer, N., and Templeton, A. S. (2017). Geological and geochemical controls on subsurface microbial life in the Samail Ophiolite, Oman. *Frontiers in microbiology*, *8*.

Rhee, I. H., Ahn, H. K., Jun, G. H., and Ho, S. C. (2010) Effect of temperature on buffer intensity of amine solutions in water-steam cycle of PWRs. New Aspects of Fluid Mechanics, Heat Transfer and Environment, 8th IASME /WSEAS International Conference, 300-303.

Richner, G. (2013) Promoting CO2 absorption in aqueous amines with benzylamine. *Energy Procedia*, *37*, 423-430.

Ridley, M. K., Xiao, C., Palmer, D. A., and Wesolowski, D. J. (2000). Thermodynamic properties of the ionization of morpholine as a function of temperature and ionic strength. *Journal of Chemical and Engineering Data*, *45*(3), 502-507.

Robuchon, G., and Nimmo, F. (2011). Thermal evolution of Pluto and implications for surface tectonics and a subsurface ocean. *Icarus*, *216*(2), 426-439.

Rogalinski, T., Herrmann, S., and Brunner, G. (2005). Production of amino acids from bovine serum albumin by continuous sub-critical water hydrolysis. *The Journal of Supercritical Fluids*, *36*(1), 49-58.

Rushdi, A. I., and Simoneit, B. R. (2002). Hydrothermal alteration of organic matter in sediments of the Northeastern Pacific Ocean: Part 1. Middle Valley, Juan de Fuca Ridge. *Applied Geochemistry*, *17*(11), 1401-1428.

Russell, M. J., Hall, A. J., and Martin, W. (2010). Serpentinization as a source of energy at the origin of life. *Geobiology, 8*(5), 355-371.

Savage, P. E. (1999). Organic chemical reactions in supercritical water. *Chemical Reviews, 99*(2), 603-622.

Schadt, F. L., Bentley, T. W., and Schleyer, P. V. R. (1976). The SN2-SN1 spectrum. 2. Quantitative treatments of nucleophilic solvent assistance. A scale of solvent nucleophilicities. *Journal of the American Chemical Society, 98*(24), 7667-7675.

Schoonen, M. A., and Xu, Y. (2001). Nitrogen reduction under hydrothermal vent conditions: Implications for the prebiotic synthesis of CHON compounds. *Astrobiology, 1*(2), 133-142.

Schott, J., Pokrovsky, O. S., and Oelkers, E. H. (2009). The link between mineral dissolution/precipitation kinetics and solution chemistry. *Reviews in Mineralogy and Geochemistry, 70*(1), 207-258.

Schrenk, M. O., Brazelton, W. J., and Lang, S. Q. (2013). Serpentinization, carbon, and deep life. *Reviews in Mineralogy and Geochemistry, 75*(1), 575-606.

Schulte, M. D., and Shock, E. L. (1993). Aldehydes in hydrothermal solution: Standard partial molal thermodynamic properties and relative stabilities at high temperatures and pressures. *Geochimica et Cosmochimica Acta, 57*(16), 3835-3846.

Schwarz, H. (2011). Chemistry with methane: Concepts rather than recipes. *Angewandte Chemie International Edition, 50*(43), 10096-10115.

Seewald, J.S. (1994). Evidence for metastable equilibrium between hydrocarbons under hydrothermal conditions. *Nature, 370,* 285-287

Seewald, J. S. (2001). Aqueous geochemistry of low molecular weight hydrocarbons at elevated temperatures and pressures: Constraints from mineral buffered laboratory experiments. *Geochimica et Cosmochimica Acta, 65*(10), 1641-1664.

Seewald, J. S., Zolotov, M. Y., and McCollom, T. (2006). Experimental investigation of single carbon compounds under hydrothermal conditions. *Geochimica et Cosmochimica Acta, 70*(2), 446-460.

Shahidi, F. (1987). Partial molar volumes of phenalkylamines and their physiologically active derivatives in water. *Canadian Journal of Chemistry, 65*(8), 1924-1926.

Shipp, J., Gould, I. R., Herckes, P., Shock, E. L., Williams, L. B., and Hartnett, H. E. (2013). Organic functional group transformations in water at elevated temperature and

pressure: Reversibility, reactivity, and mechanisms. *Geochimica et Cosmochimica Acta*, *104*, 194-209.

Shipp, J. A., Gould, I. R., Shock, E. L., Williams, L. B., and Hartnett, H. E. (2014). Sphalerite is a geochemical catalyst for carbon−hydrogen bond activation. *Proceedings of the National Academy of Sciences of the U.S.A.*, *111*(32), 11642-11645.

Shock, E. L., Helgeson, H. C., and Sverjensky, D. A. (1989). Calculation of the thermodynamic and transport properties of aqueous species at high pressures and temperatures: Standard partial molal properties of inorganic neutral species. *Geochimica et Cosmochimica Acta*, *53*(9), 2157-2183.

Shock, E. L., and Helgeson, H. C. (1990). Calculation of the thermodynamic and transport properties of aqueous species at high pressures and temperatures: Standard partial molal properties of organic species. *Geochimica et Cosmochimica Acta*, *54*(4), 915-945.

Shock, E. L. (1992). Chemical environments of submarine hydrothermal systems. In *Marine Hydrothermal Systems and the Origin of Life* (pp. 67-107). Springer Netherlands.

Shock, E. L., Oelkers, E. H., Johnson, J. W., Sverjensky, D. A., and Helgeson, H. C. (1992). Calculation of the thermodynamic properties of aqueous species at high pressures and temperatures. Effective electrostatic radii, dissociation constants and standard partial molal properties to 1000 C and 5 kbar. *Journal of the Chemical Society, Faraday Transactions*, *88*(6), 803-826.

Shock, E. L. (1993). Hydrothermal dehydration of aqueous organic compounds. *Geochimica et Cosmochimica Acta*, *57*(14), 3341-3349.

Shock, E. L., Sassani, D. C., Willis, M., and Sverjensky, D. A. (1997). Inorganic species in geologic fluids: correlations among standard molal thermodynamic properties of aqueous ions and hydroxide complexes. *Geochimica et Cosmochimica Acta*, *61*(5), 907-950.

Shock, E. L., and Schulte, M. D. (1998). Organic synthesis during fluid mixing in hydrothermal systems. *Journal of Geophysical Research: Planets*, *103*(E12), 28513-28527.

Shock, E. L., Holland, M., Meyer-Dombard, D. R., and Amend, J. P. (2005). Geochemical sources of energy for microbial metabolism in hydrothermal ecosystems: Obsidian Pool, Yellowstone National Park. *Geothermal Biology and Geochemistry in Yellowstone National Park*, *1*, 95-112.

Shock, E., and Canovas, P. (2010). The potential for abiotic organic synthesis and biosynthesis at seafloor hydrothermal systems. *Geofluids*, *10*(1-2), 161-192.

Shock, E. L., Canovas, P., Yang, Z., Boyer, G., Johnson, K., Robinson, K., Fecteau, K., Windman, T., and Cox, A. (2013). Thermodynamics of organic transformations in hydrothermal fluids. *Reviews in Mineralogy and Geochemistry*, *76*(1), 311-350.

Shock, E. L., and Boyd, E. S. (2015). Principles of geobiochemistry. *Elements*, *11*(6), 395-401.

Simon, M., and Azam, F. (1989). Protein content and protein synthesis rates of planktonic marine bacteria. *Marine Ecology Progress Series*, 201-213.

Slavik, M., Šedlbauer, J., Ballerat-Busserolles, K., and Majer, V. (2007). Heat capacities of aqueous solutions of acetone; 2, 5-hexanedione; diethyl ether; 1, 2-dimethoxyethane; benzyl alcohol; and cyclohexanol at temperatures to 523 K. *Journal of Solution Chemistry*, *36*(1), 107-134.

Smith, R. M., and Hansen, D. E. (1998). The pH-rate profile for the hydrolysis of a peptide bond. *Journal of the American Chemical Society*, *120*(35), 8910-8913.

Sohlenkamp, C., and Geiger, O. (2016). Bacterial membrane lipids: diversity in structures and pathways. *FEMS Microbiology Reviews*, *40*(1), 133-159.

Streit, E., Kelemen, P., and Eiler, J. (2012). Coexisting serpentine and quartz from carbonate-bearing serpentinized peridotite in the Samail Ophiolite, Oman. *Contributions to Mineralogy and Petrology*, *164*(5), 821-837.

Střítеská, L., Hnědkovský, L., and Cibulka, I. (2004). Partial molar volumes of organic solutes in water. XI. Phenylmethanol and 2-phenylethanol at T=(298 to 573) K and at pressures up to 30 MPa. *The Journal of Chemical Thermodynamics*, *36*(5), 401-407.

Stull, D. R., Westrum, E. F., and Sinke, G. C. (1969). *The Chemical Thermodynamics of Organic Compounds.* John Wiley & Sons Inc., New York.

Suradi, S., Hacking, J. M., Pilcher, G., Gümrükċü, I., and Lappert, M. F. (1981). Enthalpies of combustion of five sterically hindered amines. *The Journal of Chemical Thermodynamics*, *13*(9), 857-861.

Swain, M. R., Vasisht, G., and Tinetti, G. (2008). The presence of methane in the atmosphere of an extrasolar planet. *Nature*, *452*(7185), 329.

Sweeton, F. H., Mesmer, R. E., and Baes Jr, C. F. (1974). Acidity measurements at elevated temperatures. VII. Dissociation of water. *Journal of Solution Chemistry*, *3*(3), 191-214.

Szponar, N., Brazelton, W. J., Schrenk, M. O., Bower, D. M., Steele, A., and Morrill, P. L. (2013). Geochemistry of a continental site of serpentinization, the Tablelands Ophiolite, Gros Morne National Park: a Mars analogue. *Icarus*, *224*(2), 286-296.

Takai, K., Nakamura, K., Toki, T., Tsunogai, U., Miyazaki, M., Miyazaki, J., Hirayama, H., Nakagawa, S., Nunoura, T., and Horikoshi, K. (2008). Cell proliferation at 122 C and isotopically heavy CH4 production by a hyperthermophilic methanogen under high-pressure cultivation. *Proceedings of the National Academy of Sciences of the U.S.A.*, *105*(31), 10949-10954.

Tanger, J. C., and Helgeson, H. C. (1988). Calculation of the thermodynamic and transport properties of aqueous species at high pressures and temperatures; Revised equations of state for the standard partial molal properties of ions and electrolytes. *American Journal of Science*, *288*(1), 19-98.

Taran, Y. A., and Giggenbach, W. F. (2003). Geochemistry of light hydrocarbons in subduction-related volcanic and hydrothermal fluids. *Special Publication-Society of Economic Geologists*, *10*, 61-74.

Taran, Y. A., Varley, N. R., Inguaggiato, S., and Cienfuegos, E. (2010). Geochemistry of H2-and CH4-enriched hydrothermal fluids of Socorro Island, Revillagigedo Archipelago, Mexico. Evidence for serpentinization and abiogenic methane. *Geofluids*, *10*(4), 542-555.

Tassi, F., Martinez, C., Vaselli, O., Capaccioni, B., and Viramonte, J. (2005). Light hydrocarbons as redox and temperature indicators in the geothermal field of El Tatio (northern Chile). *Applied Geochemistry*, *20*(11), 2049-2062.

Tassi, F., Vaselli, O., Capaccioni, B., Montegrossi, G., Barahona, F., and Caprai, A. (2007). Scrubbing process and chemical equilibria controlling the composition of light hydrocarbons in natural gas discharges: an example from the geothermal fields of El Salvador. *Geochemistry, Geophysics, Geosystems*, *8*(5).

Templeton, A. S., Chu, K. H., Alvarez-Cohen, L., and Conrad, M. E. (2006). Variable carbon isotope fractionation expressed by aerobic CH 4-oxidizing bacteria. *Geochimica et Cosmochimica Acta*, *70*(7), 1739-1752.

Thermodynamics Research Center Hydrocarbon Project. (1982). Selected values of properties of hydrocarbons and related compounds, A-84. *Texas AandM University, College Station.*

Tingle, T. N., Hochella, M. F., Becker, C. H., and Malhotra, R. (1990). Organic compounds on crack surfaces in olivine from San Carlos, Arizona and Hualalai Volcano, Hawaii. *Geochimica et Cosmochimica Acta*, *54*(2), 477-485.

Torry, L. A., Kaminsky, R., Klein, M. T., and Klotz, M. R. (1992). The effect of salts on hydrolysis in supercritical and near-critical water: reactivity and availability. *The Journal of Supercritical Fluids*, *5*(3), 163-168.

Touhara, H., Okazaki, S., Okino, F., Tanaka, H., Ikari, K., and Nakanishi, K. (1982). Thermodynamic properties of aqueous mixtures of hydrophilic compounds 2. Aminoethanol and its methyl derivatives. *The Journal of Chemical Thermodynamics*, *14*(2), 145-156.

Tsiaras, A., Rocchetto, M., Waldmann, I. P., Venot, O., Varley, R., Morello, G., Damiano, M., Tinetti, G., Barton, E. J., Yurchenko, S. N., Tennyson, J. (2016). Detection of an atmosphere around the super-Earth 55 Cancri e. *The Astrophysical Journal*, *820*(2), 99.

Uematsu, M., and Frank, E. U. (1980). Static dielectric constant of water and steam. *Journal of Physical and Chemical Reference Data*, *9*(4), 1291-1306.

Urschel, M. R., Kubo, M. D., Hoehler, T. M., Peters, J. W., and Boyd, E. S. (2015). Carbon source preference in chemosynthetic hot spring communities. *Applied and Environmental Microbiology*, *81*(11), 3834-3847.

Valentine, D. L., Chidthaisong, A., Rice, A., Reeburgh, W. S., and Tyler, S. C. (2004). Carbon and hydrogen isotope fractionation by moderately thermophilic methanogens. *Geochimica et Cosmochimica Acta*, *68*(7), 1571-1590.

Valvani, S. C., Yalkowsky, S. H., and Roseman, T. J. (1981). Solubility and partitioning IV: Aqueous solubility and octanol-water partition coefficients of liquid nonelectrolytes. *Journal of Pharmaceutical Sciences*, *70*(5), 502-507.

Vance, S. D., Hand, K. P., and Pappalardo, R. T. (2016). Geophysical controls of chemical disequilibria in Europa. *Geophysical Research Letters*, *43*(10), 4871-4879.

Vandenbroucke, M., and Largeau, C. (2007). Kerogen origin, evolution and structure. *Organic Geochemistry*, *38*(5), 719-833.

Vanderzee, C. E., and King, D. L. (1972). The enthalpies of solution and formation of ammonia. *The Journal of Chemical Thermodynamics*, *4*(5), 675-683.

Verdier-Paoletti, M. J., Marrocchi, Y., Avice, G., Roskosz, M., Gurenko, A., and Gounelle, M. (2017). Oxygen isotope constraints on the alteration temperatures of CM chondrites. *Earth and Planetary Science Letters*, *458*, 273-281.

Verevkin, S. P., and Vasiltsova, T. V. (2004). Thermochemistry of benzyl alcohol: Reaction equilibria involving benzyl alcohol and tert-alkyl ethers. *Journal of Chemical and Engineering Data*, *49*(6), 1717-1723.

Von Damm, K. V., Edmond, J. T., Measures, C. I., and Grant, B. (1985). Chemistry of submarine hydrothermal solutions at Guaymas Basin, Gulf of California. *Geochimica et Cosmochimica Acta*, *49*(11), 2221-2237.

Wadso, I. (1969). Enthalpies of vaporization of organic compounds. *Acta Chem. Scand*, *23*, 2061.

Wagman, D. D., Evans, W. H., Parker, V. B., Schumm, R. H., and Halow, I. (1982). The NBS tables of chemical thermodynamic properties. Selected values for inorganic and C1 and C2 organic substances in SI units. *National Standard Reference Data System.*

Waite, J. H., Glein, C. R., Perryman, R. S., Teolis, B. D., Magee, B. A., Miller, G., Grimes, J., Perry, M. E., Miller, K. E., Bouquet, A., and Lunine, J. I. (2017). Cassini finds molecular hydrogen in the Enceladus plume: Evidence for hydrothermal processes. *Science*, *356*(6334), 155-159.

Ward, N., Larsen, Ø., Sakwa, J., Bruseth, L., Khouri, H., Durkin, A. S., Dimitrov, G., Jiang, L., Scanlan, D., Kang., K. H., Lewis, M., Nelson, K. E., Methé, B., Wu, M., Heidelberg, J. F., Paulsen, I. T., Fouts, D., Ravel, J., Tettelin, H., Ren, Q., Read, T., DeBoy, R. T., Seshadri, R., Salzberg, S. L., Jensen, H. B., Birkeland, N. K., Nelson, W. C., Dodson, R. J., Grindhaug, S. H., Holt, I., Eidhammer, I., Jonasen, I., Vanaken, S., Utterback, T., Feldblyum, T. V., Fraser, C. M., Lillehaug, J. R., and Eisen, J. A.. (2004). Genomic insights into methanotrophy: the complete genome sequence of Methylococcus capsulatus (Bath). *PLoS biology*, *2*(10), e303.

Winstein, S., Brown, M., Schreiber, K. C., and Schlesinger, A. H. (1952). Neighboring carbon and hydrogen. IX. Neighboring phenyl in benzylmethylcarbinyl p-toluenesulfonate1 2. *Journal of the American Chemical Society*, *74*(5), 1140-1147.

Winstein, S., Lindegren, C. R., Marshall, H., and Ingraham, L. L. (1953). Neighboring carbon and hydrogen. XIV. Participation in solvolysis of some primary benzenesulfonates 1. *Journal of the American Chemical Society*, *75*(1), 147-155.

Wolery, T. J. (1992). *EQ3/6: A software package for geochemical modeling of aqueous systems: package overview and installation guide (version 7.0)* (p. 70). Livermore, CA: Lawrence Livermore National Laboratory.

Xie, W. W., and Tremaine, P. R. (1999). Thermodynamics of aqueous diethylenetriaminepentaacetic acid (DTPA) systems: apparent and partial molar heat capacities and volumes of aqueous H 2 DTPA 3−, DTPA 5−, CuDTPA 3−, and Cu 2 DTPA− from 10 to 55 C. *Journal of Solution Chemistry*, *28*(4), 291-325.

Yang, Z., Gould, I. R., Williams, L. B., Hartnett, H. E., and Shock, E. L. (2012). The central role of ketones in reversible and irreversible hydrothermal organic functional group transformations. *Geochimica et Cosmochimica Acta, 98*, 48-65.

Yang, Z., Lorance, E. D., Bockisch, C., Williams, L. B., Hartnett, H. E., Shock, E. L., and Gould, I. R. (2014). Hydrothermal photochemistry as a mechanistic tool in organic geochemistry: The chemistry of dibenzyl ketone. *The Journal of Organic Chemistry, 79*, 7861-7871.

Yang, Z., Hartnett, H. E., Shock, E. L., and Gould, I. R. (2015). Organic oxidations using geomimicry. *The Journal of Organic Chemistry, 80*, 12159-12165.

Young, E. D., Kohl, I. E., Lollar, B. S., Etiope, G., Rumble, D., Li, S., Haghneghdar, M. A., Schauble, E. A., McCain, K. A., Foustoukos, D. I., Sutclife, C., Warr, O., Ballentine, C. J. (2017). The relative abundances of resolved $^{12}CH_2D_2$ and $^{13}CH_3D$ and mechanisms controlling isotopic bond ordering in abiotic and biotic methane gases. *Geochimica et Cosmochimica Acta, 203*, 235-264.

APPENDIX A

SUPPORTING DATA FOR CHAPTER 2

The following descriptions and figures are the supporting data for the experimental methods, results, and interpretation in Chapter 2. The sections are presented in the same order in which they are referenced in Chapter 2.

Gas chromatography with flame ionization detection (GC-FID), sometimes complemented with mass spectrometry (GC-MS), was used to identify and quantify organic compounds abundances in experiments. All gas chromatography analyses used the same GC oven heating method (Table A1).

A key objective of this work was to study the deamination of protonated amines, and thus to ensure that amines with different structures (e.g., α-methyl, and ring substituents) were near-completely protonated under the experimental hydrothermal conditions (250°C, P_{sat}). Evidence for protonation was provided for benzylamine (**BA**) and α-methylbenzylamine (**α-CH$_3$-BA**; see Chapter 2 and Fig. 2) by estimating experimental pH (3.3) and estimating the pK_a values for these amines under experimental conditions. The latter was done by comparing existing pK_a values that have been measured to high temperatures (pK_a values range from 5 – 6 at 250°C) for a variety of amines that possess similar low temperature pK_a values (8.5 – 10.7) to **BA** and **α-CH$_3$-BA** (9.4 and 9.9, respectively) (Richner, 2013; Gluck and Cleveland Jr., 1994). In Fig. A1, we show that low temperature pK_a values for ring-substituted benzylamines also span a range (8.6 – 9.6) that is encompassed by the range of existing pK_a values for amines. Some of these values are experimental (Blackwell et al., 1964), and some were estimated using a linear relationship between the pK_a values of the ring-substituted benzylamines and their

Table A1
GC oven heating method used for all calibration standards and experiments.

T (°C)[a]	Rate (°C/min)[b]	Hold (min)[c]
40.0	-	0
140.0	10.0	0
220.0	5.0	0
300.0	20.0	5.0[d]

[a]target heating temperatures for the oven
[b]rate of heating between target temperatures
[c]hold times at each target temperature
[d]sometimes this hold time was extended to ensure that no larger compounds eluted at later times.

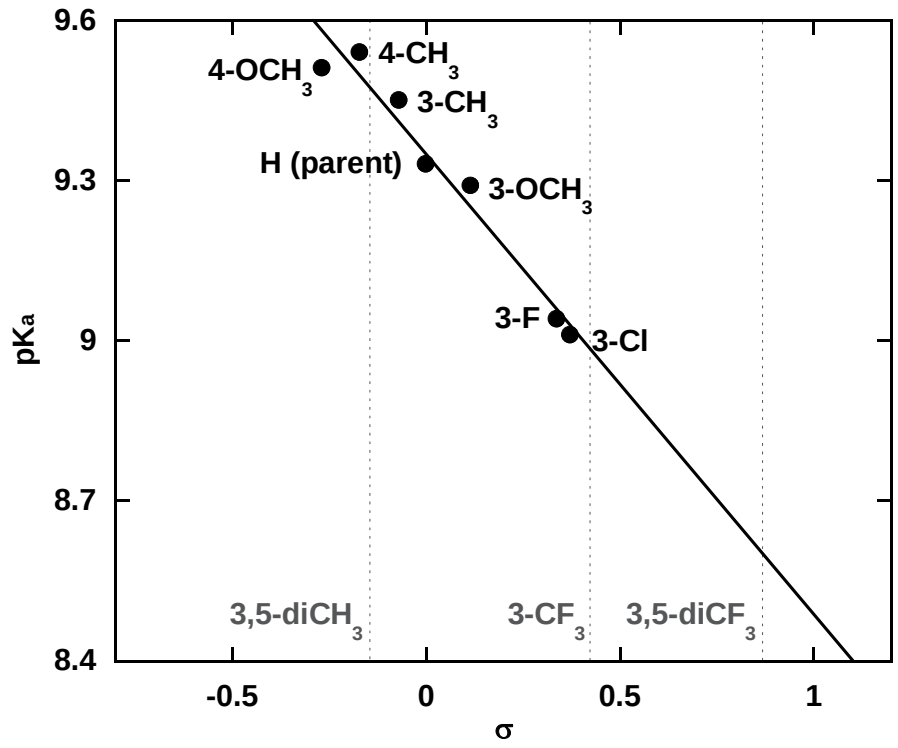

Fig. A1. pK_a values (black filled circles) at 25°C vs. sigma values (σ) for ring-substituted **BA** from Blackwell et al. (1964); the pK_a values are to be accurate to ± 0.02 units. A linear regression provides pK_a predictions for the remaining **BA** derivatives (grey text) used in this study. Sigma values were obtained from Gordon and Ford (1972). For the two-substituent compounds (e.g., 3,5-diCH_3), σ values were calculated by doubling the sigma values of their one-substituent counterparts (e.g., 3-CH_3).

Hammett σ values (Fig. A1); description of the Hammett σ values are found in Chapter 2 (Section 2.3.4) and in previous literature (Hammett, 1935).

The major products of reaction of benzylamine under acidic hydrothermal conditions were benzyl alcohol (**BAL**) and ammonium (NH_4^+). The time series concentration data for **BA** decomposition, **BAL** production, and NH_4^+ production (see Chapter 2 and Fig. 3) look strikingly similar to data from a subcritical (340 °C) hydrothermal experimental study that observed the decomposition of benzylphenylamine and the production of benzyl alcohol, aniline (analogous to ammonia), and toluene (Abraham and Klein, 1985), suggesting that benzylphenylamine might decay via a similar mechanism to that of **BA**. However, reactions with benzylphenylamine were not buffered, so mechanisms for it and **BA** should not be expected to be identical. Additionally, the extensive diversity of organic compound products seen in **BA** experiments was not reported for benzylphenylamine.

Fig. A2 shows GC-FID chromatograms for 68-hour (top) and 140-hour (bottom) experiments with 0.05 molal **BA**. Organic compound peaks are labeled, or if not visible, labels for approximate organic compound retention times are indicated. The scale in the top image is more extensive in order to show the most major products and their relative retention times, while the scale for the bottom image is zoomed in to display the product regions where two, three, and four phenyl ring compounds are expected to elute. The numerous peaks in these regions are suspected to be a large diversity of electrophilic aromatic substitution (**EAS**) products, and in fact, three isomers of benzyl-benzyl alcohol (expected **EAS** products) were identified for this and longer

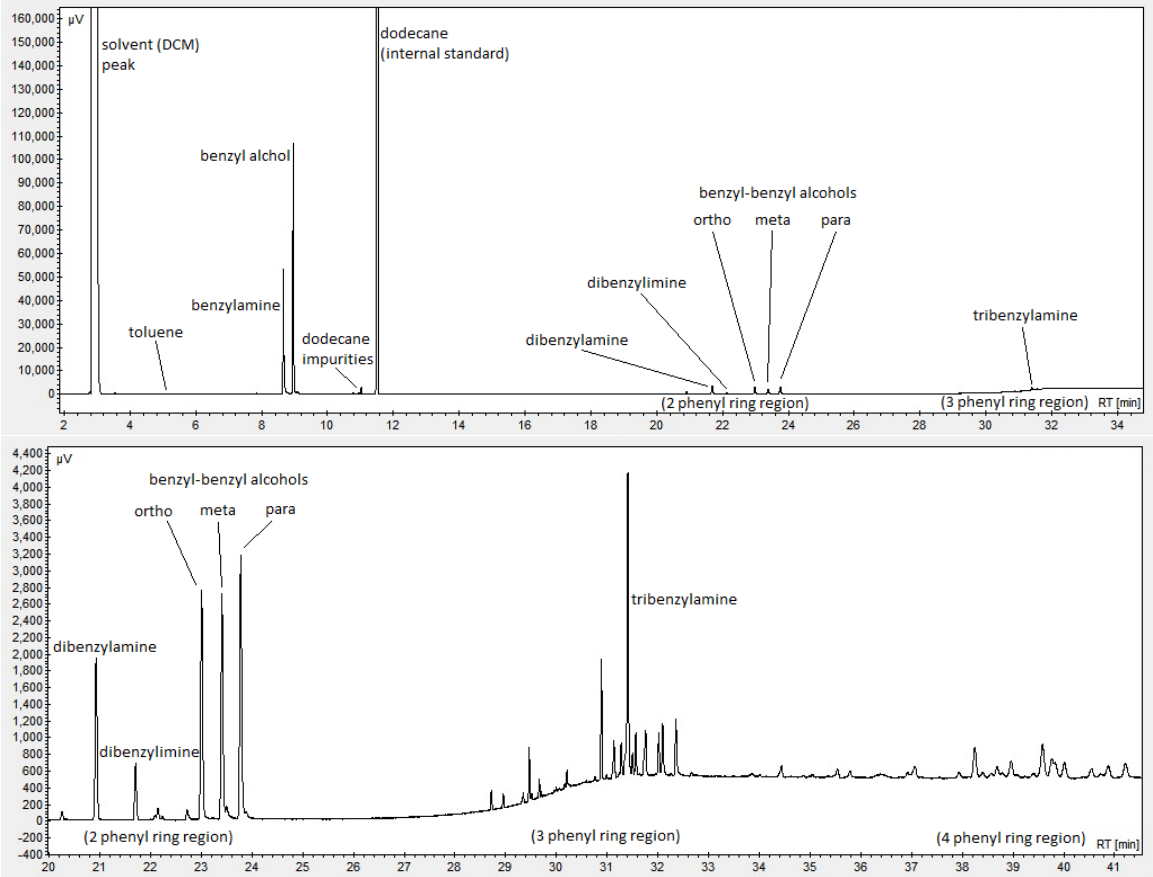

Fig. A2. Gas chromatograms (signal intensity, µV, vs. retention time, min) from 0.05 molal benzylamine experiments with 0.1 molal phosphate buffer (pH of 3.3) heated at 250°C (P_{sat}) for 68 hours (top) and 140 hours (bottom). The top image shows the chromatogram until after the three phenyl ring products no longer elute (34 min) from the column, since no four ring products were seen in 68-hour experiments. The bottom image shows a zoomed in scale of the chromatogram from the 140-hour experiment, displaying the plethora of unidentified peaks in the two, three, and four phenyl ring regions, assumed to mainly be products of EAS reactions. There are also numerous peaks that are not visually resolved in the bottom image. Note that peak heights do not necessarily correspond to relative abundance, because different compounds have different peak shapes. These images were obtained using CompassCDS software.

time experiments.

The primary focus of this work was to characterize deamination mechanisms for amines under acidic hydrothermal conditions. Comparing decomposition kinetics of ring-substituted **BA** and **α-CH_3-BA** provided the strongest evidence that the former reacts via two deamination mechanisms (S_N1 and S_N2), while the latter reacts via a single deamination mechanism (S_N1). Table A2 shows the time-dependent concentration data for experiments involving these ring-substituted compounds. From these data, first-order rate constants and the R^2 values for their fits were calculated. Also shown in the table are R^2 values for second-order rate constants that were calculated from the same data. Comparing the first- and second-order R^2 values demonstrates that the first-order fits were better, a finding that is in accordance with the proposed S_N1 (first-order) and S_N2 (pseudo-first-order) mechanisms of deamination.

Similar preliminary hydrothermal experiments with benzylamine buffered at high pH (250°C, 40 bar, pH 9) were also performed, revealing a more complicated set of competing reactions. These experiments were performed with 0.5 molal benzylamine and 0.1 molal phosphate buffer; the calculations for the buffer were performed using the same methods as described in Chapter 2. The reactant and product concentrations observed at different experimental times are shown in Table 3A. There is quite a contrast between these experimental data and those of protonated benzylamine at low pH. Protonated benzylamine (at high pH) decomposes much more slowly and produces much higher abundances of potential primary products, including: toluene (up to ~20%), dibenzylamine (up to ~5%), and dibenzylimine (up to ~10%); this indicates that it likely undergoes different primary reactions.

Table A2
Ring substituent experimental time series with concentration data and kinetics calculations

substituent(s)	σ^+ [a]	# expts.[c]	time [d] s x 10^{-3}	[reactant] [e] molal	S.D. [f] molal	log *k* [g] s^{-1}	1st order R^2 [h]	2nd order R^2 [h]
4-OCH3	-0.648	8	0.0	0.02354	0.00036	-2.23	0.982	0.842
t_{heat} = 5 min			0.1	0.01080	0.00075			
			0.2	0.00698	0.00053			
			0.2	0.00579	0.00004			
			0.3	0.00455	0.00010			
			0.3	0.00328	0.00012			
			0.4	0.00178	0.00012			
			0.5	0.00118	0.00002			
4-CH3	-0.256	7	0.0	0.04130	0.00028	-4.62	0.972	0.970
t_{heat} = 5min			0.0	0.04395	0.00006			
			7.2	0.03425	0.00012			
			7.2	0.03304	0.00020			
			14.4	0.03163	0.00013			
			21.6	0.02469	0.00009			
			28.8	0.02104	0.00008			
3,5-diCH3	-0.13 [b]	10	0.0	0.01771	0.00030	-4.81	0.937	0.915
t_{heat} = 240 min			0.0	0.01756	0.00012			
			28.8	0.00998	0.00005			
			28.8	0.00945	0.00024			
			30.6	0.01499	0.00004			
			30.6	0.01463	0.00009			
			72.0	0.00571	0.00005			
			72.0	0.00482	0.00004			
			118.8	0.00212	0.00002			
			158.4	0.00192	0.00001			
3-CH3	-0.065	8	0.0	0.03254	0.00011	-5.05	0.964	0.885
t_{heat} = 240 min			0.0	0.03029	0.00003			
			72.0	0.02218	0.00005			
			72.0	0.01968	0.00023			
			72.0	0.01660	0.00015			
			118.8	0.01253	0.00016			
			158.4	0.00654	0.00004			
			244.8	0.00401	0.00001			
H (parent)	0	8	0.0	0.04760	0.00024	-5.29	0.995	0.863
t_{heat} = 240min			32.4	0.03539	0.00001			
			72.0	0.03375	0.00025			
			72.0	0.03037	0.00020			
			160.2	0.01954	0.00007			
			244.8	0.01432	0.00003			
			244.8	0.01321	0.00005			
			504.0	0.00334	0.00002			
3-OCH3	0.047	8	0.0	0.02716	0.00032	-5.13	0.990	0.877
t_{heat} = 240min			45.9	0.02288	0.00032			
			72.0	0.01483	0.00024			

			143.1	0.00997	0.00016			
			143.1	0.00846	0.00006			
			236.7	0.00502	0.00008			
			236.7	0.00484	0.00005			
			333.9	0.00234	0.00005			
3-F	0.352	10	0.0	0.04666	0.00003	-5.68	0.961	0.891
t_{heat} = 240min			0.0	0.04320	0.00046			
			72.0	0.03476	0.00002			
			158.4	0.03311	0.00009			
			158.4	0.02957	0.00007			
			331.2	0.02298	0.00002			
			417.6	0.02257	0.00011			
			594.0	0.01228	0.00004			
			594.0	0.01169	0.00005			
			261.9	0.02845	0.00012			
3-Cl	0.399	12	0.0	0.04092	0.00013	-5.59	0.971	0.807
t_{heat} = 240min			0.0	0.04030	0.00006			
			0.0	0.03816	0.00023			
			72.0	0.03446	0.00008			
			72.0	0.03310	0.00005			
			261.9	0.01850	0.00006			
			309.6	0.01980	0.00020			
			309.6	0.01965	0.00012			
			504.0	0.01590	0.00006			
			504.0	0.00982	0.00009			
			504.0	0.00897	0.00004			
			1022.4	0.00278	0.00004			
3-CF3	0.52	11	0.0	0.03682	0.00031	-5.49	0.976	0.840
t_{heat} = 240min			0.0	0.03900	0.00005			
			72.0	0.03423	0.00025			
			72.0	0.03388	0.00016			
			302.4	0.01673	0.00008			
			302.4	0.01572	0.00001			
			504.0	0.00753	0.00007			
			504.0	0.00676	0.00006			
			504.0	0.00565	0.00001			
			504.0	0.00585	0.00005			
			1022.4	0.00171	0.00003			
3,5-diCF3	1.04 [b]	8	0.0	0.04765	0.00013	-5.70	0.997	0.941
t_{heat} = 240min			72.0	0.04352	0.00010			
			158.4	0.03813	0.00014			
			327.6	0.02587	0.00007			
			327.6	0.02582	0.00005			
			504.0	0.01974	0.00002			
			838.8	0.00910	0.00002			
			1022.4	0.00692	0.00001			
			0.0	0.00000	0.00000			
3-CH3, α-CH3	-0.065	8	0.0	0.02998	0.00008	-2.73	0.934	0.909

t_{heat} = 5min			0.12	0.02678	0.00006			
			0.3	0.01657	0.00005			
			0.42	0.01625	0.00009			
			0.6	0.00970	0.00001			
			0.72	0.00587	0.00001			
			0.9	0.00451	0.00008			
			1.2	0.00442	0.00007			
α-CH3	0	10	0.0	0.02119	0.00007	-3.10	0.901	0.705
t_{heat} = 5min			0.6	0.01247	0.00002			
			1.2	0.00523	0.00012			
			1.2	0.00457	0.00003			
			1.8	0.00706	0.00000			
			1.8	0.00354	0.00004			
			1.8	0.00333	0.00002			
			2.7	0.00150	0.00003			
			3.6	0.00230	0.00002			
			3.6	0.00099	0.00000			
3-CF3, α-CH3	0.52	7	0.0	0.05378	0.00003	-4.37	0.985	0.834
t_{heat} = 120min			7.2	0.03123	0.00006			
			16.2	0.02085	0.00001			
			21.6	0.01251	0.00003			
			21.6	0.01140	0.00003			
			86.4	0.00058	0.00001			
			165.6	0.00004	0.00001			
3,5-diCF3, α-CH3	1.04	7	0.0	0.05436	0.00007	-5.67	0.976	0.909
t_{heat} = 240min			72.0	0.04159	0.00010			
			72.0	0.03828	0.00007			
			248.4	0.02628	0.00003			
			504.0	0.01350	0.00004			
			504.0	0.01234	0.00003			
			1281.6	0.00241	0.00002			

[a] σ^+ values were obtained from Gordon and Ford, 1972.
[b] This was calculated by multiplying meta σ^+ value by 2.
[c] The number of rate experiments performed with each compound.
[d] The time of each experiment conducted, in seconds x 10^{-3}. Note, time zero begins after a heating time, t_{heat}
[e] Average reactant concentrations from 3 autosampler injections on the GC-FID.
[f] Analytical uncertainties determined from 3 autosampler injections on the GC-FID.
[g] These values were calculated from 1st order kinetics fits in KaleidaGraph.
[h] These R^2 values were determined by fitting 1st and 2st order kinetics fits in KaleidaGraph.

Table A3
Hydrothermal experiments (250 °C, 40 bar) with 0.5 molal benzylamine buffered with 0.1 molal phosphate at pH 9.0.

time [a] s x 10^{-3}	benzyl-amine molal	benzyl alcohol molal	dibenzy-lamine molal	tribenz-ylamine molal	dibenz-ylimine molal	tol-uene molal
79.2	0.46875	0.00068	0.00221	B.D.L.	0.00237	0.00052
79.2	0.47210	0.00002	0.00003	B.D.L.	0.00007	0.00003
194.4	0.33057	0.01242	0.01055	B.D.L.	0.01718	0.01556
194.4	0.33060	0.01390	0.01069	B.D.L.	0.01862	0.01645
320.4	0.27910	0.02583	0.01480	0.00170	0.02628	0.03062
320.4	0.34269	0.01161	0.01205	B.D.L.	0.01345	0.01287
406.8	0.20302	0.05519	0.02391	0.00178	0.03920	0.05808
406.8	0.22561	0.05572	0.02481	0.00178	0.04169	0.06721
604.8	0.12570	0.08275	0.03167	0.00198	0.04506	0.09212
604.8	0.13658	0.07752	0.03015	0.00193	0.04382	0.08987
867.6	0.04809	0.10401	0.02716	0.00236	0.04031	0.10806
867.6	0.06544	0.09518	0.02693	0.00214	0.03793	0.09850

[a] The time of each experiment conducted, in seconds x 10^{-3}.
Organic concentrations are averages from 2 autosampler injections on the cation IC.
B.D.L. indicates when concentrations were below detection limits of the instrument.

The presence of second-order kinetics was also investigated by performing **BA** experiments with starting concentrations of initial reactant and phosphate buffer species that were a factor of three greater than the rest of the experiments conducted in the study (0.15 vs. 0.05 molal **BA**). The resulting time-dependent concentrations are shown in Table A4, along with first-order decomposition rate constants which were calculated from that data. The difference in rate constants is small, suggesting that there are only minor contributions to decomposition kinetics from second-order reactions, interactions with buffer species, or ionic strength effects.

Table A4
Experimental concentration-dependence and NH_4^+ measurements

starting conditions	time [a] s x 10^{-3}	[BA] [b] molal	S.D. [c] molal	log k [d] s^{-1}	[BAL] [b] molal	S.D. [c] molal	[NH_4^+] [e] molal	S.D. [c] molal
0.05 molal	0.0	0.04760	0.00024	-5.29	0.00279	0.00002	0.00240	0.00171
BA	32.4	0.03539	0.00001		0.00753	0.00002		
0.10 molal	72.0	0.03375	0.00025		0.01534	0.00014	0.01658	0.00101
buffer	72.0	0.03037	0.00020		0.01427	0.00010		
t_{heat}=240min	160.2	0.01954	0.00007		0.02133	0.00009		
	165.6						0.03088	0.00036
	244.8	0.01432	0.00003		0.02173	0.00008	0.03703	0.00020
	244.8	0.01321	0.00005		0.02186	0.00003		
	504.0	0.00334	0.00002		0.01715	0.00040	0.04680	0.00418
0.15 molal	0.0	0.12990	0.00011	-5.16				
BA	72.0	0.08183	0.00022					
0.30 molal	158.4	0.03985	0.00015					
buffer	158.4	0.03326	0.00010					
t_{heat}=240min	244.8	0.02839	0.00013					
	331.2	0.01611	0.00001					
	331.2	0.01633	0.00004					
	504.0	0.00859	0.00001					

[a] The time of each experiment conducted, in seconds x 10^{-3}. Note, time zero begins after a heating time, t_{heat}.
[b] Average reactant concentrations from 3 autosampler injections on the GC-FID.
[c] Analytical uncertainties determined from 3 autosampler injections on the GC-FID.
[b] Calculated from simple first-order kinetic fits using KaleidaGraph.
[e] Average reactant concentration from 2 autosampler injections on the cation IC.
[f] Solutions were buffered using phosphate salts.

Also shown in Table A4 are concentrations of benzyl alcohol (**BAL**) and NH_4^+ over time for the lower concentration **BA** experiments. These values show that for the first 20 hours of reaction (72.0 x 10^{-3} s), benzyl alcohol and NH_4^+ increase proportionally with a 1:1 ratio to benzylamine conversion, according to the reaction scheme in Fig. 4 of Chapter 2. This suggests that deamination and hydration are the dominant primary reactions occurring in the experiments.

For the reaction of **α-CH_3-BA** under acidic hydrothermal conditions, styrene was one of the observed products, assumed to come from an elimination reaction, potentially either from the alcohol (**α-CH_3-BAL**) as a secondary product or from the amine as a primary product. Amine elimination would complicate the extraction of kinetic parameters and also jeopardize comparison of **α-CH_3-BA** and **BA** kinetics. Therefore it was necessary to investigate whether the decomposition kinetics of the amine were significantly enhanced by a reaction to form styrene. The following two lines of evidence suggest that the major primary reaction of **α-CH_3-BA** is substitution to form α-methylbenzyl alcohol (**α-CH_3-BAL**), and then the alcohol rapidly eliminated to form styrene:

1) After 5 minutes of heating (t_{heat} = 5, t = 0 minutes, see Section 2.2.3) **α-CH_3-BA** at 250°C, the ratio of **α-CH_3-BAL** to styrene is 4.3. Then, at t = 10 minutes the ratio is 1.0 and thereafter the average ratio is approximately 0.8, seemingly reaching steady state in favor of styrene (Table A5). The inversion of the ratio suggests that **α-CH_3-BAL** is formed first, and then dehydrates rapidly to form styrene as a secondary product. An experiment with **α-CH_3-BA** was also conducted at 200°C to observe the ratio of the alcohol to styrene after even less reaction progress. At t = 10 minutes the ratio is 19.7,

Table A5.
α-CH_3-BA experimental time-dependent concentrations and products

time s x 10^{-3}	[**α-CH_3-BA**] molal	S.D. [a] molal	[**α-CH_3-BAL**] molal	S.D. [a] molal	styrene molal	S.D. [a] molal
0.00	0.02114	0.00007	0.00077	0.00001	0.00018	0.00000
0.01	0.01248	0.00002	0.00304	0.00001	0.00316	0.00002
0.02	0.00528	0.00012	0.00436	0.00002	0.00620	0.00006
0.03	0.00357	0.00004	0.00439	0.00000	0.00609	0.00003
0.03	0.00706	0.00000	0.00442	0.00001	0.00415	0.00001
0.06	0.00232	0.00002	0.00507	0.00001	0.00491	0.00001
0.06	0.00099	0.00000	0.00465	0.00001	0.00612	0.00002

[a] Analytical uncertainties determined from 3 autosampler injections on the GC-FID

clearly demonstrating that **α-CH$_3$-BAL** was first being produced at a rapid rate, followed by the more sluggish reaction to produce styrene. This finding is depicted in the previous reaction path shown in Fig. 10, above.

2) Another experiment was conducted with chiral R-(+)-**α-CH$_3$-BAL** under similarly buffered hydrothermal conditions at 200°C. The products of this experiment were analyzed using a chiral column. Both S-(-)-**α-CH$_3$-BAL** and styrene are produced, presumed to be the results of a substitution (S_N1 or S_N2) reaction and an elimination (E1 or E2) reaction, respectively. At t = 10 minutes, the mixture of R and S alcohols is nearly racemic (R/S ratio of 1.03), and the ratio of total alcohol to styrene is 4.8, suggesting that the substitution reaction must be much more rapid than the elimination reaction. The near-racemic mixture shows that water rapidly substitutes for the hydroxyl at these conditions. Comparatively, **α-CH$_3$-BA** decomposes very little (< 5%) by t=10 minutes at 200°C, indicating that water substitutes much more rapidly with the alcohol than the amine. Therefore the alcohol likely racemizes via an S_N1 mechanism, since a protonated hydroxyl group should be the best leaving group in any experiments herein based on pK_b (p$K_{b\ H2O}$ < p$K_{b\ NH3}$ < p$K_{b\ OH-}$ < p$K_{b\ NH2-}$). This finding suggests that the alcohol protonates and dehydrates to form the benzyl cation much more rapidly, strengthening the case for the general reaction path of alcohol to **EAS** products outlined above (Chapter 2, Fig. 6 and 9).

APPENDIX B

SUPPORTING DATA FOR CHAPTER 3

As mentioned in Section 3.2.2, total ammonia (ΣNH_3) measurements were only made for 72-hour experiments of each time series. These measurements were used only for calculating reaction quotients that were compared with independently calculated equilibrium constants in Section 3.3.5. The measurements were also compared to the amount of ΣNH_3 in solution according to how much nitrogen was bonded to identified organic compounds, according to Eq. (B1):

$$\Sigma[NH_3] = 0.5 - (\Sigma[BA] + \Sigma[DBA] + \Sigma[TBA] + \Sigma[DBI]) \qquad \text{(B1)},$$

where each species (BA: benzylamine, DBA: dibenzylamine, TBA: tribenzylamine, DBI: dibenzylimine) concentration in the equation is the sum of its protonated and unprotonated forms and the value 0.5 corresponds to the intended molal concentration of nitrogen added to each experiment. As seen in Table B1, the 72-hour ΣNH_3 measurements accounted for an average of 73.1 ± 6.1% (±1 standard deviation) of the total ammonia calculated by equation Eq. (B1). The discrepancy between measured and estimated ΣNH_3 at 72 hours was probably due to the lack of quantification of the numerous unidentified organics that appear at later reaction times (Section 3.3.2), some of which could contain nitrogen. It is also possible that some larger products at later reaction times were not analyzable via GC due to their lack of solubility or volatility; these could also contain unaccounted nitrogen. However, since reaction quotients calculated for the four sets of experiments spanned up to 5 orders of magnitude, this discrepancy, a factor of 0.73, was not expected to make a large difference in the trends of Fig. 15 or 9, nor in the resulting interpretations. Most importantly, since ΣNH_3 was

Table B1
Measurements and estimates of total ammonia concentration, $\Sigma[NH_3]$, in hydrothermal experiments

initial organic reactant	time hours	calculated[a] $\Sigma[NH_3]$ molal	measured $\Sigma[NH_3]$ molal	substract $NH_3(g)$ $\Sigma[NH_3]$ molal
benzyl	2.0	0.488		0.477
alcohol	22.0	0.431		0.420
	22.0	0.435		0.424
	45.5	0.407		0.398
	28.0	0.439		0.429
	72.0	0.418	0.264	0.258*
benzyl-	2.0	0.181		0.177
amine	5.0	0.222		0.217
	9.0	0.277		0.270
	22.0	0.210		0.205
	28.0	0.349		0.340
	45.5	0.374		0.365
	72.0	0.392	0.308	0.301*
	72.0	0.394	0.308	0.301*
dibenzyl-	2.0	0.305		0.298
amine	22.0	0.339		0.331
	28.0	0.359		0.350
	28.0	0.362		0.353
	45.5	0.411		0.401
	45.5	0.428		0.418
	72.0	0.405	0.293	0.286*
tribenzyl-	2.0	0.299		0.292
amine	22.0	0.356		0.347
	28.0	0.377		0.368
	45.5	0.346		0.337
	72.0	0.409	0.303	0.296*

a: calculated using Eq. (B1): $\Sigma[NH_3] = 0.5 - ([BA] + [DBA] + [TBA] + [DBI])$
* measured $\Sigma[NH_3]$ used to calculate this value

measured for 72 hours experiments, the reaction quotients calculated from these experiments are more robust than if Eq. (B1) had been used to calculate $\Sigma[NH_3]$.

Calculations were performed to determine how much gaseous NH_3 would partition into the headspace of the reaction vessels using the software program, SUPCRT92 (Johnson et al., 1992), which employs the Helgeson-Kirkham-Flowers revised equation of state (Kelley, 1960; Wagman et al., 1982; Tanger and Helgeson, 1988; Shock et al., 1989; 1990; 1992; 1997). This was necessary because NH_3 was the most volatile reactant/product in experiments. Based on the density of water at 250°C the experimental solution:headspace volume ratio was determined to be 3.1. The calculations predict that 3.4% of the ΣNH_3 measured at 72 hours would be in the gas phase at the calculated experimental pH of 5.4 (Section 3.2.3). Therefore, the estimated ΣNH_3 values were multiplied by a factor of 0.976 to properly calculate all reaction quotients (Table B1).

The eight major products that were monitored and quantified in experiments were benzyl alcohol, benzylamine, dibenzylamine, tribenzylamine, dibenzylimine, toluene, benzyl ether, and benzaldehyde. Cumulative concentrations of unidentified two and three phenyl ring products (the two ring group included three identified benzyl-benzyl alcohol isomers) were also estimated (see Section 3.2.2). Concentrations of these compounds can be seen for each of the four sets of experiments over time in Table B2.

Table B2
Organic compound concentrations from time series experiments

initial organic reactant	time hours	benzyl alcohol molal	benzyl-amine molal	dibenzyl-amine molal	tribenzyl-amine molal	dibenzyl-imine molal	tol-uene mmol	benzyl ether mmol	benzal-dehyde mmol	2 ring region mmol*	3 ring region mmol*
benzyl	2.0	0.4387	0.00731	0.00309	0.000331	0.00092	0.05	3.90	0.15	1.09	0.08
alcohol	22.0	0.2925	0.04739	0.01789	0.002819	0.00132	0.99	6.17	0.07	7.56	3.64
	22.0	0.2647	0.04467	0.01576	0.001775	0.00299	0.76	4.38	0.09	7.35	3.54
	45.5	0.2044	0.05364	0.02455	0.005504	0.00893	5.31	2.85	0.11	6.96	6.97
	28.0	0.2036	0.0454	0.01360	0.001288	0.00039	0.45	2.20	0.08	6.89	2.64
	72.0	0.1787	0.04533	0.02156	0.007965	0.00708	6.02	2.36	0.11	12.60	20.44
benzyl	0.0	0.0133	0.27486	0.04122	0.001759	0.00121	0.23	B.D.L	0.02	0.01	0.02
amine	3.0	0.0317	0.20385	0.06595	0.006255	0.00200	0.63	0.03	0.02	0.03	0.12
	7.0	0.0721	0.13557	0.06845	0.014481	0.00468	1.63	0.23	0.04	0.15	0.54
	22.0	0.0896	0.09955	0.10778	0.068673	0.01382	7.06	N.Q.	N.Q.	N.Q.	N.Q.
	28.0	0.1432	0.06931	0.04786	0.017751	0.01629	14.52	1.27	0.13	1.64	2.74
	45.5	0.1523	0.05584	0.03756	0.013213	0.01981	16.26	1.52	0.14	2.73	5.02
	72.0	0.1592	0.0413	0.02931	0.008481	0.02891	28.40	1.18	0.22	4.99	8.96
	72.0	0.1567	0.03861	0.02855	0.007678	0.03069	28.51	1.10	0.26	4.64	8.33
dibenzyl	2.0	0.0193	0.03756	0.13966	0.014337	0.00322	0.99	0.01	0.05	0.04	0.29
amine	22.0	0.1234	0.06807	0.05038	0.026022	0.01671	9.38	0.97	0.12	1.16	2.03
	28.0	0.148	0.06378	0.04053	0.018580	0.01806	15.38	1.08	0.15	1.84	2.68
	28.0	0.1435	0.05963	0.03959	0.019905	0.01925	16.69	1.14	0.15	1.95	2.84
	45.5	0.1446	0.05308	0.02247	0.002570	0.01106	6.96	1.08	0.18	3.67	3.21
	45.5	0.1180	0.04101	0.01491	0.004493	0.01148	8.34	1.05	0.19	3.55	3.10
	72.0	0.1578	0.03712	0.02365	0.004753	0.02997	25.99	1.48	0.27	6.19	8.89
tribenzyl	2.0	0.0140	0.00262	0.01366	0.180857	0.00339	3.03	0.11	4.28	0.54	0.01
amine	22.0	0.0737	0.02243	0.02105	0.085544	0.01523	12.45	0.77	1.09	1.16	0.53
	28.0	0.0881	0.03315	0.02402	0.052041	0.01383	9.91	1.02	0.23	1.12	0.65
	45.5	0.1288	0.03374	0.03513	0.055684	0.02990	22.85	3.23	0.35	5.12	1.58
	72.0	0.1437	0.03353	0.02224	0.008661	0.02680	22.97	3.60	0.28	3.76	1.65

B.D.L.: This product was below the detection limits of the instrument
N.Q.: This product was not quantified for this experiment
One standard deviation from the mean measurement (3 injections per sample) was typically < 2%
*estimations using dibenzylamine and tribenzylamine calibration curves for 2 and 3 ring product regions, respectively

The same compounds in Table B2 are labeled on a gas chromatogram (Fig. B1, top) from an experiment with 0.25 molal benzylamine and 0.25 molal benzylamine hydrochloride heated at 250°C (P_{sat}) for 72 hours. Each peak on the chromatogram (signal intensity, μV, vs. retention time, min) represents an organic compound. In addition to the compounds mentioned above, three isomers of benzyl-benzyl alcohol were identified as was the compound bibenzyl. The two, three, and four phenyl ring regions are also shown on a zoomed in version of this chromatogram (Fig. B1, bottom). The sum of peak areas from unidentified two ring regions and three ring regions (including identified benzyl-benzyl alcohol isomers) were used separately to calculate their cumulative concentrations, as shown in Fig. 16 of Chapter 3 and Table B2.

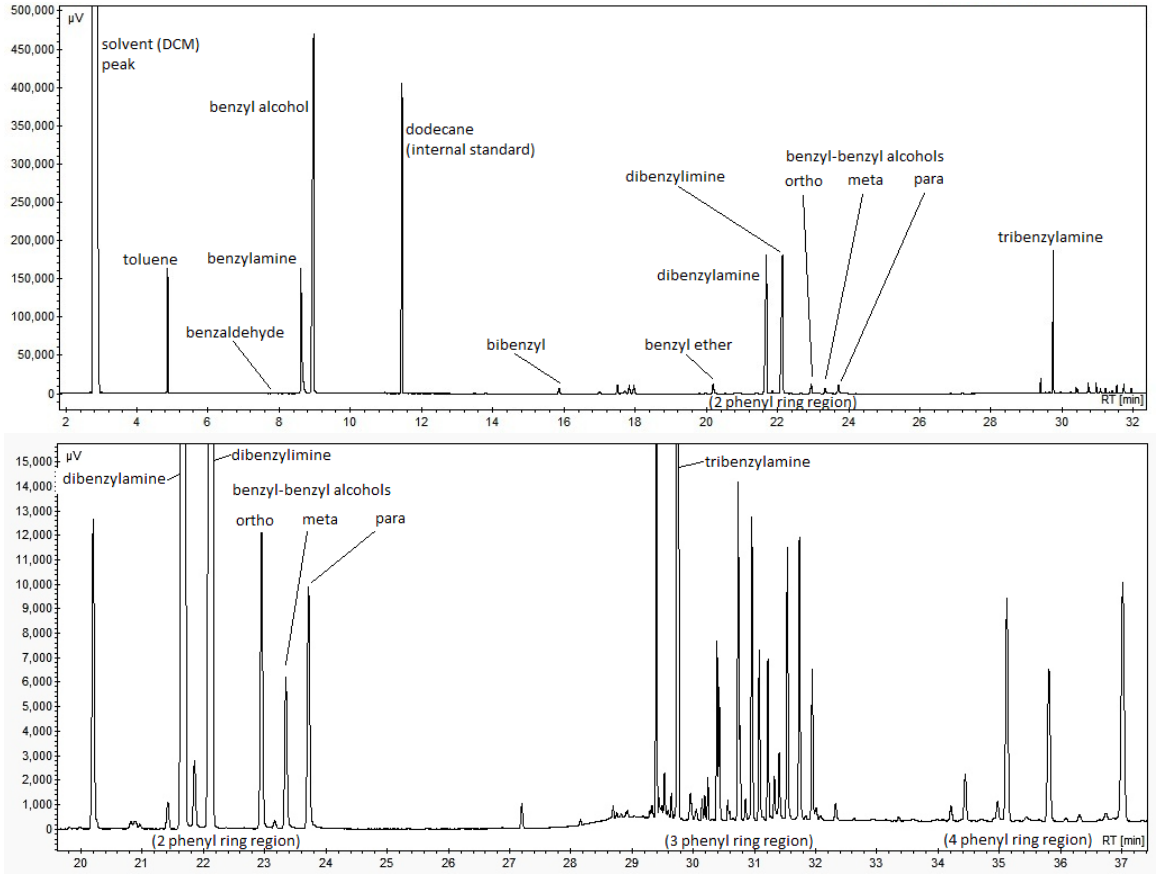

Fig. B1. Gas chromatogram from a hydrothermal experiment with 0.25 molal benzylamine and 0.25 molal benzylamine hydrochloride heated at 250°C (P_{sat}) for 72 hours. The top image shows the chromatogram at a scale where all major identified products and their retention times can be seen. The bottom image shows a zoomed in scale of the same chromatogram to display the numerous unidentified peaks in the two, three, and four phenyl ring regions; these are assumed to be products of EAS reactions. There are numerous peaks that are not visually resolved in the bottom image. Note that peak heights do not necessarily correspond to relative abundance, because different compounds have different peak shapes. These images were obtained using CompassCDS software.

APPENDIX C

ESTIMATING THERMODYNAMIC PROPERTIES OF PRIMARY, SECONDARY, AND TERTIARY AMINES AND AMINIUMS

Thermodynamic calculations were performed to independently test whether the approach to steady state reaction ratios observed in hydrothermal experiments was indeed an approach to metastable equilibrium. To do this, equilibrium constants for amination reactions as well as ionization constants for amines were needed at experimental conditions (250°C, P_{sat}). Since high temperature and pressure thermodynamic data sets do not exist for aqueous benzyl alcohol, benzylamine, dibenzylamine, and tribenzylamine, and since data for the amines at reference conditions (25°C, 1 bar) are scarce, a combination of thermodynamic property estimation strategies and equations of state were used to calculate equilibrium constants under experimental conditions.

The revised Helgeson-Kirkham-Flowers equations of state (HKF) were ultimately used to calculate thermodynamic properties of individual organic compounds and hence equilibrium constants for reactions at experimental conditions via the Microsoft Excel-based Deep Earth Water (DEW) model (Kelley, 1960; Wagman et al., 1982; Tanger and Helgeson, 1988; Shock et al., 1989; 1990; Sverjensky et al., 2014). In order to use the HKF equations of state for the desired reactions the minimum requirements for the DEW model are the standard state partial molar properties of individual compounds at reference conditions, including: Gibbs energy of formation ($\Delta_f\overline{G}°$), enthalpy of formation ($\Delta_f\overline{H}°$), third law entropy ($\overline{S}°$), constant pressure heat capacity ($\overline{C}°_P$), and volume ($\overline{V}°$). These data exist for benzyl alcohol (see below), and most of these types of data exist in the literature for benzylamine and benzylaminium. However, similar data is lacking for dibenzylamine, tribenzylamine, and their protonated forms, so group additivity relationships were explored for a variety of other primary, secondary, and tertiary amines and applied to estimate the thermodynamic properties of benzylamines. Thermodynamic

properties for a variety of individual amines as well as reaction properties that were used to develop estimation strategies can be seen in Table C1. This table also presents the properties of benzylamines that exist or can be calculated from current data (labeled calc.), and those that were estimated from correlation strategies shown in the figures below (Fig. number indicated in table). Other non-amine compounds that were used in the development of correlation strategies are also shown in this table.

The correlation strategies for estimating thermodynamic properties of primary, secondary, and tertiary amines at reference conditions can be seen in Fig. C1. These plots show that the properties of each amine change in a linear fashion (solid lines) with respect to increasing the degree of the amine. Essentially, consecutively replacing each hydrogen of ammonia with a given functional group changes each thermodynamic property by a consistent amount. We assume that this relationship holds for benzylamines, and linear functions (dashed lines) were used to calculate the properties of dibenzylamine and tribenzylamine from those of ammonia and benzylamine. A correlation strategy following the same principles was applied to estimate the properties of benzylaminiums (Fig. C2).

Also seen in Fig. C1 and C2 are labels which indicate that $\overline{S}°$ and $\overline{C}°_P$ were estimated (hollow symbols) for benzylamine and benzylaminium, respectively. These estimations required separate correlation strategies, which are shown in Fig. C3 and C4. These figures compare the respective thermodynamic properties of primary amines (or aminiums) to those of other organic compounds that serve as representatives of single functional groups attached to nitrogen. The properties of amines and their corresponding organic compounds that are plotted against one another follow Eq. (C1) and (C2):

Table C1
Thermodynamic partial molar standard state properties of aqueous organic compounds used to estimate aqueous properties of primary, secondary, and tertiary amines and aminiums

	properties of individual compounds[d]				properties of ionization reactions[e]			
aqueous species[a b]	$\Delta_f\bar{H}°$ J mol^{-1}	$\bar{S}°$ J mol^{-1} K^{-1}	$\bar{C}°_P$ J mol^{-1} K^{-1}	$\bar{V}°$ cm^3 mol^{-1}	$\Delta_{ion}\bar{H}°$ J mol^{-1}	$\Delta_{ion}\bar{S}°$ J mol^{-1} K^{-1}	$\Delta_{ion}\bar{C}°_P$ J mol^{-1} K^{-1}	$\Delta_{ion}\bar{V}°$ cm^3 mol^{-1}
methylamine	-68280[f]	127.6[f]	154.8[f]	41.9[h]	-55150[i]	18.8[i]		-5.6[i]
methylaminium	calc.	calc.	122.2[j]	calc.				
dimethylamine	-69630[k]	163.5[l]	260.4[m]	58.7[m]	-49620[i]	37.2[i]		
dimethylaminium	calc.	calc.	187.0[n]	55.1[n]				
trimethylamine	-73910[k]	165.3[o]	360[j]	78.8[p]	-36860[i]	64.0[i]		
trimethylaminium	calc.	calc.	216[j]	72.8[p]				
ethylamine	-99700[f]	140.6[f]	237.7[f]	58.6[h]	-57360[i]	12.13[i]	-31.0[q]	-5.4[i]
ethylaminium	calc.	calc.	calc.	calc.				
diethylamine	-137600[r]	190.9[s]	486[p]*	91.68[p]	-53260[i]	32.22[i]	-63.2[q]	-2.8[i]
diethylaminium	calc.	calc.	calc.	calc.				
triethylamine	-162500[r]	214.2[s]	609[j]	120.9[p]	-43180[i]	60.25[i]		-0.10[i]
triethylaminium	calc.	calc.	457.2[j]	calc.				
propylamine	-128400[f]	170.7[f]	326.4[f]	74.2[h]	-57910[i]	7.95[i]	-31.8[q]	-4.7[i]
propylaminium	calc.	calc.	calc.	calc.				
dipropylamine	-188800[r]	242.0[t]	652[j]	123.06[p]	-55100[i]	25.94[i]		-2.2[i]
dipropylaminium	calc.	calc.	577[u]	calc.				
tripropylamine	-239800[v]							
tripropylaminium								
butylamine	-151100[f]	197.5[f]	422.6[f]	89.8[h]	-584900[i]	7.53[i]	-9.2[q]	-4.3[i]
butylaminium	calc.	calc.	calc.	calc.				
dibutylamine	-247100[w]	303.3[t]		155.4[p]	-571500[i]	23.85[i]		-2.5[i]
dibutylaminium	calc.	calc.		calc.				
ethanolamine			193[x]	59.78[x]			-26.4[q]	-6.2[i]
ethanolaminium			calc.	calc.				
diethanolamine			310.5[y]	83.08[y]				
diethanolaminium			291[y]	88[y]				
ammonia	-81340[z]	108.0[p]	77.0[aa]	24.3[aa]				
ammonium	-133300[bb]	111.3[bb]	66.9[bb]	18.1[bb]				
benzylamine	24370[cc]	Fig. C3	375[dd]	104.7[dd]	-55600[ee]	-6.3[ee]		-5.79[ff]
benzylaminium	calc.	calc.	Fig. C4	calc.				
dibenzylamine	Fig. C1	Fig. C1	Fig. C1	Fig. C1	-47400[gg]	4[gg]		
dibenzylaminium	calc.	calc.	Fig. C2	Fig. C2				
tribenzylamine	Fig. C1	Fig. C1	Fig. C1	Fig. C1	-50500[gg]	-76[gg]		
tribenzylaminium	calc.	calc.	Fig. C2	Fig. C2				
benzyl alcohol	-88700[hh]	214.6[ii]	402.1[ij]	101.36[kk]				
pentylamine		223.8[ll]						
hexylamine		251.9[ll]						
acetamide		165.3[mm]						
methane		87.8[nn]						
ethane		112.2[nn]						
propane		139.6[nn]						
butane		167.4[nn]						
pentane		198.7[nn]						
hexane		221.3[nn]						
acetaldehyde		138.1[oo]						
toluene		183.7[f]	430.1[pp]					
glyince			39.3[qq]					
alanine[c]			141.4[qq]					
ethylene diaminium			185[rr]					
hexylaminium			574.2[j]					
acetate			25.9[ll]					
propionate			129.3[ll]					
ethanol			260.2[ss]					

a. Functional group always bonded to the farthest carbon from the nitrogen except where otherwise noted. b. All alkyl groups are straight chain “n-alkyl” groups. c. Note in the case of alanine, the carboxylate functional group is not bonded to the farthest carbon from the nitrogen. d. The designation "calc." means the value was determined from the properties in the line above, while reference to a Fig. indicates the property was estimated from the strategy used the given figure. e. Ionization for the reaction: $H^+ + NR_3 = HNR_3^+$. f. Calculated from standard partial molal reaction properties given by Abraham (1984) using standard partial molal properties of gases taken from Stull et al. (1969). g. Cabani et al., 1981. h. Høiland, 1986. i. Cabani et al., 1977. j. Bergström and Olofsson, 1977 combined with SUPCRT92 OH-. k. Calculated from standard partial molal reaction properties given by Florián and Warshel (1999) using standard partial molal properties of gases taken from Cox and Pilcher (1970). l. Calculated from standard partial molal reaction properties given by Florián and Warshel (1999) using standard partial molal properties of gases taken from Stull et al. (1969). m.

Shvedov and Tremaine, 1997. n. Calculated from standard partial molal properties of aminium chloride solutions taken from Shvedov and Tremaine (1997) and corrected with chloride values from Collins et al. (2000). o. Calculated from standard partial molal reaction properties given by Florián and Warshel (1999) using standard partial molal properties of gases taken from Aston et al. (1944). p. Cabani et al., 1974. q. Jones and Arnett, 1974. r. Calculated from standard partial molal reaction properties given by Cabani et al. (1981) using standard partial molal properties of gases taken from Wadso (1969). s. Calculated from standard partial molal reaction properties given by Cabani et al. (1981) using standard partial molal properties of gases taken from Stull et al. (1969). t. Calculated from standard partial molal reaction properties given by Cabani et al. (1981) using estimated standard partial molal properties of gases taken from Domalski and Hearing, 1993. u. Calculated from standard partial molal properties of aminium chloride solutions taken from Bergström and Olofsson, (1977) and corrected with chloride values from Collin et al. (2000). v. Calculated from standard partial molal reaction properties given by Jones and Arnett (1974) using standard partial molal properties of gases taken from Lebedeva (1966). w. Calculated from standard partial molal reaction properties given by Cabani et al. (1981) using standard partial molal properties of gases taken from Suradi et al. (1981). x. Pagé et al., 1993. y. Collins et al., 2000. z. Vanderzee and King, 1972. aa. Allred and Wooley, 1981. bb. CODATA, 1978. cc. Calculated from standard partial molal reaction properties given by Nichols and Wadso (1975) using standard partial molal properties of gases taken from Carson et al. (1977). dd. Derived from standard state partial molal enthalpy of formation by Nichols and Wadso, 1975. ee. Calculated from temperature-dependent pKa values from Bunting and Stefanidis, 1990. ff. Shahidi, 1987. gg. Canle L. et al., 2004. hh. Verevkin and Vasiltsova, 2004. ii. Calculated with solubility data from Valvani et al. (1981) and partial molar reaction properties from Nichols and Wadso (1975) using standard properties of pure liquids from Parks et al. (1936) and Verevkin and Vasiltsova (2004). jj. Slavik et al., 2007. kk. Stříteská et al., 2004. ll. Estimated by Shock and Helgeson, 1990. mm. Estimated by Shock, 1993. nn. Calculated from standard partial molal reaction properties given by Olofsson et al. (1984) using standard partial molal properties of gases taken from the Thermo. Res. Cent. Hydrocar. Proj. (1982). oo. Calculated in Schulte and Shock, 1993. pp. Gill et al., 1976. qq. Jolicoeur et al., 1986. rr. Nichols et al., 1976. ss. Jolicoeur and Lacroix, 1976.

*Heat capacity value not referenced to infinite dilution, but expected to be within 5 J mol^{-1} K^{-1} of infinite dilution value based on comparisons in Belousov and Panov, 1994.

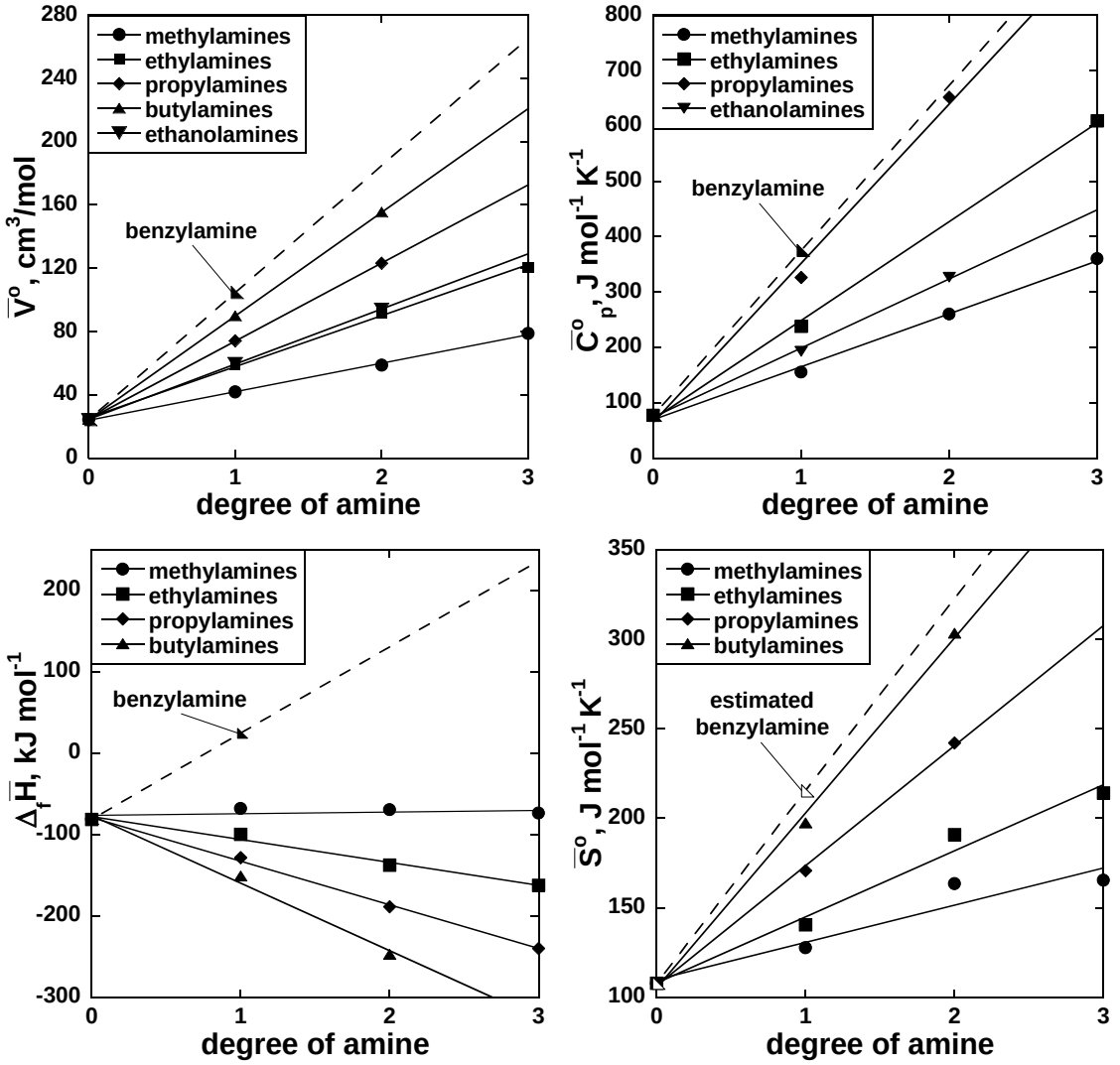

Fig. C1. Standard state thermodynamic properties (at 25°C, 1 bar) for a variety of amines vs. their degree, including methylamines (circles), ethylamines (squares), propylamines (diamonds), butylamines (triangles), ethanolamines (inverted triangles), and benzylamine (indicated). The experimental data show linear relationships, suggesting that increasing the degree of a particular amine (e.g., (0°) ammonia to (1°) methylamine to (2°) dimethylamine to (3°) trimethylamine) incrementally changes each property by a consistent value. Assuming this remains true for benzylamine, the dotted line can be used to calculate the properties of dibenzylamine and tribenzylamine from the experimental properties of benzylamine and ammonia. Data used in this figure can be found in Table C1, along with sources of the data. Note that the partial molar standard state third law entropy ($\overline{S}°$) of benzylamine (hollow symbol) was estimated using a correlation method (see text and Fig. C3).

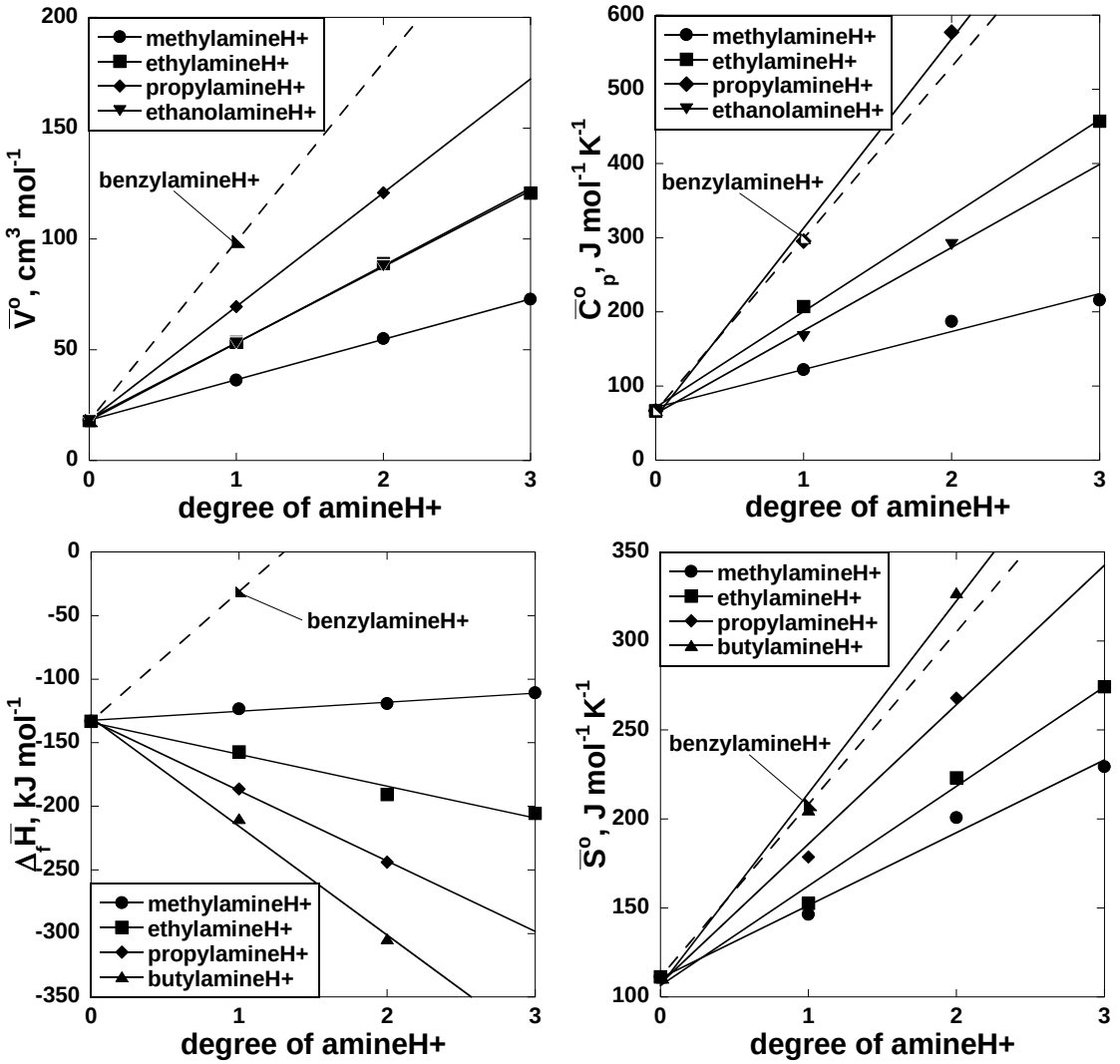

Fig. C2. Standard state thermodynamic properties (at 25°C, 1 bar) for a variety of aminiums vs. their degree, including methylaminiums (circles), ethylaminiums (squares), propylaminiums (diamonds), butylaminiums (triangles), ethanolaminiums (inverted triangles), and benzylaminium (indicated). The experimental data show linear relationships as with amines (Fig. C1). The dotted line can be used to calculate the properties of dibenzylaminium and tribenzylaminium from the experimental properties of benzylaminium and ammonium. Data used in this figure can be found in Table C1, along with sources of the data. Note that the partial molar standard state heat capacity at constant pressure ($\overline{C}°_P$) of benzylamine (hollow symbol) was estimated using a correlation method (see text and Fig. C4).

$$\bar{S}°(\text{amine}) \text{ vs. } \bar{S}°(\text{organic}) \quad ; \quad (\text{amine}) + H_2 = (\text{organic}) + NH_3 \qquad (C1)$$

$$\bar{C}°_P(\text{aminium}) \text{ vs. } \bar{C}°_P(\text{organic}) \quad ; \quad (\text{aminium}) + H_2 = (\text{organic}) + NH_4^+ \qquad (C2)$$

Note that the reaction equations in Eq. (C1) and (C2) are only used to describe the properties being plotted, but the generic reactions themselves are of no additional use for this study. Because Fig. C3 and C4 display strong linear relationships, the properties of toluene (indicated with arrows) were used to estimate the missing properties ($\bar{S}°$ and $\bar{C}°_P$) for benzylamine and benzylaminium, respectively. As mentioned above, these estimated values were then used to further estimate the same properties for dibenzylamine, tribenzylamine, and their protonated forms, respectively (Fig. C1 and C2).

The resulting standard state partial molar thermodynamic properties for benzyl alcohol, benzylamine, dibenzylamine, tribenzylamine, and the protonated aminiums can be seen in Table C2, which contains values from previous literature as well as estimated values described above. These values were inputted into the DEW model (Sverjensky et al., 2014) to calculate the revised HKF equations of state parameters (a_1, a_2, a_3, a_4, c_1 ,c_2, ω_e) for each compound (Kelley, 1960; Wagman et al., 1982; Tanger and Helgeson, 1988; Shock et al., 1989; 1990; Sverjensky et al., 2014), also shown in the table. The DEW model was then used to calculate amination reaction equilibrium constants going from benzyl alcohol to tribenzylamine (Chapter 3, Fig. 14) and ionization constants for each amine. Notably, the resulting pK_a of tribenzylaminium was calculated to be 0.27, confirming assumptions that were used in Section 3.2.3 to estimate the maximum deviation in pH for experiments which used tribenzylamine as the intial reactant. These

constants were then used to compare experimental reaction ratios to independently calculated equilibrium constants, yielding good agreement (Chapter 3, Fig. 20).

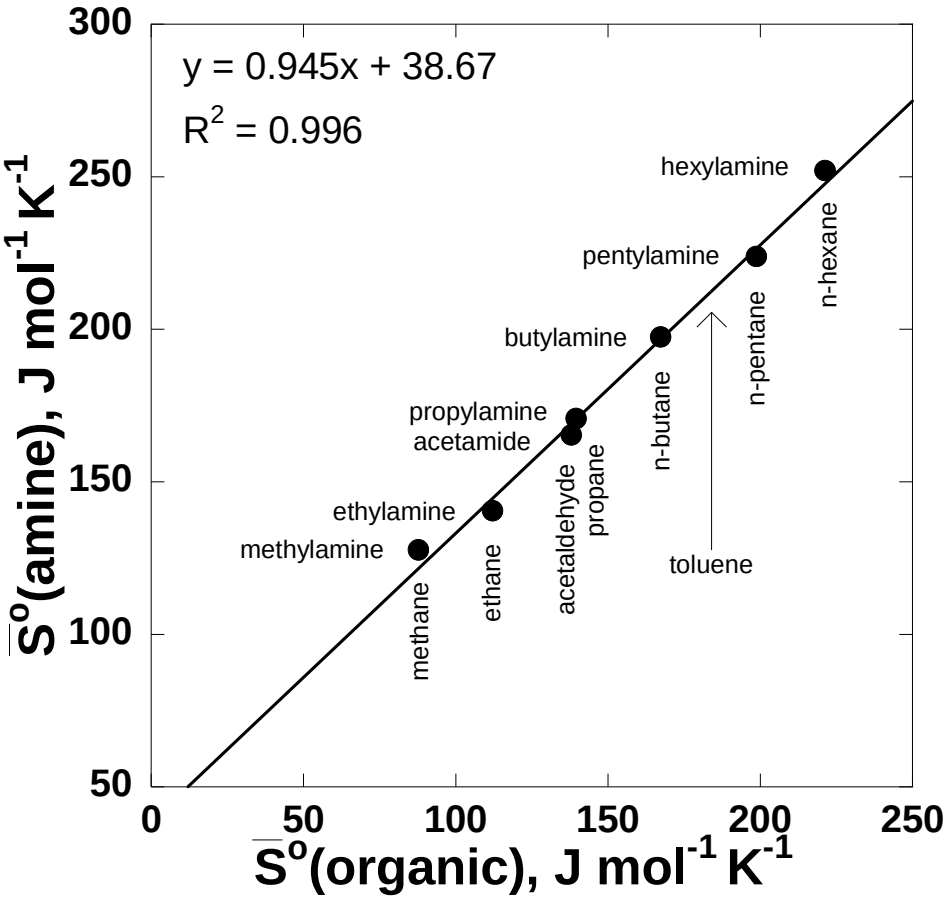

Fig. C3. Standard state partial molar third law entropy ($\bar{S}°$) at 25°C for amines vs. their associated organic compounds, according to Eq. C1 (i.e., (amine) + H_2 = (organic) + NH_3). The linear trend observed was used to calculate $\bar{S}°$ for benzylamine from that of toluene. Note that acetamide (not a traditional amine) seems to follow this trend as well. References for data used in this figure can be found in Table C1.

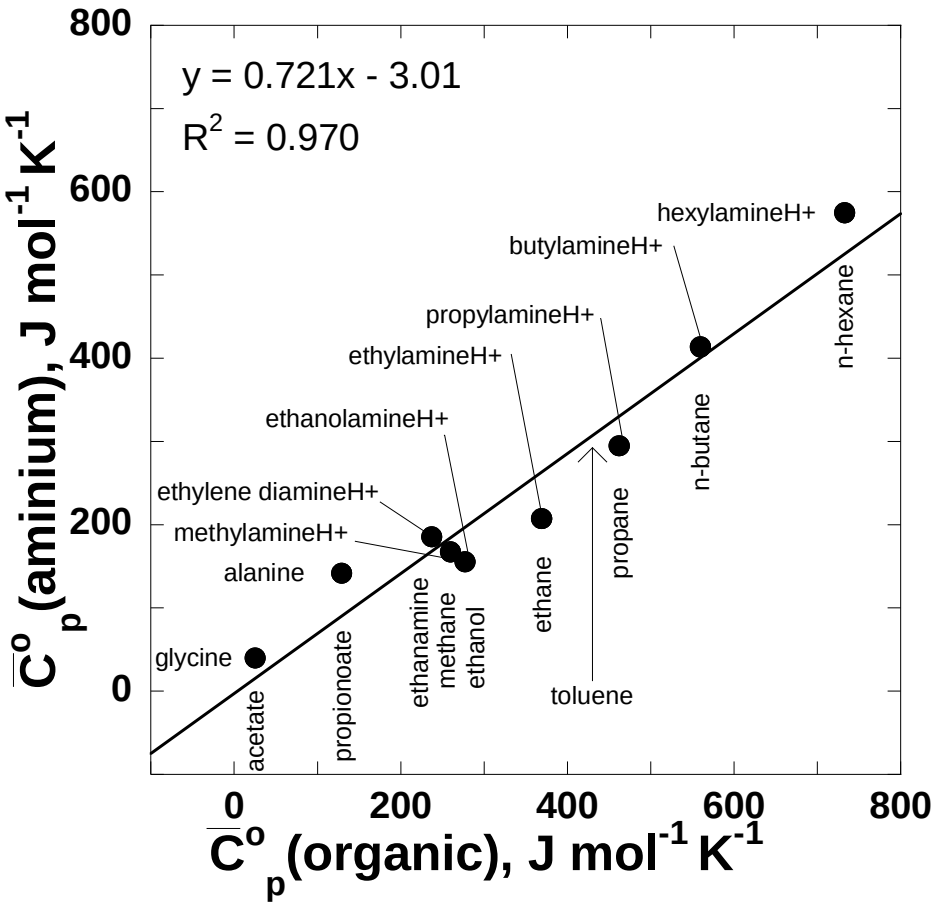

Fig. C4. Standard state partial molar heat capacity at constant pressure ($\bar{C}°_P$) at 25°C for aminiums vs. their associated organic compounds, according to Eq. C2 (i.e., (aminium) + H_2 = (organic) + NH_4^+). The linear trend observed was used to calculate $\bar{C}°_P$ for benzylaminium from that of toluene. References for data used in this figure can be found in Table C1.

Table C2
Thermodynamic properties and revised HKF equation of state parameters used in the DEW model to calculate pK_a values and amination reaction equilibrium constants

aqueous species	$\Delta_f\bar{G}^{\circ}$ [a] J mol^{-1}	$\Delta_f\bar{H}^{\circ}$ J mol^{-1}	$\bar{S}^{\circ}$ J mol^{-1} K^{-1}	$\bar{C}^{\circ}_P$ J mol^{-1} K^{-1}	$\bar{V}^{\circ}$ cm^3 mol^{-1}	a_1 x 10 J mol^{-1} bar^{-1}	a_2 x 10^{-2} J mol^{-1}	a_3 J K mol^{-1} bar^{-1}	a_4 x 10^{-4} J K mol^{-1}	c_1 J mol^{-1} K^{-1}	c_2 x 10^{-4} J K mol^{-1}	ω_e J mol^{-1}
benzyl alcohol	-19744	-154010[hh]	215[ii]	402.1[jj]	101.36[kk]	88.6477	66.4807	-35.5008	-14.3756	259.9814	69.2074	-0.1590
benzylamine	176799	24370[cc]	212.3	375[dd]	104.7[dd]	91.3617	69.0647	-37.6675	-14.4825	244.1094	63.6907	-0.1590
benzylaminium	123078	-31230	206.0	307.1	98.9	86.3439	64.2874	-33.6617	-14.2850	198.3058	49.8595	-0.8114
dibenzylamine	380180	130080	316.6	673	185.1	156.6927	131.2663	-89.8229	-17.0539	418.7558	124.3933	-0.1590
dibenzylaminium	331588	82680	320.6	547.3	179.7	151.1757	126.0136	-85.4186	-16.8367	323.0889	98.7882	-2.5469
tribenzylamine	583561	235790	420.9	971	265.5	222.0237	193.4679	-141.9784	-19.6253	593.4022	185.0959	-0.1590
tribenzylaminium	555721	185290	344.9	787.5	260.5	216.6552	188.3566	-137.6926	-19.4140	460.4706	147.7170	-2.9149

a. Calculated from columns $\Delta_f\bar{H}^{\circ}$ and $\bar{S}^{\circ}$, along with $\bar{S}^{\circ}$ of the elements from Wagman et al., 1982.
Note: All other superscripts refer to those described in the caption of Table C1.

APPENDIX D

SUPPORTING DATA FOR CHAPTER 4

This appendix contains the entirety of geochemical measurements of surface fluids issuing from the Samail Ophiolite that were used in this study, as well as supporting pictures identifying sampling locations from a single mixing zone (Fig. D1 – D3) used in Fig. 22 and 25. It contains information regarding the classification of near-endmember (N-E) Type I and N-E Type II fluids that were ultimately the focus of a series of thermodynamic calculations involving aqueous carbon chemistry.

As mentioned in Section 3.3.4, Leong et al. (in prep) determined that silica concentrations are the best single geochemical variable for quantifying mixing between Type I and Type II fluids, and thus designating which fluid samples are most representative of endmembers of those fluid types. Accordingly, the same authors used aqueous silica concentrations to perform mixing calculations, and from these calculations five Type II fluid samples that showed less than 0.5% mixing with Type I fluids were designated to represent N-E Type II fluids in the current study. Similarly, four Type I fluid samples that showed less than 40% mixing with Type II fluids were designated as N-E Type I fluids. These designations can be seen in Table D1 – D4.

Notably, certain samples were omitted from qualifying as N-E Type I or Type II fluid for thermodynamic equilibrium calculations involving organic compound formation reactions. As indicated in Table D1 – D4, these samples include those with visible mixing of Type I and Type II fluids at the surface, since the chemistry of these fluids was expected to be vastly out of equilibrium and thereforee less informative for determining formation conditions for organic compounds. Other samples were omitted because they lack H_2(aq) measurements, which are essentially for performing calculations involving carbon redox reactions.

Fig. D1. Picture of Type II fluid region of single mixing zone. Sample number and Na^+ concentration are shown, which correspond to values in Table D3.

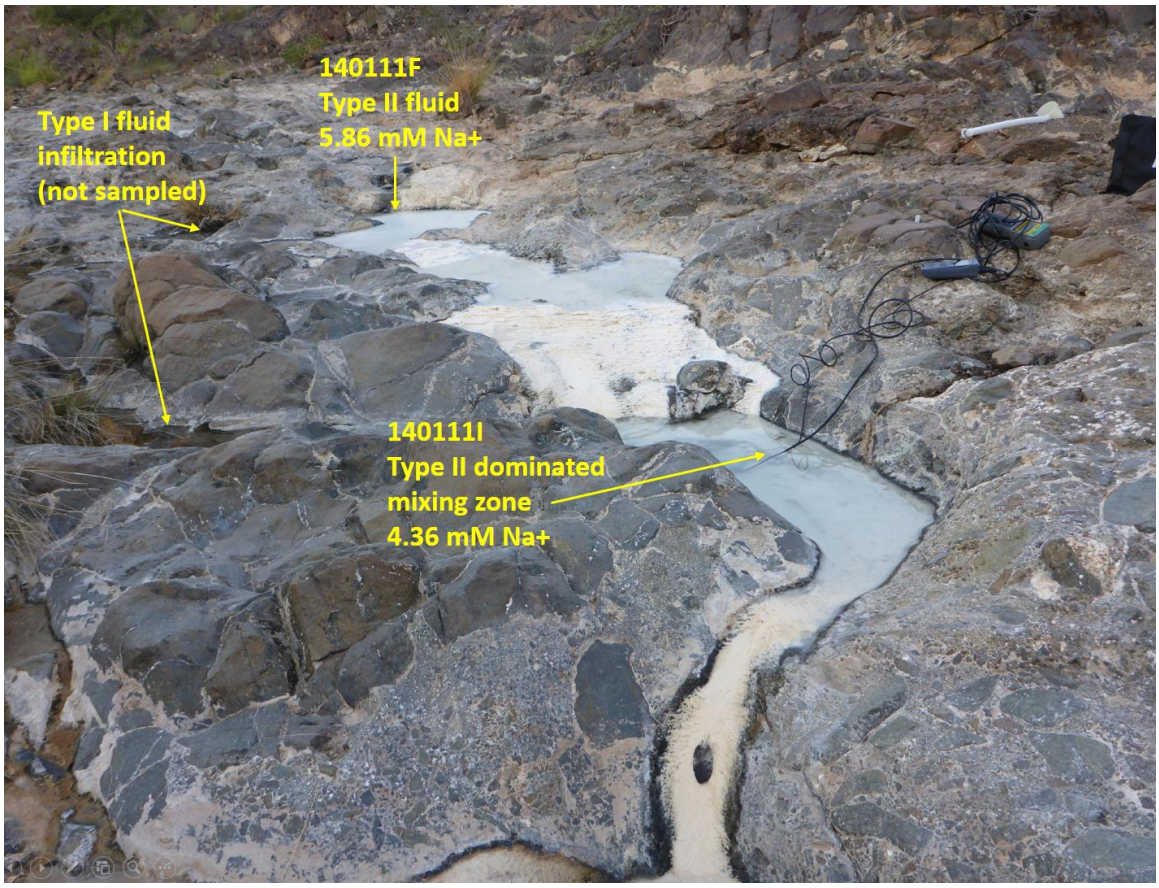

Fig. D2. Picture of Type II dominated fluid region of single mixing zone. Sample number and Na^+ concentrations are shown, which correspond to values in Table D3.

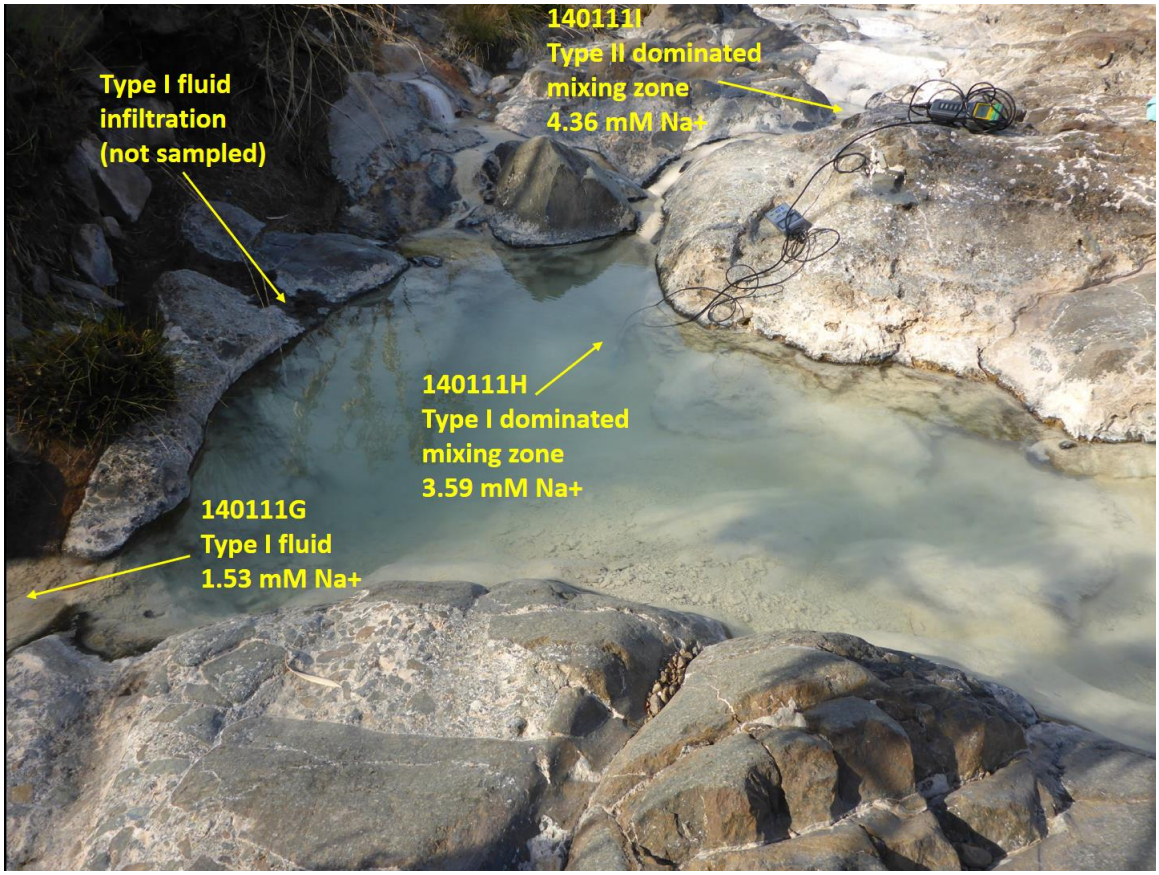

Fig. D3. Picture of Type I dominated fluid region of single mixing zone. Sample number and Na^+ concentrations are shown, which correspond to values in Table D3.

Table D1
Sample coordinates, pH, conductivity, and temperature

Sample ID	Coordinates (UTM)			cond.	temp.
YYMMDD	E	N	pH	µS cm^{-1}	°C
140116B [I]	486065	2588474	7.909	760	26.5
140116C *	486045	2588468	8.714	777	27.3
140111G [I]	646074	2533668	8.936	586	22.6
140116D *	486036	2588465	9.104	777	27.1
140110B [I]	663409	2542560	8.425	568	23.5
140114S [I]	608552	2526491	7.650	787	21.0
140111H *	646074	2533678	10.240	597	20.2
140112L *	663441	2542640	9.774	659	21.3
140111I *	646074	2533674	10.870	683	18.8
140110D *	663442	2542636	10.394	778	21.8
140117J *	486048	2588470	11.309	1387	31.6
140111F	646074	2533679	11.624	1470	23.8
140114U	608551	2526487	11.355	1479	21.7
140112M	663442	2542628	11.376	2058	28.2
140110C	663446	2542620	11.392	2011	27.0
140112K	663447	2542634	11.379	1870	26.9
140113O	608433	2525961	11.430	2329	28.4
140114V	608559	2526485	11.407	1803	24.4
140117F	NA [a]	NA [a]	11.480	1868	26.2
140117K [c]	485981	2588423	11.491	1980	27.4
140115X	487585	2575981	11.398	2949	29.5
140117I	486046	2588489	11.313	2000	32.3
140115Y [b II]	487584	2575975	11.579	2778	24.5
140113P [II]	608426	2525966	11.490	2224	25.9
140117L [d †]	485981	2588426	11.561	2087	27.3
140114T [II]	608564	2526487	11.421	2061	27.2
140117H [II]	485980	2588429	11.485	2067	29.6
140115Z [II]	487338	2576127	11.330	4050	32.2

[a] GPS reading not taken, but site is approximately one meter away from 140117G
[b] Outflow channel from 140115X
[c] Outflow channel from 140117H
[d] Outflow channel from 140117H, downstream of 140117K
[I] Designated Type I near-endmember, used in calculations
[II] Designated Type II near-endmember, used in calculations
* Not designated as near-endmember due to visible mixing at surface
† Not used in calculations due to lack of dissolved gas measurements

Table D2
Dominant analyses relevant to inorganic carbon chemistry

Sample ID YYMMDD	H_2(aq) μmolal	SD [a] μmolal	DIC mmolal	SD [b] mmolal	Mg^{2+} [b] mmolal	Ca^{2+} [b] mmolal	O_2(aq) mg L^{-1}
140116B [I]	0.062	S	5.13	0.16	2.805	0.562	4.0
140116C *	9.351	S	4.75	0.25	2.676	0.634	7.3
140111G [I]	0.240	S	4.11	0.16	2.142	0.359	7.1
140116D *	12.486	S	3.98	0.11	2.432	0.715	6.9
140110B [I]	0.016	S	3.63	0.18	1.840	0.485	7.8
140114S [I]	0.015	S	4.39	0.17	2.011	0.603	5.5
140111H	1.058	0.037	1.80	0.05	1.171	0.214	8.9
140112L	0.025	S	1.88	0.09	1.149	0.313	8.1
140111I	1.580	0.688	0.85	0.02	0.807	0.368	7.4
140110D	0.065	S	0.81	0.04	0.782	0.475	6.5
140117J	217.754	S	0.07	NA [c]	0.019	0.828	1.0
140111F	247.118	15.247	0.04	NA [c]	0.004	1.688	0.3
140114U	0.017	S	0.17	NA [c]	0.016	1.175	7.0
140112M	28.170	3.483	0.05	NA [c]	0.001	1.979	0.5
140110C	6.124	0.352	0.05	NA [c]	0.001	1.958	0.6
140112K	0.476	0.012	0.04	NA [c]	0.002	1.890	0.3
140113O	31.478	8.769	0.06	NA [c]	0.001	2.085	1.9
140114V	0.551	0.670	0.23	NA [c]	0.006	1.715	6.1
140117F	264.613	S	0.03	NA [c]	0.002	1.848	0.8
140117K	NA	-	0.03	NA [c]	0.001	2.082	1.2
140115X	214.031	19.076	0.03	NA [c]	0.000	1.887	1.4
140117I	227.347	S	0.05	NA [c]	0.008	1.859	0.4
140115Y	20.789	S	0.11	NA [c]	0.001	1.792	4.5
140113P	56.286	8.531	0.05	NA [c]	0.001	2.031	1.6
140117L [†]	NA	-	0.02	NA [c]	0.001	2.145	0.7
140114T	27.293	0.780	0.04	NA [c]	0.002	1.915	0.5
140117H	225.403	S	0.03	NA [c]	0.001	2.079	0.7
140115Z	211.761	20.345	0.03	NA [c]	0.000	2.368	1.1

[a] Sampling error calculated from multiple samples unless otherwise stated
[b] Analytical error from two injections is typically < 1%
[c] Only a single injection was performed
NA: No sample taken; definition specific to only this table.
S: Singlet sample; analytical error calculated from three injections typically < 5%
* Not designed as near-endmember due to visible mixing subsurface
[†] Not used in calculations due to lack of dissolved gas measurements

Table D3
Major dissolved ions, sulfide, and silica

Sample ID YYMMDD	Na^{+} [a] mmolal	NH_4^{+} [a] μmolal	Cl^{-} [a] mmolal	SO_4^{-2} [a] mmolal	NO_3^{-} [a] μmolal	Σ sulfide μg L^{-1}	silica(aq) μmolal
140116B I	1.058	0.233	1.277	0.696	433.763	8	302.59
140116C *	1.371	1.158	1.536	0.680	406.935	20	278.69
140111G I	1.529	0.566	1.525	0.326	124.958	3	276.35
140116D *	1.863	2.543	1.918	0.612	361.387	21	260.49
140110B I	1.308	BDL	1.579	0.346	159.410	11	183.39
140114S I	3.202	0.305	3.186	0.443	295.663	1	200.48
140111H	3.592	3.798	3.079	0.182	31.784	39	145.00
140112L	3.724	3.379	3.751	0.243	93.220	7	111.13
140111I	4.362	5.966	3.686	0.154	21.417	65	100.25
140110D	4.921	6.610	4.794	0.180	68.486	42	91.38
140117J	5.828	16.852	4.713	0.111	0.193	74	48.94
140111F	5.859	15.486	4.659	0.011	3.806	217	10.52
140114U	8.093	11.874	4.718	0.176	66.723	109	7.43
140112M	7.895	21.097	7.361	0.011	0.148	515	5.60
140110C	7.914	19.831	7.447	0.011	1.187	438	4.26
140112K	7.592	22.660	7.160	0.018	0.282	535	3.88
140113O	9.400	33.634	7.919	0.004	0.467	187	3.68
140114V	8.431	20.283	6.980	0.018	3.261	266	2.75
140117F	6.408	18.323	5.347	0.004	1.113	151	2.65
140117K	7.164	21.266	5.760	0.002	0.237	101	2.26
140115X	13.854	58.734	11.407	0.005	0.889	223	2.22
140117I	6.276	19.364	5.322	0.006	0.251	104	1.96
140115Y	14.279	50.536	11.752	0.010	4.102	115	2.16
140113P	9.528	29.234	7.896	0.008	8.860	63	1.94
140117L †	7.328	22.723	5.814	0.002	0.247	115	1.87
140114T	7.974	30.625	6.893	0.013	1.572	568	1.84
140117H	7.138	23.542	5.766	0.002	0.282	175	1.66
140115Z	17.131	87.604	12.643	0.003	0.317	200	1.38

[a] Analytical error from two injections is typically < 1%
BDL: below the detection limits of the instrument
* Not designated as near-endmember due to visible mixing at the surface
† Not used in calculations due to lack of dissolved gas measurements

Table D4
Dissolved organic species

Sample ID YYMMDD	formate µmolal	SD [a] µmolal	acetate µmolal	SD [a] µmolal	CH_4(aq) µmolal	SD b µmolal	$\delta^{13}CH_4$(aq) ‰	SD [c] ‰	DOC µmolal
140116B	BDL	-	1.471	0.031	0.003	S	-35.4	5.3	21.74
140116C *	BDL	-	1.581	-	0.899	S	-12.7	3.9	37.22
140111G	BDL	-	1.206	0.031	1.624	S	2.2	2.2	30.92
140116D *	BDL	-	1.361	0.062	0.122	S	NA [d]	-	36.84
140110B	0.435	0.133	BDL	-	0.004	S	NA [d]	-	23.637
140114S	BDL	-	0.854	0.156	0.018	S	-30.1	5.3	34.061
140111H	1.974	0.027	0.656	0.062	7.714	0.311	1.8	2.9	33.193
140112L	0.735	0.133	BDL	-	0.464	S	NA [d]	-	23.738
140111I	1.280	0.106	0.920	0.062	7.754	S	6.6	2.5	48.476
140110D	0.754	0.106	BDL	-	8.912	S	NA [d]	-	21.647
140117J	0.528	0.053	BDL	-	13.277	S	-11.2	2.1	20.98
140111F	1.918	0.053	1.757	0.125	141.334	18.320	NA [d]	-	32.347
140114U	3.270	0.159	2.484	0.405	0.090	S	-12.1	5.3	24.783
140112M	0.735	0.080	BDL	-	226.529	14.013	6.9	1.8	12.573
140110C	4.190	0.080	1.294	0.156	200.971	2.839	NA [d]	-	19.299
140112K	0.942	0.159	0.788	0.249	256.821	16.724	NA [d]	-	14.604
140113O	4.791	0.027	3.893	0.218	4.119	0.694	-5.0	1.9	11.08
140114V	0.979	-	BDL	-	1.489	0.045	-5.0	2.1	22.678
140117F	1.223	0.027	1.449	-	13.296	S	-11.9	2.2	30.94
140117K	0.547	0.080	1.294	0.343	NA	-	NA [d]	-	13.16
140115X	4.303	0.027	4.113	0.218	6.847	1.054	-4.4	1.9	13.85
140117I	0.491	0.319	BDL	-	13.591	S	NA [d]	-	16.18
140115Y	1.711	0.027	2.858	-	3.248	S	-7.2	2.7	21.34
140113P	1.599	0.080	2.197	0.374	13.320	0.964	-9.4	2.4	19.029
140117L †	0.491	0.053	0.964	0.062	NA	-	NA [d]	-	10.45
140114T	5.505	0.080	3.034	0.187	38.952	2.681	-7.9	2.4	14.913
140117H	1.073	0.398	BDL	-	12.707	S	-11.3	1.9	11.44
140115Z	3.045	0.106	3.210	0.311	18.187	1.103	NA [d]	-	12.04

[a] Analytical uncertainty, one standard deviation, calculated from two injections
[b] Sampling uncertainty, one standard deviation, calculated from multiple samples unless otherwise stated
[c] Analytical uncertainty, one standard deviation, calculated from three injections
[d] No analysis; sample bags leaked prior to isotopic analysis
BDL: Below the detection limit of the instrument
S: Single sample; analytical uncertainty, one standard deviation, calculated from three injections typically < 5%
* Not designated as near-endmember due to visible mixing at surface
† Not used in calculations due to lack of dissolved gas measurements